State of Oregon
Oregon Department of Geology and Mineral Industries
Brad Avy, State Geologist

SPECIAL PAPER 49

BEACH AND SHORELINE DYNAMICS IN THE CANNON BEACH LITTORAL CELL: IMPLICATIONS FOR DUNE MANAGEMENT

by Jonathan C. Allan[1], Laura L. Gabel[1], and Fletcher O'Brien[2]

2018

[1]Oregon Department of Geology and Mineral Industries, Coastal Field Office, P.O. Box 1033, Newport, OR 97365
[2]Oregon Department of Geology and Mineral Industries, 800 NE Oregon Street, Suite 965, Portland, OR 97232

DISCLAIMER

This product is for informational purposes and may not have been prepared for or be suitable for legal, engineering, or surveying purposes. Users of this information should review or consult the primary data and information sources to ascertain the usability of the information. This publication cannot substitute for site-specific investigations by qualified practitioners. Site-specific data may give results that differ from the results shown in the publication.

Cover photo: Oblique aerial photo of the Chapman Point beach, located immediately north of Ecola Creek, Clatsop County. Photo taken by D. Best, March 09, 2015.

Oregon Department of Geology and Mineral Industries Special Paper 49
Published in conformance with ORS 516.030

For copies of this publication or other information about Oregon's geology and natural resources, contact:
Administrative Offices
800 NE Oregon Street, Suite 965
Portland, OR 97232
Telephone (971) 673-1555
http://www.oregongeology.org
http://www.oregon.gov/DOGAMI/

TABLE OF CONTENTS

LIST OF FIGURES

LIST OF TABLES

EXECUTIVE SUMMARY

This study provides an assessment of the physical processes contributing to changes in the morphology of beaches and dunes in the Cannon Beach littoral cell, located in southern Clatsop County, Oregon. The work presented here updates an earlier investigation by Rosenfeld (1997). Since 1939, the City of Cannon Beach has experienced significant accumulation of sand along its beaches, especially in its dunes north of Haystack Rock (**Figure 1** and **Figure 33**). In particular, north of Ecola Creek, the combination of a large sand supply and the proliferation of European beach grass (*A. arenaria*) has contributed to the formation of dunes that have reached heights of 16 m (53 ft, relative to the North American Vertical Datum of 1988 [NAVD88]) In response to considerable sand buildup north of Ecola Creek, the City of Cannon Beach initiated a process to evaluate their existing dune management plan on the basis of updated scientific information on physical processes and coastal geomorphology occurring along the Cannon Beach littoral cell. The overarching objective is to use the updated information to help establish new guidelines for the relocation of excess sand that periodically builds up along the coastline. This sand buildup within the dune is presently affecting the views of local residents, while sand blowing inland has become a nuisance, migrating where it has begun to inundate buildings and properties. The broad findings of this study include the following:

- Since 1997 the Cannon Beach littoral cell has gained ~209,220 m^3 (273,649 $yards^3$) of sand.
- Large positive sediment gains have occurred in all areas north of Tolovana Park, with the largest accumulation having occurred north of Ecola Creek in the Chapman Point dune management region. This region alone has accumulated ~225,080 m^3 (294,390 $yards^3$) of sediment since 1997.
- Sand volume gains have also occurred in the Presidential dune management area (south of Ecola Creek and north of Haystack Rock), which accumulated ~24,287 m^3 (31,767 $yards^3$) of sand since 1997.
- Minor sand gains were also observed in the Haystack Rock (~1,770 m^3 [2,315 $yards^3$]) and Arch Cape (~9,180 m^3 [~12,000 $yards^3$]) sub-region areas.
- Net sand losses since 1997 have dominated all other sub-regions including:
    - Tolovana North — lost ~4,350 m^3 (5,690 $yards^3$);
    - Tolovana South — lost ~17,500 m^3 (22,890 $yards^3$);
    - Silver Point — lost ~1,660 m^3 (2,170 $yards^3$);
    - Arcadia Beach — lost ~9,670 m^3 (12,650 $yards^3$);
    - Hug Point — lost ~5,070 m^3 (6,630 $yards^3$); and
    - Falcon Cove — lost ~12,800 m^3 (16,740 $yards^3$).
- The total volume of sand contained in the entire Cannon Beach littoral cell measured between the 6 m (19 ft) contour (approximately the dune or bluff toe) and mean lower low water (MLLW), is ~3.6 million m^3 (4.67 million $yards^3$). Incorporating the volume of sand contained in the dunes increases the total volume to ~4.2 million m^3 (5.4 million $yards^3$) of sand.
- In the Chapman Point dune management area, we found that ~195,600 m^3 (~255,900 $yards^3$) of sand is located at elevations greater than the 10 m (33 ft) contour; ~63,000 m^3 (~82,400 $yards^3$) is located in the southern portion of Chapman Point (i.e., ~one third of the total sand volume is located south of 5th Street).
- Our assessment of wind and wave processes over the past two to three decades suggests that the combination of persistent El Niño conditions since the early 1980s coupled with the prevalence of strong southerly winds have contributed to a net northward drift in beach sand within the littoral cell.

- The formation of dunes north of Haystack Rock is thus a function of three main factors:
    - A sufficiently large supply of sand that is transported by nearshore processes;
    - A prevailing wind—of particular importance is the wind speed, which needs to be strong enough to entrain and mobilize sand within the intertidal zone and at the back of the beach, and their subsequent landward and northward transport; and,
    - Obstacles to trap the sand such as woody debris, vegetation, and micro-topography.
- Because the volume of sand released from erosion of dunes in the Cannon Beach cell account for ~38% of the total sand that accumulated north of Haystack Rock, this strongly suggests that much of the sand is locally derived from the nearshore region (i.e., the surf zone to depths of 10 to 15 m [30 to 45 ft]) and from erosion of the beach (particularly south of Haystack Rock).
- The introduction European beach grass (*Ammophila arenaria*) to the Oregon coast in the 1900s has profoundly changed the morphology of the dunes. At Cannon Beach, *A. arenaria* was introduced sometime in the 1950s, and major plantings occurred in the 1960s. These initial efforts effectively stabilized the dunes at Chapman Point and by 1967 had greatly increased its capacity to retain sand.
- From a management standpoint, an effective dune scraping management plan must adhere to the following principles:
    - Minimize the height at which the dune is lowered, thereby avoiding the potential for wave overtopping during an extreme storm(s). Analyses of extreme 100-year total water levels (TWL, the combined effect of wave runup superimposed on tides) undertaken in the Cannon Beach cell indicate the potential for storms to generate wave runup is on the order of 7 to 7.5 m (23 to 25 ft). Incorporating a 1.2 m (4 ft) factor of safety adopted by the City of Cannon Beach yields design dune crest elevations that potentially could range from 8.2 to 8.7 m (27 to 28.5 ft);
    - Retain the sand that is removed from the crest of the dune by placing it back onto the beach, thereby retaining a sufficient buffering capacity against future storms; and,
    - Replant the scraped area in order to quickly stabilize the dune, minimizing the subsequent entrainment of sand by wind processes and their landward incursion into backshore properties.
        - Following dune scraping, it is <u>imperative</u> that steps be taken to stabilize the exposed area as quickly as possible, in order to minimize the transport of exposed dune sand back in among properties located behind the dunes.
        - We recommend NOT using European beach grass (*A. arenaria*) to stabilize the dune, because this species is directly contributing to the buildup of higher dunes at Cannon Beach, affecting the view from shorefront homes.
        - A more effective approach is to plant either the non-native American (*A. breviligulata*) or Pacific Northwest native dune grass (*E. mollis*), or some combination of both grasses; both species have been demonstrated to build lower, broader dunes.

Because of the variability in the forces that both sustain and erode beaches and dunes on the Oregon coast and our uncertainty in changes that will likely affect the beach over longer time scales (10 to 30 years), an adaptive management approach based on a sound knowledge of beach and dune processes, guided by systematic monitoring and evaluation of the system as a whole is essential.

1.0 INTRODUCTION

Cannon Beach, located on the northern Oregon coast in Clatsop County. The City of Cannon Beach is evaluating their existing dune management plan. This plan establishes guidelines for the relocation of excess sand (dune scraping) that periodically builds up along the coastline north of Haystack Rock and south of Chapman Point (**Figure 1**). This accumulation of sand over the past few decades has resulted in substantial aggradation of the dunes located north of Ecola Creek, which impacts the views of residents located adjacent to the beach. Furthermore, wind-blown sand has been demonstrated to be a nuisance, migrating inland, where it has begun to inundate buildings and properties.

Development of the Cannon Beach dune management plan was originally completed in 1997 (Rosenfeld, 1997). Although the study emphasis was directed at understanding sediment dynamics along the entire littoral cell, Cape Falcon to Tillamook Head, the study mainly focused on the beach north of Ecola Creek. The study ultimately led to the establishment of a framework for dune management north of Ecola Creek and south of Chapman Point. The Cannon Beach dune management plan was subsequently modified by Marra (2001) to allow for additional dune scraping activities south of Kramer Point and north of Harrison Street.

The City of Cannon Beach has contracted with the Oregon Department of Geology and Mineral Industries (DOGAMI) to undertake an updated study of the physical processes driving sediment movement along the length of the Cannon Beach littoral cell. The impetus for this work stems from recent efforts to remove about 60,000 yards^3 of sand from the frontal dunes north of Ecola Creek and deposit the sand out on the beach. Placement of such a large amount of sand on the beach has raised concern over the potential effect the sand could have on the physical system.

The proposed study is being undertaken according to a phased approach, consisting of:

1. **Science Background Report:** The existing report is the outcome of this task and reflects a synthesis of scientific information and data-gathering that spans the entire littoral cell (Cape Falcon to Tillamook Head). The report also reviews earlier dune management work undertaken by previous coastal consultants including Rosenfeld (1997) and Marra (2001). In addition to addressing the sediment budget and sand movement in the littoral cell, the City of Cannon Beach has requested additional information on the following topics:
    - The patterns and rates of dune growth;
    - Impacts of dune grading and disposal practices on beach contours, habitat, and sand supply;
    - Seasonal differences and timing considerations in dune grading and disposal;
    - Vegetation/revegetation impacts; and
    - Impacts on recreational use, including beach access.

    One additional task associated with the science background report is to:
    - Undertake updated surveys of beach profiles established along the Cannon Beach cell (**Figure 1**) in 2009 for the purposes of FEMA flood mapping. Two surveys were to be carried out: the first at the end of summer 2015, and a follow-up survey in late winter 2016.
2. **Implementation Strategy:** This task involves applying the findings/conclusions/recommendations from the Science Background Report to policy decisions. The products are:
    - Draft comprehensive plan background report: this document would address the legal requirements and policy implications not covered in the science background report.
    - Policy report: this document would convert the science background report findings into enforceable policy language, zoning ordinance requirements, and implementation procedures.

3. **Public Hearings and Adoption:** This task takes the finished products and presents them for public review. Minimally, this task will involve a hearing before the Planning Commission and a hearing before the City Council. If needed, additional public review may be pursued prior to the Planning Commission hearings, where the Background Report and Implementation Strategy are presented, and public comment is taken in a less structured forum than a Planning Commission or City Council hearing.

Section **2.0** of this report examines the physical processes driving coastal changes on the northern Oregon coast, including the role of tides, observed sea level changes (including future projections), and waves. Alongshore sediment transport processes, a function of wave approach relative to the shore, are also examined. Section 2 concludes with an overview of the tsunami hazard facing the Oregon coast due to its proximity to the Cascadia subduction zone (CSZ) and the probability of occurrence of another great earthquake on the subduction zone. A discussion of dune morphology and the processes that drive dune growth is provided in Section **3.0**. The local geology and geomorphology of the Cannon Beach littoral cell, including historical shoreline changes is examined in Section **4.0**. Section **5.0** discusses the Cannon Beach littoral cell monitoring network, rates, and patterns of coastal change and concludes with an examination of recent beach sand volume changes taking place along the entire littoral cell. Section **6.0** explores the implications of dune management along the north end of the littoral cell including the effects of dune erosion, high wave runup levels, and approaches for disposing of scraped dune sand. Critical to any dune scraping activity is the need to stabilize the graded dune as quickly as possible; this need is examined in Section **6.5.**

Figure 1. Location map of the Cannon Beach littoral cell showing subcells, place names, and beach profile locations.

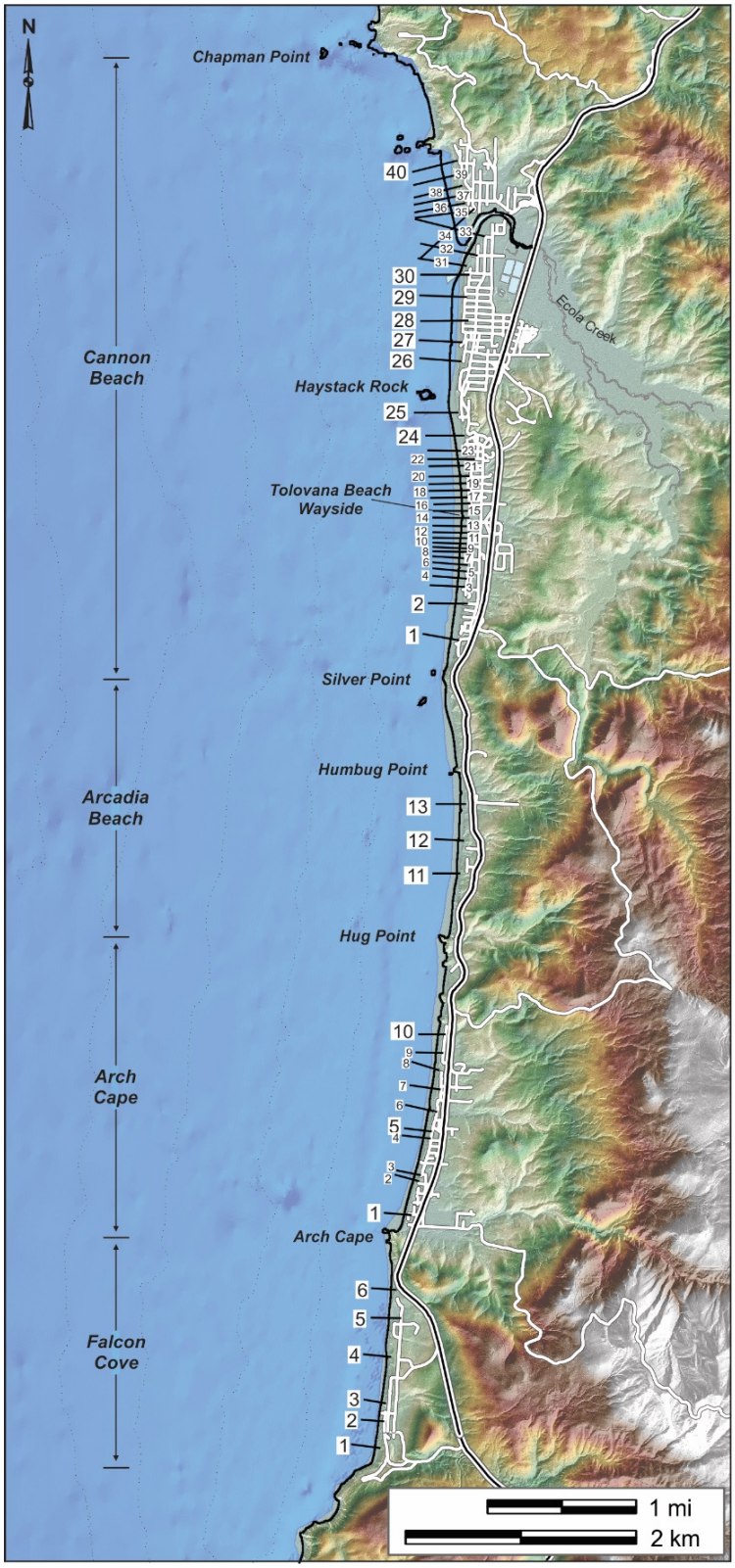

2.0 BEACH PROCESSES ON THE OREGON COAST

2.1 Background

This section explores the characteristics of waves and water levels observed on the northern Oregon coast. Much of this information stems from analyses of National Ocean Service (NOS) tide gauge data measured at several sites, e.g., the Columbia River (Astoria, #9439040), Tillamook Bay (Garibaldi, #9437540), and Newport (South Beach, #9435380), as well wave statistics measured by deepwater wave buoys operated by the National Data Buoy Center (NDBC).

2.2 Tides

Tides along the Oregon coast are classified as moderate, with a maximum range of up to 4.3 m (14 ft) and an average range of about 1.8 m (6 ft) (Komar, 1997). There are two highs and two lows each day, with successive highs (or lows) usually having markedly different levels. Tidal elevations are given in reference to the mean of the lower low water levels (MLLW), and can be easily adjusted to the North American Vertical Datum of 1988 (NAVD88) vertical datum. As a result, most tidal elevations are positive numbers with only the most extreme lower lows having negative values.

For the purposes of this study, we have based our analyses on tides measured at the South Beach gauge (#9435380) in Yaquina Bay (1967–2017), which is representative of tidal conditions along the coast. **Figure 2** shows tidal elevation statistics derived from the South Beach tide gauge (the longest temporal record), with a mean range of 1.91 m (6.3 ft) and a diurnal range of 2.54 m (8.3 ft). The highest tide measured from this record reached 3.73 m (12.2 ft), recorded in December 1969 during a major storm. These values are comparable to those measured at the Garibaldi site (mean = 1.9 m, diurnal = 2.53 m), nearest to Cannon Beach, with the only real difference being that the Garibaldi gauge recorded a peak water level of 3.64 m (11.9 ft) in December 2005 due to its shorter record; the Garibaldi gauge began tide measurements in July 2005.

Figure 2. Daily tidal elevations measured at South Beach (Newport) on the central Oregon coast. Data from National Ocean Service (NOS) (http://www.co-ops.nos.noaa.gov/waterlevels.html?id=9435380).

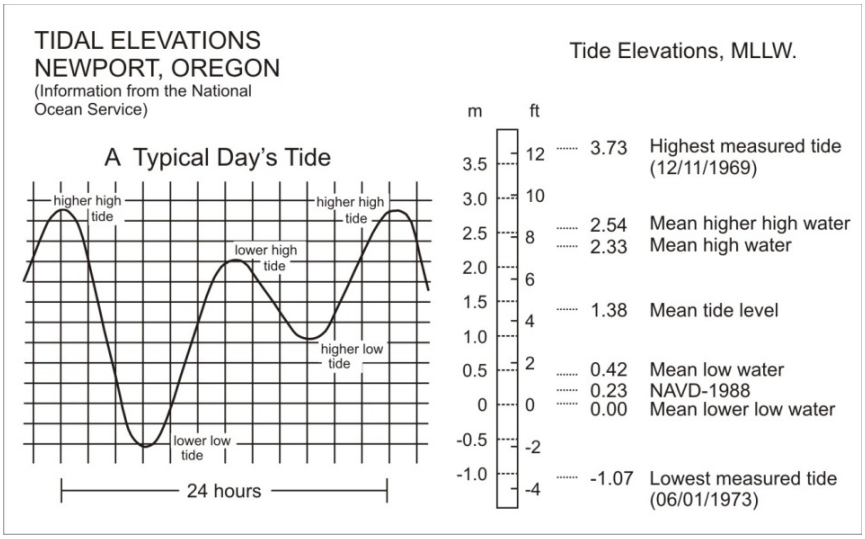

Tides on the Oregon coast tend to be enhanced during the winter months due to warmer water temperatures and the presence of northward flowing ocean currents that raise water levels along the shore; the effect persists throughout the winter rather than lasting for only a couple of days as is the case for a storm surge. This effect can be seen in the monthly averaged water levels derived from the combined time series (**Figure 3**), but where the averaging process has removed the water-level variations of the tides, yielding a mean water level for the entire month. The results in **Figure 3**, from 50 years of data, show that on average monthly-mean water levels during the winter are nearly 25 cm (0.8 ft) higher than in the summer. Water levels are most extreme during El Niño events, due to an intensification of the processes, largely, enhanced ocean sea surface temperatures offshore from the Oregon coast. This occurred particularly during the unusually strong 1982-1983 and 1997-1998 El Niños, and most recently in the 2015-2016 El Niño. As seen in **Figure 3**, water levels during those climate events were approximately 25 to 30 cm (0.8 to 1 ft) higher than the seasonal peak, and as much as 56 cm (1.8 ft) higher than during the preceding summer. These water levels enabled wave swash processes to reach much higher elevations on the beach during the winter months, with storm surges potentially raising water levels still further.

Figure 3. Seasonal cycles in monthly-mean water levels based on data from the South Beach tide gauge (1967–2017).

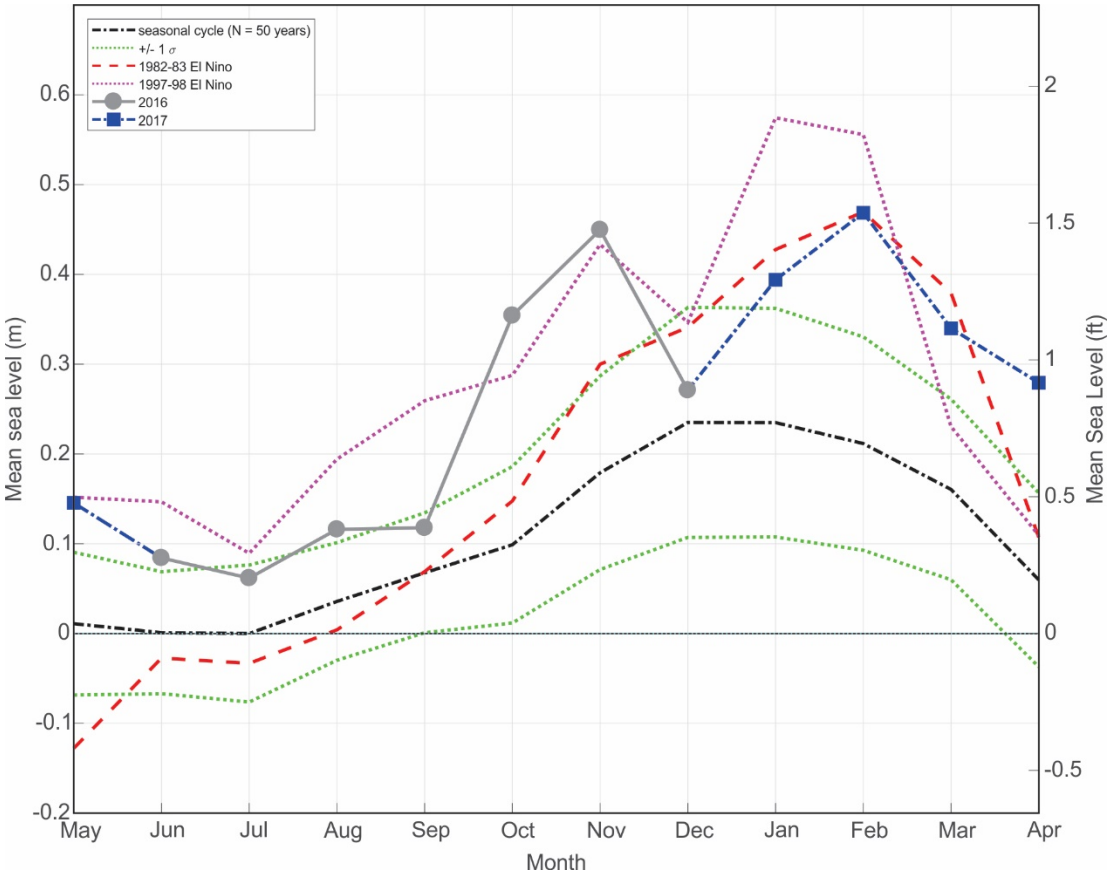

Aside from seasonal to interannual effects of climate events on ocean water levels, also of interest are the long-term trends associated with relative sea level changes on the Oregon coast. **Figure 4** presents results from an analysis of the Newport time series based on a separate analysis of the summer and winter tide levels (Komar and others, 2011). For our purposes "winter" is defined as the combined average tide level measured over a 3-month period around the peak of the seasonal maximum in winter water levels, typically the months of December through February. Similarly, "summer" water levels reflect the combined average tide level measured over a 3-month period around the seasonal minimum, typically the months of May through July when water levels also tend to be less variable. As observed previously in **Figure 3**, the winter tidal elevations are systematically displaced upward by about 25 cm (0.8 ft) above the summer elevations, with the difference between the two regression lines reflecting the seasonal change in ocean water levels from summer to winter. The winter patterns presented in **Figure 4** also emphasize the extremes associated with major El Niños. In contrast, the summer regression line is characterized by significantly less scatter in the residuals because it effectively excludes the influence of storms and El Niños that are dominant during the winter. By using this approach, it can be seen that the central Oregon coast is currently being transgressed by rising sea level at a rate of ~0.85 ± 0.77 mm/yr.

Figure 4. The trends of "winter" (red) and "summer" (blue) mean-sea levels (MSL) measured by the South Beach tide gauge. Results for the summer regression are statistically significant, while the estimated winter rate is not significant at the 95% confidence level (updated plot of Komar and others, 2011). RSL is relative sea level; RMSE is root mean square error.

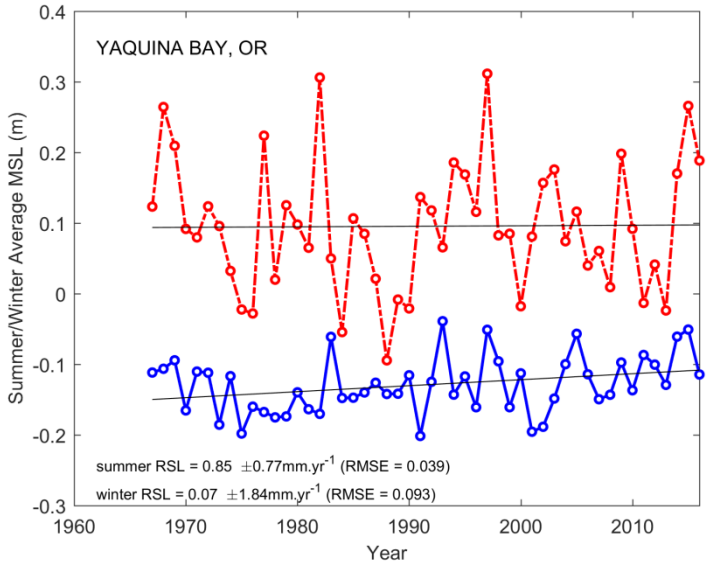

2.2.1 Projected Future Sea Levels for the Oregon Coast

In 2012 the National Research Council completed a major synthesis of the relative risks of sea level rise on the U.S. West Coast (NRC, 2012). The consensus from that report is that sea level has risen globally by on average 1.7 mm/yr, while rates derived from satellite altimetry indicate an increase in the rate of sea level rise to 3.28 mm/yr since 1993; regional estimates for the North Pacific indicate that mean sea level is increasing at a slightly lower rate of 2.7 mm/yr (Aviso, 2017). By combining knowledge of glacial isostatic rebound (the rate at which the earth responds to the removal of ice from the last glaciations), regional tectonics, and future temperature patterns, the NRC committee concluded that the mid-range forecast for mean sea level on the Oregon coast would increase by approximately 0.64 m (2.1 ft) by 2100 (NRC, 2012). **Table 1** presents a summary of the NRC findings for the Central Oregon coast, including the uncertainty range, which varies significantly depending on the modeled global temperature change projected for the future. As can be seen from the table, the upper projected range suggests an increase in regional sea level of 1.43 m (4.7 ft) by 2100.

Projections of future sea level assume that sea level is uniform year round. However, as noted previously, sea level on the Oregon coast exhibits a pronounced seasonal cycle of about 25 cm (0.8 ft) between summer and winter, increasing to as much as 60 cm (2 ft) in response to the development of a strong El Niño. Thus, when combined with projected future increases in regional sea level, it becomes apparent that the potential increase in sea level could be substantially greater depending on the time of year (**Figure 5**). For example, by 2100, sea level during an El Niño winter will have increased by a total of 2 m (6.6 ft); this change would raise the mean shoreline position by 2 m as well, as the shoreline shifts upward and landward as beaches respond to the change in mean water levels.

Table 1. Projected sea level rise for the central Oregon coast. Data from National Research Council (NRC, 2012).

	Project Sea Level Rise	
	(m)	(ft)
2030 Projection	0.06	0.2
Range	−0.03 to 0.21	−0.1 to 0.7
2050 Projection	0.18	0.6
Range	−0.02 to 0.49	−0.07 to 1.6
2100 Projection	0.64	2.1
Range	0.12 to 1.43	0.4 to 4.7

Figure 5. Projected future changes in regional mean sea levels (MSL) on the Oregon coast. Sea level change data from National Research Council (NRC, 2012). IPCC is the Intergovernmental Panel on Climate Change.

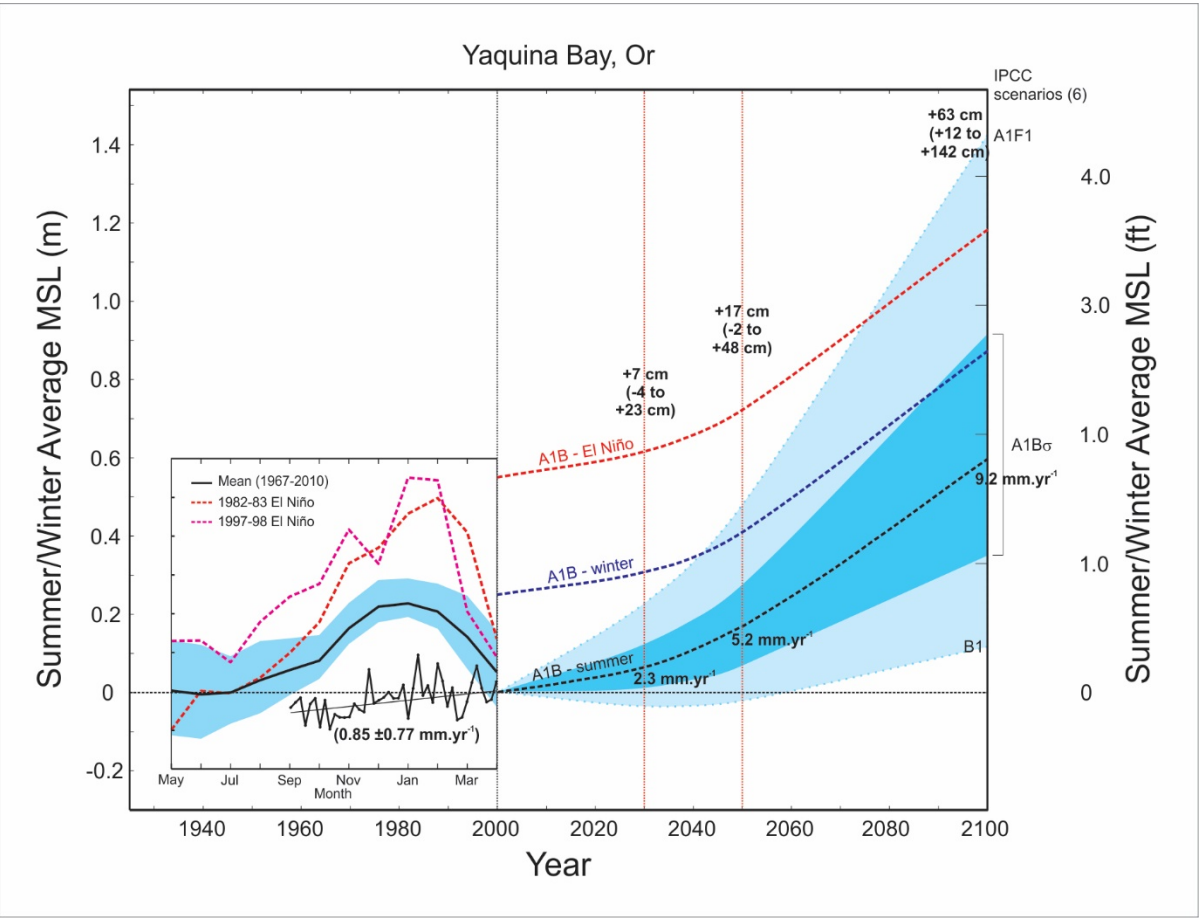

Finally, it is important to appreciate that the trends shown in **Figure 4** reflect relative sea level changes due to the fact that the Pacific Northwest (PNW) coast of Oregon and Washington is locally influenced by changes in the elevation of the land due to regional tectonics as well as by the global rise in sea level, with the net change being important to both coastal erosion and flood hazards.

Figure 6 presents a synthesis of both tectonic land elevation changes and sea level trends derived for multiple stations along the PNW coast (Komar and others, 2011), correlated against differential surveys of first-order National Geodetic Survey (NGS) benchmarks (e.g., Burgette and others, 2009) and GPS CORS (Continuously Operating Reference Station) stations. Results here indicate that in general the southern Oregon coast is an emergent coast with tectonic uplift of the land outpacing sea level rise. In contrast, the central to northern Oregon coast is slowly being transgressed by the rising sea exceeding the tectonic uplift of the land. In the far north in Clatsop County, the overall pattern suggests that this portion of the coast varies from slight submergence in the Cannon Beach littoral cell to emergent in the north along the Clatsop Plains. From NRC (2012) projected changes in regional mean sea level, it can be expected that areas presently classified as emergent (e.g., the southern Oregon coast) will become submergent as the rate of sea level rise surpasses tectonic uplift. Furthermore, erosion and flood hazards on the northern Oregon coast will almost certainly accelerate, increasing the risk to property.

Figure 6. Assessments of changes in relative sea level (RSL) based on tide-gauge records compared with benchmark (Burgette and others, 2009) and Global Positioning System (GPS) measurements of land-elevation changes, with their corresponding RSL rates obtained by adding the 2.28 mm/yr Pacific Northwest eustatic rise in sea level (Komar and others, 2011). Note: Station P407 is located near Cannon Beach and indicates approximately the northern extent of the current rate of sea level transgression (rise).

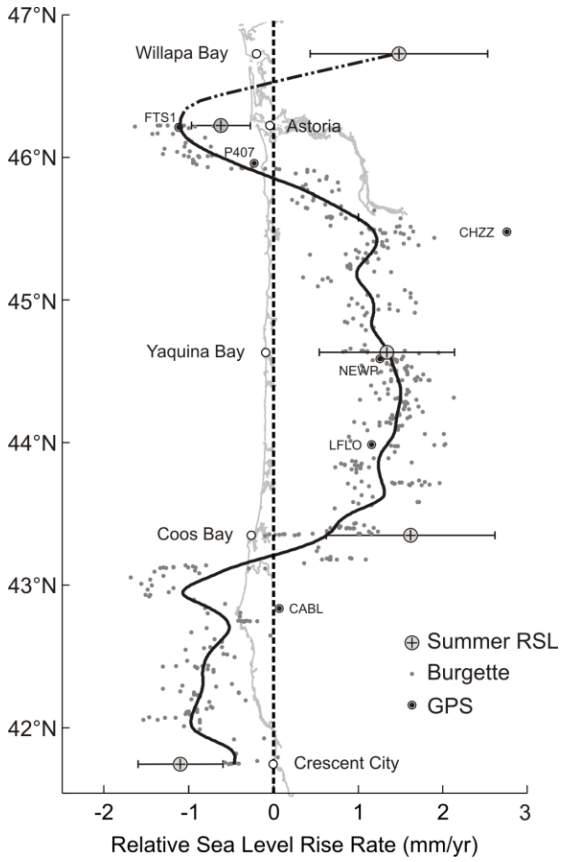

2.3 Waves

Along dune- and bluff-backed shorelines, waves are the major process affecting the shape and composition of beaches. Waves transport sand onshore (toward the beach), offshore (seaward to form nearshore bars, etc.), and along the beach (longshore transport). Short-term beach and shoreline variability (i.e., storm related changes) is directly dependent on the size of the waves that break along the coast, along with high ocean water levels and cell circulation patterns associated with rip currents. In contrast, long-term shoreline changes are dependent on additional factors including the balance in the beach sediment budget, changes in sea level, patterns of storminess, and regional tectonics.

The Oregon coast is exposed to one of the most extreme ocean wave climates in the world, due to coast's long fetches and the strength of the extratropical storms that develop and track across the North Pacific. These storms exhibit a pronounced seasonal cycle (**Figure 7**, solid blue line), producing the highest waves (mean significant wave height = 3.45 m [11.3 ft]) in the winter when strong storms commonly generate deepwater wave heights greater than 10 m (33 ft); the largest storms in the region generated waves in the range of 14 to 15 m (45 to 50 ft). Estimates of the 100-year or 1% extreme storm wave range from 14.4 m (47 ft) (Ruggiero and others, 2010) to 15.6 m (51 ft) (Allan and Komar, 2006). Conversely, summer months are dominated by considerably smaller wave heights (mean = 1.54 m [5.0 ft]), enabling beaches to rebuild and gain sand eroded during the preceding winter (**Figure 7**). Thus, there is a seasonal exchange in the volume of sand present between summer (accreted) and winter (eroded). When large waves are superimposed on high tides, they can reach much higher elevations at the back of the beach, contributing to significantly higher rates of coastal erosion and flood hazards. It is the combined effect of these processes that leads to erosion of coastal dunes and bluffs, causing them to retreat landward.

Figure 7. Seasonal variability of ocean waves measured offshore from Newport. Gray lines reflect all measurements since 1987. The seasonal cycle is depicted by the blue line for the means. The two magenta lines show the range ±1σ, accounting for 68% of the variability; the red line shows +2σ, accounting for 95% of the observations.

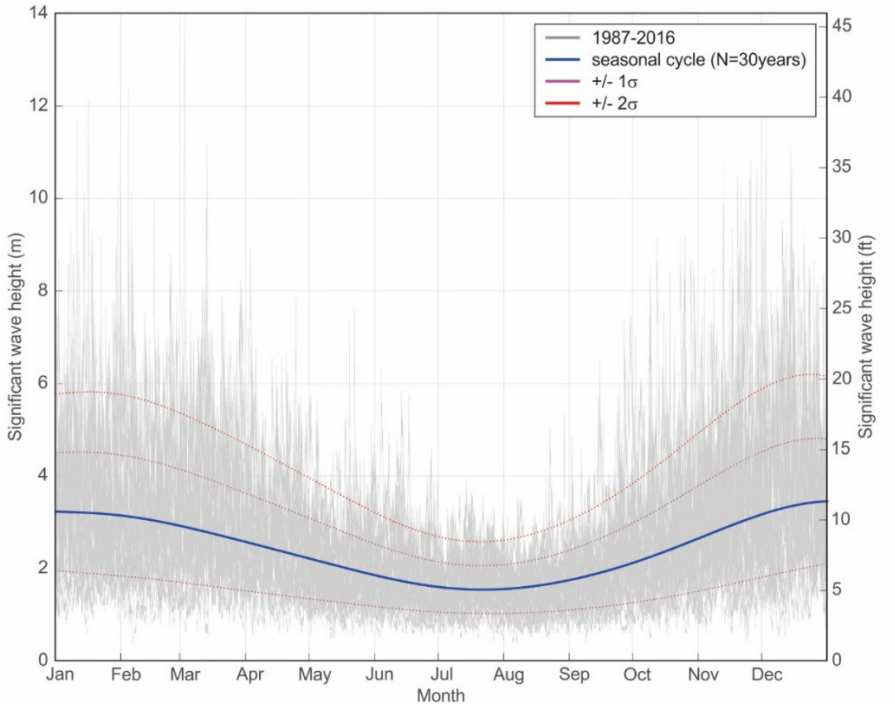

Besides seasonal variations in ocean waves characteristic of the PNW, several studies have identified a progressive long-term increase in winter wave heights affecting the North Pacific (Allan and Komar, 2000, 2006; Ruggiero and others, 2010). Over the long term, such changes could be expected to result in increased erosion and cause a significant change to the overall beach sediment budget (i.e., increased sand movement and potentially losses) and, ultimately, the instability of beaches (potentially increased erosion). While the progressive increase in wave heights is evident in records up through the mid-2000s, more recent analyses undertaken here point to a reversal in this pattern, with average winter wave heights falling significantly since mid-2000 (**Figure 8**). **Figure 8** presents "decadal scale" probability distributions for waves measured by buoy #46002 located 480 km west of Cape Blanco, Oregon, for the periods 1975–1990, 1991–2005, and the most recent period covering wave observations since 2006. We have used buoy #46002 as opposed to 46050 (shown in **Figure 7**), because #46002 has been in operation since the mid-1970s and hence has a much longer record. As can be seen from **Figure 8**A, there is a general shift in the wave height distribution during the middle "decade" toward generally larger wave heights. This shift is most pronounced for waves >1 m (3 ft) but smaller than ~6 m (20 ft). Of interest is the even greater reverse (leftward) shift (i.e., toward smaller waves) in the wave height distribution during the most recent "decadal" period. This recent change indicates that winter wave heights are on average lower than waves heights observed during the first decade (1975–1990).

The upper plot does not reveal anything meaningful with respect to the more extreme waves, because this type of plotting favors smaller, more frequent waves compared with larger, less frequent wave heights. **Figure 8**B addresses this problem by plotting the actual numbers of observations on a log scale to emphasize extreme but rare occurrences (Komar and Allan, 2007; Komar and others, 2009). As can be seen, the measured numbers of wave heights greater than 10 m are now readily apparent, although there are only a few occurrences of extreme storms resulting in such large wave heights per decade. Furthermore, the overall shift to smaller waves in the latest decade (2005–2017) is now even more obvious, extending up to even larger wave heights (~10 m [33 ft]). This decrease includes the left limb of the histograms (the lowest measured wave heights), indicating that there has been a decrease in the entire wave height distribution (i.e., small to large waves).

Figure 8C depicts the empirical cumulative distribution function (ECDF) for the three "decadal" periods. The ECDF also includes the 0.5 (median), 0.8, and 0.95 quantile values, which have shifted over time. For example, the median increased from 3 to 3.2 m (9.8 to 10.5 ft) in the first two decadal periods, and decreased to 2.8 m (9.2 ft) in the current period. Of further interest are the larger waves, which are most important for the erosion of beaches. Again, it can be seen that the wave heights increased during the first two periods (6 to 6.14 m [19.7 to 20.2 ft]), and have since decreased to ~5.5 m (18 ft).

Although not presented here, similar analyses were undertaken for summer wave conditions; these analyses showed the same overall pattern identified for the winter waves. From these findings, we can speculate that the overall shift to lower wave heights (and hence lower wave energy) observed in the most recent period is likely to have had a corresponding effect on coastal beach responses observed in the Cannon Beach cell. Certainly, the shift to generally lower wave heights since mid-2000 and the accompanying increase in volume of sand north of Ecola Creek is coincident. However, in reality, changes in ocean waves are but one of several processes that may be contributing to observed morphological changes. Furthermore, how long the current phase, characterized by lower wave heights, remains dominant is difficult to tell. Despite this, in time we can fully expect a return to conditions similar to the late 1990s, characterized by generally larger storms and bigger waves, resulting in a return to more erosional conditions. To that end, the management strategy for beaches within the Cannon Beach cell should account for such shifts in storminess.

Figure 8. Comparison of histograms (probability distributions) of wave heights for the periods 1975–1990, 1991–2005, and 2006-2017 documenting the shift in the wave climate to higher waves: *A)* standard probability distribution, *B)* number distribution plotted on a semi-log scale, and *C)* empirical cumulative distribution function. Wave data measured at buoy #46002, located 480 km west of Cape Blanco.

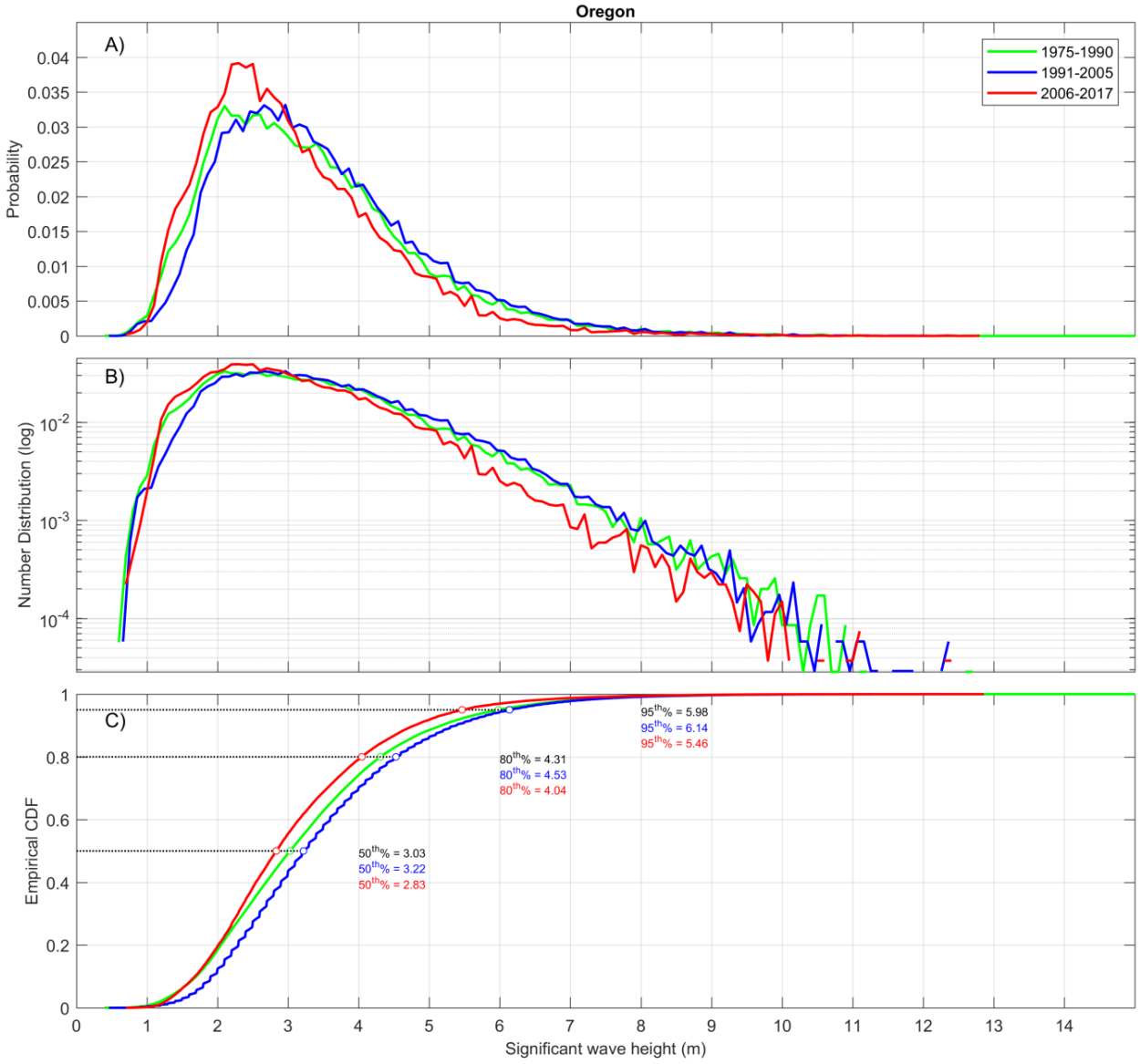

2.4 Sediment Transport

The culmination of the transformation of waves across the nearshore occurs in the surf zone where waves break and then swash up the beach face, carrying sediments or eroding the beach and dunes. Within the surf zone, sediments are entrained due to the turbulent action of wave breaking and are then transported by nearshore currents. Sediment transport in the littoral zone can be divided between the movement of sediment that is directed in primarily onshore-offshore directions (cross-shore sediment transport), and the movement of sediments parallel to the beach (longshore transport). The latter is especially significant when waves approach the shore at an angle, as they then generate stronger currents confined to a narrow zone landward of the breaker zone and can be responsible for the movement of substantial volumes of sediment along the shore.

On the Oregon coast the role of longshore currents is especially important due to a seasonal variation in the directions of wave approach between summer and winter (**Figure 9,** left). During a "normal year," summer waves, driven by north to northwesterly winds, approach the coast from the northwest, transporting significant volumes of sand alongshore toward the southern ends of the littoral cells, and also onshore, causing the dry part of the beach to build out, also resulting in aggradation of the dunes (Komar, 1998). In contrast, the arrival of large waves from the southwest during the winter results in a reversal in the net sediment transport, which is now directed toward the north, as well as cutting back the dry summer beach by moving the sand back offshore (**Figure 9,** left). Over several normal years there can be an equilibrium balance such that net sediment transport is close to zero (i.e., there is no net long-term buildup [accretion] of sediment at either end of the littoral cells). However, this pattern may be periodically disrupted by the occurrence of major El Niño events that can contribute to a significantly larger net northward movement of the sediment (**Figure 9,** right).

Figure 9. Patterns of sediment transport during *(left)* "normal" and *(right)* El Niño years (after Komar, 1986).

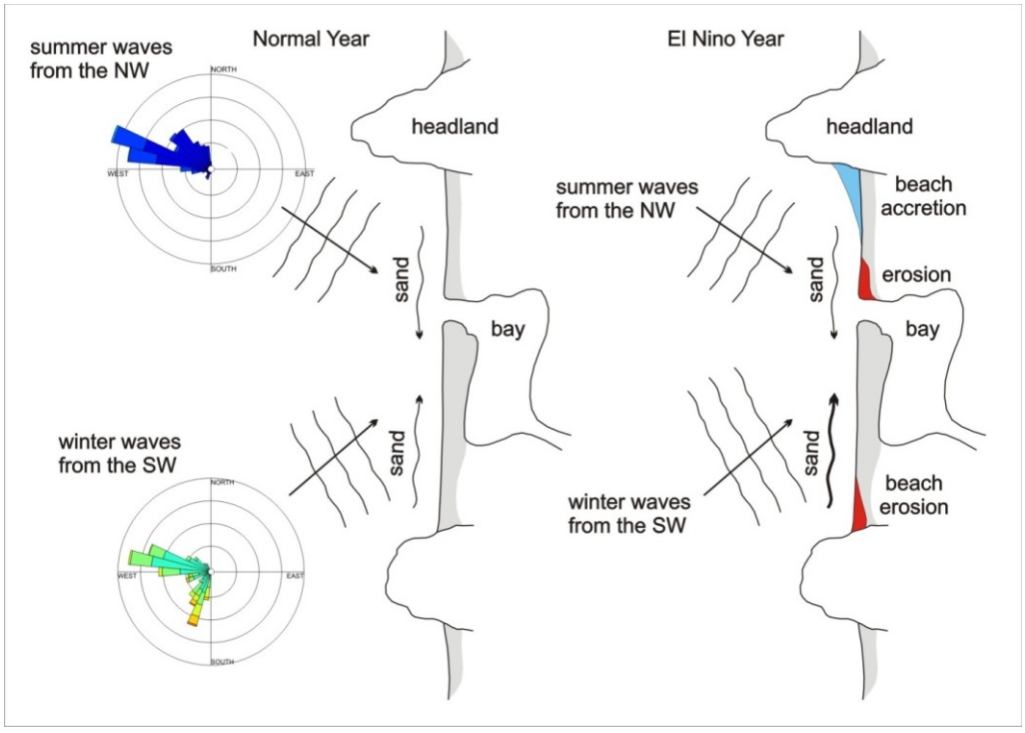

One of the earliest descriptions of the effect of El Niños on the displacement of sand in the pocket beach littoral cells on the Oregon coast is that of Komar (1986). In a study of the effects of the 1982-1983 El Niño in the Beverly Beach littoral cell north of Newport, Komar observed an unusually high northward drift of sand in the cell, with erosion immediately north of Yaquina Head and accretion in the north at Otter Rock. He attributed this response to a combination of factors, including the southward displacement of the storm systems, larger waves (and hence higher wave energy levels), and more acute wave approach angles from the southwest that contribute to the development of strong northward directed currents and sediment transport within the surf zone (Komar, 1986).

Peterson and others (1990) were also interested in the effects of the 1982-1983 El Niño, but focused their study on the quantification of the northward displacement of sand between Yachats and Seal Rock on the central Oregon coast. They estimated some 4.8×10^6 m^3 (6.3×10^6 yards^3) of sand were displaced during the event along ~7.4 km (4.6 mi) of shoreline (Peterson and others, 1990). However, their analyses were based on only a few discrete transects along with speculation of the thickness of the sand and beach slopes; their volume estimate seems large relative to more recent beach volume estimates (Allan and Hart, 2007, 2008) and changes observed elsewhere on the Oregon coast. Regardless, Peterson and others concluded that the sand shift was the result of a southward 10 to 15 degree latitude shift in the winter geostrophic wind, a proxy for the seasonal storm tracks. Essentially, this means that the predominant storm tracks are shifted to the south, so that the storm waves arrive at acute angles relative to the shore, contributing to a stronger than normal northward directed wave energy flux.

In anticipation of potentially large erosional responses expected for the 1997-1998 El Niño, airborne lidar was flown along the entire U.S. West Coast. These data were subsequently analyzed in two studies in the Netarts littoral cell to assess the patterns and volume of sand transported as a result of the El Niño (Revell and others, 2002; Allan and others, 2003). In general, Revell and others found that the sand largely moved northward in the Netarts cell, with the greatest amount of erosion occurring at the south end of the cell at Cape Lookout State Park. They noted that the seasonal cycle of cross-shore sediment and beach change was about 320,000 m^3 (418,500 yards^3) of sand, while about 70,000 m^3 (91,557 yards^3) of sand was shifted to the north. Allan and others (2003) identified that the mean shoreline position along the southern 3 km (1.9 mi) of the Netarts cell (i.e., seaward of Cape Lookout State Park) eroded by ~20 m (66 ft). More recently, Allan and others (2009) documented a rotational shift in the mean shoreline position in the Rockaway littoral cell located between Cape Meares and Neahkahnie Head in Tillamook County. Erosion was observed to occur at the south ends of all three subcells, while accretion dominated the northern ends of the cells (Allan and others, 2009). In total, some 1.4×10^6 m^3 (1.9×10^6 yards^3) of sand were removed from the cell due to enhanced wave erosion; some of this sand was removed to the north where it accumulated on Nehalem Spit. These data reflect the accumulated change that took place over two major winters, the 1997-1998 El Niño and 1998-1999 when a series of particularly extreme storms occurred (Allan and Komar, 2002b).

Recently, Anderson and Ruggiero (2015) analyzed a 60-year record of hindcast waves (1950–2010) in order to calculate the monthly alongshore wave energy flux (a measure of the sediment transport potential). They found that the average monthly climatology of all 63 years results in zero net annual longshore directed wave energy flux, consistent with the hypothesis of Komar (1998). However, when individual years are examined, such as years of major El Niños, the northerly directed energy flux was found to be an order of magnitude greater than the climatological mean (i.e., more sand was transported to the north). Conversely, major La Niña events produced a comparable response but in the opposite direction. Incorporating a one-line shoreline change model and the long-term wave energy flux, Anderson and Ruggiero (2015) identified decadal oscillations in the position of the shoreline between 1950 and 2010, which were

strongly coupled to the occurrence of the El Niño/La Niña climate phenomena, as well as the longer-term Pacific Decadal Oscillation (PDO).

The PDO operates over a cycle of 20 to 30 years and is strongly coupled with El Niño/La Niña events (**Figure 10**). When the PDO is in its positive phase (characterized by generally warmer sea surface temperatures near the coast), there is a significant increase in the incidence of El Niños. Conversely, when the PDO is in its negative phase (characterized by generally cooler sea surface temperatures), there is a higher incidence of La Niñas. As an example, the period from the mid-1940s to the mid-1970s reflected a cool PDO, dominated by La Niñas (**Figure 10**). The PDO switched to its warmer phase in the mid-1970s, characterized by abundant El Niños, including two of the strongest events on record. As a result of this change, we can speculate that the increased erosion observed throughout the 1980s and 1990s, coupled with a more dominant and persistent northward directed wave energy flux, has been instrumental in causing the counterclockwise rotation (characterized by increased erosion in the south and accretion in the north) observed in a number of beach settings along the Oregon coast. This pattern is consistent with changes observed in the Cannon Beach cell, particularly the recent aggradation occurring north of Ecola Creek.

Figure 10. The Pacific Decadal Oscillation (PDO) and the Multivariate El Niño (MEI) Index; red indicates positive "warm" phase, blue indicates negative "cool" phase. Gray shading indicates the "normal" range of variability. Dashed lines reflect periods when the PDO switched between cool/warm phases.

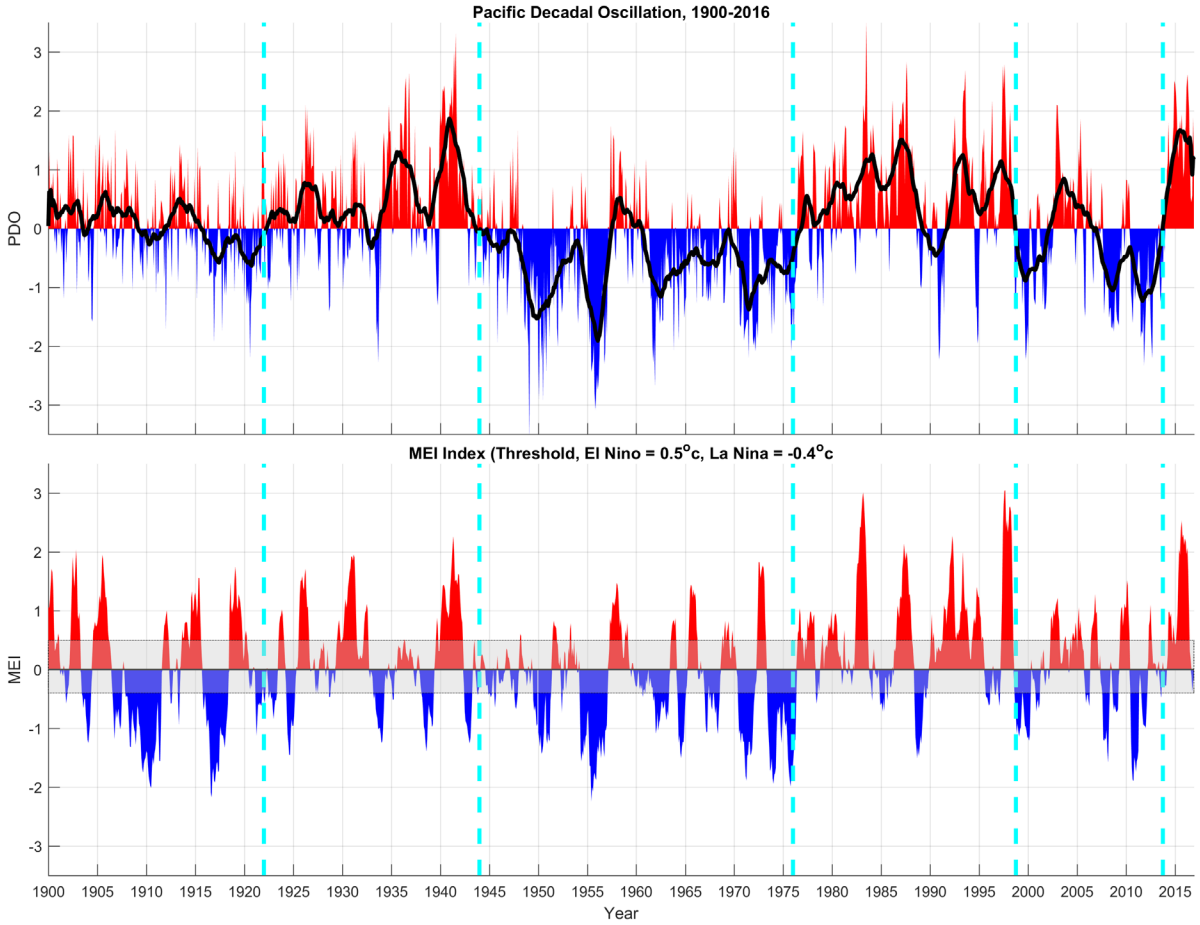

Despite the brief cooling phase beginning in 1998 (**Figure 10**) that persisted up until late 2014 (dominated by more La Niña conditions), accompanied by a general decrease in wave energy, we have yet to see any evidence of a reversal in the process with sand returning to the south. Furthermore, the current pattern of net northward transport is likely to persist for some time yet, until we see a return to a more dominant northwesterly wind and wave pattern, which could help to drive sand back to the south. In addition, new research (Bond and others, 2015; Hartmann, 2015) suggests that the current PDO phase may be ending, ushering in a return to a warm phase dominated by El Niños. This probably means a return to conditions characteristic of the previous warm phase of the 1980s and 1990s with additional net sand transport to the north; for example, the most recent major El Niño in 2015-2016 is possibly evidence of that change (**Figure 10**).

In summary, these findings suggest that the current phase of sand accumulation north of Ecola Creek is similar to what has been observed elsewhere on the Oregon coast and that it is strongly coupled to the current phase of waves arriving from a predominantly southwest direction, especially during the major El Niños.

2.5 Oregon Tsunami Hazards

Considerable geologic data from estuaries and coastal lakes along the Cascadia subduction zone provides evidence for episodic occurrences of abrupt coastal subsidence at times of major earthquakes, immediately followed by significant ocean flooding associated with major tsunamis that swept across the ocean beaches and also traveled well inland through the bays and estuaries. Coastal paleoseismic records document the impacts of as many as 13 major subduction zone earthquakes and associated tsunamis over the past ~7,000 years (Witter and others, 2003, 2010; Kelsey and others, 2005), while recent studies of turbidite records within sediment cores collected in deep water at the heads of Cascadia submarine canyons provide evidence for at least 46 distinct tsunami events over the past ~10,200 years (Goldfinger and others, 2003, 2012, 2017; Goldfinger, 2009). The length of time between these events varies from as short as 100 years to as long as 1,200 years, with the average recurrence interval for major Cascadia earthquakes (magnitude >[Mw] 9) estimated to be ~530 years (Witter and others, 2010). Recently, Goldfinger and others (2017) provided a revised assessment for the central to northern Oregon coast, which was found to have a mean recurrence time of ~340 years. Goldfinger and others estimate the conditional probability of the next Cascadia event taking place in the next 50 years is 16 to 22%.

The most recent Cascadia subduction zone earthquake occurred on January 26, 1700 (Satake and others, 1996; Atwater and others, 2005) and, from the size of the tsunami documented along the coast of Japan, is estimated to have been magnitude (Mw) 9 or greater. This event probably ruptured the full length (~1,200 km) of the subduction zone, based on correlations between tsunami deposits identified at multiple sites along the length of the PNW coast. Analyses of tsunami paleo-deposits in the Ecola Creek valley at Cannon Beach indicate that the AD 1700 event inundated the creek valley to a distance of at least 1.45 km (0.9 mi) (Witter, 2008). To the north on the Washington coast, there is evidence indicating that the 1700 event overtopped the Long Beach Peninsula (Atwater and others, 1995).

There is now increasing recognition that great earthquakes do not necessarily result in a complete rupture of the Cascadia subduction zone (i.e., rupture along the full 1,200-km fault zone); paleo-records show partial ruptures of the plate boundary have occurred due to smaller earthquakes with magnitudes (Mw) < 9 (Witter and others, 2003; Kelsey and others, 2005). These partial-segment ruptures appear to occur more frequently on the southern Oregon coast, as determined from paleotsunami studies (stratigraphic coring, radiocarbon dating, and marine diatom analyses) undertaken at several locations on the

southern Oregon coast, including Bradley Lake located just south of Bandon, the Sixes River, and the Coquille estuary. According to Kelsey and others (2005), initial estimates of the recurrence intervals of Bradley Lake tsunami incursion is typically shorter (~380 to 400 years) than the average recurrence intervals inferred for great earthquakes (~530 years). Furthermore, they have documented from those records that local tsunamis from Cascadia earthquakes occur in clusters (~250 to 400 years) followed by gaps of 700 to 1,300 years, with the highest tsunamis associated with earthquakes occurring at the beginning and end of a cluster.

Recent analyses of turbidite records (Goldfinger, 2009; Goldfinger and others, 2012, 2017) suggest that of the 46 events in the geologic past:

- 19 events were probably associated with a rupture of the full Cascadia subduction zone, characterized by a magnitude (Mw) ~8.5–9.1 or greater earthquake;
- 3 events reflected a near-full rupture (~90%) of the length of the subduction zone, characterized by an estimated earthquake magnitude (Mw) of ~8.5–8.7;
- 8 events were associated with a partial rupture (~75%) of the length of the subduction zone (Cape Mendocino to Neah Bay), characterized by an estimated earthquake magnitude (Mw) of ~8–8.6;
- 2 events reflected a partial rupture (~50%) of the length of the subduction zone (Cape Mendocino to Heceta Bank), characterized by an estimated earthquake magnitude (Mw) of ~8.4;
- 9 events reflected a partial rupture (~25%) of the length of the subduction zone (Cape Mendocino to Cape Blanco), with an estimated earthquake magnitude (Mw) of ~7.4–8.2; and,
- 4 events reflected a partial rupture (~15%) of the length of the subduction zone (Cape Mendocino to Smith River), with an estimated earthquake magnitude (Mw) of ~7.6–7.9.

These last 15 shorter ruptures are concentrated in the southern part of the margin and have estimated recurrence intervals of ~220 to 320 years. (The 46th event occurred off the coast of Washington and is not characterized here.)

Aside from local tsunamis associated with the Cascadia subduction zone, the Oregon coast is susceptible to impacts from tsunamis generated by distant events, particularly along the coast of Japan, along the Aleutian Island chain, and from the Gulf of Alaska. The most recent distant tsunami event occurred on March 11, 2011, when a magnitude (Mw) 9.0 earthquake occurred 129 km (80 miles) offshore from the coast of Sendai, northeast Honshu, Japan (Allan and others, 2012). This earthquake triggered a catastrophic tsunami that within minutes inundated the northeast coast of Japan, sweeping far inland; most recent reports indicate 15,894 dead and another 2,562 missing. Measurements derived from a tide gauge on the impacted shore (Ayukawa, Ishinomaki, Miyagi Prefecture) recorded a tsunami amplitude of 7.6 m before the gauge was destroyed by the initial tsunami wave (Yamamoto, 2011), while post-tsunami surveys indicated tsunami water levels within the inundation zone reached as high as 19.5 m (Mori and others, 2011). The tsunami also propagated eastward across the Pacific Ocean, impacting coastal communities in Hawaii and along the west coast of the continental United States—Washington, Oregon, and California. The tsunami arrived 9 hours 37 minutes after the earthquake shaking began, reaching Port Orford on the southern Oregon coast at 7:23 am (Pacific Standard Time) and Garibaldi in Tillamook County approximately 18 minutes later (Allan and others, 2012). Luckily, the tsunami wave arrival coincided with low tide, minimizing its potential impact on the Oregon coast.

Damage in Oregon, Washington, and northern California from the tsunami was almost entirely confined to harbors, including Depoe Bay, Coos Bay, and Brookings in Oregon, and in Crescent City, California, having been moderated by the arrival of the tsunami's highest waves during a relatively low tide (Allan

and others, 2012). At Crescent City, an open-coast breakwater, the to-and-fro surge of the water associated with the tsunami waves overturned and sank 15 vessels and damaged 47, while several boats were swept offshore. Flood damage also occurred during the early hours of March 12; for example, an RV park near the mouth of Elk Creek was flooded when a 1.05 m (3.4 ft) tsunami wave arrived, coinciding with high tide. The total damage to the Crescent City harbor and from the effects of the flooding has been placed at $12.5 million. At Brookings on the southern Oregon coast, 12 fishing vessels put to sea at about 6 am, prior to the arrival of the tsunami waves. However, the Hilda, a 220-ton fishing boat and the largest in the harbor, broke loose under the forces of the wave-induced currents, washing around the harbor and smashing into and sinking several other boats. Much of the commercial part of the harbor and about one third of the sports basin were destroyed; the total damage has been estimated at about $10 million.

Prior to the Tōhoku tsunami, the previous most significant distant tsunami occurred on March 27, 1964, when a magnitude (Mw) 9.2 earthquake occurred near Prince William Sound in Alaska. This earthquake generated a catastrophic local tsunami in Alaska, while the effects of the tsunami were also felt around the Pacific Basin. The tsunami caused significant damage to infrastructure in the coastal communities of Seaside and Cannon Beach and killed four people camping along Beverly Beach in Lincoln County. At Cannon Beach the tsunami arrived ~11:34 pm, coinciding with a rising tide (Witter, 2008), while the runup elevations were found to range from 6.7 to 7.9 m (22 to 26 ft, relative to mean lower low water [MLLW[1]]) in Seaside, Oregon (Horning, 2006). Witter noted that runup elevations did not exceed 6.1 m (20 ft) as there were no reports to suggest that the tsunami wave overtopped the barrier spit that fronts Cannon Beach. Newspaper reports of water depths at two sites in Cannon Beach suggest minimum water level elevations of ~6.1 m (20 ft), with flooding having occurred in two city blocks in downtown Cannon Beach (Witter, 2008). The tsunami resulted in damage of ~$50,000 to Cannon Beach city infrastructure and $180,000 to private property—over $0.37 million and $1.32 million in 2017 dollars. The most dramatic impact was the destruction of the primary bridge across Ecola Creek; the bridge was carried up the creek some 275 m (900 ft).

In 2009 the Oregon Department of Geology and Mineral Industries (DOGAMI) initiated a multi-year study to accelerate remapping of the Oregon coast for tsunami inundation using state of the art computer modeling and laser-based terrain mapping (lidar). The outcome of this effort was the creation of new and more accurate tsunami evacuation maps for the entire length of the coast. DOGAMI, in collaboration with researchers (Zhang and Baptista) at the Oregon Health and Science University (OHSU), Oregon State University (Goldfinger), and the Geological Survey of Canada (Wang), developed a new approach to produce a suite of next-generation tsunami hazard maps for Oregon (Priest and others, 2010; Witter and others, 2010). Modeling tsunami inundation on the southern Oregon coast began late in 2009 and consisted of a range of scenarios, including 15 Cascadia events and two distant earthquake source events (e.g., 1964 Prince William Sound earthquake magnitude [Mw] 9.2 earthquake [Witter, 2008]). The last of the suite of new evacuation maps (TIM series) was released in 2013; the maps are also available in an online tsunami hazard portal (http://nvs.nanoos.org/TsunamiEvac).

Associated with great Cascadia earthquakes is a near-instantaneous lowering (subsidence) of the coast by ~0.4 m (1.3 ft) to as much as 3 m (9.8 ft) (Witter and others, 2003). This process equates to raising sea level by the same amount along the entire Pacific Northwest coastline. Following a Cascadia earthquake, coastal erosion is expected to accelerate everywhere as beaches and shorelines adjust to a new equilibrium condition that, over time, would likely decrease asymptotically (Komar and others, 1991). On the southern Oregon coast, Komar and others have suggested that the extensive development of sea stacks

[1] At Cannon Beach, MLLW is located approximately 0.22 m (0.72 ft) below the North American Vertical Datum of 1988 (NAVD88).

offshore from Bandon may be evidence for that erosion response following the last major subduction zone earthquake in 1700. Over the past century, the erosion appears to have stabilized, as there is little evidence for any progressive erosion trend. This suggests that the south coast of Oregon is now being uplifted (estimated to be ~0.6 to 1.1 m) due to the Cascadia subduction zone having become locked again, such that strain is now building toward the next major earthquake. With the release of that energy and land subsidence, cliff erosion along the Bandon shore (and elsewhere on the Oregon coast) would be expected to begin again.

3.0 OREGON COAST DUNES – PROCESS AND MORPHOLOGIES

Coastal sand dunes are large geomorphic aggradational features located at the back of the beach that form when sand is blown inland by wind and becomes trapped among the beach wrack and vegetation (Woodhouse, 1978). Where vegetation is absent or sparsely present, the dunes are able to drift in response to the prevailing wind direction. In some situations, the drifting dune sand can become a nuisance as the sand accumulates in and around coastal properties, while in others the migrating dune may engulf buildings contributing to their eventual destruction (Komar, 1997). Consequently, maintaining a stable, vegetated dune system is essential where community assets worthy of protection have been built either on or immediately landward of the dune. In addition, stable dunes form an essential component of the coastal beach sediment budget and a primary control on the backshore ecosystem, providing several important ecosystem services that include (Elko and others, 2016):

- Habitat for endangered species;
- Sites of high tourism value;
- Groundwater recharge zones; and,
- Protection of coastal infrastructure and properties from wave erosion and storm surge flooding.

In the case of the latter, dunes serve a critical yet flexible barrier to wave runup and ultimately wave overtopping, providing a natural stockpile of sand, which is periodically drawn on during times of storm wave attack. The eroded sand is typically removed offshore to form nearshore bars or is transported elsewhere within the physical system (see Section **2.0** on sediment transport). With the transition to lower wave heights in the summer (as occurs on the Oregon coast), the eroded sand is returned to the subaerial beach through a combination of wave and aeolian (wind) processes, where the sand once again accumulates at the back of the beach, allowing the dunes to rebuild. As a result, the formation of dunes is dependent on three simple requirements:

- A sufficient supply of sediment;
- A prevailing wind. Wind speed is important because the wind needs to be strong enough to entrain and mobilize sediments across the beach and provide subsequent landward transport to enable dune formation. The predominant wind direction is also important as it governs the types of dunes that could develop; and,
- Obstacles to trap the sand such as woody debris, vegetation, and micro-topography. To this can be added engineering solutions such as the use of sand fencing.

The erosion of dunes is controlled entirely by the frequency and magnitudes of storms, combined with high ocean water levels that enable waves to reach higher elevations at the back of the beach. Once dunes are eroded, their recovery can take years to decades, with the rate of recovery dependent on the supply of sediment from the beach system. Hence, littoral systems that have a sufficiently large and positive beach

sediment budgets are more likely to recover quickly, compared with littoral systems that have lower sediment inputs or transport. Dune recovery may be accelerated through a variety of approaches including the establishment of dune fences, which encourage sand trapping and enable dune growth within a couple of years (Nordstrom and others, 2007), as well as through the planting of vegetation (Simm and others, 1996; Elko and others, 2016). Where sediment supply is sufficient, dunes provide more effective coastal protection and at a significantly lower cost when compared with coastal engineering structures such as a seawall or riprap revetment (Woodhouse, 1978).

Dunes are thus maintained naturally through the interaction of littoral processes (i.e., sand that is delivered to the beach by waves), aeolian processes (the transportation of sand by wind), and important ecological processes (sand trapping and vertical accretion by plants). Dunes may also be the product of engineering through the establishment of artificial dunes (e.g., at Cape Lookout State Park [Allan and Komar, 2004]). Regardless of how dunes are formed, a challenge facing coastal communities fronted by dunes is finding a balance between:

- Maintaining the ecosystem services offered by dunes;
- Preserving the height and volume of dunes in order to provide protection to properties located on or behind the dune; and,
- Enabling residents to maintain their views of the ocean.

Due to our uncertainty in the processes that enable and contribute toward dune formation, including their periodic destruction, "managing a dynamic dune system at a range of spatial and temporal scales requries an adaptive management approach that is based on sound scientific knowledge of coastal dune processes and grounded by systematic, accurate monitoring" (Elko and others, 2016, p. 2). Such an approach is even more critical as one considers potential longer-term climate change impacts, which are likely to tip the current equilibrium balance toward a state of sand deficit that could see increased erosion of beaches and dunes in the near future. Understanding these trade-offs is key toward developing a sound dune management approach for communities such as Cannon Beach.

3.1 Oregon Dune Morphology

The shape and size of dunes on the Oregon coast are strongly dependent on the supply of sand to the back of the beach and the presence of vegetation (OCZMA, 1979; Allan, 2004; Hacker and others, 2012; Zarnetske and others, 2012, 2015), especially *Ammophila arenaria* (European beach grass), *Ammophila breviligulata* (a non-native American dune grass introduced from the U.S. East Coast), and *Elymus mollis*, a dune grass native to the PNW coast. Without question, the introduction of European beach grass (*A. arenaria*) early in the 1900s, first in the Coos Bay area in 1910 and on the Clatsop Plains in 1935 (OCZMA, 1979), resulted in the most profound changes to the morphology and sizes of dunes on the Oregon coast (Cooper, 1958). According to Hacker and others (2012), *A. breviligulata* was introduced into the Warrenton area in 1935. However, although *A. breviligulata* can be found in select areas on the Oregon coast (e.g., South Beach State Park and on the Clatsop Plains), it is much more prevalent on the Washington coast.

Prior to their introduction, much of the Oregon coast was dominated by broad low-lying dunes, generally devoid of beach grass. The dunes were unconstrained and shifted about in response to predominant wind directions (OCZMA, 1979). However, with the introduction of dune grass during last century, and particularly in the 1950s to 1970s when dune grass plantings accelerated, the dunes stabilized rapidly and their form began to change. Once introduced, the grass rapidly spread along the entire PNW coast, eventually producing the densely vegetated continuous foredune ridges characteristic of the coast today.

For example, Lund (1973 *in* OCZMA, 1979) noted that areas of open active sand on the south-central Oregon coast narrowed by almost 50% within 30 years. This is borne out in our own examination of historical aerial photos collected in 1939 and again in 1967 for the coast of Oregon.

In Cannon Beach, there is no evidence of dune grass plantings having occurred prior to the 1950s (**Figure 11**). As shown in **Figure 11**, early 1939 photos of the area clearly show a broad dune devoid of any vegetation, with the 1939 shoreline located about where the existing vegetation line is located today (compare with the cover photo of this report, which was taken in 2015). Rosenfeld (1997) noted that European beach grass (*A. arenaria*) was probably introduced sometime around the 1950s, with major plantings occurring during the 1960s at Chapman Point. These initial efforts effectively stabilized the dunes and by 1967 had greatly increased the retention of sand throughout the area (**Figure 11**). Today, those initial dune plantings have resulted in the formation of a conditionally stable dune that fronts homes built on older Holocene stabilized dune sand. Seaward of the stable dunes is a new area of active dune formation that is currently taking place and is the impetus for this study.

Dune management activities, implemented by the Breaker's Point Homeowners Association, have taken place along the south end of Chapman Point since 1979. These activities commenced with dune grass plantings to help further stabilize sand blowing inland toward the homes. According to Rosenfeld (1997), a major storm in 1981 resulted in a considerable amount of sand being deposited over the entire condominium complex, including roofs of two-story residences. The Association responded by lowering the dune crest and replanting badly damaged areas. As a result of the 1982-1983 El Niño, large volumes of sand began to accumulate along Chapman Point, requiring more aggressive dune management strategies between 1983 and 1990 in order to reduce sand encroachment around homes. These measures included continuous sand fencing during the winter months, when sand is highly mobile, coupled with raking to expose the beach grass, as well as the application of fertilizer (Rosenfeld, 1997).

Figure 11. Aerial photos flown in 1939 and 1967 as well as lidar collected in 2009 depict historical shoreline changes, dune stabilization, and accompanying morphological changes in the beach and dunes at Chapman Point, Cannon Beach. Note the wide expanse of dune sand that characterizes the area in 1939. The image on the right is of a 2009 lidar DEM and shows the degree of beach progradation and sand accumulation that has taken place over the past 70 years.

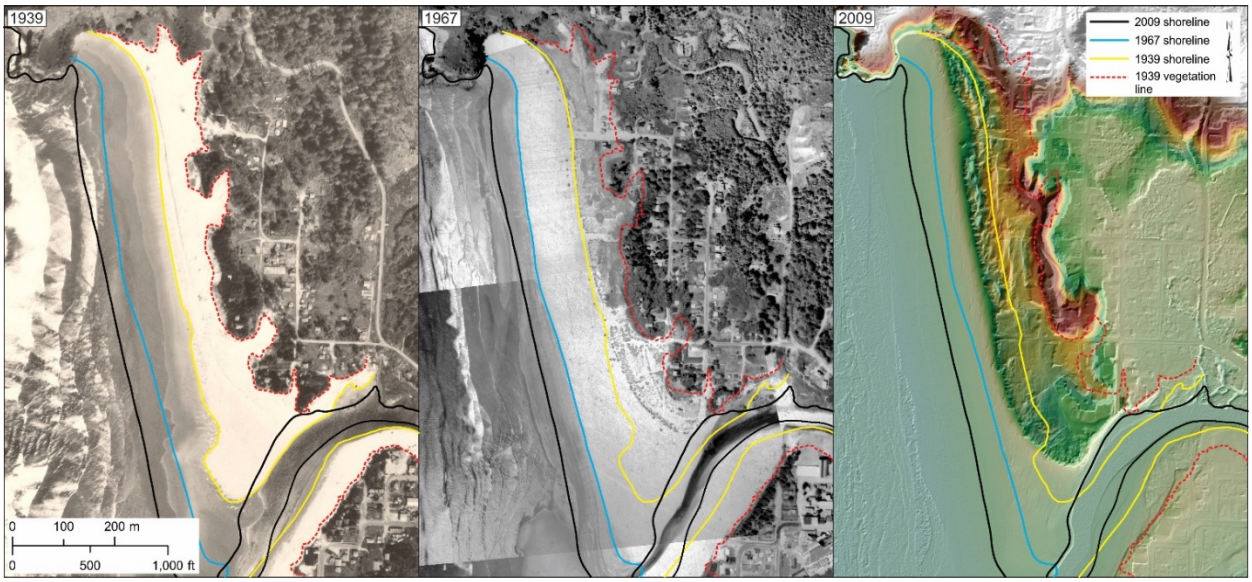

A number of studies have been undertaken to assess the relative roles of *A. arenaria*, *A. breviligulata*, and *E. mollis* in dune building (Hacker and others, 2012; Zarnetske and others, 2012). Hacker and others (2012) discussed the distribution of the dune grass species along the PNW coast of Oregon and Washington, noting that the non-native American beach grass (*A. breviligulata*) has increased its dominance over the European dune grass (*A. arenaria*). This is especially the case on the Washington coast. Zarnetske and others (2012) derived a conceptual model (**Figure 12**) showing the biophysical feedback between vegetation and sediment supply. Furthermore, Zarnetske and others (2012), by undertaking detailed experiments of the grasses in a wind tunnel, provided the most comprehensive assessment to date of the performance of the three dune grasses to trap sand. Their study revealed the following results:

- The dense vertical growth habit of European beach grass (*A. arenaria*) allows it to capture sand more efficiently, produce more vertical tillers (the above-ground branch of a plant), and builds taller, narrower dunes (**Figure 12**).

Figure 12. *A)* Conceptual model showing the relationship between sediment supply and vegetation that directly affects the geomorphology of dunes. *B)* Biophysical feedback associated with three dune grass species influence the dune morphology (Zarnetske and others, 2012).

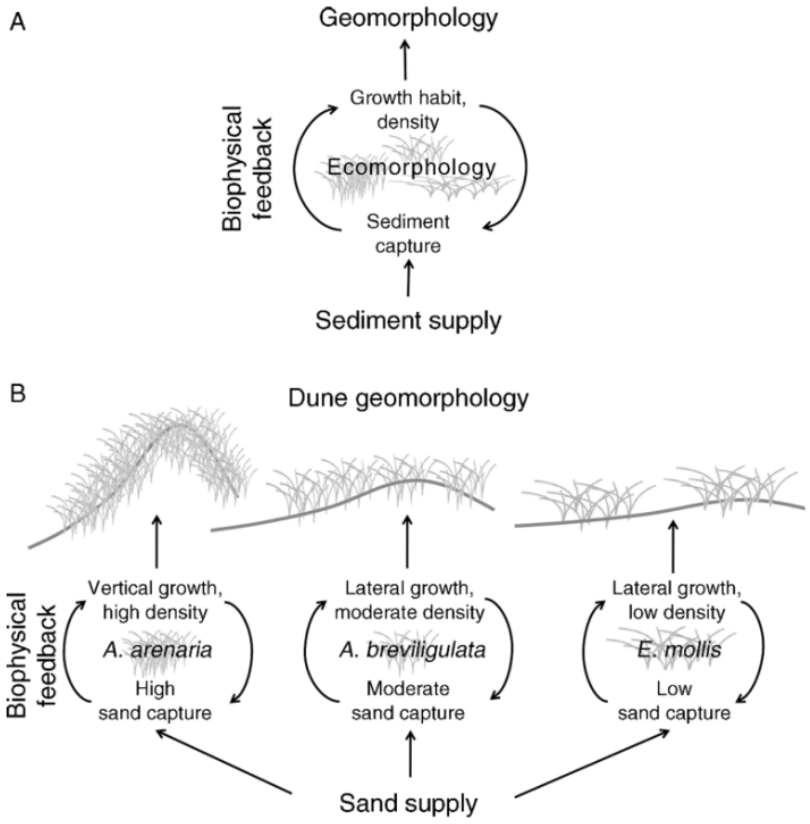

- The non-native American dune grass (*A. breviligulata*) has a more lateral growth habit and is generally less dense when compared with *A. arenaria* and, as a result, is more suited for building lower, wider dunes (**Figure 12**).
- *E. mollis* (the native Oregon dune grass) was found to have the highest sand capture efficiency of the three species due to its low spreading habit and much wider tiller. Because of the width of its tiller, each branch has a significantly larger surface area, enabling more sand to be trapped. However, because its tiller density is lower when compared with *A. arenaria* and *A. breviligulata*, *E. mollis* is not able to trap as much sand and, accordingly, tends to produce broad dunes with lower heights (**Figure 12**). Although there are few natural examples where *E. mollis* is prevalent on the Oregon coast, examples of its success in building broad sand dunes have been identified elsewhere. For example, *E. mollis* was introduced in the Chiba Prefecture located on the central east coast of Japan in the late 1960s to stabilize and build foredunes along its coast (Suzuki and Numata, 1982). According to Suzuki and Numata, the zone containing *E. mollis* advanced seaward at a rate of 5 m/year (16 ft/year). This was almost entirely due to the elongation of new rhizomes, with the dune grass preferring to grow in areas where sand was rapidly accumulating. Furthermore, Suzuki and Numata (1982) observed that *E. mollis* performed best on the seaward side of the foredune. Their results suggest that any plantings of *E. mollis* on the Oregon coast may best be concentrated on the seaward face of the dunes.
- Despite the broader tiller morphology of *E. mollis*, higher vegetation (tiller) density significantly increases sediment capture and hence deposition. As a result, both the European and non-native American dune grass significantly outperform the native beach grass;
- In environments subject to high sediment deposition rates, European beach grass (*A. arenaria*) has been found to perform extremely well due to its aggressive vertical tiller growth habit, which allows it to keep pace with the supply of sediment and leads to the building of taller dunes. Conversely, as sand supply increases, *A. breviligulata* sends out lateral tillers, which increases the amount of sand being trapped on the front face of the foredune, resulting in a broader, lower dune.
- Zarnetske and others (2012) noted that although there are no *E. mollis* dominant foredunes, their results suggest that it would produce dunes that are broadly similar to *A. breviligulata*.
- Finally, Zarnetske and others (2015) expressed some concern about using *A. breviligulata* in dune management areas, in part due to the fact that it produces lower foredunes, and hence could result in dunes that would potentially be subject to periodic overtopping under high wave energy regimes (e.g., under a future climate regime). However, providing the dunes are allowed to build seaward and their heights are maintained at a high enough elevation to withstand periodic wave runup and overtopping, such concerns are probably unwarranted at least in the immediate future. This is because the effects of the storms would be concentrated well seaward of the existing line of properties. All of this assumes that coastal managers refrain from allowing any further development out on the developing dune.

3.2 Wind Processes on the Oregon Coast

Besides wave processes that redistribute sand within Oregon's pocket beach littoral cells, important to the development of dunes is the prevailing wind climate experienced along the coast (Cooper, 1958; Komar, 1976; Hunter and Richmond, 1983). Similar to PNW ocean waves, the regional wind climatology is typified by a strong seasonal pattern that is a function of the atmospheric climatology across the North Pacific. During the summer, the regional mean atmospheric circulation in the North Pacific is dominated by a subtropical area of high pressure termed the North Pacific High (Favre and Gershunov, 2006), which results in the development of fine weather and mild north to northwesterly winds. In winter, the North Pacific High is shifted southward toward the equator and is replaced by the Aleutian Low, an area of significantly lower atmospheric pressures that develops across the far North Pacific. This system favors the development and propagation of strong storms (Gyakum and others, 1989), which result in increased precipitation and strong west to southwesterly winds that directly affects the ocean and atmospheric climatology of the Pacific Northwest.

Figure 13A is a seasonal wind rose plot derived for the Newport Oregon C-Man climate station[2], operated by the National Data Buoy Center of NOAA. The Newport climate station is an ideal site for assessing the predominant wind patterns due to its location at the mouth of Yaquina Bay, away from any localized topographic influences (i.e., it is open to winds arriving from any direction). As can be seen from **Figure 13**A, the general wind climatology is one of prevailing winds out of the northwest during spring and summer, and winds from the southwest in winter. Of interest also is the presence of light easterly winds that form in the fall and winter. These winds may reflect cold air drainage down the Yaquina valley and are of such low velocity that they are unlikely to transport much sand, most of which would be directed toward the beach and ocean. Figure 13A also identifies the entrainment thresholds required to mobilize sand under both dry (~5 m/s) and wet (~15 m/s) conditions (Bauer and others, 1990; Shoreland Solutions 1998a). These are generalized thresholds and will vary depending on site-specific factors. Further discussion of sand transport potential by Oregon coastal winds is provided below.

[2] Consists of hourly wind speed and direction measurements undertaken from January 10, 1985 – April 7, 2017.

Figure 13. ***A)*** **Wind roses showing the seasonal distributions of wind speeds by direction for the Newport[3], Oregon C-Man climate station operated by the National Data Buoy Center (NDBC). The arms point in the** ***direction from which the winds are blowing*****;** ***B)*** **Seasonal wind speed empirical cumulative distribution function (ECDF); and** ***C)*** **diurnal pattern of mean wind speeds. Data reflect all hourly measured values spanning the period 1985 through March 2017.**

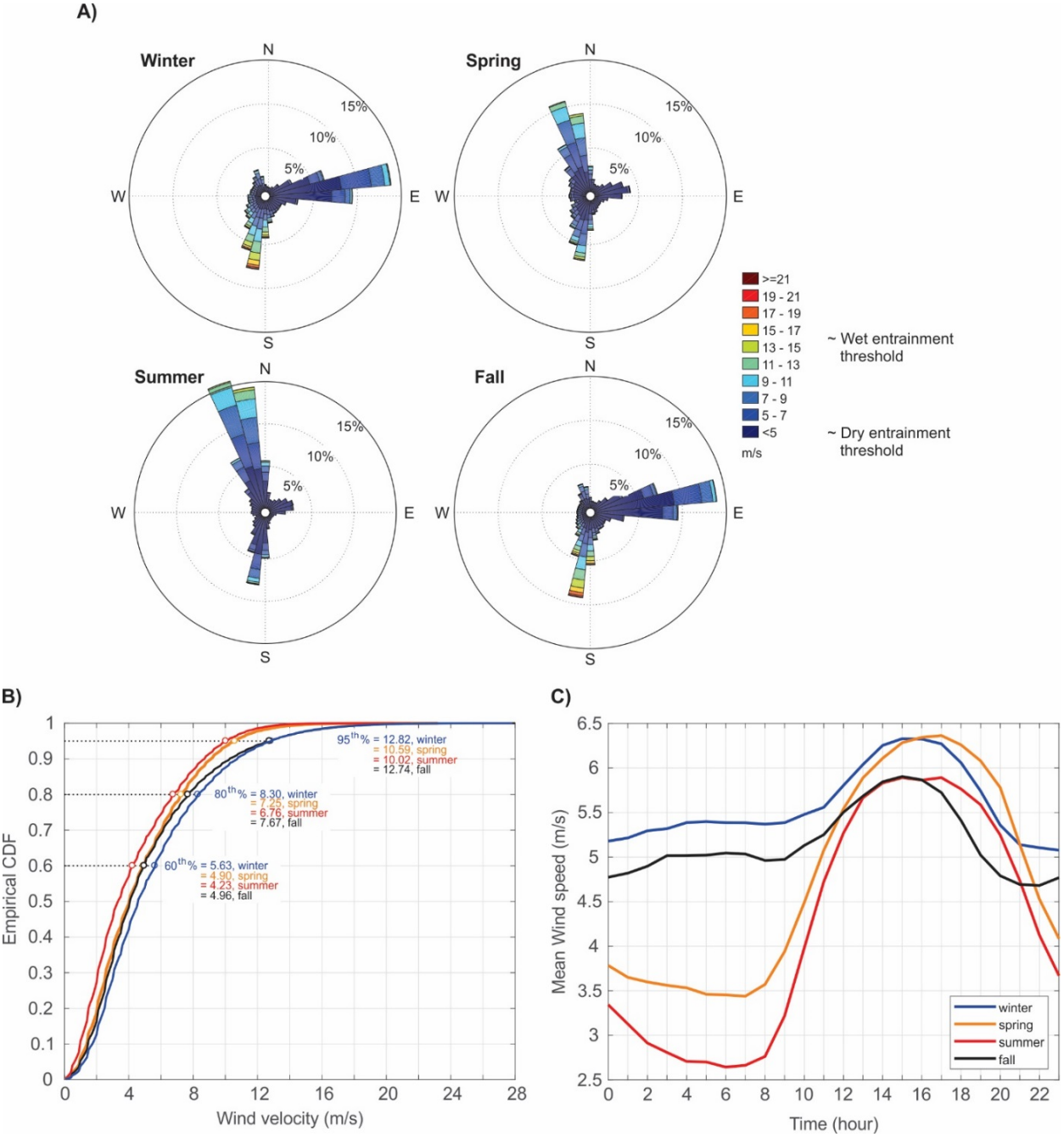

[3] http://www.ndbc.noaa.gov/station_page.php?station=NWPO3

Figure 13B is an empirical cumulative distribution function that has been fitted to the seasonal wind speeds in order to better assess the prevalence of certain wind velocities. In general, the plot demonstrates the expected seasonal response with spring and summer wind speeds characterized by lower velocities when compared with fall or winter conditions; overall, it can be seen that the lowest wind velocities occur in summer (**Figure 13**B). More specifically, **Figure 13**B indicates that for 60% of the time in summer, wind speeds are <4.2 m/s (~9.4 mi/hr); Note, the threshold velocity (u_{*t}) required to mobilize dry sand is ~5.6 m/s (12.5 mi/hr). This compares with wind speeds in the winter, which are <5.6 m/s (~12.5 mi/hr) for 60% of the time. Conversely, for 20% of the time wind speeds during the winter exceed 8.3 m/s (~18.6 mi/hr), and for 10% of the time they exceed 12.8 m/s (~28.6 mi/hr). This compares with summer winds, which exceed 6.8 m/s (~15.2 mi/hr) for 20% of the time, and 10 m/s (~22.4 mi/hr) for 10% of the time (**Figure 13**B). We find that for 1% of the time, wind speeds exceed 17.2 m/s (~38.5 mi/hr) during the fall and winter and exceed ~13 m/s (29 mi/hr) in the summer. Note, in all cases, these statistics reflect steady winds and not the wind gusts, which may reach hurricane force during the most extreme storms. From these data, we can speculate that with respect to sediment transport potential, more sand is likely to be mobilized and transported in the winter than in summer.

Figure 13C shows the mean hourly diurnal pattern for each of the seasons. Overall, wind speeds are generally at their lowest during the late evening/early morning, increase over the course of the day, and reach their peak by mid-afternoon. This pattern is most pronounced for winds occurring during the spring and summer. In contrast, the transition from lower to stronger wind speeds is much less pronounced during the fall and winter.

3.2.1 Calculated Sand Transport

To understand the potential for sand transport on Oregon beaches, we use the sand-transport rate equation for a given wind speed and direction proposed by Bagnold (1941):

$$q \begin{cases} = 0 & \text{when } u_* \leq u_{*t} \\ = C\sqrt{\frac{d}{D}}\,\frac{\rho_a}{g}\,u_*^3 & \text{when } u_* > u_{*t} \end{cases} \qquad \text{Eqn. 1}$$

where q is the bulk volume of sand crossing a unit width of ground surface per unit time, C is an empirical constant assumed to be 1.8 (Bagnold, 1941), ρ_a is air density (1.225 kg/m^3), g is acceleration due to grav-ity (9.81 m/s), d is the mean sediment diameter (mm), D is a reference grain size of 0.25 mm, and u_* is the shear velocity required to move the particles and is calculated from:

$$u_* = \frac{K(u_z - u_f)}{\ln(z/f)} \qquad \text{Eqn. 2}$$

where K is the von Karman constant (0.4), u_z is the wind velocity at height z (for Newport this is 10 m [33 ft]), u_f is the wind velocity at the focal height f of the velocity profiles during conditions of transport. The values of u_f and f (a roughness factor) are assumed to be 2 m/s and 5 mm, respectively, which are approximate averages derived by Bagnold. The threshold velocity (u_{*t}) is assumed to be 5.6 m/s (12.5 mi/hr) at a height of 10 m (33 ft) (Hunter and Richmond, 1983). Although there are other more modern proposed equations for calculating sand-transport rates, the Bagnold (1941) equation still yields the most reliable indicator of the sediment transport rate (Sherman and others, 1998).

Using Equations 1 and 2, we calculated the sand-transport rate using the entire wind record from the Newport C-Man station (**Figure 14**, *top*). The results confirm the largely bi-modal wind transport potential, with south to southwesterly winds dominating in the fall and winter, which helps drive sand toward the north. Conversely, north to northwesterly winds dominate in the spring and summer, which help return sand to the south ends of Oregon's pocket beach littoral cells. Our analyses also indicate that westerly winds enable sand to be moved from the subaerial beach to the back of the beach, where it may accumulate along the toe of the dune. However, the role of westerly winds in transporting sand onshore is smaller compared with the potential for northerly or southerly transport. Hence, these winds are more likely to contribute to the development of ephemeral dunes that form at the back of the beach.

We can take these data one step further by focusing purely on the role of winds blowing from the north (±22.5° about north) and south (±22.5° about south), to better define the seasonal pattern in the sand-transport potential (**Figure 14**, *bottom*). Using this approach, we find that ~79% of the sand-transport is directed to the north, while the southerly sand-transport accounts for ~21% of the volume of sand moved. Hence, we find that the net transport to the north is approximately 4 times greater than the southward transport and is consistent with previous estimates made by Shoreland Solutions (1998a). This means that for the period studied, there has been a greater potential for net northward sediment transport, much of which is the product of strong south to southwesterly winds (**Figure 13**A,B) that form in late fall and winter.

Finally, given that winter is characterized by significant precipitation, is it reasonable to expect large volumes of sand being entrained and transported by the wind, especially in light of the larger threshold wind speeds required to entrain the sediment (**Figure 13**A). However, apparent from **Figure 13** is that winds do in fact exceed this threshold in the fall and winter, providing a mechanism for sand transport. Thus, despite the incidence of south to southwesterly winds being relatively infrequent on the coast, in terms of their transport potential what they may lack in frequency they likely make up for in wind strength. **Figure 15** shows two qualitative examples that reinforce the assumption that even wet sand is capable of being transported. The upper photo shows sand burying beach grass adjacent to homes at Pacific City, Oregon; the storm resulted in very heavy precipitation on the northern Oregon coast. The lower photo shows blowing sand piling up around the buildings. Furthermore, our experience from having worked on Oregon beaches throughout the seasons collecting beach-change information under a range of conditions, strongly points to the ability of winter storms to transport large quantities of sand to the north (due to their greater winder velocities) despite heavy wet weather. This observation is supported by other researchers (Hunter and Richmond, 1983).

Figure 14. ***(top)*** **Calculated wind direction and sand-transport potential based on wind records measured at the Newport C-Man climate station. Wind barbs indicate the direction from which the sand is coming.** ***(bottom)*** **Seasonal variability in the ability of northerly (±22.5° about north) and southerly (±22.5° about south) winds to transport sand.**

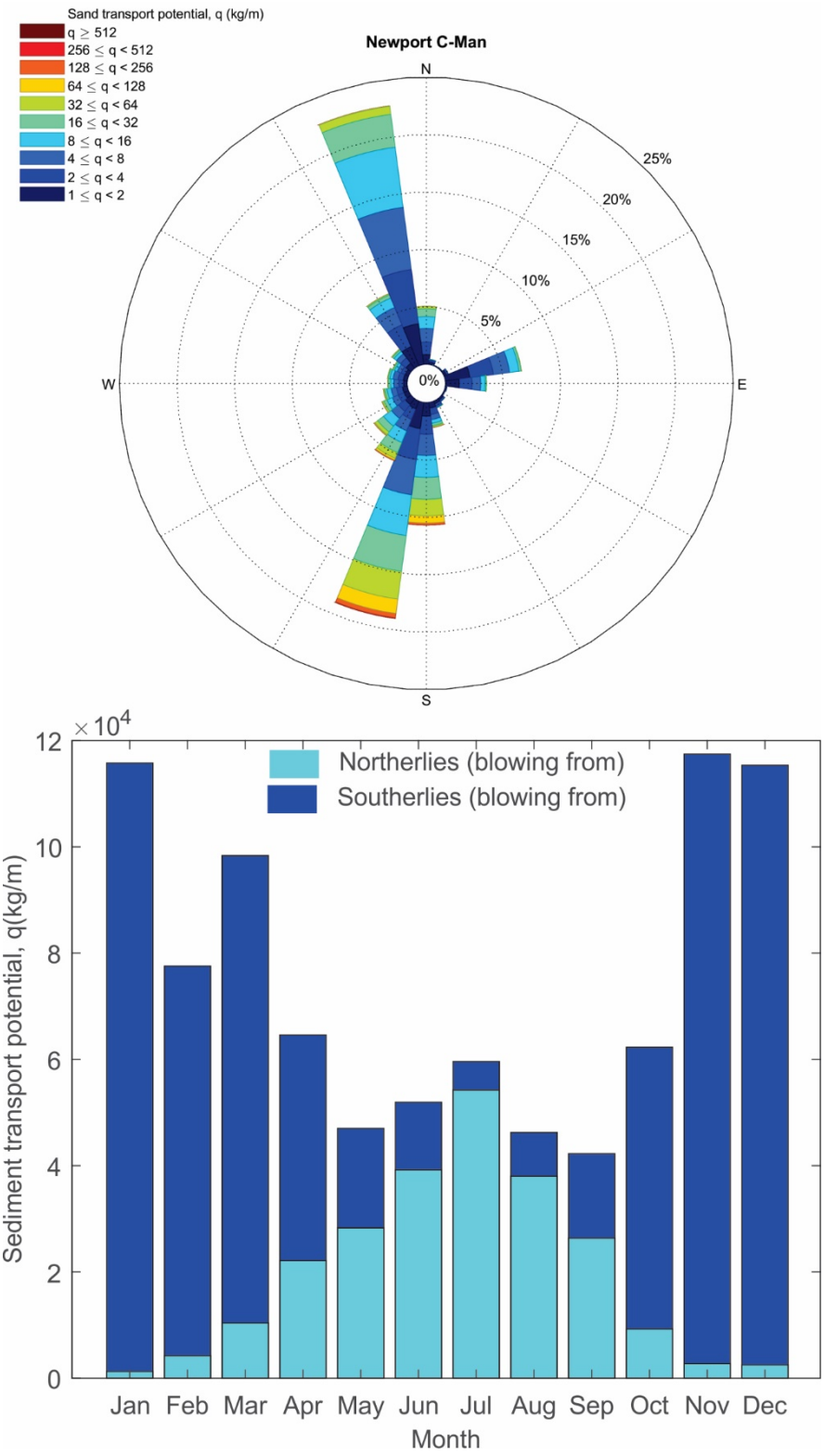

Figure 15. ***A)*** **The transport of wet sand onto the 16 to 18 m (53 to 59 ft) high primary foredune in Pacific City during a major storm on November 30, 2001.** ***B)*** **The same event is moving sand toward the north in among the homes built on the foredune. (Photo credit: J. Allan, DOGAMI, 2001)**

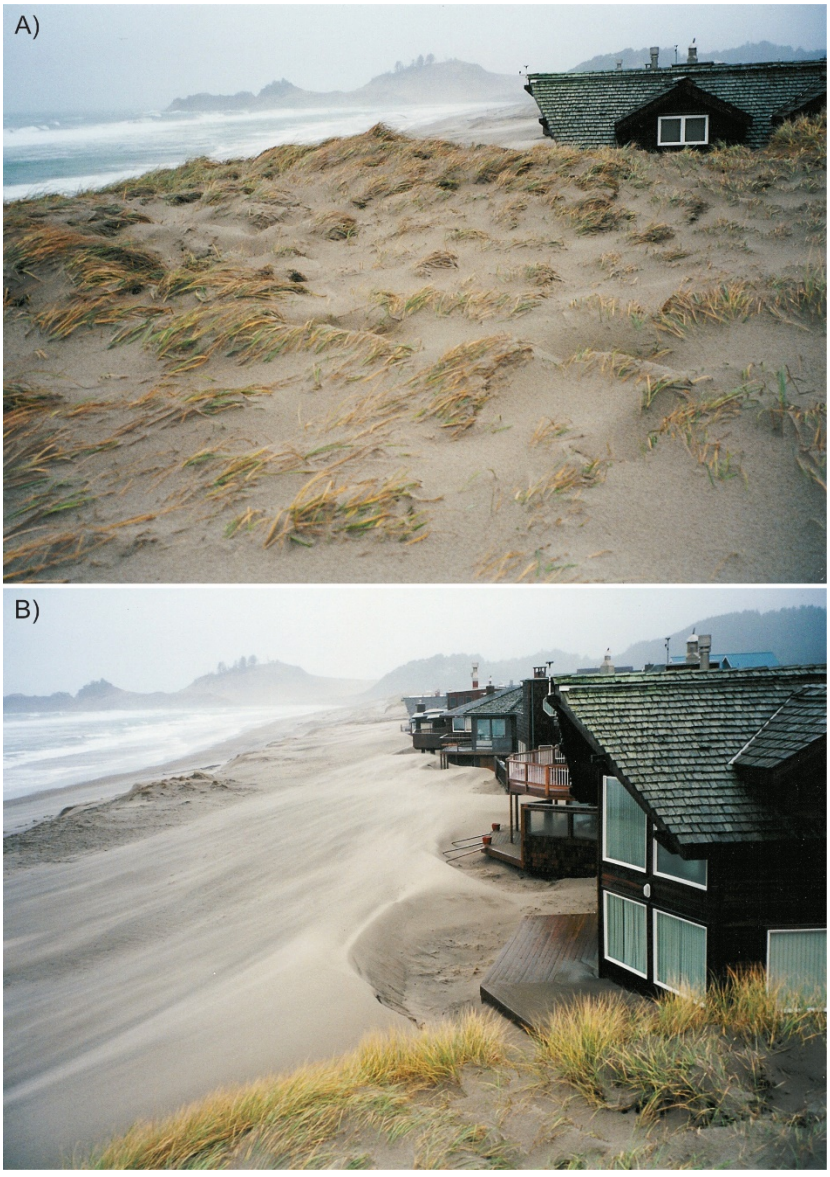

4.0 COASTAL GEOLOGY AND GEOMORPHOLOGY OF THE CANNON BEACH LITTORAL CELL

Cannon Beach is located in south central Clatsop County on the northwest Oregon coast, between latitudes 45°55′04.8″N (Tillamook Head) and 45°46′59.24″N (just north of Cape Falcon) (**Figure 1**). The total length of the coastal strip in the county is 57 km (35.4 mi) and varies in its geomorphology from wide sandy beaches backed by broad dunes, cobble and boulder beaches, and bluff-backed shorelines. Bold headlands formed of resistant basalt (e.g., Cape Falcon and Tillamook Head) provide natural barriers to alongshore sediment transport, effectively dividing the county coastline into two littoral cells:

- The Cannon Beach cell, which is approximately 23 km (14.3 mi) long and extends from Cape Falcon to Tillamook Head; and
- The Columbia River cell, which is approximately 185 km (115 mi) long and extends from Tillamook Head to Point Grenville on the Washington coast.

Clatsop County is bounded in the north by the Columbia River and the broad expanse of its lower estuary. Prior to jetty construction and discharge control, this river system historically transported to the coast large volumes of sediment that played a significant role in the evolution of the Clatsop Plains (Sherwood and others, 1990; Kaminsky and others, 2010). However, under modern conditions (essentially the last 5,000 to 7,000 years) Columbia River sediments are unlikely to have been transported south of Tillamook Head (Clemens and Komar, 1988).

To the south, smaller streams such as the Necanicum and Ecola Creeks flow out of the Coast Range mountains. Due to generally low flow discharges and the kind of terrain in which they are downcutting, these creeks contribute minimal beach sediment to the coast today. Hence, there is presently no significant source of sediment to the coast other than from erosion of the backshore. This is especially true in the Cannon Beach littoral cell located south of Tillamook Head. The Cannon Beach cell is also at a juncture between an area where the rate of sea level rise exceeds the local tectonic rate of uplift (**Figure 6**, area south of GPS Station P407 located near Tillamook Head) and the area north of Tillamook Head where rates of sea level rise are falling relative to the land (Komar and others, 2011). In essence, under current patterns of sea level change, the area south of P407 is being transgressed (flooded) by a rising sea level, while north of P407 the coast is emerging.

4.1 Local Geology

The predominant geologic units in the Cannon Beach cell consist of recent Holocene beach sand present along the full length of the coastline (**Figure 16**). These beaches are backed by a variety of geologic units that clearly influence the contemporary geomorphology of the coast (Schlicker and others, 1972; Witter and others, 2009). Travelling north to south, the broad geology of the coast can be divided into the following components:

- Late Pleistocene to Holocene colluvial deposits that overlay Middle Miocene intrusive Grande Ronde Basalt (e.g., much of Tillamook Head). These are fronted by late Holocene gravels and boulders;
- Relatively flat, late Pleistocene coastal terrace deposits on which most of the City of Cannon Beach and Tolovana Park have been developed (**Figure 16** and **Figure 17**). These sediments include well-cemented fluvial gravels, beach sand, and poorly bedded mud with fossil shell from estuarine environments. In many areas, low bluffs of the coastal terrace presently are protected from storm

wave erosion by a ramp of dune sand and are well vegetated, suggesting that they have been stable for some time. Nevertheless, parts of the shoreline (e.g., Arch Cape, Tolovana Beach) have also been hardened with coastal engineering structures, a testament to previous storm induced erosion processes (**Figure 16**, *left*);

Figure 16. Geology of the Cannon Beach littoral cell. Data from Witter and others (2009).

- Between Silver Point and Hug Point the shore consists predominantly of unstable bluffs, with several major landslides (e.g., the Silver Point landslide). The geology in this region is characterized as consisting mostly of Astoria Formation (Middle to lower Miocene) sandstone/mudstone units. Pleistocene terrace deposits underlie much of the Arcadia Beach area, while in the south, exposures of Angora Peak sandstone form prominent bluffs. In many areas, broad sand beaches are backed by gravel berms, followed by bluffs of varying heights;

- The community of Arch Cape occupies a broad coastal terrace with few active landslides impacting relatively low (<10 m high) bluffs (**Figure 16**, *right*). The entire shoreline is naturally armored by a gravel beach, which is periodically covered with sand during summer months (**Figure 18**); and,
- At the south end of this stretch of coast, Cove Beach borders a crescent-shaped reentrant in the coast between Arch Cape and Cape Falcon (**Figure 16**, *right*). The small beach community of Falcon Cove that overlooks Cove Beach faces the most severe erosion and landslide hazards among coastal communities in southern Clatsop County, with more than 65 percent of the bluffs that back Cove Beach showing evidence of active or prehistoric mass movement (Witter and others, 2009). Deposits that comprise these bluffs are inferred to be mostly late Pleistocene rock avalanche deposits.

Figure 17. Haystack Rock at Cannon Beach. Homes present along the shore have been constructed on marine terrace deposits that form low, well-vegetated bluffs. (Photo credit: E. Harris, DOGAMI, 2011)

Figure 18. Gravel beach at Arch Cape. (Photo credit: E. Harris, DOGAMI, 2011)

4.2 Provenance of Cannon Beach Sediments

The beach sand present on the Oregon coast consists primarily of grains of quartz and feldspar. The beaches also contain small amounts of heavier minerals (e.g., garnets, hypersthene, augite, and hornblende) (**Figure 19**), which can be traced to various sediment sources along the Pacific Northwest coast (Clemens and Komar, 1988). For example, garnet and hypersthene are derived from the Klamath Mountains in southern Oregon and in North California. Because the headlands today extend well out in deep water, they effectively limit sand transport around their ends under the current process regime. This suggests that these heavier minerals were probably transported northward along the coast at a time when sea level was much lower, with few barriers to interrupt their northward movement (Komar, 1997).

With distance from their source, the sediments combined with other minerals derived locally from erosion processes in the Coast Range. As shown in **Figure 19**, the concentrations of garnet and hypersthene decrease to the north, while concentrations of augite increase significantly; augite is a mineral that is prevalent in the volcanic rocks present throughout Tillamook County. At Tillamook Head the concentration of garnet is very small, suggesting that Tillamook Head reflects the most northerly transport of garnet. North of Tillamook Head, concentrations of hypersthene and hornblende increase again. These latter sediments are locally derived from the Columbia River, which contributed to the formation of the Clatsop Plains, Long Beach Peninsula, and Grayland Plains. Thus, sediments derived from the Columbia River were transported mainly to the north, supplying the Washington coast and shelf.

With the end of the last glaciation, sea level rose rapidly and the beaches began to migrate landward. New sediments were derived from erosion of the coastal plain that makes up the continental shelf today. About 5,000 to 7,000 years ago, the rate of sea level rise slowed as it approached its current level (Komar, 1997). In this stage the prominent headlands began to interrupt sediment transport. Modern barrier spits and beaches began to form within the headland bounded littoral cells that make up the coast today.

Figure 19. Variations in the percent abundances of various heavy minerals observed on the central to northern Oregon coast (after Clemens and Komar, 1988).

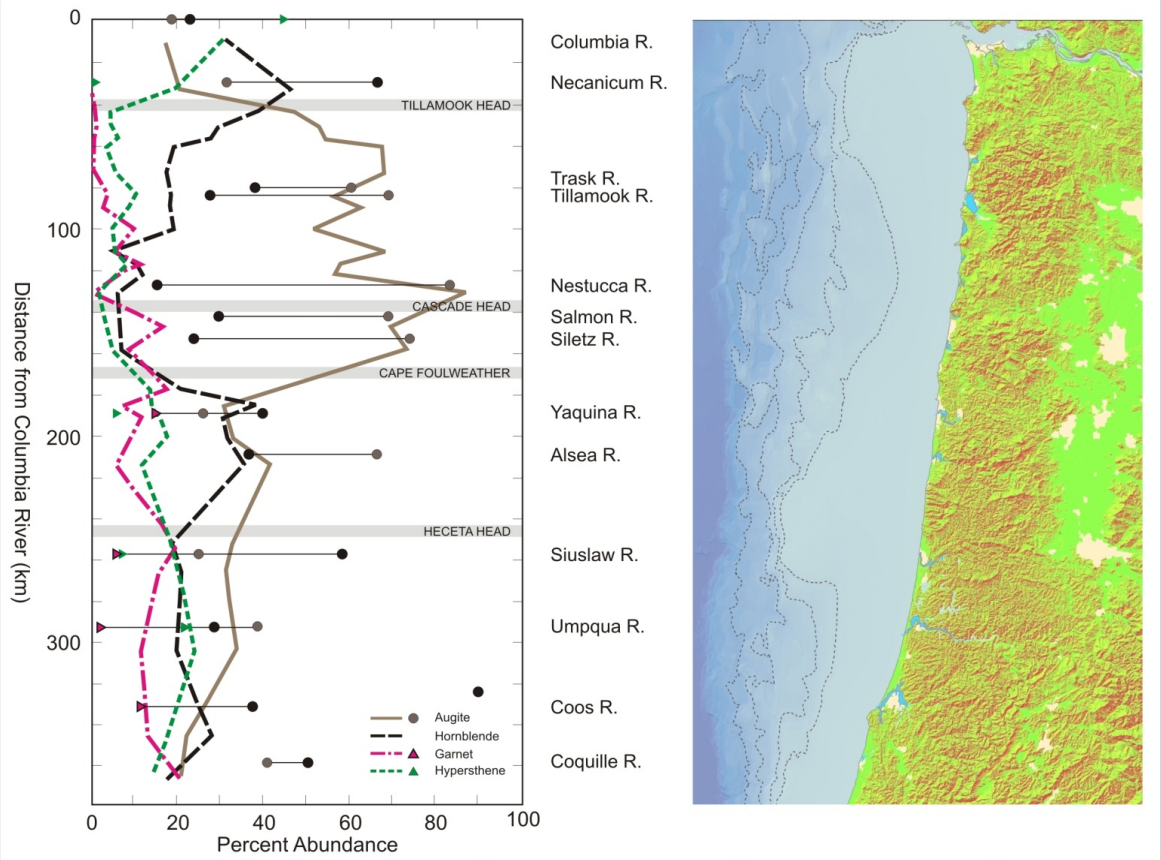

Analyses of the sediments in the estuaries in Tillamook County to the south indicate an abundance of augite, indicative of their having been derived locally (**Figure 19**). This suggests that local rivers and streams draining from the Coast Range carried these sediments out to the coast, where they subsequently mixed with other sediments. These concentrations have probably increased during the past 150 years as human settlement accelerated, leading to increased deforestation and sediment loads in the rivers (Peterson and others, 1984; Komar and others, 2004). Furthermore, analyses of sediments in Tillamook Bay indicate that while fine sediments pass through the estuary, most of the coarser sediments remain behind, where they accumulate as bars and shoals (Komar and others, 2004). In addition, sediments within Tillamook Bay are predominantly of marine origin (60%), while river sediments make up 40% of the remaining sediment. This finding is consistent with the work of Peterson and others (1984) and Clemens and Komar (1988), who noted that because of the combination of low river discharge and high tidal regime in Oregon estuaries, the majority of the estuaries are in fact natural "sinks" for the sediment.

Clemens and Komar (1988) concluded that the beaches of Oregon receive very little sediment input from rivers and streams today. Accordingly, sediment supply today is essentially confined to areas backed by coastal bluffs, particularly those areas overlain by more erosive Pleistocene marine terrace sandstones (raised ancient beach and dune sands) and more recent Holocene dune sands that drape the landscape.

Finally, prior to the 1940s, many of the barrier spits were devoid of significant vegetation. With the introduction European beach grass (*Ammophila arenaria*) in the early 1900s and its subsequent proliferation along the Oregon coast, the grass essentially contributed to the stabilization of the dunes and barrier spits. The product today is an extensive foredune system, which consists of large "stable" dunes containing significant volumes of sand. As the dunes stabilized, humans have settled on them, building in the most desirable locations, typically on the most seaward foredune. As will be shown throughout this report, construction of homes and facilities in such areas poses a significant risk as storms periodically erode into the dunes. This has resulted in many cases where the foundations of homes may be undermined, eventually requiring riprap coastal engineering structures to mitigate the erosion problem.

4.3 Coastal Geomorphology

On the basis of local geology and geomorphology, the Cannon Beach shoreline can be broadly divided into the following morphological beach types (**Figure 20**).

1. ***Dune-backed beaches:*** Dune-backed beaches make up a small (5%) proportion of the Cannon Beach shoreline and are confined to a small section of the shore north of Ecola Creek in Cannon Beach (**Figure 20**). The geomorphology of the beach can be generalized as having wide, dissipative surf zones with low, sloping foreshores backed by broad, high dunes. Dune crest elevations reach 18 m (59 ft), while the average beach slope (tan β) for these beaches is 0.038 (i.e., ~a 1:26 slope or 3.8% slope).
2. ***Cliffed shore:*** Cliffed shores make up the second largest (24%) geomorphic "type" in the cell (**Figure 20**). Examples of this type of shore exist around Tillamook Head, along discrete sections of the shore to the south of Cannon Beach, Arch Cape, and at Cape Falcon. This particular shore type may be fronted by either prominent cobble/boulder beaches (e.g., Tillamook Head) or wide dissipative sand beaches, backed with a veneer of gravel (e.g., Arcadia Beach).
3. ***Bluff-backed beaches:*** Bluff-backed beaches are the most prominent geomorphic type in the Cannon Beach cell, comprising approximately 63% of the shore (**Figure 20**). The bluffs that back the beaches vary in height from ~7 m (23 ft) to greater than 40 m (131 ft). Beach slopes (tan β) seaward of the bluffs average about 0.028 ($\sigma = 0.007$, i.e., ~a 1:37 slope [2.8% slope]). Geomorphically, these beaches may be characterized as "composite" using the terminology of Jennings and Shulmeister (2002), such that the beaches consist of a wide dissipative sandy beach backed by a steeper upper foreshore composed of gravels. In addition, several of the bluff-backed sections are characterized by well-vegetated faces, indicating that they have not been subject to significant wave erosion processes along the toe of the bluffs during the late 20th and early 21st centuries.
4. ***Cobble berm backed by bluffs:*** Finally, an extensive cobble berm fronts moderately high bluffs in Falcon Cove at the south end of the county. Similar to the bluff-backed beaches to its north, this particular beach type is also characterized as of the "composite" type. Although it is fronted by a wide, dissipative sand beach, much of this is presently located below water and is mostly visible near low tide. However, prior to the storms of the late 1990s, the sand beach at Falcon Cove was more substantial; its loss is likely due to the removal of sand during the 1997-1998 El Niño, transported to the north around Arch Cape and into the Cannon Beach littoral cell.

Figure 20. Geomorphic classification of the Cannon Beach littoral cell.

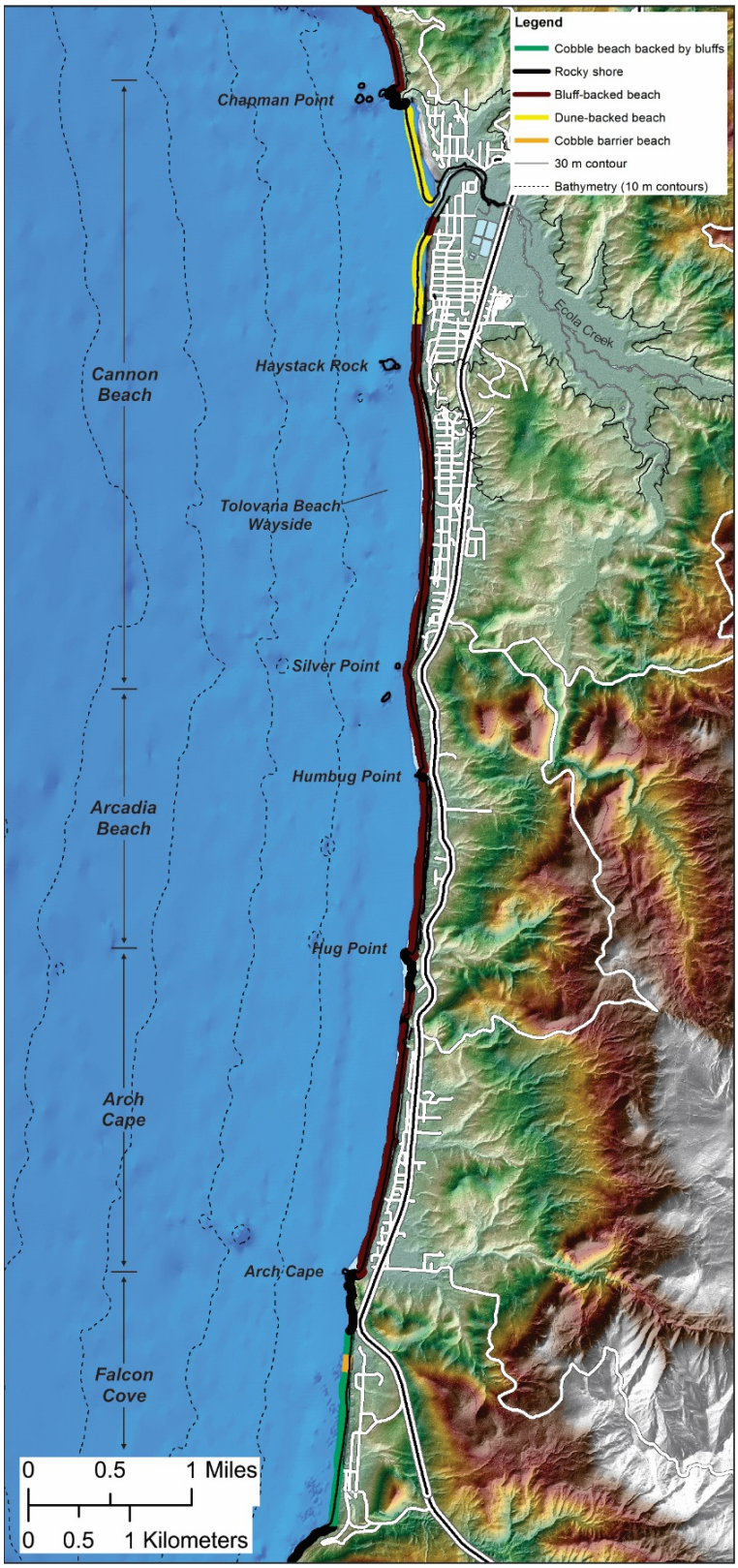

4.4 Historical Coastal Changes

This section presents a discussion of large-scale morphological changes derived from analyses of historical and contemporary shorelines derived in the Cannon Beach cell. This summary stems from work undertaken by researchers at DOGAMI and OSU over the past two decades (Priest and others, 1993; Allan and Priest, 2001; Allan and others, 2003, 2015b; Allan and Hart, 2007, 2008; Allan and Harris, 2012; Allan and Stimely, 2013; Ruggiero and others, 2013).

National Ocean Service (NOS) Topographic (T)-sheet shoreline positions covering the 1920s and 1950s were previously obtained from NOAA (Allan and Priest, 2001). These lines reflect the mean high water (MHW) position mapped by early NOS surveyors, on an average tide typically in mid to late summer. Additional shorelines were derived from a variety of other sources including: 1967 digital orthophotos (Ruggiero and others, 2013); 1980s era U.S. Geological Survey topographic maps; 1994 digital orthophotos; and 1997, 1998, and 2002 lidar data (Allan and Priest, 2001). Pre-lidar historical shorelines use the high water line (HWL) as a shoreline proxy. The HWL has been used by researchers for more than 150 years because it can be visually identified in the field or from aerial photographs. In contrast, shorelines derived from lidar data are datum-based and can be extracted objectively using a tidal datum, such as MHW or mean higher high water (MHHW). Studies by Moore (2000) and Ruggiero and others (2003) note that HWL-type shoreline proxies are virtually never coincident with datum-based MHW-type shorelines. In fact, they are almost universally estimated to be higher (landward) on the beach profile when compared to MHW shorelines (Ruggiero and others, 2013). According to Ruggiero and others, the average absolute horizontal offset between the HWL and MHW ranges from ~6 m (~19 ft) to as much as 50 m (164 ft), while the average is typically less than 20 m (65 ft). Offsets are typically greatest on flat, dissipative beaches where the wave runup may be large, and smallest where beaches are steep (e.g., gravel beaches).

Estimates of the uncertainty of HWL shoreline measurements have been assessed in a number of studies (Moore, 2000; Ruggiero and others, 2013). These uncertainties reflect the following errors: 1) mapping methods and materials for historical shorelines (including the offset between the HWL and MHW shoreline), 2) the registration of shoreline positions relative to Cartesian coordinates, and 3) shoreline digitizing, and are summarized in **Table 2**.

Shorelines measured by DOGAMI staff using Real-Time Kinematic Differential Global Positioning System (RTK-DGPS) surveys of the beach are available for the Cannon Beach littoral cell. These data sets provide the most up-to-date assessments of the changes taking place along the Cannon Beach cell and were collected in April 2016 at the end of the 2015-2016 winter. In all cases, the GPS shorelines reflect measurements of the MHHW line located at an elevation of 2.3 m (7.5 ft). We have relied on the latter as opposed to the MHW line, because previous studies indicate that MHHW line most closely approximates the MHW line surveyed by early NOS surveyors. Errors associated with these various products are described by Moore (2000). GPS shoreline positioning errors, a function of the orientation of the GPS receiver relative to the slope of the beach, are estimated to be approximately ±0.1 to ±0.2 m (±0.3 to ±0.6 ft) and are thus negligible.

Table 2. Average uncertainties for Pacific Northwest shorelines (Ruggiero and others, 2013).

	NOS T-Sheets (1800s to 1950s)		DRGs (1940s to 1990s)		Aerial Photography (1960s to 1990s)		Lidar	
Total shoreline position uncertainty	18.3 m	60 ft	21.4 m	70 ft	15.1 m	50 ft	4.1 m	14 ft

NOS is National Ocean Service; T is Topographic sheet; DRG is digital raster graphic.

The approach adopted here is to describe the broad morphological changes identified along the coast, beginning in the north at Cannon Beach, and progressing south toward Cape Falcon.

4.4.1 Cannon Beach

Major coastal storms battered the Cannon Beach area on January 3, 1939; December 2- 3; 1967, February 18, 1976; and most recently in January 1983 and February 1986 (FEMA, 2010). The most recent severe storms occurred in the 1998-1999 winter, when the equivalent of four 100-year storms occurred in close succession, contributing to significant erosion along much of the northern Oregon coast.

Several storms have resulted in ocean flooding in downtown Cannon Beach. This typically occurs when Ecola Creek is in flood, coupled with high tides, locally induced surges, and large waves. These combined processes cause the creek to back up, which leads to flooding in low-lying areas adjacent to town (**Figure 21**). For example, a major storm on December 2-3, 1967, resulted in water ponding to an elevation of 3.5 m (11.5 ft), a depth of 0.76 m (2.5 ft) above the street surface, at the intersection of 2nd and Hemlock Streets, the center of the city's business district (FEMA 2010). Approximately 35 stores and business establishments, several public buildings, the conference complex, and three residential properties were flooded. Water and sanitary facilities were also damaged, creating a health hazard. Similar, but less severe, flooding has occurred three other times in the last 20 years.

Figure 21. Oblique view looking west-northwest over downtown Cannon Beach toward Chapman Point. (Photo credit: D. Best, 2015)

Analyses of the shoreline variability along the Cannon Beach shore indicate no predominant trends of erosion immediately south of Ecola Creek, while the beach north of the creek has built seaward by 40 to 60 m (131 to 197 ft) since 1967, enabling large dunes to form at the back of the beach (**Figure 21**). This is most evident when comparing the location of the main vegetation line in 1939, 1967, and most recently in 2009 (**Figure 22**). Farther south near Tolovana Park, similar efforts to identify the vegetation line in 1939 and 1967 indicate that much of this shore has remained relatively stable, having experienced minimal change (erosion or accretion) over the years, particularly since the late 1960s.

Figure 22. Variability in historical shoreline positions at Cannon Beach (1926–2016).

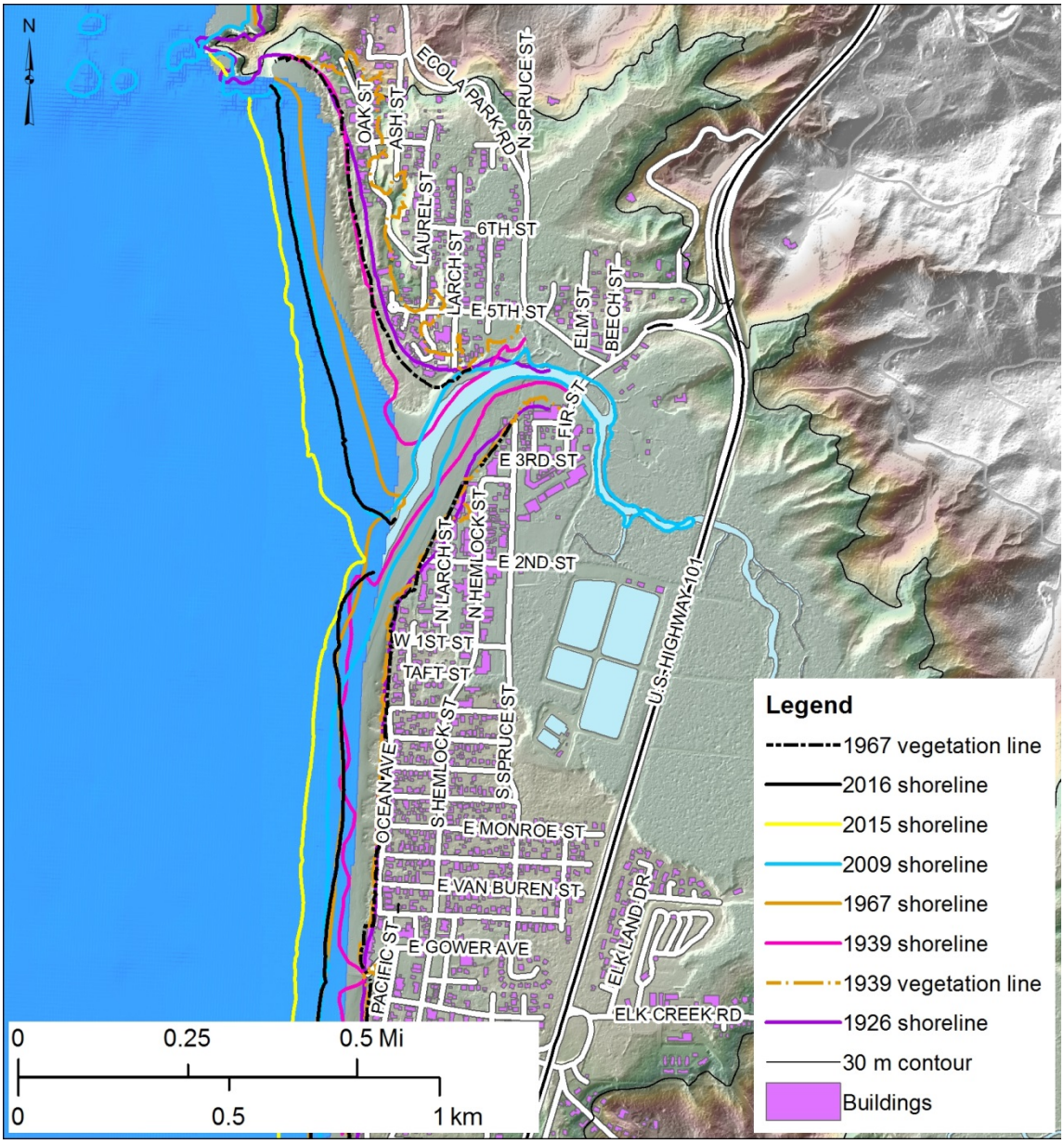

Ruggiero and others (2013) performed short- (1960s to 2002) to long-term (1800s to 2002) analyses of changes in the MHW shoreline in order to understand shoreline change patterns taking place in the Pacific Northwest. The authors used historical shoreline information from a variety of sources, including NOS topographic "t-sheets" aerial photos and lidar data, similar to those presented here. Their results for the Cannon Beach cell suggest that over the long-term the average shoreline change rate was not statistically different from zero (**Figure 23**). That is, the cell is considered to be stable, neither accreting nor eroding. Between the 1960s and 2002, Ruggiero and others identified that 75% sites in the Cannon Beach cell were eroding at rates of −0.5 m/yr, while 25% of these were eroding at rates greater than −1 m/yr. Erosion rates were highest in the southern part of the cell near Arch Cape, while the majority of the beaches fronting Cannon Beach remained stable. Measurable accretion (~+1-2 m/yr) were observed to have taken place north of Ecola Creek since the 1960s, consistent with our own observations presented here and in Section **3.0**.

Despite any obvious trends and patterns in shoreline response south of Ecola Creek, it is apparent that this beach has periodically been affected by major storms. Evidence for this includes the presence of numerous coastal engineering structures, including riprap (the most common structure), few concrete seawalls, and wooden bulkheads (**Figure 16**). For example, a substantial wooden bulkhead has been constructed along 270 m (886 ft) of the shore fronting downtown Cannon Beach (between 2nd Street and 3rd Street), while a major seawall built after the January 1939 storm is located in front of the Ecola Inn. Analysis of the permit records held by the Oregon State Parks and Recreation Department (OPRD), which manages the public beach, indicates that many of the smaller riprap structures were constructed in the early 1970s (~1973-1974), following the 1982-1983 El Niño. Interestingly, however, very few coastal engineering structures were constructed after the major 1997-1998 El Niño (second strongest on record) or following the extreme 1998-1999 winter, which generated the equivalent of four 100-year storms in the space of two months (Allan and Komar, 2002b).

Figure 23. Long- (1800s through 2002) and short-term (1960s through 2002) shoreline change rates (solid black line) for the Cannon Beach littoral cell. Shaded gray banded area represents uncertainty associated with the rate calculation (Ruggiero and others, 2013).

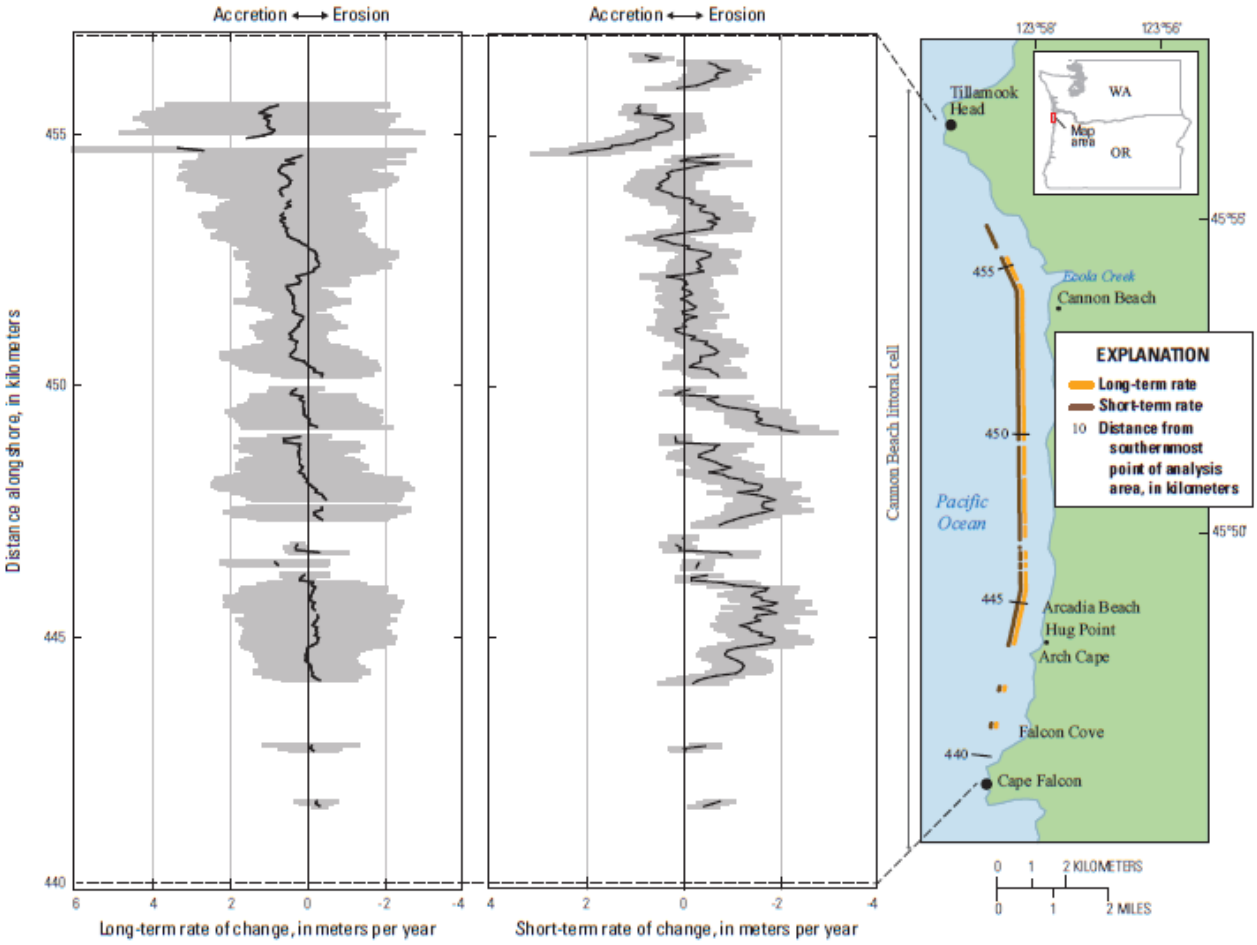

4.4.2 Arch Cape

Shoreline changes in the Arch Cape subcell are broadly similar to those observed along the Cannon Beach shore. **Figure 24** documents various responses from 1928 to the present. Apparent from **Figure 24**, the shoreline in 1939 and 1967 tracks farther seaward of its position in 2009. This would imply that the shore is currently eroding. However, in reality, this simply highlights the strong seasonal excursions to which PNW beaches are subjected, which can be as much as 20 to 30 m (65 to 100 ft), and even greater during an El Niño climate event. Hence, a better measure of the long-term pattern of change is to assess changes taking place on the backshore (near the vegetation or dune line). **Figure 24** includes vegetation lines determined from 1939 and 1967 photos, overlaid on 2009 lidar data. In general, the southern half of the Arch Cape subcell indicates little long-term evidence for erosion or accretion, with vegetation lines in 1939 and 1967 tracking very close to the 2009 bluff face (**Figure 24**). However, in the northern half of Arch Cape there is some suggestion that this section has been gradually eroding landward, with most of the change having taken place between 1939 and 1967. Estimated rates of erosion are low ~0.03 to 0.1 m, with calculated photo errors (uncertainty) producing numbers as large as the rates themselves, reinforcing the fact that the long-term change is slow. Regardless, it is interesting to note that the bulk of the existing coastal engineering structures present in the Arch Cape subcell are located in the northern third of the shore where most of the erosion has been taking place. Furthermore, the majority of these were constructed in the early 1980s; a few were built in the late 1970s.

Figure 24. Variability in historical shoreline positions at Arch Cape, 1926–2016. *(left)* southern half, *(right)* northern half.

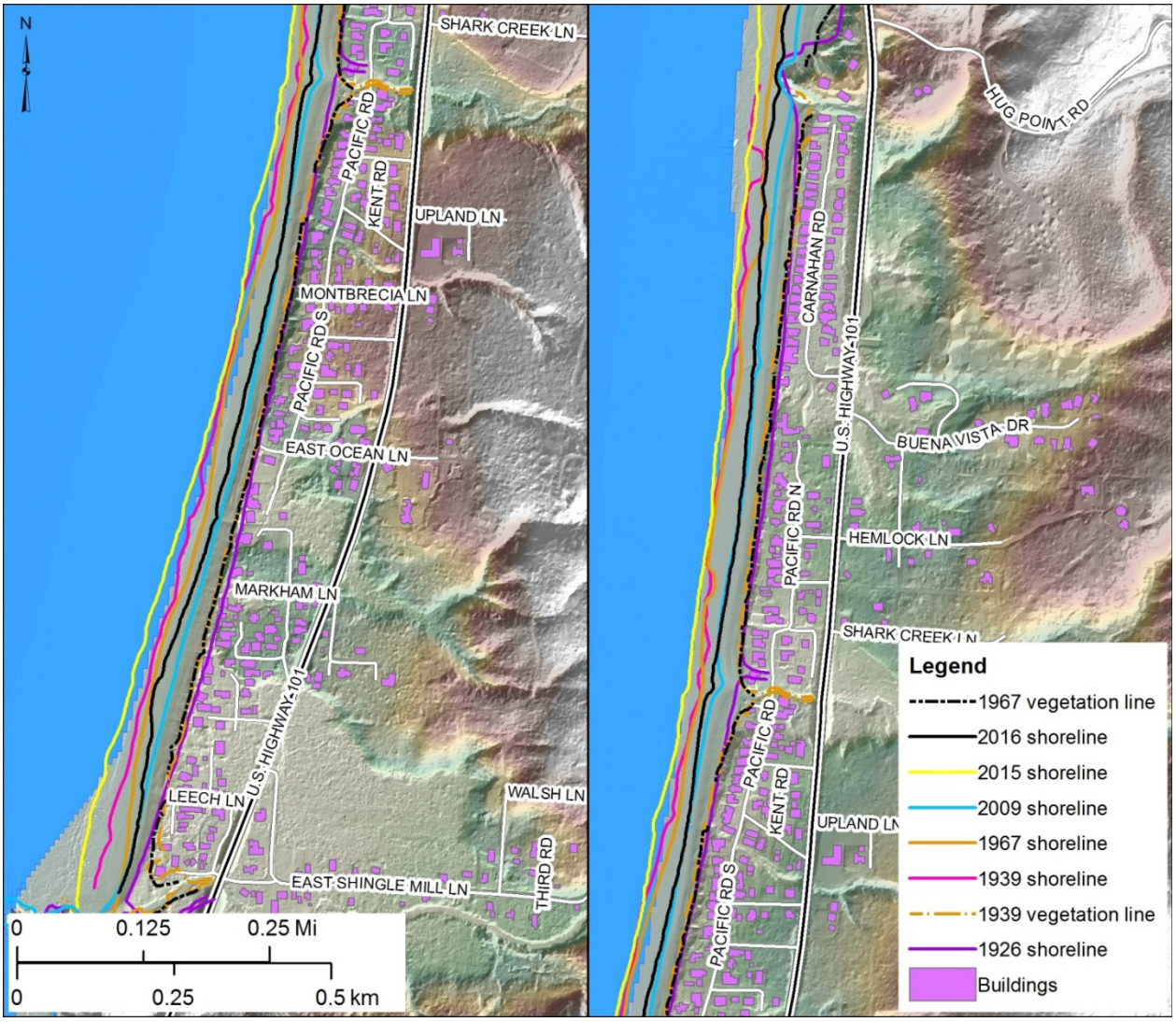

4.4.3 Falcon Cove

By far the highest erosion rates observed in the Cannon Beach littoral cell occur in Falcon Cove, located between Cape Falcon and Arch Cape. More than 65 percent of coastal bluffs backing Cove Beach show evidence of active or prehistoric mass movement (Witter and others, 2009). Deposits that comprise these bluffs are inferred to reflect mostly late Pleistocene to Holocene colluviums that are easily eroded. As noted previously, the coastal geomorphology reflects a wide dissipative sandy beach backed by a prominent cobble berm and bluffs. **Figure 25** presents the shoreline history in Falcon Cove. An attempt was made to rubbersheet a single 1939 photo at the south end of the pocket beach, the results of which are included in the figure. While suitable ground-control points could be identified in the southern half of the photo, the northern half lacked sufficient points. Hence, vegetation results derived from the 1939 photo likely contain higher errors compared with other Cannon Beach sites to the north. In general, erosion rates in the southern half of Falcon Cove have ranged from about 0.1 m to 0.4 m (0.3 ft to 1.3 ft) since 1967. If we include results from 1939, these numbers effectively double for a number of sites.

Figure 25. Variability in historical shoreline positions at Falcon Cove, 1926–2016. Bold red line denotes problem sites where bluffs are actively eroding and homes are either already affected or could be affected soon.

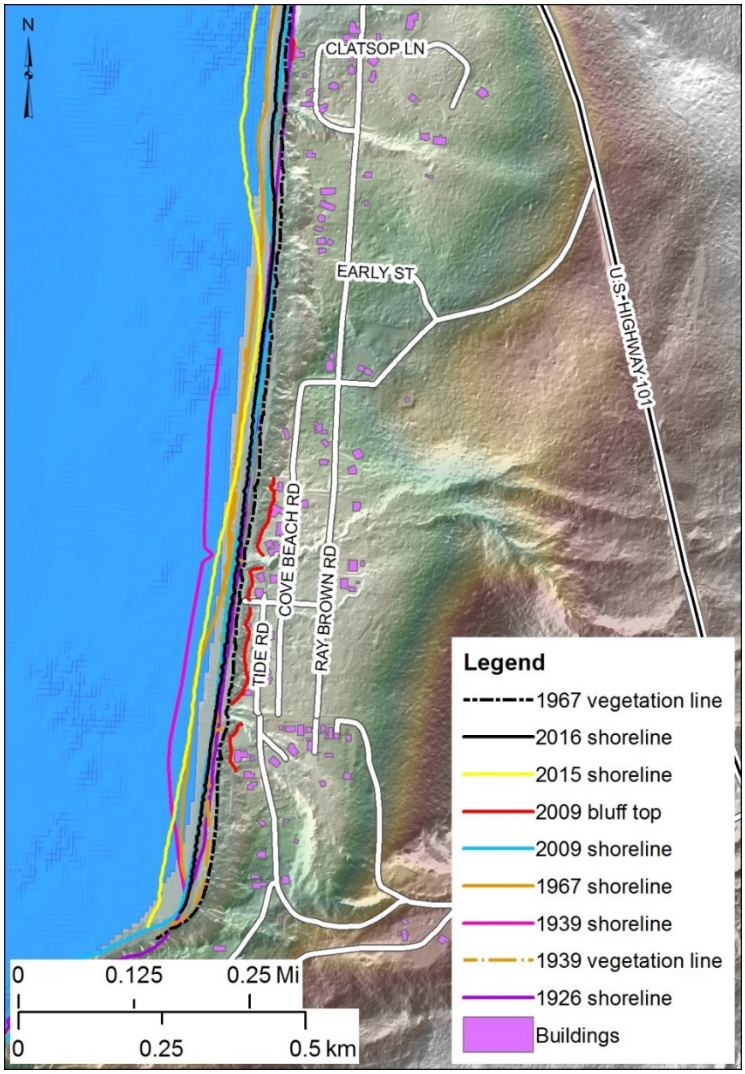

5.0 OBSERVATIONS OF CANNON BEACH CHANGES: 1997–2016

5.1 Topographic Beach Mapping

5.1.1 Background

Beach profiles that are oriented perpendicular to the shoreline can be surveyed using a variety of approaches, including a graduated rod and chain, surveying level and staff, Total Station theodolite and reflective prism, lidar airborne altimetry, and Real-Time Kinematic Differential Global Positioning System (RTK-DGPS) technology. Traditional techniques such as leveling instruments and Total Stations can provide accurate representations of the morphology of a beach but are demanding in terms of time and effort. At the other end of the spectrum, high-resolution topographic surveys of the beach derived from lidar are ideal for capturing the 3-dimensional (3D) state of the beach over an extended length of coast within a matter of hours; other forms of lidar technology are now being used to measure nearshore bathymetry out to moderate depths but are dependent on water clarity. However, lidar technology remains expensive and is impractical along small segments of shore and, more importantly, the high costs effectively limit the temporal resolution of the surveys and hence the ability of the end-user to understand short-term changes in beach morphology (Bernstein and others, 2003).

Within this range of technologies, the application of RTK-DGPS for surveying the morphology of both the subaerial and subaqueous portions of the beach has become the accepted standard (Morton and others, 1993; Ruggiero and Voigt, 2000; Bernstein and others, 2003; Ruggiero and others, 2005) and is the surveying technique used in this study. The GPS is a worldwide radio-navigation system formed from a constellation of 24 satellites and their ground stations, originally developed by the U.S. Department of Defense; in 2007 the Russian government made their Global Navigation Satellite System (GLONASS) satellite network available, increasing the number of satellites to ~46 (as of February 2011). In its simplest form, GPS can be thought of as triangulation with the GPS satellites acting as reference points, enabling users to calculate their position to within several meters (e.g., using inexpensive off the shelf hand-held units), while survey grade GPS units can provide positional and elevation measurements accurate to a centimeter. At least four satellites are needed to determine mathematically an exact position, although more satellites are generally available. The process is complicated because all GPS receivers are subject to error, which can significantly degrade the accuracy of the derived position. These errors include the GPS satellite orbit and clock drift plus signal delays caused by the atmosphere and ionosphere and multipath effects (where the signals bounce off features and create a poor signal). For example, hand-held autonomous receivers have positional accuracies typically less than about 10 m (<~30 ft), but can be improved to less than 5 m (<~15 ft) using the Wide Area Augmentation System (WAAS). This system is essentially a form of differential correction that accounts for the above errors, which is then broadcast through one of two geostationary satellites to WAAS-enabled GPS receivers.

Greater survey accuracies are achieved with differential GPS (DGPS) by using two or more GPS receivers to simultaneously track the same satellites, enabling comparisons to be made between two sets of observations. One receiver is typically located over a known reference point, and the position of an unknown point is determined relative to that reference point. With the more sophisticated 24-channel dual-frequency RTK-DGPS receivers, positional accuracies can be improved to the subcentimeter level when operating in static mode and to within a few centimeters when in RTK mode (i.e., as the rover GPS is moved about). In this study we used Trimble® 24-channel dual-frequency R7/R8 GPS receivers. This system consists of a GPS base station (R7), Zephyr Geodetic™ antenna (model 2), HPB450 radio modem, and

R8 "rover" GPS (**Figure 26**). Trimble (2005) reported that both the R7/R8 GPS systems have horizontal errors of approximately ±1 cm + 1 ppm (parts per million × the baseline length) and ±2 cm in the vertical.

To convert a space-based positioning system to a ground-based local grid coordinate system, a precise mathematical transformation is necessary. Although some of these adjustments are accomplished by specifying the map projection, datum, and geoid model prior to commencing a field survey, an additional transformation is necessary whereby the GPS measurements are tied to known ground control points (**Figure 27**). This step is called a GPS site calibration, such that the GPS measurements are calibrated to ground control points with known vertical and horizontal coordinates using a rigorous least-squares adjustments procedure. Calibration is initially performed in the field using the Trimble TSC2 GPS controller and then re-evaluated in the office using the Trimble Business Office software (version 3.6).

Figure 26. The Trimble R7 base station antenna in operation on the Clatsop Plains. Corrected GPS position and elevation information is then transmitted by an HPB450 Pacific Crest radio to the R8 GPS rover unit. (Photo credit: J. Allan, DOGAMI)

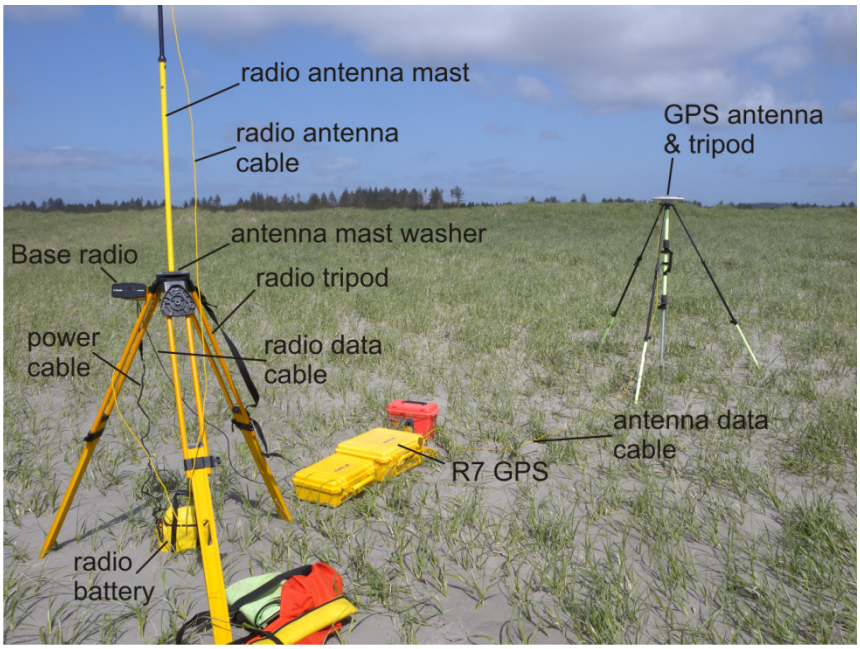

5.1.2 Cannon Beach Survey Control

Survey control in the Cannon Beach littoral cell was provided by occupying three benchmarks established by National Geodetic Survey (CANN), Watershed Sciences, Inc. (PW3), and DOGAMI (NEH8) (**Table 3**). Coordinates assigned to these monuments were derived using the Online Positioning User Service (OPUS) maintained by the NGS (http://www.ngs.noaa.gov/OPUS/). In many cases, the same benchmarks were observed multiple times and the horizontal and vertical coordinates were continually updated, while the root mean square (RMS) errors associated with the multiple reoccupations were found to be low (typically subcentimeter). More detailed information describing the derivation of local coordinates at the GPS control sites was provided by Allan and others (2015b). In all cases we used the Oregon State Plane coordinate system, northern zone (meters), while the vertical datum is relative to the North American Vertical Datum of 1988 (NAVD88).

Figure 27. A 180-epoch calibration check is performed on a survey monument. This procedure is important for bringing the survey into a local coordinate system and for reducing errors associated with the GPS survey. (Photo credit: J. Allan, DOGAMI)

Table 3. Survey benchmarks used to calibrate GPS surveys in the Cannon Beach littoral cell. BASE signifies the location of the GPS base station during each respective survey.

Benchmark Name	Northing (m)	Easting (m)	Elevation (m)
CANN (BASE)	249672.887	2231374.944	30.577
PW3	254233.448	2231555.564	3.999
NEH8	234997.630	2232106.115	9.101

Notes: Coordinates are expressed in the Oregon State Plane Coordinate System, northern zone (meters) and the vertical datum is NAVD88.

Control was provided using both horizontal and vertical values derived by averaging multiple separate GPS occupations with survey control provided by the Oregon Reference Geodetic Network (ORGN).

5.1.3 Profile Surveys

For the purposes of this study, we re-occupied 54 transects established by Allan and others (2015b) and added two new sites north of Haystack Rock/south of Ecola Creek and three new sites north of Ecola Creek (**Figure 1**). In total, 6 sites are in Falcon Cove, 13 are in the Arch Cape/Arcadia Beach subcell, and 40 are in the Tolovana/Cannon Beach area.

Having established the profile network, we located the R7 GPS base station on the CANN benchmark monument (**Table 3**), using a 2.0-m fixed-height tripod. Survey control was provided by undertaking 180 GPS epoch measurements (~3 minutes of measurement per calibration site) using the calibration sites indicated in **Table 3**, enabling us to perform a site calibration that brought the survey into a local coordinate system. This step is important in order to eliminate various survey errors that may be compounded by factors such as poor satellite geometry, multipath, and poor atmospheric conditions that, combined, increase the total error to several centimeters. After site calibration, a mapper wearing the R8 GPS rover unit mounted on a backpack measured cross-shore beach profiles. Mapping undertaken during periods of low tide, enabling more of the beach to be surveyed. **Table 4** documents dates when beach monitoring sites were measured and when lidar data were collected.

To supplement the beach surveys, lidar data measured by Watershed Sciences, Inc. in 2009 for DOGAMI were also analyzed and integrated into the beach profile data set. This was especially important for backshore areas where it was not possible to easily survey with the GPS gear. In addition, lidar data flown by NASA/NOAA/USGS in 1997, 1998, and 2002 were used to extend the time series of the beach and bluff profile data. In particular, the 1998 lidar data measured at the end of the major 1997-1998 El Niño was analyzed, providing additional measurements of the beach in an eroded state that can be compared with more recent winter surveys of the beach. The 1997, 1998, 2002, 2010, and 2016 lidar data were downloaded from the NOAA Coastal Service Center (http://www.csc.noaa.gov/digitalcoast/data/coastallidar/index.html) and gridded in ArcGIS using a nearest-neighbor algorithm to produce a digital elevation model (DEM). Distance and elevation data were then extracted from the lidar DEM.

Table 4. Dates when beach surveys and mapping efforts were undertaken.

Measurement Date	Type
October 1997	lidar (NASA/NOAA/USGS)
April 1998	lidar (NASA/NOAA/USGS)
September 2002	lidar (NASA/NOAA/USGS)
September 2009	lidar (DOGAMI)
August 2010	lidar (USACE)
September 10, 2010	RTK-DGPS
March 24, 2011	RTK-DGPS
September 29, 2015	RTK-DGPS
March 31, 2016	RTK-DGPS
March-April 2016	lidar (USGS)

Notes: Lidar data collected by NASA/NOAA/USGS in 1997, 1998, and 2002 have a point density of ~1 point/m^2; lidar data collected by DOGAMI in 2009 and by the USGS in 2016 have a point density of ~8 points/m^2.

The approach used to measure the cross-shore beach profiles typically consisted of walking from the landward edge of the primary dune or bluff edge, down the beach face, and out into the swash zone. Where dunes are present, our survey lines allow us to traverse the dunes, enabling the backshore topography to be measured. Conversely, because many coastal bluffs on the Oregon coast are too high to allow for safe navigation by the mapper down the bluff face, in these areas we rely on lidar to capture morphological changes. In all cases, a straight line perpendicular to the shore was achieved by navigating along a predetermined line displayed on a hand-held Trimble TSC2 computer connected to the R8 receiver. The computer shows the position of the operator relative to the survey line and indicates the deviation of the GPS operator from the line. The horizontal variability during the survey is generally minor, being typically less than about ±0.25 m (0.8 ft) either side of the line, which results in negligible vertical uncertainties due to the relatively uniform nature of beaches characteristic of much of the Oregon coast (Allan and others, 2015b). From our previous research at numerous sites along the Oregon coast, this method of surveying can reliably detect elevation changes on the order of 4 to 5 cm (0.13 to 0.16 ft), that is, well below normal seasonal changes in beach elevation, which typically varies by 1 to 2 m (3 to 6 ft) (Ruggiero and others, 2005; Allan and Hart, 2007, 2008).

Analysis of the beach survey data involved a number of stages. The data were first processed in Trimble Business Center (TBC) software and then exported in comma-delimited form. The xyz values were then imported into MathWorks® MATLAB® environment (a suite of computer programming languages) using a customized script and further processed. A least-squares linear regression was fit to the profile data. The purpose of this script is to examine the reduced data and eliminate data point residuals that exceed a ±0.75 m (±2.5 ft) threshold (i.e., the outliers) either side of the predetermined profile line. The data are then exported into a Microsoft® Excel® database for archiving purposes. A second MATLAB script uses the Excel profile database to plot the survey data (relative to the earlier surveys) and outputs the generated figure as a Portable Network Graphics (PNG) file. The **Appendix: Cannon Beach Profiles** shows the reduced beach profile plots for the Cannon Beach transects; these data may also be viewed online via the NANOOS Beach and Shoreline Change mapping portal (http://nvs.nanoos.org/BeachMapping).

5.2 Beach Characterization

Analyses of the beach profile data were undertaken in order to quantify various physical characteristics of the beaches. These included heights of the primary dunes and bluffs backing the beach, the beach-dune junction (E_j) elevations and positions, and the slope of the beach (tan β). Beach slope was determined by fitting a linear regression through the measured GPS data. In all cases, the slope of the beach face was determined to be the region of the beach located between mean sea level (~1.4 m, MLLW) and the highest observed tide (~3.8 m, MLLW), an approach that is consistent with methodologies adopted by Ruggiero and others (2005) and Stockdon and others (2006). Beach-dune junction (E_j) locations were determined by assessing the major breaks in slope between the seaward face of the dune and the more gently sloping beach face (Allan and others, 2015b). For most sites along the Oregon coast, beach-dune junctions (E_j) typically occur at elevations between about 4 and 6 m (13 and 20 ft, NAVD88). **Figure 28** provides an example of repeat surveys undertaken at the Cannon Beach 35 profile site, located north of Ecola Creek. In this example, the two earliest surveys occurred in 1997 and 1998 (pre- and post-El Niño), and show little change between the surveys. Evident also is the considerable amount of accretion that has taken place over the past 19 years, with the dune face having advanced seaward by ~38 m (125 ft) since 1997 as measured at the 10 m (33 ft) contour elevation. Of interest, the dune crest height did not change appreciably between 1997 and 2010 (**Figure 28**). However, since 2010 the dune has built vertically by about

1.5 m (4.9 ft). Furthermore, it is apparent that additional dune building has been occurring on the seaward face of the dune (below the 10 m [33 ft] contour, **Figure 28**). We speculate that some of this sand accumulation is due to anthropogenic lowering of the dune crest, with the sand being bulldozed seaward over the front face of the dune, where the sand has generally remained.

Figure 28 also identifies the positions of the beach-dune junction (E_j) over time. Examination of these data indicates that the beach-dune junction (E_j) has varied in elevation, a function of repeated phases of both erosion and accretion events. As of late winter 2016, a steep erosion scarp had formed, and the beach-dune junction reflected the toe of the scarp, located at an elevation of 5 m (16.4 ft; black star in **Figure 28**). Two other characteristics of **Figure 28** are worth noting. First, the dark gray shaded region depicts the typical range of beach variability about the mean profile. This range is based on measured changes that occurred between 2009 and the present. This range depicts the seasonal variability in the beach that occurs between summer and winter. Second, the yellow-gray shading denotes the maximum/minimum measured changes identified from all surveys between 2009 and the present, providing an initial reference point on which to base subsequent comparisons. However, in both cases because the measured record reflects a few discrete points in time, the identified ranges are likely to be on the low side, such that much larger responses would not be unusual.

Figure 28. Plot showing beach-dune junctions (stars) identified from various surveys at the Cannon Beach 35 profile site. Dark gray shading denotes the normal range of variability (mean profile ±1σ range), while the yellow-gray indicates the maximum/minimum measurements determined from all surveys (latter excludes surveys undertaken in 1997 and 1998). E_j is beach-dune or beach-bluff junction elevation, MHHW is mean higher high water, MLLW is mean lower low water, and NAVD88 is North American Vertical Datum of 1988.

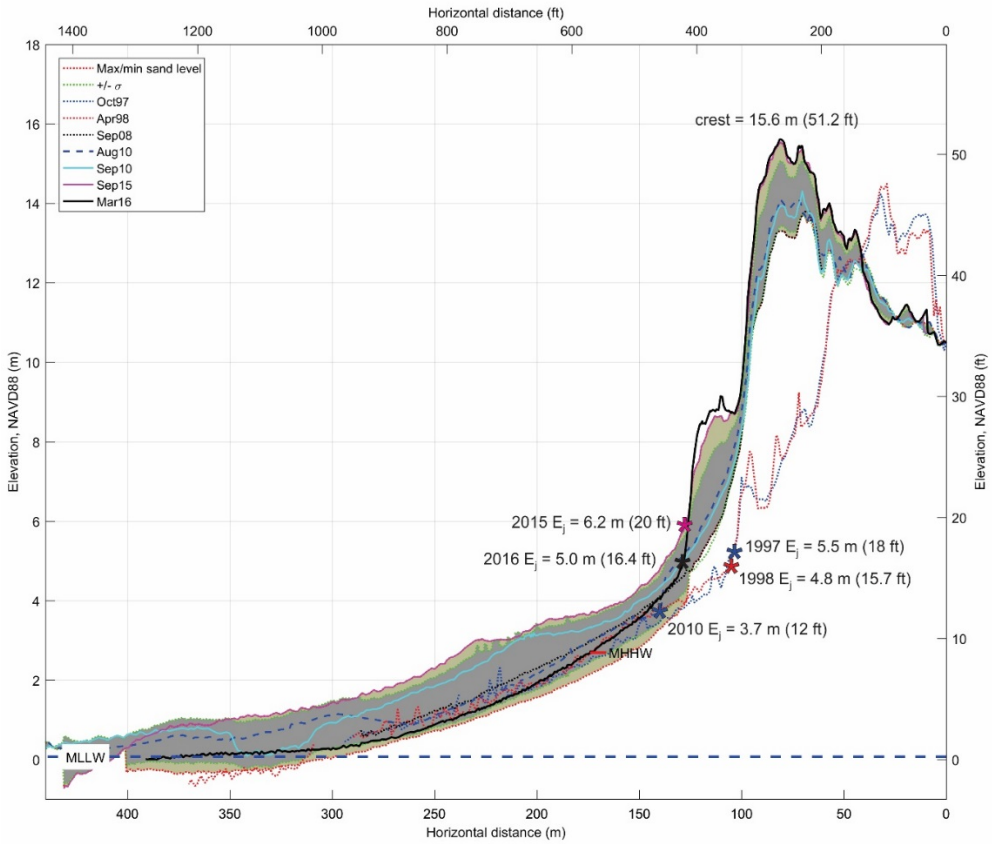

Figure 29 provides a plot of the alongshore changes in beach slopes (tan β), mean sediment grain sizes (M_z), beach-dune and beach-bluff junction (E_j) elevations, and the dune crest and/or bluff top heights along the length of the Cannon Beach cell. In general, the steepest slopes (e.g., Falcon Cove and Arch Cape) are confined to those beaches with coarse sediments (gravels) on the foreshore, while sites exhibiting generally lower beach slopes typically occur near the mouths of estuaries and creeks (e.g., Ecola Creek). At many beach study sites, sediment grain sizes vary both in the alongshore and cross-shore directions. For example, at Arch Cape a substantial gravel berm is present on the upper foreshore that backs a wide sandy beach (**Figure 18**), providing significant protection to the backshore (Allan and others, 2005). Such beach types are characterized as "composite" using the naming convention of Jennings and Shulmeister (2002), such that they consist of a wide dissipative sandy beach composed of fine to medium sand (mean grain sizes (M_z) range from 2.8Ø to 2.1Ø (0.14 to 0.23 mm [Peterson and others, 1994]), **Figure 29**), backed by a thin veneer of gravel on the upper foreshore. North of Hug Point, the beaches become increasingly dissipative, such that they are more gently sloping (**Figure 29**). Nevertheless, much of this shoreline still contains a thin veneer of gravel at the back of the beach that is most exposed at the end of the winter, when the beaches are in their most eroded state.

The gravel beach at Falcon Cove is without doubt one of the more dramatic examples of a gravel (predominantly cobble) beach on the Oregon coast. Along much of its length the cobble beach fronts an actively eroding bluff. At least two homes have had to be moved landward, and several other homes remain threatened. At the north end of the beach, the gravel forms a barrier beach that has impounded a small lake behind it. However, the site is subject to frequent overtopping, as evidenced by the many logs and debris along the crest of the berm and on its landward side leading into the lake. The beach is actively being fed by gravel and boulders from the south end of the cell in the form of landslides off Cape Falcon, while the south central portion of Cove Beach is primarily supplying sand and colluvial material to the system. As material is released from Cape Falcon, the sediment is rapidly transported northward along the beach where it is assimilated into the gravel beach (**Figure 30**). Gravels are also being supplied by the bluff immediately north of the lake. The gravel beach is characterized by a wide range of grain sizes, from coarse sand and granules to large cobbles and boulders. The sediment is classified as "well sorted," which indicates a uniform mixing of the predominant grain sizes present on the beach. Mean grain sizes (M_z) ranged from –5.74Ø (53 mm) in the south to –6.19Ø (73 mm) in the north. **Figure 29** indicates that the beaches in Falcon Cove are very steep, varying from ~9° to 14° (tan β = 0.16 to 0.26; 15.8% to 24.9% slope), which is entirely a function of the coarse nature of the sediments present along this subcell.

Figure 29 also plots the beach-dune and beach-bluff junction elevations (E_j) for the study sites. In general, values for beach-bluff junction elevations tend to be highest along the shores of Falcon Cove and parts of Arch Cape (mean = 5.6 to 6.4 m [18 to 21 ft]). In contrast, the lowest E_j values are confined to much of the Cannon Beach shore (mean = 4.75 m [15.6 ft]). **Figure 29** also identifies the bluff top and/or dune crest heights. Not surprisingly, these heights vary substantially, with the lowest crest heights in the vicinity of Tolovana and in Cannon Beach and the highest dunes north of Ecola Creek. Along the remainder of the shore, the beaches are protected by prominent bluffs (e.g., Falcon Cove) with crest elevations that range from 14 to 21 m (46 to 69 ft).

Figure 29. Alongshore changes in beach slopes (tan β), beach-dune junction (E_j) elevations, and dune/bluff crest/tops along the Cannon Beach cell. Red squares indicate mean sediment grain sizes measured by Peterson and others (1994). Note: tan β slope of 0.1 = a 10% slope.

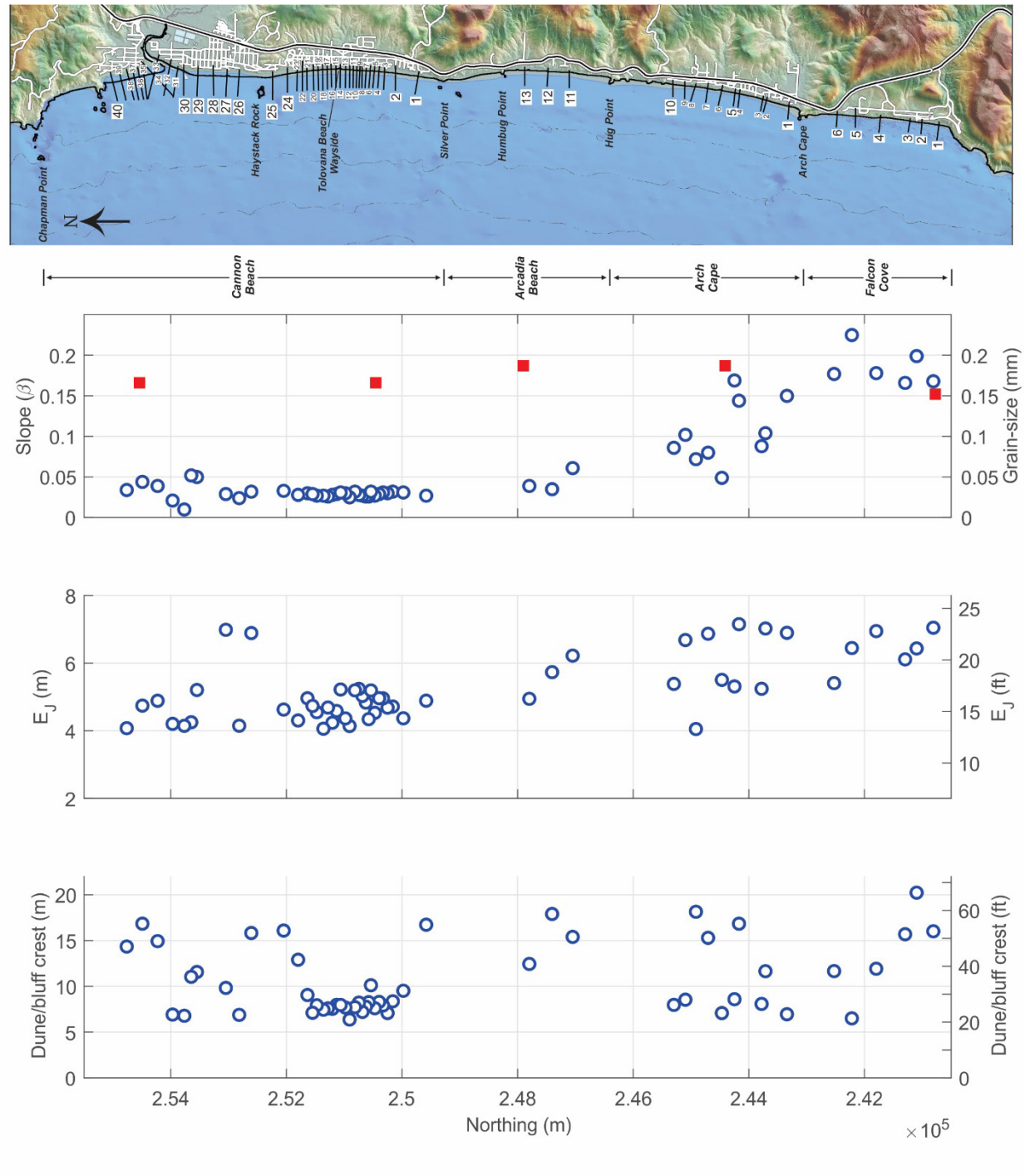

Figure 30. ***(A)*** **Recent landsliding at the south end of Falcon Cove, and** ***(B)*** **bluff erosion to the north that is actively supplying new sediment (predominantly gravels) to the littoral system. (Photo credit: J. Allan, DOGAMI, March 2016)**

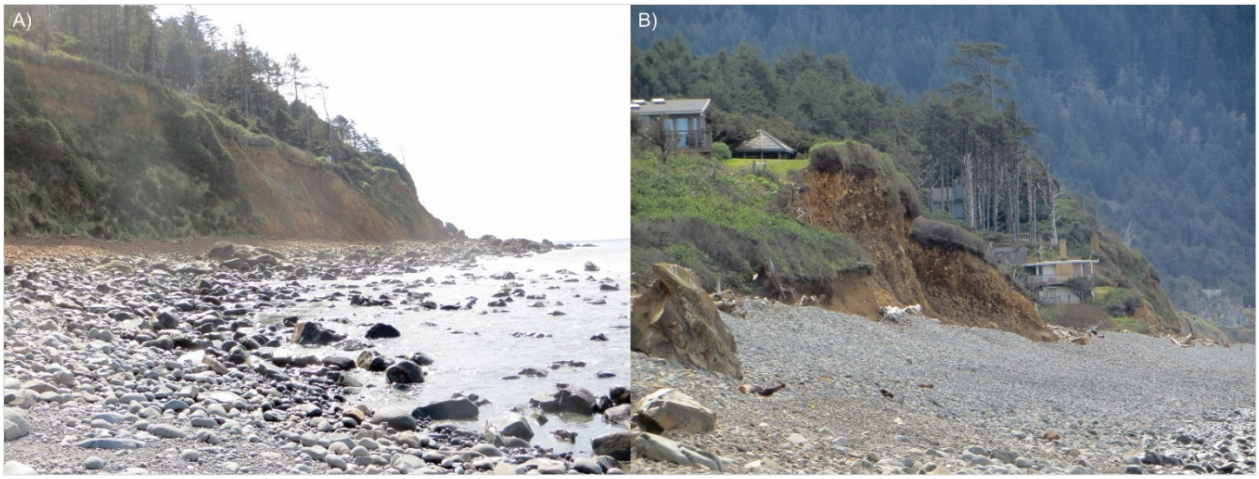

5.3 Recent Beach and Shoreline Changes in the Cannon Beach Littoral Cell

Here we present a brief discussion of recent coastal changes in the Cannon Beach littoral cell. The assessment is based on repeat beach surveys at discrete Cannon Beach (CB) transect locations since 1997, as well as analyses of changes in the position of the 6 m (19.7 ft) contour between 1997 and 2009. The 6 m (19.7 ft) elevation contour is used here because it is an excellent proxy for capturing the effects of major storms.

Figure 31 shows the profile changes measured at four transect sites north of Ecola Creek, south of Chapman Point: CB34, CB35, CB37, and CB39. Site locations are shown in **Figure 1**. From south to north, each transect highlights the degree of sand buildup that has occurred since 1997. By far the largest sand accumulation has occurred in the south at CB34 and CB35 (adjacent to Ecola Creek), which has caused the foredune to build and advance seaward. Measurements indicate that the foredune has built seaward by 42 m (139 ft) at CB34 and 25 m (81 ft) at CB35.

More recent changes (post 2009) are highlighted by the shaded gray zone included in **Figure 31**. Below the 6 m (19.7 ft) contour, this shaded region effectively captures the interannual variability in the elevation of the beach. This response reflects the buildup of sand over the summer and subsequent erosion and removal offshore in the winter. In contrast, changes taking place above the 6 m (19.7 ft) contour essentially characterize the long-term accumulation of sand on the dune. The exceptions to this are those periodic occasions when the dune may be artificially lowered by dune grading. For example, at CB34 adjacent to Ecola Creek it is evident that the dune was lowered sometime after 1998, with the sand removed seaward. This is shown by the removal of the 1998 dune crest, and the relatively broad flat crest at the ~11 m (36 ft) contour; the region of grading extends from the condominiums seaward some 70 m (235 ft) toward the west. Since about 2010, new sand has begun to accumulate at the seaward edge of the dune, further raising its crest.

Modifications to the dune crest appear to also characterize the CB35 transect, which was modified after the 1997-1998 El Niño. In contrast, there does not appear to have been any apparent dune grading north of CB35. Finally, three of the transects (CB34, CB35, and CB39) capture the effects of the 2015-2016 winter, with the presence of a near vertical scarp, indicating that wave runup reached and eroded the toe of the dune.

Analyses of shoreline changes as defined at the 6 m (19.7 ft) contour is presented in **Figure 32** for the entire littoral cell. These results are the product of changes in the position of the 6 m (19.7 ft) contour between 1997 and 2009 and were derived from lidar. As can be seen in the figure, the results confirm that significant accretion has occurred immediately north of Ecola Creek, with the amount of accretion decreasing toward Chapman Point. The amount of shoreline advance reaches a maximum of 42 m (139 ft) immediately next to the creek, decreasing rapidly to the north where it averages ~14 m (46 ft) between CB36 and CB38, and ~3.8 m (12.4 ft) north of CB38. Accretion also characterizes the section of shore to the north of Haystack Rock and south of Ecola Creek (north of the CB26 profile site, **Figure 1**).

Figure 31. Beach morphological changes as measured by DOGAMI between 1997 and 2016 for selected sites in the Cannon Beach cell, north of Ecola Creek. Dark gray shading denotes the normal range of variability (mean profile ±1σ range), while yellow-gray shading indicates the maximum/minimum measurements determined from all surveys (latter excludes surveys undertaken in 1997 and 1998). MHHW is mean higher high water.

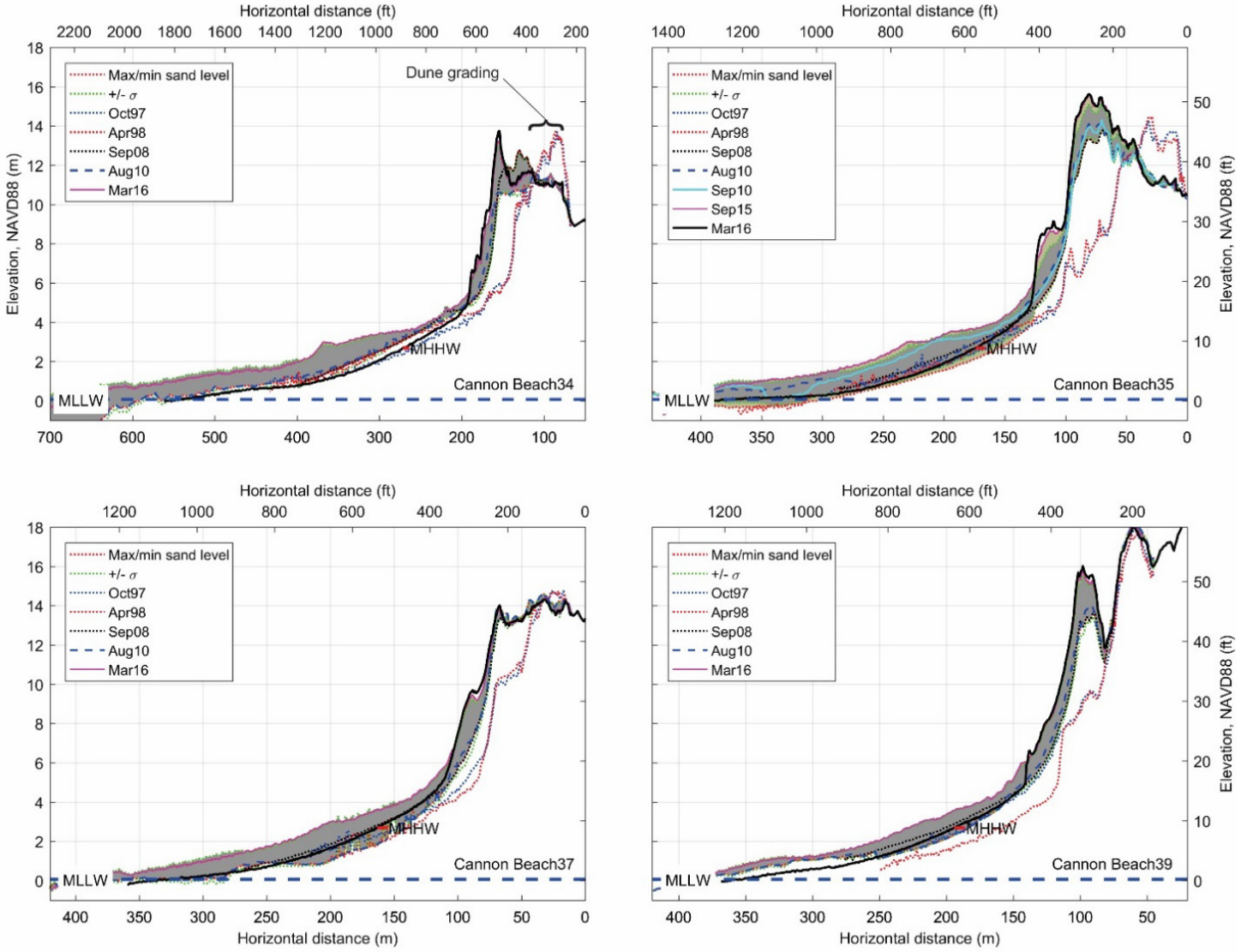

Analyses of shoreline changes as defined at the 6 m (19.7 ft) contour are presented in **Figure 32** for the entire littoral cell. These results are the product of changes in the position of the 6 m (19.7 ft) contour between 1997 and 2009 and were derived from lidar. As can be seen in the figure, the results confirm that significant accretion has occurred immediately north of Ecola Creek, with the amount of accretion decreasing toward Chapman Point. The amount of shoreline advance reaches a maximum of 42 m (139 ft) immediately next to the creek but decreases rapidly to the north, where it averages ~14 m (46 ft) between CB36 and CB38 and ~3.8 m (12.4 ft) north of CB38. Accretion also characterizes the section of shore to the north of Haystack Rock and south of Ecola Creek (north of the CB26 profile site, **Figure 1**).

Figure 32. Net shoreline excursions along the Cannon Beach littoral cell as measured at the 6 m (19.7 ft) contour for the period 1997–2009. Blue dots indicate accretion (seaward advance of the contour), while red dots indicate erosion (landward retreat). Light blue stripe denotes the location of Ecola Creek; the gray stripes denote the locations of Silver Point, Hug Point, and Arch Cape.

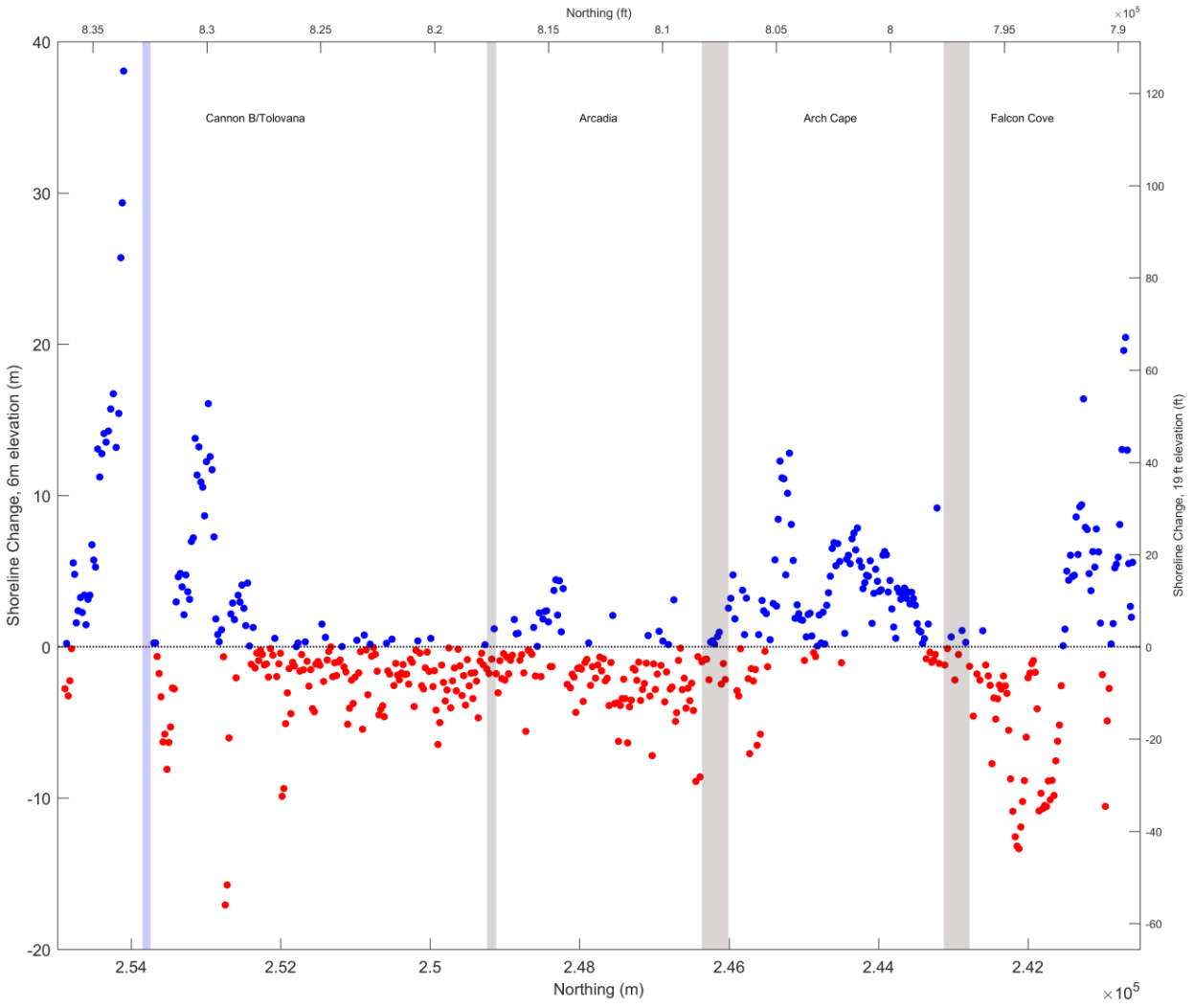

Much of the shoreline south of Haystack Rock and north of Silver Point has experienced predominantly erosion, ranging from negligible to several meters over the past 12 years. The average change in this region is -1.8 m (6 ft) between 1997 and 2009. This pattern also characterizes much of the shore between Arcadia Beach and Arch Cape. Again, the degree of erosion over the past decade is relatively small. In contrast, beaches in the Arch Cape subcell (south of Hug Point, north of Arch Cape) are mostly stable, having accreted several meters as the gravel berm gained sediment and built higher. Finally, shoreline changes in Falcon Cove indicate significant erosion (up to 15 m [49 ft] of retreat) in the central to northern half of the cell, while the south end is considered to be relatively stable, having gained additional cobble. However, these latter responses probably reflect mostly fluctuations in the position and volume of the cobble berm that fronts the bluffs. For example, analyses of beach profile measurements in this area indicate that the bluffs themselves have eroded several meters during the past 15 years.

5.4 Sand Volume Changes in the Cannon Beach Littoral Cell

To better understand changes in the volumes of sediment within the Cannon Beach cell, analyses have been undertaken of lidar collected in 1997, 1998, 2002, and 2009; lidar data collected in 2010 was ignored as these data are considered to be less reliable. Lidar collected in 1997, 1998, and 2002 are described as single-return only. This means that the returned laser pulse will be associated with the highest feature in the landscape, which could include features such as treetops or the top of a building. However, the first return can also represent the ground itself, assuming the lidar pulse is able to penetrate through a canopy and then be reflected by the ground surface. This is possible in areas where the vegetation cover is scrubby (e.g., grasses), enabling the laser to penetrate all the way to the ground. Regardless, care must be taken when interpreting lidar measured in 1997, 1998, and 2002 in areas away from the beach. This contrasts with lidar collected in 2009, which is characterized as multi-return lidar, enabling the vegetation to be stripped out to render a bare-earth digital representation of the ground surface.

High-resolution (8 points/m^2) lidar was flown along the Oregon coast in March-April 2016 (**Table 5**). Like the data collected by DOGAMI in 2009, these 2016 data are multi-return lidar that allow one to extrapolate a bare-earth model of the ground. These 2016 measurements enable us to better document changes that have taken place since 2009. This is important since the past 5 years have been dominated by relatively mild winters that have contributed to significant beach and dune building along the coast.

The approach undertaken here focused on volume changes occurring above the 4 m (13 ft) contour to the back edge of the dunes, physical features such as concrete paths, back edge of gravel berms, or the bluff toe. The decision to ignore changes taking place in the intertidal zone (below 4 m [13 ft]) is based on the knowledge that this lower region is largely dominated by seasonal fluctuations and that the more lasting changes are seen higher on the back of the beach. In addition, the 2009 and 2016 lidar flights were not flown at low tide and thus the DEM includes effects from the ocean measured at the time of the survey.

To assist with the volume analysis, the Cannon Beach cell was divided into 10 discrete compartments (**Figure 33**) and the volume of material present in each compartment and year determined. **Figure 33** also includes the net volume change measured between 1997 and 2016. Using this approach, we are able to minimize the vegetation error that is present in the earlier lidar data by focusing on those areas where there is an absence of dense vegetation (i.e., we can target the more open areas dominated by dune grass that likely allow for some of the lidar points measured to reflect true ground). We used 1997 data as our baseline for comparison. **Table 5** summarizes the calculated volume changes identified in each compartment along the Cannon Beach littoral cell, while **Table 6** presents a summary for the entire littoral cell.

Figure 33. Beach sand volume compartments identified for the Cannon Beach littoral cell showing the net sand volume change from 1997 to 2016. Green indicates accretion, red denotes erosion. Sand volumes are calculated for the area above the 4 m (13 ft) contour to the back edge of the dunes, physical features such as concrete paths, back edge of gravel berms, or the bluff toe.

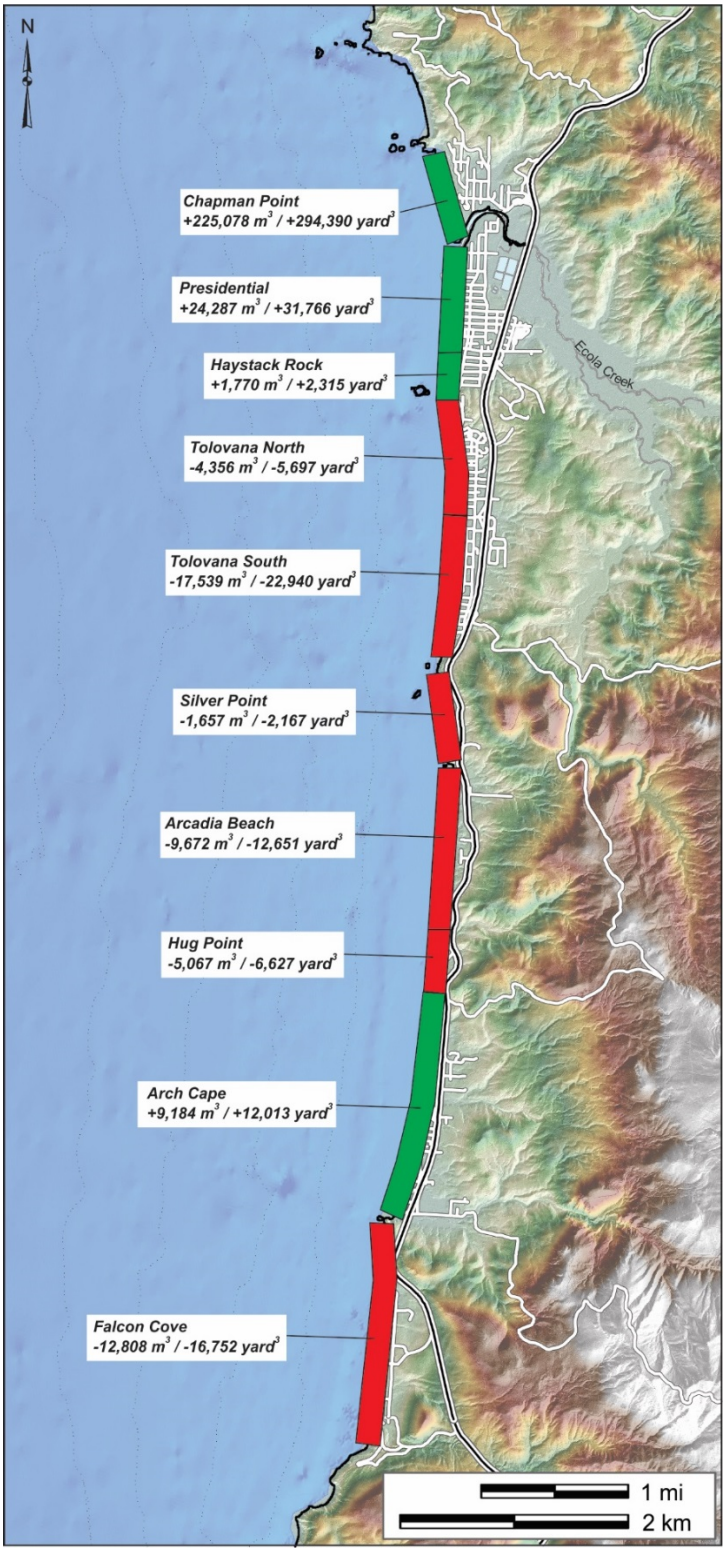

Table 5. Net volume change estimates derived from analyses of 1997, 1998, 2002, 2009, and 2016 lidar data for discrete shoreline compartments. The sand volume baseline is relative to 1997. Sand volumes are calculated for the area above the 4 m (13 ft) contour to the back edge of the dunes, physical features such as concrete paths, back edge of gravel berms, or the bluff toe.

Region	Year	Volume Change (m^3)	Volume Change (yd^3)	Region	Year	Volume Change (m^3)	Volume Change (yd^3)
Chapman Point	1997	0	0	Silver Point	1997	0	0
	1998	−3,458	−4,523		1998	−2,978	−3,896
	2002	19,228	25,150		2002	930	1,216
	2009	119,310	156,051		2009	−868	−1,136
	2016	225,078	294,390		2016	−1,657	−2,167
Presidential	1997	0	0	Arcadia Beach	1997	0	0
	1998	−3,642	−4,763		1998	−4,207	−5,502
	2002	345	451		2002	−12,872	−16,836
	2009	13,138	17,184		2009	−13,174	−17,231
	2016	24,287	31,766		2016	−9,672	−12,651
Haystack Rock	1997	0	0	Hug Point State Park	1997	0	0
	1998	−2,639	−3,449		1998	−8,255	−10,798
	2002	−9,765	−12,772		2002	−2,769	−3,621
	2009	−3,895	−5,095		2009	−2,945	−3,852
	2016	1,770	2,315		2016	−5,067	−6,627
Tolovana North	1997	0	0	Arch Cape	1997	0	0
	1998	−11,050	−14,453		1998	−9,552	−12,494
	2002	−15,834	−20,710		2002	13,952	18,248
	2009	−10,665	−13,948		2009	14,743	19,283
	2016	−4,356	−5,697		2016	9,184	12,013
Tolovana South	1997	0	0	Falcon Cove	1997	0	0
	1998	−1,359	−1,777		1998	5,326	6,966
	2002	−23,813	−31,146		2002	2,365	3,093
	2009	−13,266	−17,351		2009	−4,967	−6,497
	2016	−17,539	−22,940		2016	−12,808	−16,752

Table 6. Volume change estimates derived from analyses of 1997, 1998, 2002, 2009, and 2016 lidar data for the entire Cannon Beach cell. Sand volumes are calculated for the area above the 4 m (13 ft) contour to the back edge of the dunes, physical features such as concrete paths, back edge of gravel berms, or the bluff toe.

		Year	Volume Change* (m^3)	Volume Change (yd^3)
		1997	0	0
		1998	−41,812	−54,734
		2002	−28,233	−36,927
		2009	97,410	127,408
Cannon Beach Cell		2016	209,220	273,649
	1997 to 1998	*1997 to 2002*	*1997 to 2009*	*1997 to 2016*
Net gain (m^3)	5,326	36,819	147,190	260,320
Net loss (m^3)	−47,138	−65,052	−49,780	−51,100
Net gain (yd^3)	6,966	48,157	192,518	340,485
Net loss (yd^3)	−61,655	−85,085	−65,110	−66,836

*Volume change estimates are relative to 1997.

Figure 34 presents in graphical form the data listed in **Table 5**, allowing for more direct comparisons of the changes taking place along the Cannon Beach littoral cell. These data are presented in two forms:

- (Figure 34A) net volume change for four periods:
  - 1997 to 1998 (El Niño);
  - 1997 to 2002 (includes the effects of the extreme 1998-1999 winter storms);
  - 1997 to 2009; and,
  - 1997 to 2016.
- (Figure34B) net volume change for each of the *inter-survey* periods:
  - 1997 to 1998 (El Niño);
  - 1998 to 2002 (includes the effects of the extreme 1998-1999 winter storms);
  - 2002 to 2009; and,
  - 2009 to 2016.

We identify several interesting characteristics about the sediment volume in the Cannon Beach cell:

- The total volume of sand contained in the Cannon Beach littoral cell measured between the 6 m (19 ft) contour (approximately the dune or bluff toe) and MLLW is 3.6×10^6 m^3 (4.67×10^6 yards^3). This volume estimate is determined from our repeat transect surveys undertaken in summer 2015 and will vary from year to year. Incorporating the volume of sand contained in the dunes (i.e., above the 6 m [19 ft] contour) increases the total volume of sand to ~4.2×10^6 m^3 (5.4×10^6 yards^3), consistent with estimates made by Rosenfeld (1997);
- The seasonal exchange of sand on the beach between September 2015 (late summer) and March 2016 (late winter) was ~2.0×10^6 m^3 (2.6×10^6 yards^3). However, this estimate will vary from year to year as it is dependent on seasonal variations in winter (i.e., storminess) and summer waves; and,
- The total volume of beach sand north of Silver Point is approximately twice as much as the amount of beach sand to the south of the point. This is consistent with observations by Rosenfeld (1997).

With respect to the effects of the 1997-1998 El Niño, we identified the following:

- During the 1997-1998 El Niño, the back of the beach lost ~41,812 m^3 (~54,734 yards^3) of sediment in the entire littoral cell (**Table 6**, **Figure 34**). Given the strength of the El Niño and the impacts observed elsewehere on the Oregon coast, the 1997-1998 El Nino did not significantly affect the beaches in the Cannon Beach cell; and,
- With the exception of the Falcon Cove subcell in the south, which gained ~5,300 m^3 (~7,000 yards^3) of sediment over the 1997-1998 El Niño winter, all areas experienced net erosion during this period (**Table 5**).

With the transition from El Niño to La Nina/neutral type conditions between 1998 and 2002, the following occurred:

- Erosion continued to dominate the beaches between Haystack Rock and Arcadia Beach. These beaches lost an additional ~39,122 m^3 (51,170 yards^3) of sand;
- In contrast, the Chapman Point and Presidential compartments (combined ~+26,700 m^3 [34,900 yards^3]) as well as the Arch Cape subcell (+23,500 m^3 [30,700 yards^3] gained sand (**Figure 34B**); and,
- The overall change between 1998 and 2002 across the entire cell reflected a net sediment gain of ~13,600 m^3 (17,800 yards^3). However, due to the degree of erosion that took place in the 1997-1998 El Niño and ongoing erosion between Haystack Rock and Arcadia Beach, the Cannon Beach littoral cell remained in a state of deficit of ~−28,300 m^3 (37,000 yards^3)(**Table 6**). In summary, by summer 2002 the beaches had still not yet fully recovered.

Figure 34. Beach volume changes in the Cannon Beach littoral cell, divided into 10 sub-regions. *A)* net volume change for four periods: 1997 to 1998 (El Niño), 1997 to 2002 (includes the effects of the extreme 1998-1999 winter storms), 1997 to 2009, and 1997 to 2016; *B)* net volume changes for each of the inter-survey period: 1997 to 1998, 1998 to 2002, 2002 to 2009, and 2009 to 2016. Sand volumes are calculated for the area above the 4 m (13 ft) contour to the back edge of the dunes, physical features such as concrete paths, back edge of gravel berms, or the bluff toe.

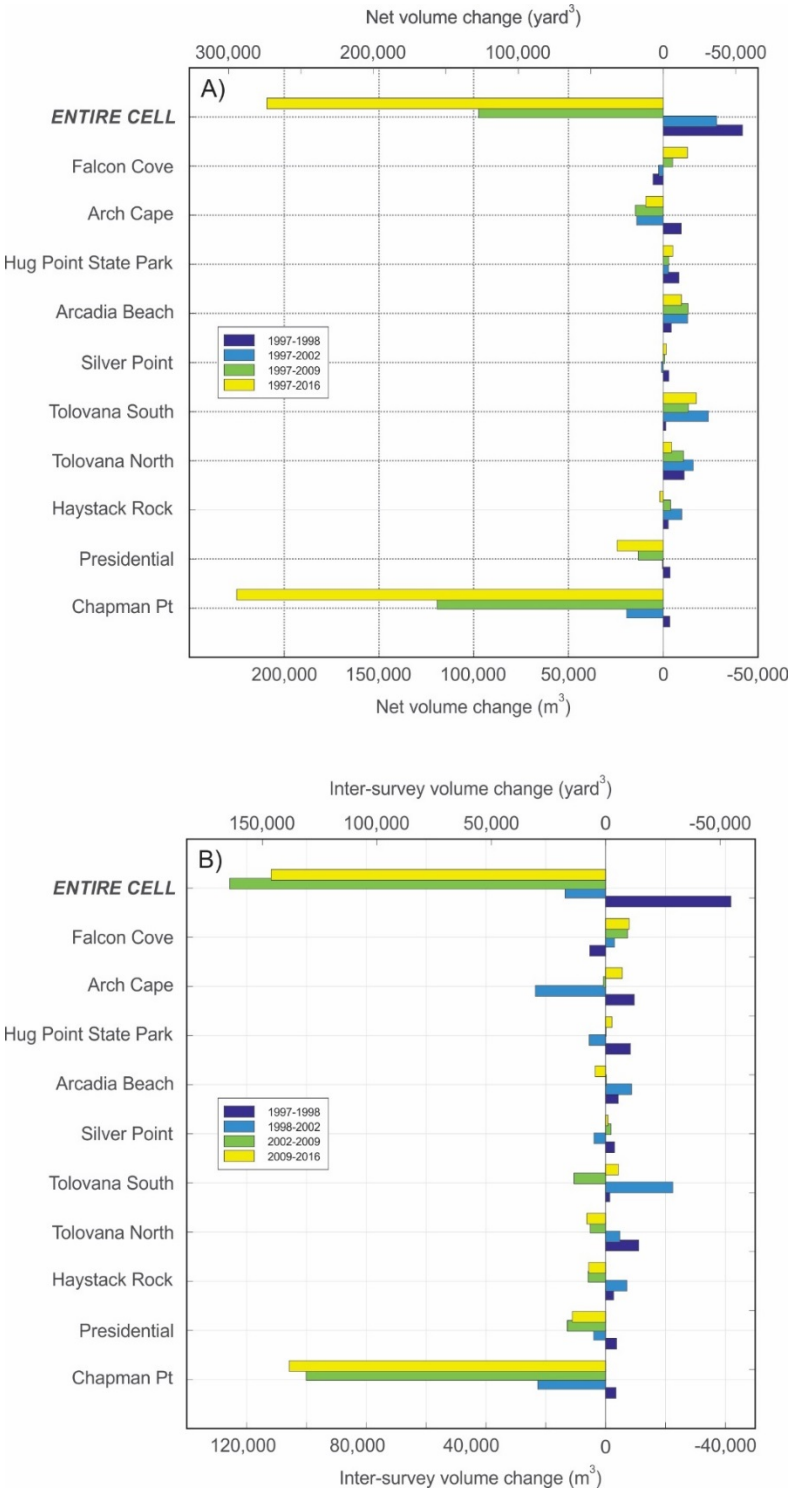

Between 2002 and 2009, summer and winter wave conditions reverted back to more typical seasonal states, which have contributed to the following responses:

- The Cannon Beach littoral cell gained ~125,700 m^3 (164,300 $yards^3$) of sediment over this period (**Figure 34B**, *green bar, entire cell*). Relative to the 1997 baseline, this amounted to a net gain of ~97,400 m^3 (127,400 $yards^3$) overall (**Table 6**);
- Positive sediment gains occurred north of Silver Point (**Figure 34**B), with the largest accumulation of sediment north of Ecola Creek in the Chapman Point region: ~119,300 m^3 (156,000 $yards^3$) of sediment by 2009 (**Table 5**). Significant sand volume gains also occurred in the Presidential dune management area, which accumulated ~13,100 m^3 (17,200 $yards^3$) of sediment;
- **Figure 35** shows the degree of elevation changes (analogous to volume gains) that occurred in the Chapman Point and Presidential dune management compartments from 1997 to 2009. Significant sand gains occurred immediately north of Ecola Creek, with the dune having built vertically by ~3 to 5 m (10 to 16 ft), while some areas at the distal south end accreted by up to 6 m (~20 ft, red shading, **Figure 35**). Smaller accumulations occurred in the Presidential dune management area with elevations gains being typically ~1 to 3 m (3 to 10 ft);
- The northern end of the Presidential dune management compartment has generally lost sand, with the dune there have been lowered by ~1 to 2 m (3 to 6 ft) since 1997. Dune lowering along the dune crest is likely due to dune grading activities, while erosion along the toe of the dune is a product of wave erosion coupled with scour caused by Ecola Creek; and,
- Interestingly, the central portion of the Cannon Beach cell (north of Hug Point and south of Haystack Rock) has been eroding. However, the amount of erosion that has taken place in this area reflects about 38% of the total sand volume that has accumulated in the Chapman Point area. This indicates that much of the sand that has been accumulating north of Haystack Rock is probably locally derived from the beach and nearshore region (i.e., the surf zone to depths of 10 to 15 m (30 to 45 ft). Unfortunately, because we do not have repeat measurements of sediment changes across the surf zone we are unable to define exactly the sources of all the sediment.

Since 2009, winter wave conditions have generally become milder, characterized by few large storms. These changes have probably contributed to the following responses:

- The Cannon Beach littoral cell gained an additional ~111,800 m^3 (146,230 $yards^3$) of sediment since 2009 (**Figure 34B**, *yellow bar, entire cell*). Relative to the 1997 baseline, this amounted to a net gain of ~209,220 m^3 (273,649 $yards^3$) (**Table 6**);
- Positive sediment gains occurred in all areas north of Tolovana Park (**Figure 34**B), with the largest accumulation of sediment occurring north of Ecola Creek in the Chapman Point region: ~105,770 m^3 (138,340 $yards^3$) of sediment since 2009 (**Table 5**). This means the Chapman Point sub-region has accumulated ~225,080 m^3 (294,390 $yards^3$) of sediment since 1997.
- Sand volume gains also continued in the Presidential dune management area, which gained ~11,150 m^3 (14,580 $yards^3$) of sediment since 2009; the net gain in this sub-region is +24,287 m^3 (31,766 $yards^3$) of sand since 1997;
- **Figure 36** shows the degree of elevation changes (analogous to volume gains) that occurred in the Chapman Point and Presidential dune management compartments from 2009 to 2016. Significant dune building has continued since 2009 north of Ecola Creek in the Chapman Point region, with the dune having built vertically by ~3 to 5 m (10 to 16 ft). Unlike the 1997 to 2009 period shown in **Figure 35**, the degree of dune building is widespread throughout the area. **Figure 36** also indicates the most significant area of dune building is to the southwest of W. 5th

Street. Sand accumulations have also continued to occur in the Preesidential dune management area with elevations gains being typically ~1 to 2 m (3 to 6 ft), while the landward edge of this region has been lowered by ~1 m (3 ft). The latter may be due to dune grading;

- Net gains of sand were also observed in the Haystack Rock (~5,670 m^3 [7,416 yards^3]), Tolovana North (~6,310 m^3 [8,253 yards^3]), and Arcadia Beach (~3,500 m^3 [4,578 yards^3]) sub-region areas (**Table 5**); and,
- Net sand losses continue to dominate the Falcon Cove sub-region (~7,840 m^3 [10,256 yards^3]), while the Arch Cape beach also lost a significant amount of its sand reserve (~5,560 m^3 [7,272 yards^3]) (**Table 5**).

Figure 35. Sand elevation changes in the Chapman Point *(left)* and Presidential *(right)* dune management areas from 1997 to 2009. Hot colors reflect sediment gains; cooler colors reflect erosion. Gray boxes denote buildings.

Figure 36. Sand elevation changes in the Chapman Point *(left)* and Presidential *(right)* dune management areas from 2009 to 2016. Hot colors reflect sediment gains; cooler colors reflect erosion. Gray boxes denote buildings.

Given the amount of sand that has accumulated north of Ecola Creek, we explore the volume of sand present throughout the Chapman Point compartment in more detail to better assess the volume of sand present at different elevations. This is accomplished by subdividing the Chapman Point compartment into three sub-regions (**Figure 36**) and comparing those data to the volume of sand contained in the entire area. Sub-region 1 extends from Ecola Creek north to about the CB35 transect, while sub-region 2 extends north to just south of CB37; sub-region 3 includes the remaining portion of the Chapman Point dune management area. Sand volumes are presented in **Table 7** for the entire region and for the two sub-regions. Based on these data, we note the following:

- The total sand volume in the Chapman Point area above the 4 m (13 ft) contour is ~608,700 m^3 (~796,100 $yards^3$); 38% of all this sand is located in the two sub-regions shown in **Figure 36**;
- ~99,900 m^3 (~130,600 $yards^3$) of sand is located at elevations greater than the 12 m (39 ft) contour; ~24,600 m^3 (~32,200 $yards^3$) is located in the combined southern two sub-regions;
- Above the 10 m (33 ft) contour, the volume of sand increases to ~195,600 m^3 (~255,900 $yards^3$) for the entire area; ~63,000 m^3 (~82,400 $yards^3$) of sand is located in the southern two sub-regions (i.e., about one third of the total sand volume is located south of 5th Street, **Figure 36**).

Accordingly, lowering the dune to the 10 m (33 ft) contour south of 5th Street would liberate ~63,000 m^3 (~82,400 $yards^3$) of sand into the littoral system;

- Above the 8 m (26 ft) contour, the volume of sand increases to ~314,900 m^3 (~411,900 $yards^3$) for the entire area; ~112,800 m^3 (~147,500 $yards^3$) is located in the southern two sub-regions (**Figure 36**).

Table 7. Volume change estimates determined for the Chapman Point dune system. Sand volumes are calculated for the area above the 4 m (13 ft) contour to the back edge of the dunes, physical features such as concrete paths, back edge of gravel berms, or the bluff toe.

	Chapman Point Volume		Chapman Point Sub-Region 1 Volume		Chapman Point Sub-Region 2 Volume	
Contour Elevation (m)	(m^3)	(yd^3)	(m^3)	(yd^3)	(m^3)	(yd^3)
>16	6,739	8,815	0	0	10	12
>14 < 16	27,300	35,708	422	552	3,527	4,613
>12 < 14	65,821	86,091	4,055	5,303	16,617	21,734
>10 < 12	95,785	125,282	17,876	23,381	20,458	26,758
>8 < 10	119,281	156,014	26,802	35,056	23,035	30,129
>6 < 8	138,894	181,667	30,323	39,661	25,437	33,271
>4 < 6	154,846	202,531	34,144	44,658	26,029	34,045
Totals	608,668	796,107	113,622	148,612	115,112	150,561
Sub-Region 1+2	228,734	299,173				

6.0 DUNE MANAGEMENT IMPLICATIONS

6.1 Background

Managing dunes is founded on three important objectives. First, to ensure the dunes sustain an adequate sand volume in order to withstand the erosional effects of an extreme storm(s) and to minimize any potential for wave overtopping and inundation (flooding) of backshore properties (Simm and others, 1996). Accordingly, the role of a dune during a storm is to withstand impact by large waves and surge—a scarped or heavily eroded dune face is evidence that the dune was successful in absorbing the storm impact (Elko and others, 2016) see the example in **Figure 28**. Furthermore, as noted by Woodhouse (1978), conserving a broad, well-nourished dune system remains the most effective, cheapest, and natural solution for combating coastal erosion while retaining valuable ecosystem services. Past experience at several locations on the Oregon coast has clearly demonstrated the problems associated with losing a dune system, resulting in the need for expensive coastal engineering in the form of "hard" structures that must be constructed and maintained at huge cost to homeowners for the life of the property (e.g., Komar, 1986; 1997).

A second goal of dune management should be to maintain weak points in the dune system (e.g., adjacent to trails), by repairing areas subject to localized blowouts from wind or waves in order to prevent the dune buffer from weakening and potentially being breached during a storm. Furthermore, such efforts are essential for helping to minimize potential problems that could contribute to the dune becoming unstable. Because dune recovery after storms or from high wind events is not immediate, vegetation plantings, aided by fences, may be required to initiate further recovery by natural processes. Such an approach has been implemented at Cannon Beach on a few occasions to mitigate problem spots (Rosenfeld, 1997).

Third, dunes provide valuable habitat for a wide range of plants and animals, including in some cases rare species. Thus, maintaining these ecosystem services may be of great importance to coastal communities due to the recreational benefits provided by the system as a whole. Great care must be taken to minimize potential ecosystem losses as a result of modifications to the dune system both in terms of dune scraping and with respect to the introduction of new plant species.

It is apparent that a fourth objective is necessary in some dune regions, particularly areas undergoing rapid vertical growth and backed by properties behind the dunes such as at Chapman Point. In these areas, there is a strong desire to maintain the dunes at a particular height in order to retain views of the ocean. It has become common practice to grade or scrape (lower) the dune down to a design elevation, pushing the sand over the seaward face of the foredune and out onto the beach. In these areas an effective management strategy that addresses the intrinsic dune management goals listed previously, while retaining secondary benefits such as views, is important. Such an approach can be accomplished, provided that the following issues are addressed in a systematic manner:

- Minimize the height at which the dune is lowered, thereby avoiding the potential for wave overtopping during an extreme storm(s);
- Retain sand that is removed from the crest of the dune by placing it back on the beach, thereby preserving a sufficient buffering capacity against future storms. On the Oregon coast this is especially important given the finite sediment budgets contained within the pocket beaches of the Oregon coast; and,
- Immediately replant the graded area in order to quickly stabilize the dune and minimize the subsequent entrainment of sand by wind processes and their accompanying landward incursion into backshore properties.

A balance must therefore be struck between these competing objectives. Furthermore, because of our uncertainty in the forces that both sustain and erode beaches and dunes on the Oregon coast, especially over longer time scales (10 to 30 years), an adaptive management approach based on a sound knowledge of beach and dune processes, guided by systematic monitoring and evaluation of the system as a whole, is essential.

6.2 Extreme Wave Erosion

The erosion potential of sandy beaches and dunes along the coast of Oregon is a function of the total water level produced by the combined effect of the wave runup (R) plus the tidal elevation (E_T), exceeding some critical elevation of the fronting beach, typically the elevation of the beach-dune junction (E_J). This basic concept is depicted conceptually in **Figure 37**A based on the model developed by Ruggiero and others, (1996) and, in the case of the erosion of a foredune backing the beach, the application of a geometric model (**Figure 37**B) formulated by Komar and others (1999). In its simplest form, the model indicates that the more extreme the total water level elevation, the greater the resulting erosion that occurs along both dunes and bluffs. As can be seen from **Figure 37**, estimating the maximum potential dune erosion (*DEmax*) is dependent on first determining the total water level elevation, TWL, diagrammed in **Figure 37A**, which includes the combined effects of extreme high tides plus storm surge plus wave runup, relative to the elevation of the beach-dune junction (E_J). Therefore, when TWL > E_J the foredune retreats landward by some distance, until a new beach-dune junction is established, the elevation of which approximately equals the extreme water level. Because beaches along the high-energy Oregon coast are typically wide and have a nearly uniform slope (tan β), the model assumes that this slope is maintained, and the dunes are eroded landward until the dune face reaches point B in **Figure 37**B. As a result, the model is geometric in that it assumes an upward and landward shift of a triangle, one side of which corresponds to the elevated water levels, and then the upward and landward translation of that triangle and beach profile to account for the total possible retreat of the dune (Komar and others, 1999).

Using the geometric model approach and a 30-year history of extreme total water levels (TWL), Allan and others (2015b), calculated that the most extreme storms have the potential to erode the Cannon Beach dunes by as much as 50 to 80 m (164 to 263 ft); the average for this area is 65 m (213 ft). However, it is unlikely that this extreme degree of response is ever fully realized. This is because the geometric model assumes an instantaneous erosional response, with the dunes retreating landward as a result of direct wave attack. However, the reality of coastal change is that it is far more complex, there in fact being a lag in the erosional response behind the forcing processes. As noted by Komar and others (1999), the extreme high runup elevations typically occur for only a relatively short period of time (e.g., the period of time in which the high wave runup elevations coincide with high tides). Because the elevation of the tide varies with time (e.g., hourly), the amount of erosion can be expected to be much less when water levels are lower, and will increase when water levels are higher (assuming the waves remain large). Thus, it is probable that several storms during a winter may be required to fully realize the degree of erosion estimated by the geometric model; this did occur during the winter of 1998-1999, for example, with the last in the series of five storms the most extreme and erosive (Allan and Komar, 2002b). In addition, as beaches erode, sediment is transported by waves offshore (or along the shore) where the sediment accumulates in nearshore sandbars. This process helps to mitigate the incoming wave energy by causing the waves to break farther offshore, dissipating some of the wave energy, and forming the wide surf zones characteristic of the Oregon coast, thereby reducing the extent of beach and dune erosion that occurs. In summary,

the actual amount of beach erosion and dune recession is dependent on many factors, the most important of which include the incident wave conditions, the TWL, and the duration of the storm event(s).

Figure 37. ***A)*** **The foredune erosion model (Ruggiero and others, 1996).** ***B)*** **The geometric model used to assess the maximum potential beach erosion in response to an extreme storm (Komar and others, 1999). See text for explanation.**

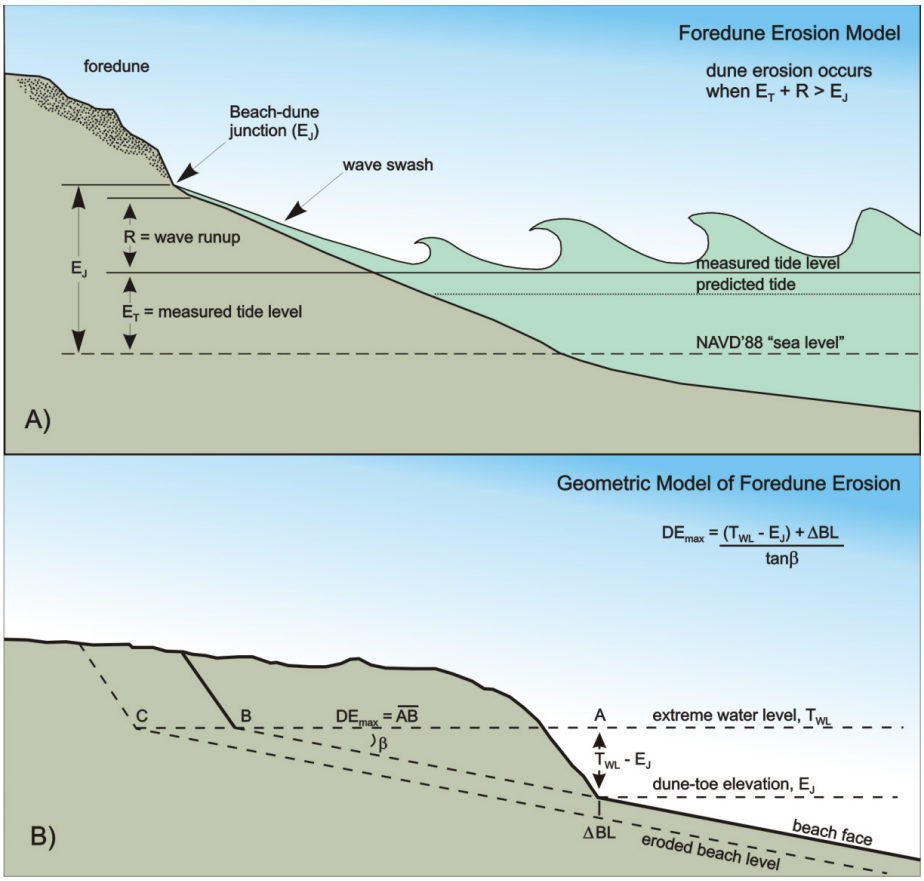

Kriebel and Dean (1993) developed a dune erosion model that is broadly similar to the Komar and others (1999) geometric model. At its core is the assumption that the beach is in statistical equilibrium with respect to the prevailing wave climate and mean water levels. As water levels increase, the beach profile is shifted upward by an amount equal to the change in water level (S) and landward by an amount R_∞, until the volume of sand eroded from the subaerial beach matches the volume deposited offshore in deeper water; note that *DEmax* and R_∞ are essentially synonymous with each other. In reality, both *DEmax* and R_∞ are almost never fully realized because storms rarely last long enough to fully erode the dune to the extent predicted by the models. Because the duration of a storm is a major factor controlling beach and dune erosion, Kriebel and Dean developed an approach to account for the duration effects of storms with respect to the response time scale required to fully erode a beach profile. Using this approach, Allan and others (2015b) performed additional erosion calculations for the Cannon Beach area. They determined that a single storm (after accounting for the duration of such an event) has the potential to erode the Cannon Beach dunes by ~8.4 to 13.2 m (27.6 to 43 ft).

In summary, calculated dune erosion analyses indicate that the maximum potential dune erosion (*DEmax*) for the Cannon Beach shore is ~65 m (213 ft). Accounting for the duration of a single storm reduces this to ~10 m (33 ft). As can be seen in **Figure 32** derived from analyses of lidar coupled with GPS beach surveys (Allan and Harris, 2012; Allan and Stimely, 2013), the typical storm-induced erosion in the Cannon Beach littoral cell has previously varied from as little as several meters to as much as 20 m (66 ft) between 1997 and 2009. Hence, any dune scraping activities will need to take into account the potential of the dunes to erode landward during future extreme storms, such that a suitable buffer of dune must be maintained in order to safeguard the properties located behind the dunes. In addition to storm-induced erosion of dunes, other factors may locally impact the erosion of dunes and bluffs. Of particular importance is the development of rip current embayments that can form locally, affecting several hundred meters (a few thousand feet) of shore, leading to additional localized erosion of the dunes. Examples of this phenomenon having occurred on the Oregon coast are numerous, such as on Siletz Spit (Komar and Rea, 1976; Allan and others, 2015a) and on Netarts and Nestucca Spits (Komar, 1986, 1997; Allan and others, 2009, 2015c). It is important to appreciate that the models of Komar and others (1999) and Kriebel and Dean (1993) do not account for such phenomena and hence the modeled storm erosion values should be treated as a minimum.

6.3 Design Elevations for Dunes at Cannon Beach

Estimates of extreme total water levels (TWL, the combined effect of wave runup superimposed on tides) have previously been calculated for Clatsop County by Allan and others (2015b). From their analyses, 100-year TWLs for the dune-backed beaches and dunes in the Cannon Beach area were found to range from 7 to 7.5 m (23 to 25 ft) NAVD88. These calculations provide guidance with respect to the absolute minimum elevation at which a dune may be lowered to avoid problems with wave runup and overtopping; note that this does not account for any dune retreat that can be expected to occur during a 100-year storm or coupled with localized erosion from a rip current embayment, discussed previously. Further consideration on how low to reduce the dune heights is also dependent on existing Federal Emergency Management Agency (FEMA) flood insurance maps and regulations, which require that the dunes be maintained at a specified elevation and with sufficient dune volume to prevent erosion and flooding. In addition, local comprehensive plans established by the city of Cannon Beach require an additional factor of safety of 1.2 m (4 ft) be applied above the FEMA flood elevation heights. Thus, the proposed new FEMA coastal base flood elevations of 7 to 7.5 m (23 to 25 ft) identified by Allan and others (2015b) and a 1.2 m [4 (ft]) factor of safety adopted by the City of Cannon Beach yields dune crest elevations that potentially could range from 8.2 to 8.7 m (27 to 29 ft)[4]. Using the calculated sand volumes presented in **Table 7** for the Chapman Point region and focusing on elevations above 10 m (33 ft), it can be demonstrated that ~63,000 m^3 (~82,400 $yards^3$) of sand could potentially be released in the southern two sub-regions at Chapman Point, while ~195,600 m^3 (~255,900 $yards^3$) could potentially be released for the entire area. Potentially, this could increase by as much as another ~60,000 m^3 (~78,500 $yards^3$) were the dune lowered to ~8.7 m (29 ft).

[4] These elevations are relative to the North American Vertical Datum of 1988 (NAVD88).

6.4 Disposal Approaches

Retaining sand within the littoral system is paramount, especially given the very limited sand sources in the Cannon Beach littoral cell. We concur with Rosenfeld (1997, p. 13), who stated that "under no circumstances should offshore disposal or transport [of sand] out of the littoral cells be considered."

For dune sand disposal, the most commonly applied approach is to bulldoze the sand seaward, placing it along the seaward face of the dune and out onto the beach below. This is not an unreasonable approach; however, timing is key. Were one to base the decision on wind transport potential alone, our analyses would suggest that the best time is likely to be in late spring/mid-summer, specifically May- July, due to stronger wind speeds in those months, ensuring the highest potential for southward transport by winds. However, the challenge with allowing nature to transport the sand is that there are no guarantees as transport is entirely dependent on having the right conditions and, importantly, the process is likely to be slow. In addition, a complication with the May-July period is that it coincides with the transition to summer wave conditions, whereby sand eroded from the beach in the previous winter is migrating back onto the subaerial beach. Hence, this is the time when beaches are actually gaining sand and building vertically. This means that waves will be ineffective in the erosion and transport of any graded sand.

Performing dune grading in winter may also be challenging, as the graded sand can be entrained due to the much stronger southerlies that characterize Oregon's winter winds (**Figure 13** and **Figure 14**), potentially returning some of the sand back onto the foredune and landward among buildings. Conversely, a significant benefit of winter disposal is that this is the period when water levels are at their highest and wave energy levels are at their most elevated; these conditions enable storm waves to reach to much higher elevations at the back of the beach, leading to erosion of the dunes. Thus, although winter winds may entrain and carry sand landward, a significant benefit of winter disposal is that the waves are able to erode, entrain, and remove the sand offshore. As a result, given the potential for winter waves to remove large quantities of sand (~100 to 200 m^3 [~130 to 262 $yards^3$] per meter of beach) during discrete events, the benefits of winter grading may in fact outweigh the potential return of some of that sand during a strong wind event.

Grading dunes in late summer (August-September timeframe) is also likely to be less than ideal, because the northerly winds (which drive the sand to the south) are predominantly of lower velocity, reducing their potential to transport sand southward and out of the area (**Figure 13** and **Figure 14**). Furthermore, as noted previously, because waves during this period are generally at their lowest in height and of longer duration, they are largely transporting sand back onto the beach. This process effectively reaches its peak during late summer. As a result, any sand graded during this period is likely to remain on the beach until the first winter storm waves arrive, which typically occurs around October-November.

Of these various periods, we believe mid-summer to be the least effective, while winter grading is probably the most effective. However, due to challenges in working in the winter a potential compromise is to undertake dune grading in early fall, when waves are transitioning from aggradational to a predominantly erosional state. This latter period increases the potential for the scraped dune sand that is placed at the toe of the foredune to be eroded by waves and removed offshore.

Rather than waiting for nature to remove the sand, an approach is to physically remove the sand from one location and transport it to another area that is currently starved of sand. For example, sand removed from Chapman Point could potentially be transported to areas such as at Tolovana South (**Figure 33**). This would entail placing the sand in trucks and driving down the beach. Although potentially less acceptable than allowing nature to perform such operations (due to having vehicles operating on the public beach), the benefits are expected to be immediate in both locations. At the source area, the removed sand

is less likely to be re-handled over multiple cycles of dune scraping, while the receiving end gains valuable beach sand increasing the buffering capacity of the beach and potentially boosting its recreational potential. Such an approach is not uncommon around the world and is something to consider for Cannon Beach. To minimize the impact to people recreating in the area, one could adopt a phased approach focusing initially on the highest points in the dunes, and expanding to other areas as deemed necessary. Alternatively, one could adopt a combination of approaches such as pushing some of the sand seaward at Chapman Point, while also relocating some of the sand to Tolovana South.

6.5 Post-Grading Responsibilities

After a dune has been scraped (graded), it is imperative that steps be taken to stabilize the exposed area as quickly as possible. This is important to minimize the transport of uncovered dune sand back to the areas behind the dunes. On the Oregon coast, there are several examples where existing approaches have failed to adequately replant dunes following dune grading and have exacerbated the problem by causing more sand to be entrained and transported inland, burying roads and piling sand up against homes. These examples include Pacific City in Tillamook County (**Figure 15**B), and Alsea Spit in central Lincoln County. The importance of re-planting has been demonstrated both qualitatively (the previously mentioned examples) and quantitatively. For example, Nordstrom and others (2007) examined the effectiveness of sediment transport by wind on a scraped dune and found that transport rates and deflation rates can be significantly greater within the foredune compared with the beach, particularly if the dune surface is poorly vegetated. Furthermore, they observed that winds blowing across poorly vegetated patches in the dune increase the potential for creating an irregular crest elevation, increasing the dune roughness, which produces feedback encouraging more sediment trapping and dune building. Their research is also supported by the work of researchers in Japan, who observed that wind transport of sand was reduced by as much as 95%, with a vegetation cover of 28% (Kuriyama and others, 2005). They concluded that when the grasses grew, the landward aeolian sand transport rate rapidly decreased landward from the seaward limit of vegetation because the grasses restrained sediment movement due to wind and trapped windblown sediments. It is thus clear that any dune scraping must be accompanied by plantings in order to stabilize the scraped dune and to minimize sand being blown into unwanted areas.

Given recent research on the capabilities of different dune grasses to trap sand, European beach grass (*A. arenaria*) is the most obvious choice for planting due to its much greater tiller density and accompanying higher trapping capabilities. *A. arenaria* is also most adept at keeping pace with sand deposition on the dune, growing vertically in response. However, it is this exact mechanism of vertical growth and higher density that is directly contributing to the building of higher dunes at Cannon Beach and elsewhere on the Oregon coast. We believe a more effective approach may be to plant either the non-native American (*A. breviligulata*) or the PNW native dune grass (*E. mollis*), or some combination of both grasses. This is because both species of dune grass have been demonstrated to build lower, broader dunes (Zarnetske and others, 2012). Thus, an approach might include the following (**Figure 38**):

- Having scrapped the dune down to a design elevation, immediately plant the scraped portion with *A. breviligulata* or *E. mollis* using conventional planting approaches already established for the Oregon coast (Woodhouse, 1978; OCZMA, 1979; Ternyik, 1979; Shoreland Solutions, 1998a,b). *E. mollis* may be the better choice for the scraped dune because it is already present in this part of the coast (S. Hacker, written communication, 2017) (**Figure 38**);
- Scraped sand dispersed out onto the seaward face of the dune should also be planted with dune grass (**Figure 38**). This step further aides the stabilization of the dune by reducing the

potential large exchange that takes place between the beach and dune, while enhancing the potential for seaward extension (progradation) of the dune. *A. breviligulata* may be a better choice for the seaward face of the dune as *E. mollis* is not expected to perform quite so well there (S. Hacker, written communication, 2017). This approach encourages more lateral growth of the dune morphology; and,

- Once stabilized, the central portion of the dune becomes somewhat self-regulating (requiring only periodic maintenance), while the area of primary trapping and deposition is increasingly shifted westward toward the ocean (**Figure 38**). Some ongoing remediation may still be required to maintain the dune at a specified elevation and to eliminate the incursion of European beach grass (*A. arenaria*) into the area. Over time, a broad, uniformly topped dune is developed, and dune erosion and wave overtopping are increasingly shifted seaward away from homes (**Figure 38**). Successful applications where wide dunes have been stabilized with subsequent periodic maintenance requirements include Manzanita and the southern Clatsop Plains (just north of Delray Road).

Figure 38. Conceptual cartoon of proposed dune plantings for Cannon Beach. *E. mollis* is used to stabilize the back of the dune, while *A. breviligulata* encourages lateral dune growth. As the dune widens over time, the hazard associated with wave erosion (and runup and overtopping) is diminished. MLLW is mean lower low water; MHHW is mean higher high water; NAVD88 is North American Vertical Datum of 1988.

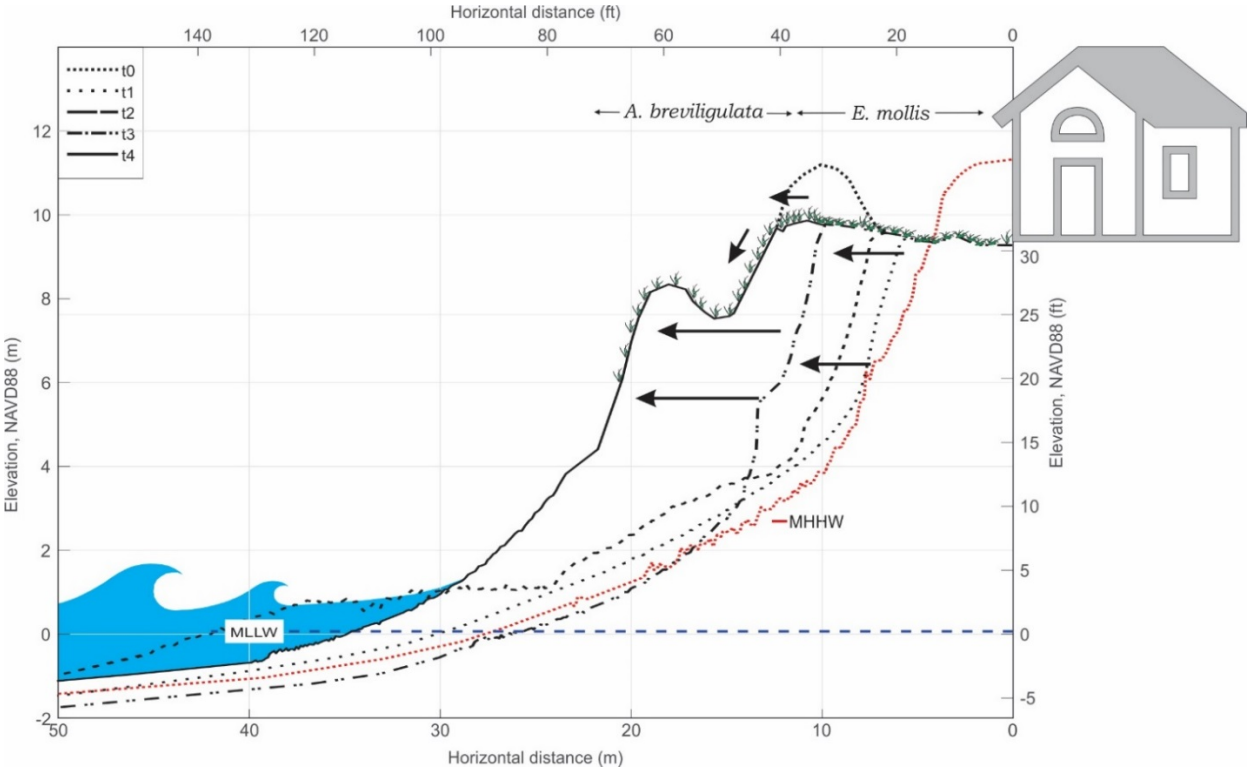

A preferable approach would be to use the PNW native beach grass (*E. mollis*), given that it is native to the U.S. West Coast and prior to the introduction of *A. arenaria* was the dominant species on the coast. Although *E. mollis* has the highest trapping efficiency of the three plants, its primary limitation is the plant's lower density. Consequently, plantings may result in some areas remaining exposed to wind

transport. However, dense planting of such a species could potentially resolve such a problem. Examples of the application of *E. mollis* on the Oregon coast to stabilize dunes are limited. We are aware of only one example at Cape Lookout State Park, in Tillamook County, where *E. mollis* has been established for the purposes of stabilizing an artificial dune (Allan and Komar, 2004; Allan and others, 2006). However, *E. mollis* is naturally present at a number of sites along the south central Oregon coast, including Tahkenitch Creek, Siltcoos River and at South Beach State Park. Unlike *A. arenaria* and *A. breviligulata, E. mollis* does die back in the winter, forming a dense mat of leaves and potentially limiting its viability as an effective dune stabilizer during the winter; however, *E. mollis* rapidly shoots up again in spring.

6.6 Ecola Creek

The locations of the Ecola Creek channel and mouth have varied significantly over the years (**Figure 39**). During the 1920s, the channel and mouth appear to have been much wider, with the creek's right bank having tracked through the Breakers Point Condominiums, while its southern bank was close to where it is today. At that time, the creek channel likely fluctuated over a much wider area, migrating both to the north and south in response to storms and subsequent infilling of the channel with sand. This is because it would have been much less constrained then compared with conditions today.

As sand began to accumulate in the Chapman Point region during the 1930s through 1960s (especially seaward of the Breakers Point Condominiums), the dunes stabilized and the beach and dune grew southward. This growth of the dunes effectively forced the channel mouth to migrate southward as well. Today, the mouth of the channel is in the south, just west of 2nd Street (**Figure 39**). Under the current regime, the channel mouth probably does not switch its position very much; a comparison of recent historical photos from 2005 to the present appears to support this view. In addition to sand accumulation seaward of the Breakers Point Condominiums, sand accumulated adjacent to the end of N. Spruce Street (**Figure 39**) and in the vicinity of the old Cannon Beach Elementary School; over the years the sand has been stabilized. A large open area of sand exists today and, combined with the southward extension of the Chapman Point dune and beach, has caused the Ecola Creek channel to shift northward up against Larch Street (north side of the creek and adjacent to the Breakers Point Condominiums). Rosenfeld (1997) noted that in 1979 the creek channel was about 26 m (85 ft) from the edge of the road and by 1983 had shifted south slightly, placing it 37 m (120 ft) from the road. Between 1983 and 1989, the channel deepened and started to migrate back northward, bringing it up against Larch Street, eventually eroding into the sandy bank at the toe of the street. An evaluation of recent aerial photos of the area, taken in 2005, 2009, and 2014, indicate the following changes near Larch Street:

- From 2005 to 2009, little to no change; and,
- From 2009 to 2014, the bank cut back ~5 to 10 m (16 to 33 ft). This most recent change is captured in **Figure 36**, which indicates that the south end of the dune is being truncated.

In response to the recent erosion, the City of Cannon Beach established a number of coir rolls (biodegradable erosion control fiber rolls) planted with willows to help stabilize the eroding bank (**Figure 40**). It remains to be seen how effective this approach will be, since the current design could still be undermined by the creek, and/or truncated with additional erosion at the ends of the rolls. As an alternative to coir rolls, another soft engineering approach that might work in this environment is the construction of a dynamic revetment or cobble berm along the toe of the eroding area. Such an approach has been successfully applied in high energy, open-coast sites at Cape Lookout State Park (Allan and Komar, 2002a; Komar and Allan, 2010) and adjacent to the south Columbia River jetty (Allan and Gabel, 2016), as well as in low wave energy environments such as next to the Hatfield Marine Science Center in Yaquina Bay (**Figure 41**).

There is some concern that the placement of large volumes of sand scraped from the Chapman Point dunes could exacerbate problems in Ecola Creek, potentially contributing to increased erosion near Larch Street, modifications to the creek's flow regime, and possibly even changes to the biology of the creek. With respect to the first two items, such effects are probably short-lived as early fall rains can be expected to flush out the creek mouth. Furthermore, these processes have clearly been ongoing since the 1930s, without any apparent long-term impact to the ability of the creek to flow. As can be seen in **Figure 39**, Ecola Creek has generally maintained its position in the south, and at times may be infilled with sand (e.g., 1967) causing its channel to narrow. Perhaps of greater concern is the potential to drive the creek channel closer to Larch Street, on the north side of the channel (**Figure 39**). This particular issue remains a valid concern and some effort to remediate the problem has already been implemented (**Figure 40**). However, as discussed previously, it remains to be seen if coir rolls and willows will safeguard the site and prevent further erosion.

Figure 39. Historical changes in the location of Ecola Creek, 1926 to 2016.

Figure 40. Coir rolls (biodegradable erosion control fiber rolls) (*A*) planted with willows and (*B*) along the toe of Larch Street (mid photo near pole) at the south end of the Breakers Point Condominiums have been installed to stem erosion by Ecola Creek and from waves that travel up the channel during storms that accompany high tides. Note the debris that has accumulated to the right of the photo along the bank and in the bushes (*A*). The debris indicates recent flooding (probably due to creek flooding). The height of the debris is about 4 m (13 ft) elevation. (Photo credit: J. Allan, DOGAMI, 2016)

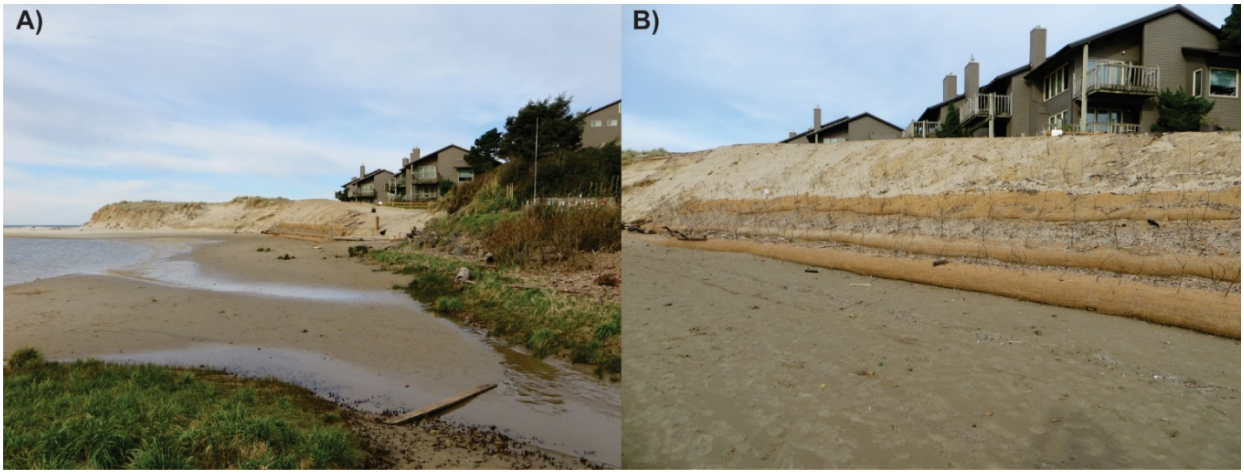

Figure 41. A cobble berm or dynamic revetment, constructed adjacent to the Hatfield Marine Science Center in Yaquina Bay, has successfully stopped erosion of the backshore. (Photo credit: J. Allan, DOGAMI, 2016)

7.0 CONCLUSIONS

Since 1939, the City of Cannon Beach has experienced a substantial accumulation of sand along its beaches and in its dunes north of Haystack Rock, especially in the Presidential dune management area located between Harrison and 1st Streets and north of Ecola Creek at Chapman Point (**Figure 33**). In the case of the Chapman Point dune management area, the combination of a large sand supply and the prevalence of European beach grass (*A. arenaria*) has contributed to dune vertical buildup, reaching elevations of 16 m (53 ft, NAVD88) in some places. In response to the large amount of sand buildup, the City of Cannon Beach initiated a process to evaluate their existing dune management plan on the basis of updated scientific information on physical processes and coastal geomorphology occurring along the Cannon Beach littoral cell. The overarching objective is to use the updated information to help establish new guidelines for the relocation of excess sand that periodically builds up along the coastline. This buildup of sand within the dunes is presently affecting the views of local residents, while sand blowing inland has become a nuisance, migrating where it has begun to inundate buildings and properties.

The purpose of this study has been to provide an update of an earlier investigation by Rosenfeld (1997) of physical processes and beach and dune geomorphology in the area. The broad findings of this study include the following:

- The total volume of sand contained in the Cannon Beach littoral cell measured between the 6 m (19 ft) contour (approximately the dune or bluff toe) and mean lower low water (MLLW) is ~3.6×10^6 m^3 (4.67×10^6 yards^3). Incorporating the volume of sand contained in the dunes increases the total volume to ~4.2×10^6 m^3 (5.4×10^6 yards^3) of sand;
- The seasonal exchange of sand on the beach between September 2015 (late summer) and March 2016 (late winter) was ~2.0×10^6 m^3 (2.6×10^6 yards^3), representing the volume of sand eroded from the inshore beach and transported to offshore bars. However, this estimate will vary from year to year as the process is dependent on seasonal variations in winter and summer waves;
- The total volume of beach sand north of Silver Point is approximately twice as much as the amount of sand contained to its south;
- Since 1997, the Cannon Beach littoral cell has experienced a net gain of ~209,220 m^3 (273,649 yards^3) of sand;
- Positive sediment gains have occurred in all areas north of Tolovana Park, with the largest accumulation occurring north of Ecola Creek in the Chapman Point dune management region, which accumulated ~225,080 m^3 (294,390 yards^3) of sediment since 1997;
- Sand volume gains have also occurred in the Presidential dune management area, which accumulated +24,287 m^3 (31,767 yards^3) of sand since 1997;
- Minor sand gains were also observed in the Haystack Rock (~1,770 m^3 [2,315 yards^3]) and Arch Cape (~9,180 m^3 [~12,000 yards^3]) sub-region areas.
- Net sand losses since 1997 have dominated all other sub-regions including:
    - Tolovana North — lost ~4,350 m^3 (5,690 yards^3);
    - Tolovana South — lost ~17,500 m^3 (22,890 yards^3);
    - Silver Point — lost ~1,660 m^3 (2,170 yards^3);
    - Arcadia Beach — lost ~9,670 m^3 (12,650 yards^3);
    - Hug Point — lost ~5,070 m^3 (6,630 yards^3); and,
    - Falcon Cove — lost ~12,800 m^3 (16,740 yards^3).

- The total sand volume in the Chapman Point dunes above the 4 m (13 ft) contour is ~613,000 m^3 (~801,770 $yards^3$). Of this, 38% of all this sand is located in two smaller sub-regions seaward of the Breaker Point Condominiums;
- In the Chapman Point dune management area, we found that ~99,900 m^3 (~130,600 $yards^3$) of sand is located at elevations greater than the 12 m (39 ft) contour; ~24,600 m^3 (~32,200 $yards^3$) is located in the combined southern two sub-regions;
- Above the 10 m (33 ft) contour, the volume of sand increases to ~195,600 m^3 (~255,900 $yards^3$) for the entire Chapman Point dune management area; ~63,000 m^3 (~82,400 $yards^3$) is located in the southern two sub-regions (i.e., about one third of the total sand volume is located south of 5th Street). Accordingly, lowering the dune to the 10 m (33 ft) contour south of 5th Street would release ~63,000 m^3 (~82,400 $yards^3$) of sand into the littoral system;
- The volume of sand released from erosion of dunes in the Cannon Beach cell would account for only ~38% of the total sand that has accumulated north of Haystack Rock. This suggests that much of the sand that has been accumulating north of Haystack Rock is probably locally derived from the nearshore region (i.e., the surf zone to depths of 10 to 15 m (30 to 45 ft) and from erosion of the beach (particularly south of Haystack Rock). Unfortunately, because we do not have repeat measurements of sediment changes across the surf zone we are unable to definitively define the source the sediment;
- The formation of dunes in the Chapman Point and Presidential dune management areas is a function of three factors:
    - A sufficient supply of sand that is transported by nearshore processes;
    - A prevailing wind. Of particular importance is the wind speed, which needs to be strong enough to entrain and mobilize sand within the intertidal zone and at the back of the beach, and their subsequent landward transport; and,
    - Obstacles to trap the sand such as woody debris, vegetation, and micro-topography.
- Analyses of a 60-year record (1950–2010) of the monthly alongshore wave energy flux (a measure of the sediment transport potential) by Anderson and Ruggiero (2015) indicate that the average monthly climatology of all 63 years results in zero net annual longshore directed wave energy flux, a zero net longshore sand transport. This is consistent with conceptual models of sediment transport for the Oregon coast proposed by Komar (1997). However, when individual years are examined, such as major El Niños, the northerly directed energy flux (and hence sediment transport potential) was found to be an order of magnitude greater than the climatological mean, indicating that more sand was transported to the north during these climate events. Conversely, major La Niña events produced a comparable response, but in the opposite direction, the transport being to the south. These responses suggest that alongshore sediment transport is strongly coupled to the occurrence of the El Niño/La Niña climate phenomena, as well as the longer-term Pacific Decadal Oscillation (PDO);
- Incorporating analyses of the potential for wind to transport sand onshore for the period 1985 to 2017, we observed the following:
    - The regional wind climatology is dominated by winds out of the northwest during spring and summer and by winds from the southwest in winter:
        - During the winter, wind speeds exceed 8.3 m/s (~18.6 mi/hr) for 20% of the time and exceed 12.8 m/s (~28.6 mi/hr) for 10% of the time;
        - Conversely, summer wind speeds exceed 6.8 m/s (~15.2 mi/hr) for 20% of the time and 10 m/s (~22.4 mi/hr) for 10% of the time;

        - For 1% of the time, wind speeds exceed 17.2 m/s (~38.5 mi/hr) during the fall and winter, and ~13 m/s (29 mi/hr) in the summer; and,
        - Hence, more sand is likely to be mobilized and transported by winds in the winter than in the summer, despite the conditions being generally wetter.
    - Application of a wind sediment transport model indicated the following:
        - The wind transport potential is largely bi-modal, with south to southwesterly winds dominating in the fall-winter and driving sand to the north, while north to northwesterly winds dominate in the spring and summer, which help return sand to the south;
        - Summing the volume of sand that could potentially be moved by wind indicates that ~79% of the sand-transport potential is directed to the north, while the southerly sand transport accounts for ~21% of the volume of sand mobilized. Thus, the net northward transport potential is approximately 4 times greater than the corresponding southward transport.
- The combined effects of nearshore waves and wind sediment transport appear to be driving more sand to the north under the current wind and wave regime;
- The introduction European beach grass (*Ammophila arenaria*) to the Oregon coast in the 1900s has profoundly changed the morphology of the dunes;
- In the Cannon Beach littoral cell, it appears that *A. arenaria* was introduced sometime in the 1950s, with major plantings occurring in the 1960s. These initial efforts effectively stabilized the dunes at Chapman Point and by 1967 had greatly increased the retention of sand;
- Studies of three different species of dune grass have revealed the following:
    - The dense vertical growth habit of European beach grass (*A. arenaria*) allows it to capture sand more efficiently, produce more vertical tillers (the above-ground branch of a plant), and build taller, narrower dunes;
    - The non-native American dune grass (*A. breviligulata*) has a more lateral growth habit and is generally less dense when compared with *A. arenaria*; as a result, the plant is more suited for building lower, wider dunes; and,
    - *E. mollis* (the native Oregon dune grass) was found to have the highest sand capture efficiency of the three species due to its low spreading habit and much wider tiller. Because of the width of its tiller, each branch has a significantly larger surface area, enabling more sand to be trapped. However, because its tiller density is considerably lower when compared with *A. arenaria* and *A. breviligulata*, *E. mollis* is not able to trap as much sand and, accordingly, tends to produce broad dunes with lower heights.
- Managing dunes is founded on three important objectives:
    - To ensure the dunes sustains an adequate sand volume in order to withstand the erosional effects of an extreme storm(s) and to minimize any potential for wave overtopping and inundation (flooding) of backshore community assets;
    - To maintain weak points in the dune system (e.g., adjacent to trails), by repairing areas subject to localized blowouts from wind or waves in order to prevent the dune buffer from weakening and potentially being breached during a storm. Because dune recovery after storms or from high wind events is not immediate, vegetation plantings, aided by fencing, may be required to initiate further recovery by natural processes; and,
    - Dunes provide valuable habitat for a wide range of plants and animals, including in some cases rare species.

  - Increasingly, we are coming to recognize a fourth objective, which is to maintain dunes at a particular height via dune scraping in order to retain views of the ocean and to minimize sand blowing inland among properties where it can become an expensive nuisance. This is particularly necessary in dune areas that are undergoing rapid vertical growth and are-backed by properties behind the dunes, such as at Chapman Point;
- An effective dune scraping management plan must adhere to the following:
  - Minimize the height at which the dune is lowered, thereby avoiding the potential for wave overtopping during an extreme storm(s);
    - Estimates of extreme 100-year total water levels (TWL, the combined effect of wave runup superimposed on tides) indicate the potential for storms to generate TWLs that are on the order of 7 to 7.5 m (23 to 25 ft). Incorporating the 1.2 m (4 ft) factor of safety adopted by the City of Cannon Beach yields dune crest elevations that potentially could range from 8.2 to 8.7 m (27 to 28.5 ft) depending on the newly revised FEMA coastal flood maps;
  - Retain the sand that is removed from the crest of the dune by placing it back onto the beach, thereby retaining a sufficient buffering capacity against future storms;
    - Using the extreme TWLs and factor of safety, we estimate that ~195,600 m^3 (~255,900 $yards^3$) of sand could be released for the entire Chapman Point area, of which ~63,000 m^3 (~82,400 $yards^3$) could potentially be released in the southern two sub-regions;
    - Retaining sand within the littoral system is paramount;
    - Existing approaches of placing the sand seaward of the foredune is not unreasonable. From data presented in this report, we believe the best time to do this is probably between May and July, when winds from the northwest have the greatest potential to transport sand to the south;
    - An alternative approach to scraping the sand seaward is to transport the scraped sand to areas such as at Tolovana South. Although potentially less acceptable than allowing nature to perform such operations (due to having vehicles operating on the public beach), the benefits are expected to be immediate in both locations. At the source area, the sand is less likely to be re-handled over multiple cycles of dune grading, while the receiving end gains valuable beach sand, increasing the buffering capacity of the beach and potentially boosting its recreational potential. Such an approach is not uncommon around the world and is something to consider;
  - Replant the scraped area in order to quickly stabilize the dune, minimizing the subsequent entrainment of sand by wind processes and their landward incursion into backshore properties;
    - After a dune has been scraped, it is <u>imperative</u> that steps be taken to stabilize the exposed area as quickly as possible. This is important to minimize the transport of uncovered dune sand back in among properties located behind the dunes;
    - We recommend NOT using European beach grass (*A. arenaria*) to stabilize the dune, because this species is directly contributing to the building of higher dunes at Cannon Beach and elsewhere on the Oregon coast, affecting the view from shorefront homes;

- A more effective approach is to plant either the non-native American (*A. breviligulata*) or the PNW native dune grass (*E. mollis*), or some combination of both grasses; both species have been demonstrated to build lower, broader dunes;

Because of the variability in the forces that both sustain and erode beaches and dunes on the Oregon coast and our uncertainty in changes that will likely affect the beach over longer time scales (10 to 30 years), an adaptive management approach based on a sound knowledge of beach and dune processes, guided by systematic monitoring and evaluation of the system as a whole, is essential.

8.0 ACKNOWLEDGMENTS

Funding for this study was provided by the City of Cannon Beach under an intergovernmental agreement (grant award #632151701). We are grateful to Mr. Mark Barnes for his technical advice throughout this project. We would especially like to acknowledge Dr. Paul Komar (Emeritus Professor, Oregon State University) and Mr. Jed Roberts (DOGAMI) for their review of the report.

9.0 REFERENCES

Allan, J.C., 2004, An evaluation of the risks from storm erosion and overwash of the Elk River Spit, Oregon, associated with restoring Western Snowy Plover breeding habitat: Oregon Department of Geology and Mineral Industries Open-File Report O-04-17, 39 p. http://www.oregongeology.org/pubs/ofr/O-04-17.pdf

Allan, J.C., and Gabel, L.L., 2016, Monitoring the response and efficacy of a dynamic revetment constructed adjacent to the Columbia River south jetty, Clatsop County: Oregon Department of Geology and Mineral Industries Open-File Report O-16-07, 50 p. http://www.oregongeology.org/pubs/ofr/p-O-16-07.htm

Allan, J.C., and Harris, E.L., 2012, An "expanded" geospatial database of beach and bluff morphology determined from lidar data collected on the northern Oregon coast: Tillamook and Clatsop counties: Oregon Department of Geology and Mineral Industries Open-File Report O-12-08, 27 p. http://www.oregongeology.org/pubs/ofr/p-O-12-08.htm

Allan, J.C., and Hart, R., 2007, Assessing the temporal and spatial variability of coastal change in the Neskowin littoral cell: Developing a comprehensive monitoring program for Oregon beaches: Oregon Department of Geology and Mineral Industries Open-File Report O-07-01, 27 p. http://www.oregongeology.org/pubs/ofr/O-07-01.pdf

Allan, J.C., and Hart, R., 2008, Oregon beach and shoreline mapping and analysis program: 2007-2008 beach monitoring report: Oregon Department of Geology and Mineral Industries Open-File Report O-08-15, 54 p. http://www.oregongeology.org/pubs/ofr/O-08-15.pdf

Allan, J.C., and Komar, P.D., 2000, Are ocean wave heights increasing in the eastern North Pacific?: Eos, Transactions of the American Geophysical Union, v. 81, no. 47, 561, 566-567.

Allan, J.C., and Komar, P.D., 2002a, A dynamic revetment and artificial dune for shore protection, in Coastal Engineering 2002: Solving Coastal Conundrums, July 7-12, Cardiff, Wales: American Society of Civil Engineers, Proceedings of the 28th International Conference on Coastal Engineering, vol. 2, p. 2044–2056.

Allan, J.C., and Komar, P.D., 2002b, Extreme storms on the Pacific Northwest Coast during the 1997-98 El Niño and 1998-99 La Niña: Journal of Coastal Research, v. 18, no. 1, 175–193. http://www.jstor.org/stable/4299063

Allan, J.C,. and Komar, P.D., 2004, Environmentally compatible cobble berm and artificial dune for shore protection: Shore & Beach, v. 72, no. 1, 9–18.

Allan, J.C., and Komar, P.D., 2006, Climate controls on US West Coast erosion processes: Journal of Coastal Research, v. 22, no. 3, 511–529. https://doi.org/10.2112/03-0108.1

Allan, J.C., and Priest, G.R., 2001, Coastal erosion hazard zones along the Clatsop Plains, Oregon: Gearhart to Fort Stevens: Oregon Department of Geology and Mineral Industries Open-File Report O-01-04, 56 p. http://www.oregongeology.org/pubs/ofr/O-01-04.pdf

Allan, J.C., and Stimely, L., 2013, Oregon Beach Shoreline Mapping and Analysis Program: Quantifying short to long-term beach and shoreline changes in the Gold Beach, Nesika, and Netarts littoral cells:, Oregon Department of Geology and Mineral Industries Open-File Report O-13-07. http://www.oregongeology.org/pubs/ofr/p-O-13-07.htm

Allan, J.C., Komar, P.D., and Priest, G.R., 2003, Shoreline variability on the high-energy Oregon coast and its usefulness in erosion-hazard assessments, *in* Byrnes, M.R., Crowell, M., and Fowler, C. (eds.), Shoreline mapping and change analysis: Technical considerations and management implications: Journal of Coastal Research, p. 83–105.

Allan, J.C., Hart, R., and Geitgey, R., 2005, Dynamic revetments for coastal erosion stabilization: A feasibility analysis for application on the Oregon coast: Oregon Department of Geology and Mineral Industries Special Paper 37, 67 p. http://www.oregongeology.org/pubs/sp/SP-37.zip

Allan, J.C., Hart, R., and Tranquilli, V., 2006, The use of Passive Integrated Transponder tags (PIT-tags) to trace cobble transport in a mixed sand-and-gravel beach on the high-energy Oregon coast, USA: Marine Geology, v. 232, no. 1-2, 63–86. https://doi.org/10.1016/j.margeo.2006.07.005

Allan, J.C., Witter, R.C., Ruggiero, P., and Hawkes, A.D., 2009, Coastal geomorphology, hazards, and management issues along the Pacific Northwest coast of Oregon and Washington, *in* O'Connor, J.E., Dorsey, R.J., and Madin, I.P. (eds.), Volcanoes to vineyards: Geologic field trips through the dynamic landscape of the Pacific Northwest: Boulder, Colo., Geological Society of America Field Guide 15, p. 495–519.

Allan, J.C., Komar, P.D., Ruggiero, P., and Witter, R.C., 2012, The March 2011 Tōhoku tsunami and its impacts along the U.S. West Coast: Journal of Coastal Research, v. 28, no. 5, 1142–1153.

Allan, J.C., and others, 2015a, Coastal flood hazard study, Lincoln County, Oregon: Oregon Department of Geology and Mineral Industries Open-File Report O-15-06. http://www.oregongeology.org/pubs/ofr/p-O-15-06.htm

Allan, J.C., and others, 2015b, Coastal flood hazard study, Clatsop County, Oregon: Oregon Department of Geology and Mineral Industries Open-File Report O-15-05. http://www.oregongeology.org/pubs/ofr/p-O-15-05.htm

Allan, J.C., and others, 2015c, Coastal flood hazard study, Tillamook County, Oregon: Oregon Department of Geology and Mineral Industries Special Paper 47, 274 p. http://www.oregongeology.org/pubs/sp/p-SP-47.htm

Anderson, D., and Ruggiero, P., 2015, Modeling interannual to multi-decadal shoreline rotations of headland-bounded littoral cells, *in* Coastal Sediments' 15, Understanding and Working with Nature, San Diego, Calif.: American Society of Civil Engineers, p. 11.

Atwater, B.F., and others, 1995, Summary of coastal geologic evidence for past great earthquakes at the Cascadia subduction zone: Earthquake Spectra, v. 11, no. 1, 1–18.

Atwater, B.F., and others, 2005, The orphan tsunami of 1700-Japanese clues to a parent earthquake in North America: U.S. Geological Survey Professional Paper 1707.

Aviso, 2017, Mean sea level rise data from altimetry [website]: http://www.aviso.altimetry.fr/en/data/products/ocean-indicators-products/mean-sea-level.html. [The altimeter products were produced by SSALTO (Segment Sol multi-missions d'ALTimetrie, d'orbitographie et de localisation précise) / DUACS (Data unification and Altimeter combination system) and distributed by Aviso, with support from Centre national d'études spatiales.]

Bagnold, R., 1941, The physics of blown sand and desert dunes: London, Methuen, 265 p.

Bauer, B. O., Sherman, D. J., Nordstrom, K. F., and Gares, P. A., 1990, Aeolian transport measurement and prediction across a beach and dune at Castroville, California, *in* Nordstrom, K. F., Psuty, N., and Carter, B. (eds.), Coastal dunes: form and process: Chicester, Wiley, p. 39-55.

Bernstein, D.J., Freeman, C., Forte, M.F., Park, J.-Y., Gayes, P.T., and Mitasova, H., 2003, Survey design analysis for three-dimensional mapping of beach and nearshore morphology, Coastal Sediments '03, St. Petersburg, Fla.: American Society of Civil Engineers,12 p. http://citeseerx.ist.psu.edu/viewdoc/download?doi=10.1.1.543.2499&rep=rep1&type=pdf

Bond, N.A., Cronin, M.F., Freeland, H., and Mantua, N., 2015, Causes and impacts of the 2014 warm anomaly in the NE Pacific: Geophysical Research Letters, v. 42, no. 9, p. 3414-3420.

Burgette, R.J., Weldon, R.E., III, and Schmidt, D.A., 2009, Interseismic uplift rates for western Oregon and along-strike variation in locking on the Cascadia subduction zone: Journal of Geophysical Research, v. 114, no. B01408, p. 24.

Clemens, K.E., and Komar, P.D., 1988, Oregon beach-sands compositions produced by the mixing of sediments under a transgressing sea: Journal of Sedimentary Petrology, v. 58, no. 3, 519–529.

Cooper, W.S., 1958, Coastal sand dunes of Oregon and Washington: Boulder, Colo., Geological Society of America Memoir 72, 169 p.

Elko, N., Brodie, K., Stockdon, H., Nordstrom, K., Houser, C., McKenna, K., Moore, L., Rosati, J., Ruggiero, P., Thuman, R., and Walker, I., 2016, Dune management challenges on developed coasts: Shore & Beach, v. 84, no. 1, 15-28.

Favre, A., and Gershunov, A., 2006, Extra-tropical cyclonic/anticyclonic activity in North-Eastern Pacific and air temperature extremes in Western North America: Climate Dynamics, v. 26, 617–629.

FEMA, 2010, Flood insurance study: Clatsop County, Oregon and incorporated areas: Federal Emergency Management Agency, Flood Insurance Study Number 41007CV001A.

Goldfinger, C., 2009, Paleoseismically derived probabilities for Cascadia great earthquakes, Session 202, Reducing risk from geologic hazards in the dynamic landscape of Oregon and Washington, GSA Annual Meeting,18-21 Oct. 18-19, 2009, Portland, Oreg.: Geological Society of America Abstracts with Programs. 41, no. 7, p. 520.

Goldfinger, C., Nelson, C.H., Johnson, J.G., and The Shipboard Scientific Party, 2003, Holocene earthquake records from the Cascadia Subduction Zone and Northern San Andreas fault based on precise dating of offshore turbidites: Annual Review of Earth and Planetary Sciences, v. 31, 555–577. doi: 10.1146/annurev.earth.31.100901.141246

Goldfinger, C., and others, 2012, Turbidite event history—Methods and implications for Holocene paleoseismicity of the Cascadia subduction zone: U.S. Geological Survey Professional Paper 1661–F, 170 p. https://pubs.usgs.gov/pp/pp1661f/

Goldfinger, C., Galer, S., Beeson, J., Hamilton, T., Black, B., Romsos, C., Patton, J., Nelson, C. Hans, Hausmann, R., and Morey, A., 2017, The importance of site selection, sediment supply, and hydrodynamics: A case study of submarine paleoseismology on the northern Cascadia margin, Washington USA: Marine Geology, v. 384, 4-16, 17, 25-46. https://doi.org/10.1016/j.margeo.2016.06.008 [available online August 2, 2016].

Gyakum, J.R., Anderson, J.R., Grumm, R.H., and Gruner, E.L., 1989, North Pacific cold-season surface cyclone activity: 1975-1983: Monthly Weather Review, v. 117, 1141–1155.

Hacker, S.D., Zarnetske, P., Seabloom, E., Ruggiero, P., Mull, J., Gerrity, S., and Jones, C., 2012, Subtle differences in two non-native congeneric beach grasses significantly affect their colonization, spread, and impact: Oikos, v. 121, no. 1, 138–148. https://doi.org/10.1111/j.1600-0706.2011.18887.x

Hartmann, D.L., 2015, Pacific sea surface temperature and the winter of 2014: Geophysical Research Letters, v. 42, no. 6, p. 1894-1902.

Horning, T., compiler, 2006, Summary of eyewitness observations from 1964 Alaska tsunami in Seaside, Oregon, Appendix C *in* Tsunami Pilot Study Working Group, Seaside, Oregon tsunami pilot study—Modernization of FEMA flood hazard maps: U.S. Geological Survey Open-File Report 2006-1234, p. C1–C7. https://pubs.usgs.gov/of/2006/1234/of2006-1234.pdf

Hunter, R.E., and Richmond, B.M., 1983, Storm-controlled oblique dunes of the Oregon coast: Geological Society of America Bulletin, v. 94, no. 12, 1450–1465.

Jennings, R., and Shulmeister, J., 2002, A field based classification scheme for gravel beaches: Marine Geology, v. 186, 211–228.

Kaminsky, G.M., Ruggiero, P., Buijsman, M.C., McCandless, D., and Gelfenbaum, G., 2010, Historical evolution of the Columbia River littoral cell: Marine Geology, v. 273, 96–126.

Kelsey, H.M., Nelson, A.R., Hemphill-Haley, E., and Witter, R.C., 2005, Tsunami history of an Oregon coastal lake reveals a 4600 yr record of great earthquakes on the Cascadia subduction zone: Geological Society of America Bulletin, v. 117, no. 7/8, 1009–1032.

Komar, P.D., 1976, Beach processes and sedimentation: Englewood Cliffs, N.J., Prentice Hall, 429 p.

Komar, P.D., 1986, The 1982-83 El Nino and erosion on the coast of Oregon: Shore & Beach, v. 54, no. 2, 3–12.

Komar, P.D., 1997, The Pacific Northwest coast: living with the shores of Oregon and Washington: Durham, N.C., Duke University Press, 195 p.

Komar, P.D., 1998, The 1997-98 El Niño and erosion on the Oregon coast: Shore & Beach, v. 66, no. 3, 33–41.

Komar, P.D., and Allan, J.C., 2007, A note on the depiction and analysis of wave-height histograms: Shore & Beach, v. 75, no. 3, 1–5.

Komar, P.D., and Allan, J.C., 2010, "Design with Nature" strategies for shore protection—The construction of a cobble berm and artificial dune in an Oregon State Park: U.S. Geological Survey Scientific Investigations Report 2010–5254.

Komar, P.D., and Rea, C.C., 1976, Erosion of Siletz Spit, Oregon: Shore and Beach, v. 44, no. 1, 9–15.

Komar, P.D., Torstenson, R.W., and Shih, S.-M., 1991, Bandon, Oregon: Coastal development and the potential for extreme ocean hazards: Shore & Beach, 59, no. 4, 14–22.

Komar, P.D., McDougal, W.G., Marra, J.J., and Ruggiero, P., 1999, The rational analysis of setback distances: Applications to the Oregon coast: Shore & Beach, v. 67, 41–49.

Komar, P.D., McManus, J., and Styllas, M., 2004, Sediment accumulation in Tillamook Bay, Oregon: Natural processes versus human impacts: Journal of Geology, v. 112, 455–469.

Komar, P.D., Allan, J.C., and Ruggiero, P., 2009, Ocean wave climates: trend and variations due to earth's changing climate, *in* Young, K.C. (ed.), Handbook of Coastal and Ocean Engineering: World Scientific Publishing, 1192 p.

Komar, P.D., Allan, J.C., and Ruggiero, P., 2011, Sea level variations along the U.S. Pacific Northwest Coast: Tectonic and climate controls: Journal of Coastal Research, v. 27, no. 5, 808–823.

Kriebel, D.L., and Dean, R.G., 1993, Convolution method for time-dependent beach-profile response: Journal of Waterway, Port, Coastal and Ocean Engineering, v. 119, no. 2, p. 206-226.

Kuriyama, Y., Mochizuki, N., and Nakashima, T., 2005, Influence of vegetation on aeolian sand transport rate from a backshore to a foredune at Hasaki, Japan: Sedimentology, v. 52, no. 5, 1123–1132.

Marra, J., 2001, Presidential Streets Management Unit (Kramer Point to Harrison Street): Newport, Oreg., Shoreland Solutions**:** 54 p.

Moore, L.J., 2000, Shoreline mapping techniques: Journal of Coastal Research, v. 16, no. 1, 111–124.

Mori, N., Takahashi, T., Yasuda, T., and Yanagisawa, H., 2011, Survey of 2011 Tohoku earthquake tsunami inundation and run-up: Geophysical Research Letters, v. 38, L00G14, no. 7. https://doi.org/10.1029/2011GL049210

Morton, R.A., Leach, M.P., Paine, J.G., and Cardoza, M.A., 1993, Monitoring beach changes using GPS surveying techniques: Journal of Coastal Research, v. 9, no. 3, 702–720.

Nordstrom, K.F., Jackson, N.L., Hartman, J.M., and Wong, M., 2007, Aeolian sediment transport on a human-altered foredune: Earth Surface Processes and Landforms, v. 32, no. 1, 102–115.

NRC, 2012, Sea-level rise for the coasts of California, Oregon, and Washington: Past, present, and future: Washington, D.C., National Research Council.

OCZMA, 1979, Beaches and dunes handbook for the Oregon coast, Report to the Oregon Department of Land Conservation and Development: Newport, Oreg., Oregon Coastal Zone Management Association.

Peterson, C., Scheidegger, K., Komar, P.D., and Niem, W., 1984, Sediment composition and hydrography in six high-gradient estuaries of the northwestern United States: Journal of Sedimentary Petrology, v. 54, no. 1, 86–97.

Peterson, C.D., Jackson, P.L., O'Neil, D.J., Rosenfeld, C.L., and Kimerling, A.J., 1990, Littoral cell response to interannual climatic forcing 1983-1987 on the central Oregon coast, USA: Journal of Coastal Research, v. 6, no. 1, 87–110.

Peterson, C.D., and others, 1994, Beach-shoreline database, Pacific Northwest region, U.S.A.: Oregon Department of Geology and Mineral Industries Open-File Report O-94-2, 29 p. http://www.oregongeology.org/pubs/ofr/O-94-02.zip

Priest, G.R., Saul, I., and Diebenow, J., 1993, Pilot erosion rate data study of the central Oregon coast, Lincoln County: Oregon Department of Geology and Mineral Industries Open-File Report O-93–10, 228 p. http://www.oregongeology.org/pubs/ofr/O-93-10.pdf

Priest, G.R., Goldfinger, C., Wang, K., Witter, R.C., Zhang, Y., and Baptista, A.M., 2010, Confidence levels for tsunami-inundation limits in northern Oregon inferred from a 10,000-year history of great earthquakes at the Cascadia subduction zone: Natural Hazards, v. 54, no. 1, 27–73.

Revell, D., Komar, P.D., and Sallenger, A.H., 2002, An application of LIDAR to analyses of El Niño erosion in the Netarts littoral cell, Oregon: Journal of Coastal Research, v. 18, no. 4, 792–801.

Rosenfeld, C.L., 1997, Cannon Beach: An integrated approach to sand management: Sept. 10, 1997, 24 p., plus 2 app. https://www.ci.cannon-beach.or.us/sites/default/files/fileattachments/planning_commission/page/20521/appsandmngmt.pdf

Ruggiero, P., and Voigt, B., 2000, Beach monitoring in the Columbia River littoral cell, 1997–2000: Olympia, Washington Department of Ecology, Coastal Monitoring and Analysis Program, Publication 00-06-026.

Ruggiero, P., Komar, P.D., McDougal, W.G., and Beach, R.A., 1996, Extreme water levels, wave runup and coastal erosion, Proceedings of the 25th Conference on Coastal Engineering, Orlando, Fla.: American Society of Civil Engineers, p. 2793–2805.

Ruggiero, P., Kaminsky, G.M., and Gelfenbaum, G., 2003, Linking proxy-based and datum-based shorelines on a high-energy coastline: Implications for shoreline change analyses: Journal of Coastal Research, no. SI 38, p. 57-82.

Ruggiero, P., Kaminsky, G.M., Gelfenbaum, G., and Voight, B., 2005, Seasonal to interannual morphodynamics along a high-energy dissipative littoral cell: Journal of Coastal Research, v. 21, no. 3, 553–578.

Ruggiero, P., Komar, P.D., and Allan, J.C., 2010, Increasing wave heights and extreme value projections: The wave climate of the U.S. Pacific Northwest: Coastal Engineering, v. 57, no. 5, 539–552.

Ruggiero, P., Kratzmann, M.G., Himmelstoss, E.A., Reid, D., Allan, J., and Kaminsky, G., 2013, National assessment of shoreline change: Historical shoreline change along the Pacific Northwest coast [Oregon and Washington]: Reston, Va., U.S. Geological Survey Open-File Report 2012-1007, 61 p., scale 1:70,000. https://pubs.er.usgs.gov/publication/ofr20121007

Satake, K., Shimazaki, K., Yoshinobu, T., and Ueda, K., 1996, Time and size of a giant earthquake in Cascadia inferred from Japanese tsunami records of January 1700: Nature, v. 379, no. 6562, 246–249.

Schlicker, H.G., Deacon, R.J., Beaulieu, J.D., and Olcott, G.W., 1972, Environmental geology of the coastal region of Tillamook and Clatsop counties, Oregon: Oregon Department of Geology and Mineral Industries Bulletin 74, 164 p., 18 pl., scale 1:62,500. http://www.oregongeology.org/pubs/B/B-074.zip

Sherman, D.J., Jackson, D.W., Namikas, S.L., and Wang, J., 1998, Wind-blown sand on beaches: an evaluation of models: Geomorphology, v. 22, no. 2, 113–133. https://doi.org/10.1016/S0169-555X(97)00062-7

Sherwood, C.R., Jay, D.A., Harvey, R.B., Hamilton, P., and Simenstad, C.A., 1990, Historical changes in the Columbia River Estuary: Progress in Oceanography, v. 25, no. 1, 299–352.

Shoreland Solutions, 1998a, Manzanita foredune management plan: Newport, Oreg., prepared for Manzanita Beachfront Homeowners Association.

Shoreland Solutions, 1998b, Pacific City foredune management plan: management strategy: Newport, Oreg., prepared for Pacific City Beachfront Homeowners Association.

Simm, J.D., Brampton, A.H., Beech, N.W., and Brooke, J.S. (eds.), 1996, Beach management manual: London, Construction Industry Research and Information Association (CIRIA) Report 153, 448 p.

Stockdon, H.F., Holman, R.A., Howd, P.A., and Sallenger, A.H., 2006, Empirical parameterization of setup, swash, and runup: Coastal Engineering, v. 53, no. 7, 573–588.

Suzuki, E., and Numata, M., 1982, Succession on a sandy coast following the construction of banks planted with *Elymus mollis*: Japanese Journal of Ecology, v. 32, no. 2, 129–142.

Ternyik, W.E., 1979, Dune stabilization and restoration: methods and criteria, *in* Beaches and dunes handbook for the Oregon coast, Report to the Oregon Department of Land Conservation and Development: Newport, Oreg., Oregon Coastal Zone Management Association, 40 p.

Trimble, 2005, Trimble 5700 GPS system datasheet: Dayton, Ohio, Trimble Navigation Limited.

Witter, R.C., 2008, Prehistoric Cascadia tsunami inundation and runup at Cannon Beach, Clatsop County, Oregon: Oregon Department of Geology and Mineral Industries Open-File Report O-08-12, 36 p. http://www.oregongeology.org/pubs/ofr/O-08-12.zip

Witter, R.C., Kelsey, H.M., and Hemphill-Haley, E., 2003, Great Cascadia earthquakes and tsunamis of the past 6700 years, Coquille River estuary, southern coastal Oregon: Geological Society of America Bulletin, v. 115, 1289–1306.

Witter, R.C., Horning, T., and Allan, J.C., 2009, Coastal erosion hazard zones in southern Clatsop County, Oregon: Seaside to Cape Falcon: Oregon Department of Geology and Mineral Industries Open-File Report O-09-06, 39 p., 16 pl., GIS data. http://www.oregongeology.org/pubs/ofr/O-09-06.zip

Witter, R.C., Zhang, Y., Goldfinger, C., Priest, G.R., and Wang, K., 2010, Validating numerical tsunami simulations in southern Oregon using late Holocene records of great Cascadia earthquakes and tsunamis, 2010 Annual Meeting, April 21–23, Portland, Oreg., Seismological Society of America.

Woodhouse, W.W., 1978, Dune building and stabilization with vegetation: Fort Belvoir, Va.: U.S. Army Corps of Engineers, Coastal Engineering Research Center, 122 p.

Yamamoto, M., 2011, IOC/UNESCO Bulletin No. 17 (April 5, 2011) — Tōhoku Tsunami March 11, 2011: Intergovernmental Oceanographic Commission of UNESCO (IOC-UNESCO). ftp://ftp.ngdc.noaa.gov/hazards/publications/20110311_iocbulletin17.pdf

Zarnetske, P.L., Hacker, S. D., Seabloom, E.W., Ruggiero, P., Killian, J.R., Maddux, T.B., and Cox, D., 2012, Biophysical feedback mediates effects of invasive grasses on coastal dune shape: Ecology, v. 93, no. 6, 1439–1450. https://doi.org/10.1890/11-1112.1

Zarnetske, P.L., Ruggiero, P., Seabloom, E.W., and Hacker, S.D., 2015, Coastal foredune evolution: the relative influence of vegetation and sand supply in the US Pacific Northwest: Journal of the Royal Society Interface, v. 12, no. 106, 20150017. DOI: 10.1098/rsif.2015.0017 http://rsif.royalsocietypublishing.org/content/12/106/20150017

10.0 APPENDIX: CANNON BEACH PROFILES

The following profiles (Falcon Cove: FC1–FC6; Arch Cape: AC1–AC13; and Cannon Beach: CB1–CB40) depict the measured beach profile changes from 1997 to 2016 for selected sites in the Cannon Beach littoral cell. Dark gray shading in the plots depicts the normal range of variability (mean profile ±1σ range), while the yellow-gray indicates the maximum/minimum measurements determined from all surveys (latter excludes surveys undertaken in 1997 and 1998).

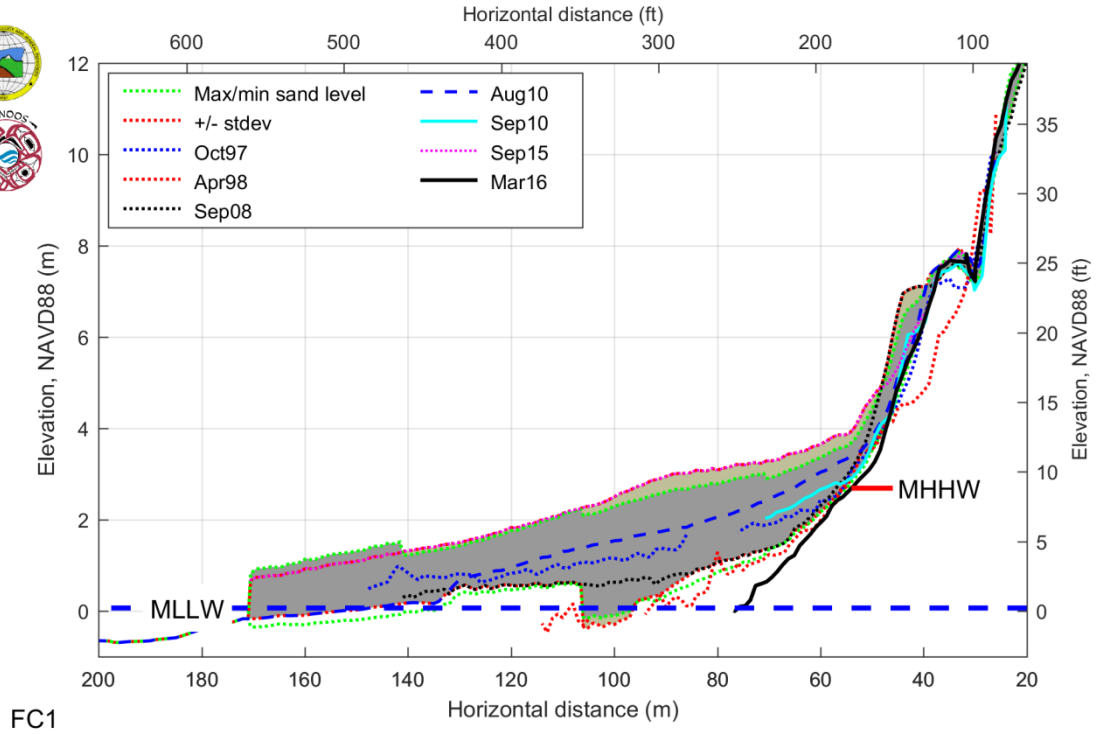

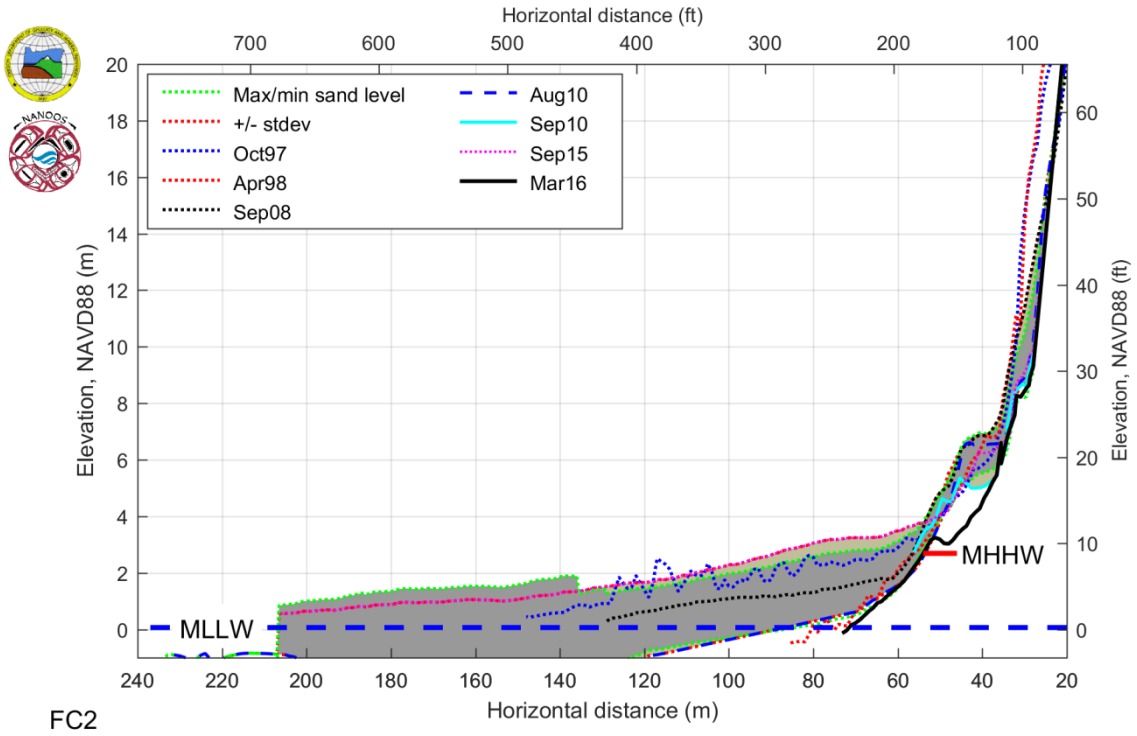
Horizontal distance (ft)
700
600
500
400
300
200
100
Max/min sand level
+/- stdev
Oct97
Apr98
Sep08
Aug10
Sep10
Sep15
Mar16
Elevation, NAVD88 (m)
Elevation, NAVD88 (ft)
MHHW
MLLW
240
220
200
180
160
140
120
100
80
60
40
20
Horizontal distance (m)

FC2

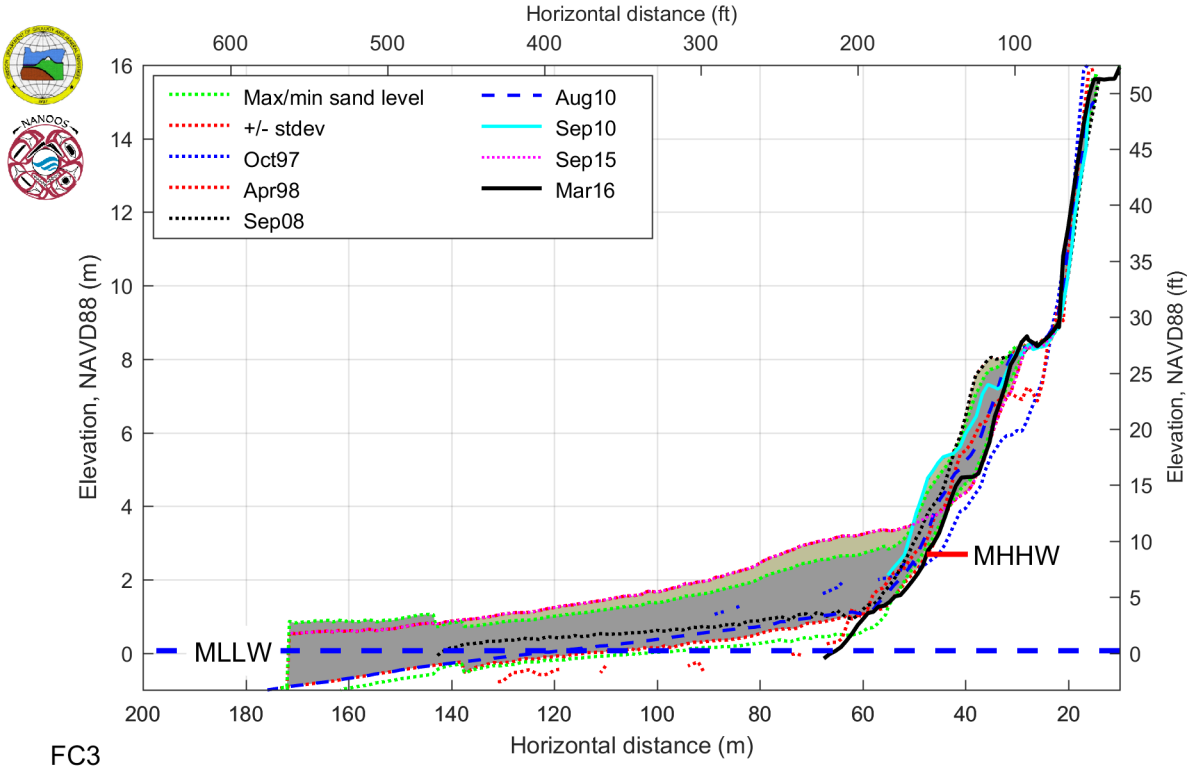
Horizontal distance (ft)
600
500
400
300
200
100
Max/min sand level
+/- stdev
Oct97
Apr98
Sep08
Aug10
Sep10
Sep15
Mar16
Elevation, NAVD88 (m)
Elevation, NAVD88 (ft)
MHHW
MLLW
200
180
160
140
120
100
80
60
40
20
Horizontal distance (m)

FC3

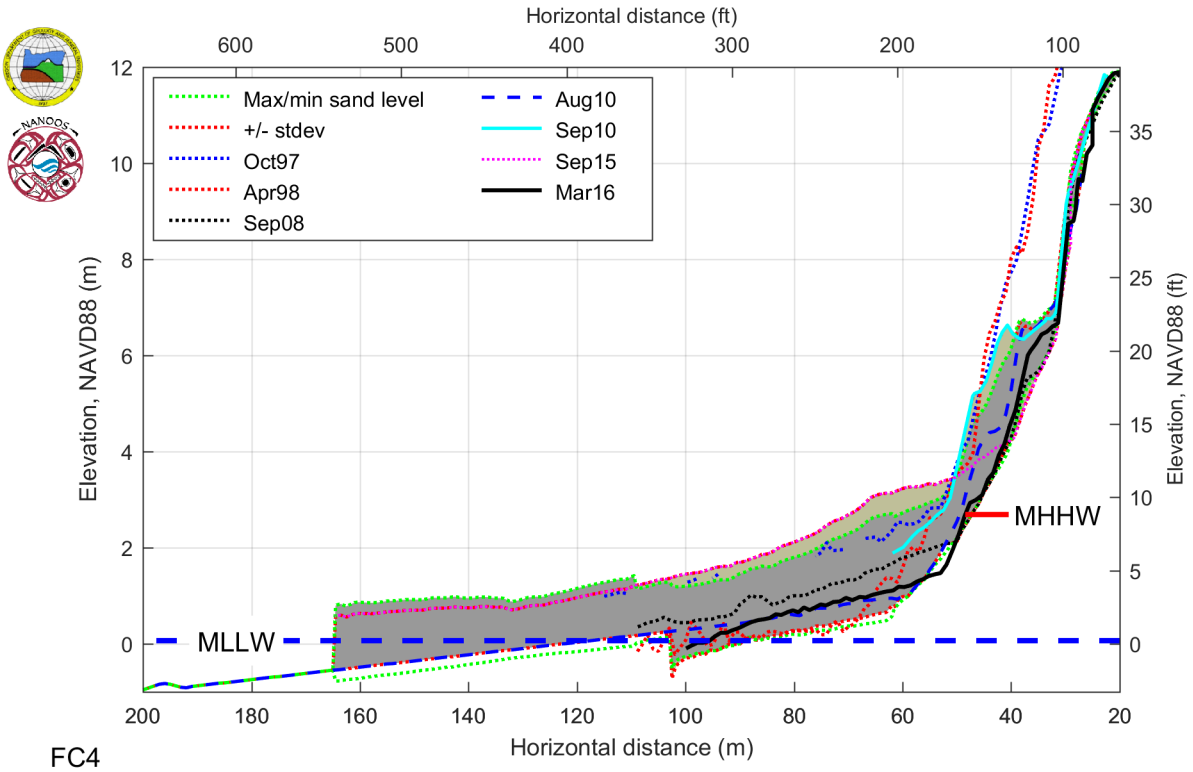
Horizontal distance (ft)
600
500
400
300
200
100
Max/min sand level
+/- stdev
Oct97
Apr98
Sep08
Aug10
Sep10
Sep15
Mar16
Elevation, NAVD88 (m)
Elevation, NAVD88 (ft)
MHHW
MLLW
200
180
160
140
120
100
80
60
40
20
Horizontal distance (m)

FC4

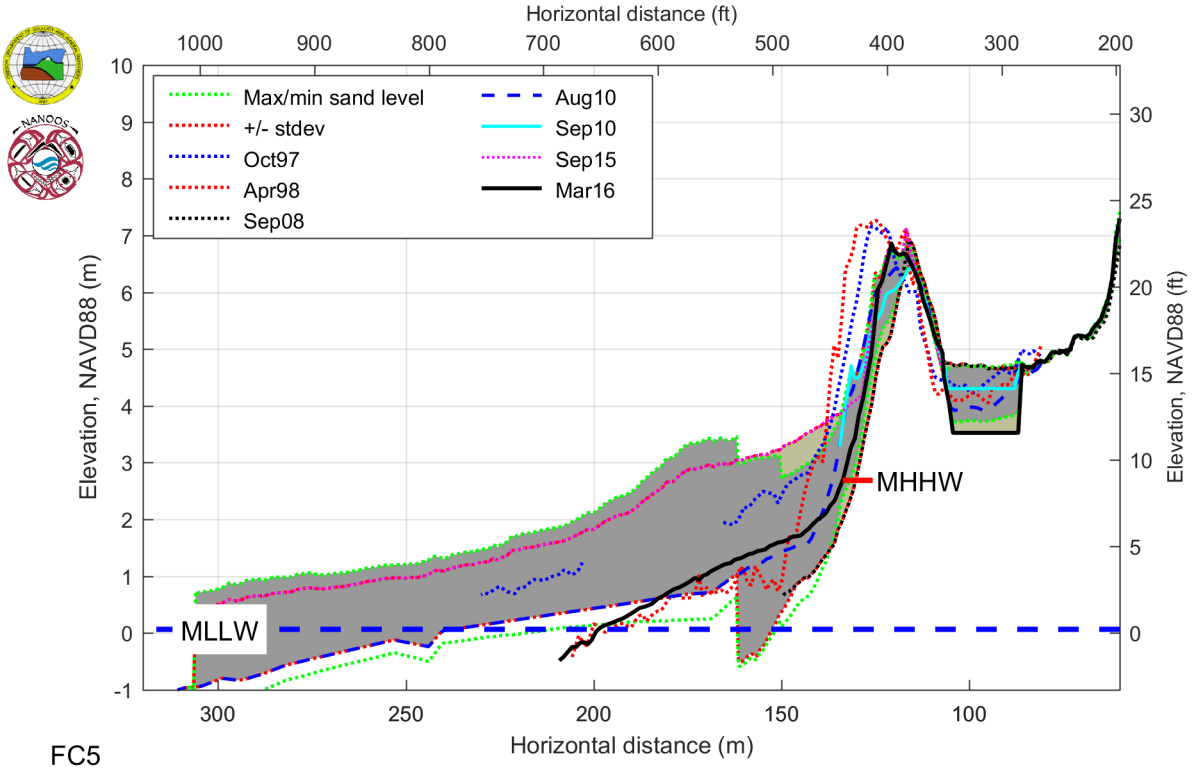
Horizontal distance (ft)
1000
900
800
700
600
500
400
300
200
Max/min sand level
+/- stdev
Oct97
Apr98
Sep08
Aug10
Sep10
Sep15
Mar16
Elevation, NAVD88 (m)
Elevation, NAVD88 (ft)
MHHW
MLLW
300
250
200
150
100
Horizontal distance (m)

FC5

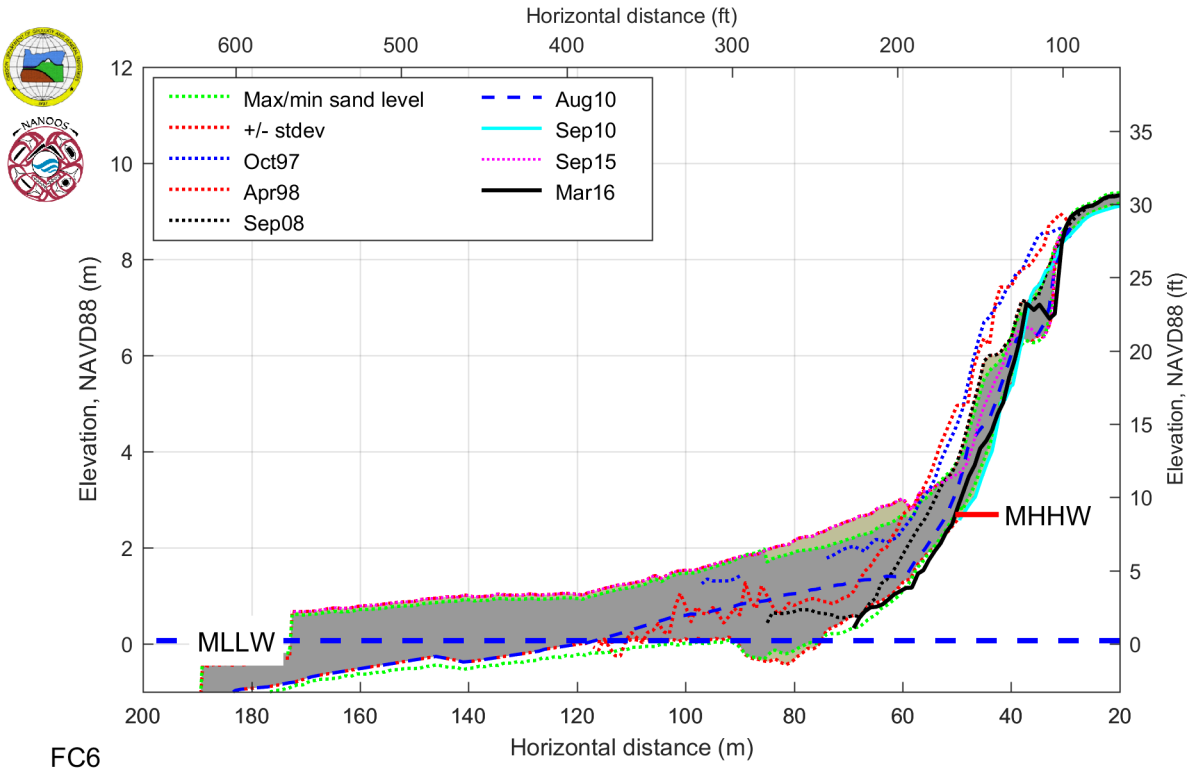
Horizontal distance (ft)
600
500
400
300
200
100
Max/min sand level
+/- stdev
Oct97
Apr98
Sep08
Aug10
Sep10
Sep15
Mar16
Elevation, NAVD88 (m)
Elevation, NAVD88 (ft)
MHHW
MLLW
200
180
160
140
120
100
80
60
40
20
Horizontal distance (m)

FC6

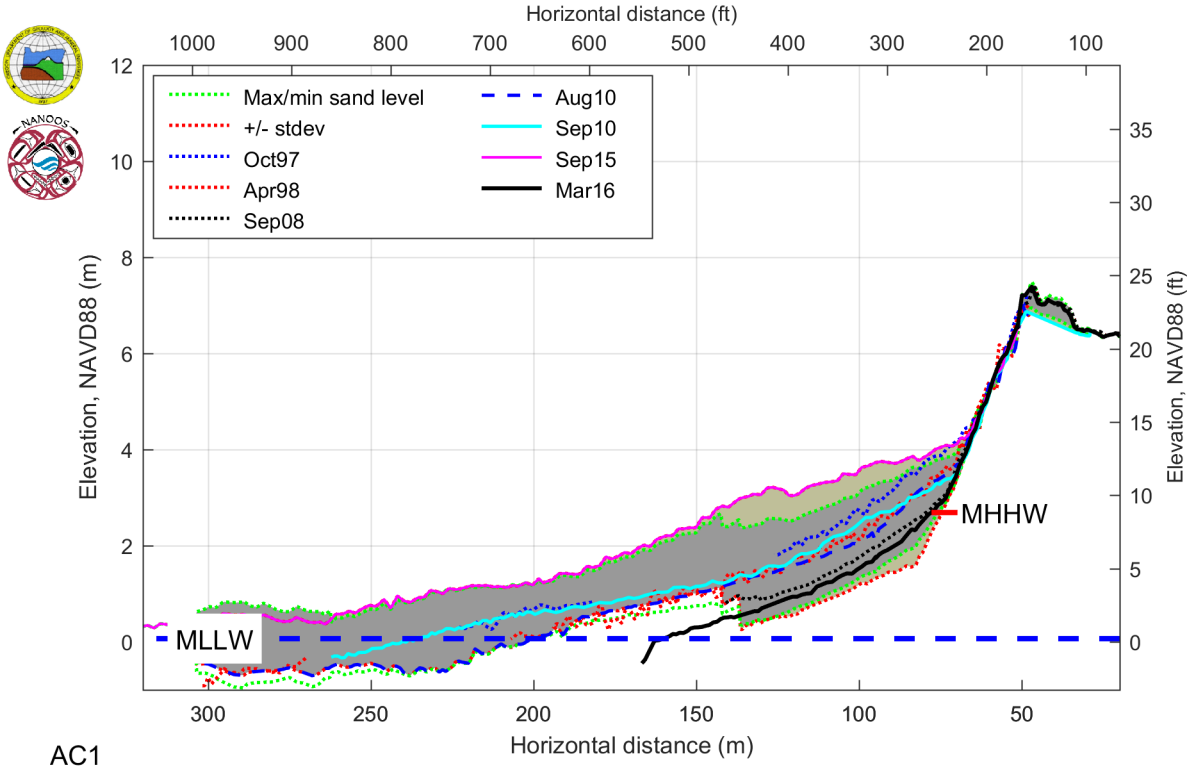
Horizontal distance (ft)
1000
900
800
700
600
500
400
300
200
100
Max/min sand level
+/- stdev
Oct97
Apr98
Sep08
Aug10
Sep10
Sep15
Mar16
Elevation, NAVD88 (m)
Elevation, NAVD88 (ft)
MHHW
MLLW
300
250
200
150
100
50
Horizontal distance (m)

AC1

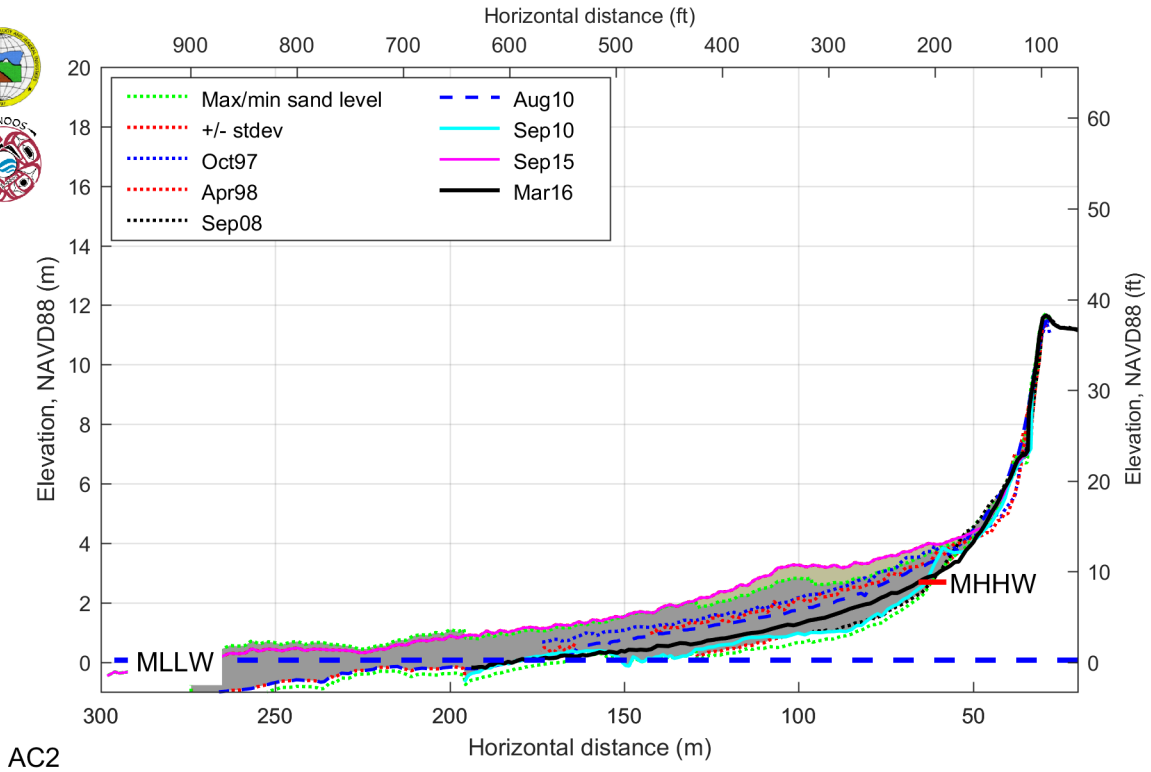
Horizontal distance (ft)
900 800 700 600 500 400 300 200 100
Max/min sand level
+/- stdev
Oct97
Apr98
Sep08
Aug10
Sep10
Sep15
Mar16
Elevation, NAVD88 (m)
Elevation, NAVD88 (ft)
MHHW
MLLW
300 250 200 150 100 50
Horizontal distance (m)

AC2

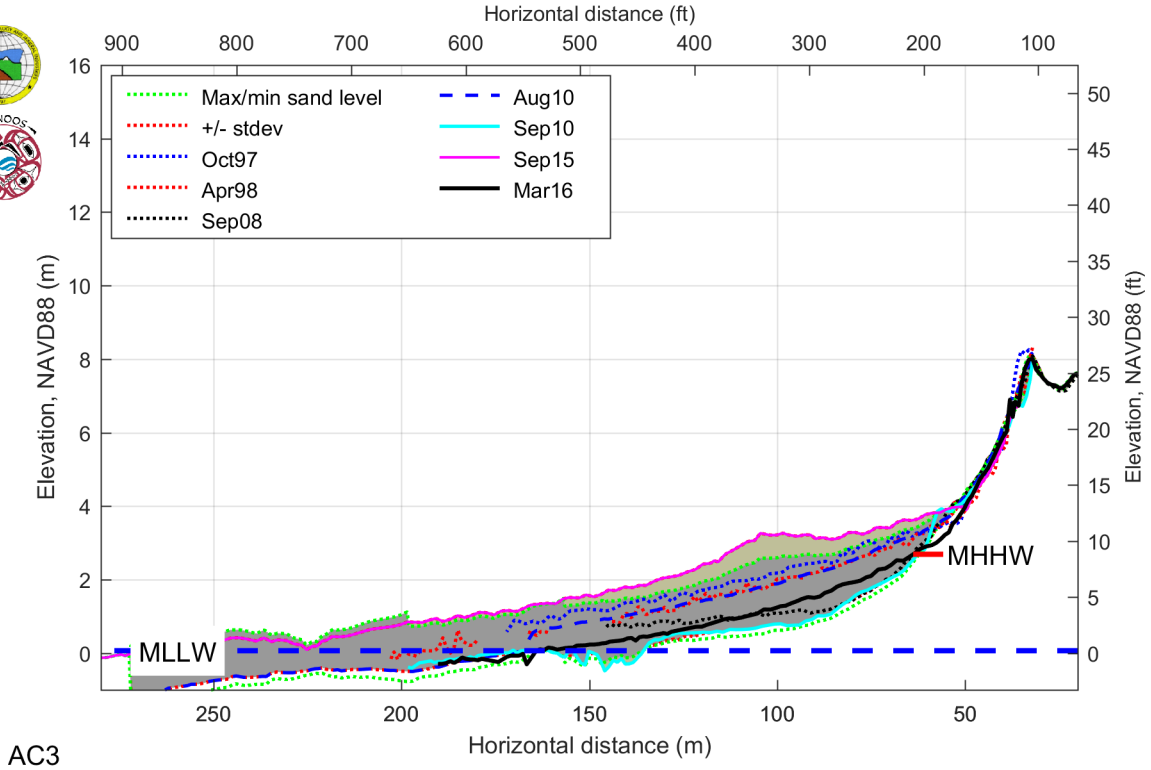
Horizontal distance (ft)
900 800 700 600 500 400 300 200 100
Max/min sand level
+/- stdev
Oct97
Apr98
Sep08
Aug10
Sep10
Sep15
Mar16
Elevation, NAVD88 (m)
Elevation, NAVD88 (ft)
MHHW
MLLW
250 200 150 100 50
Horizontal distance (m)

AC3

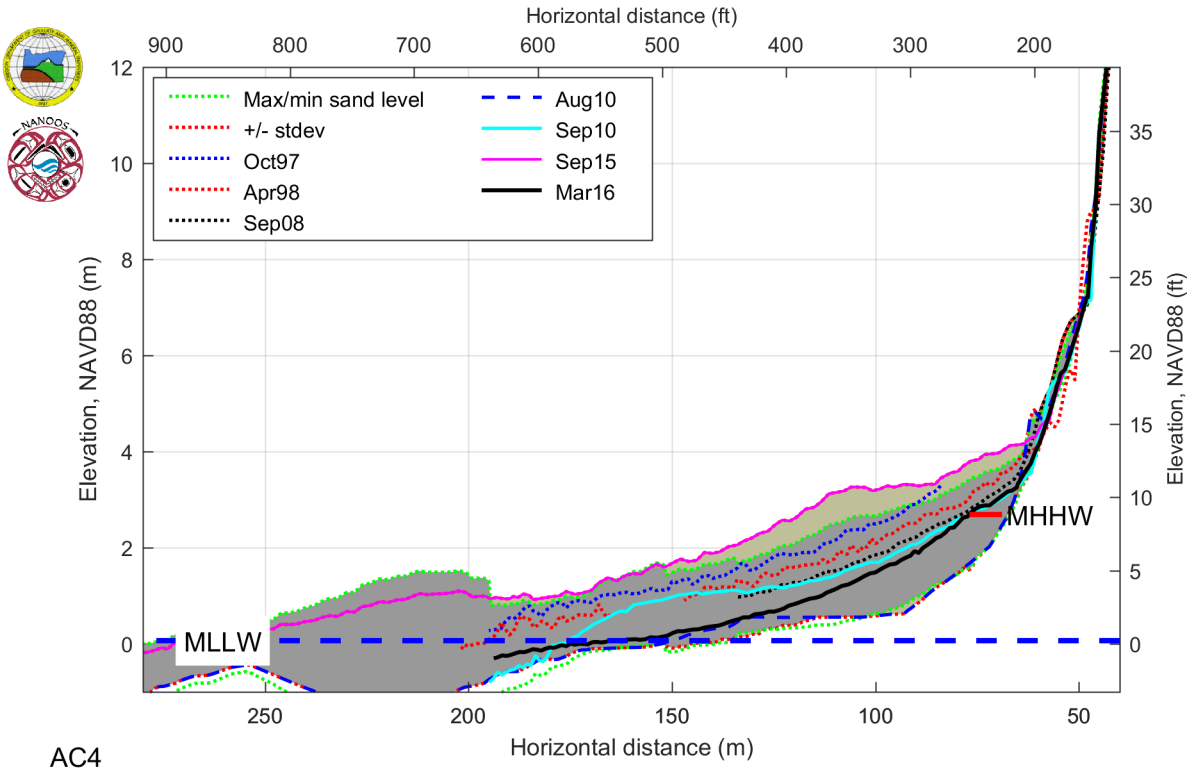
Horizontal distance (ft)
900
800
700
600
500
400
300
200
Max/min sand level
+/- stdev
Oct97
Apr98
Sep08
Aug10
Sep10
Sep15
Mar16
Elevation, NAVD88 (m)
Elevation, NAVD88 (ft)
MHHW
MLLW
250
200
150
100
50
Horizontal distance (m)

AC4

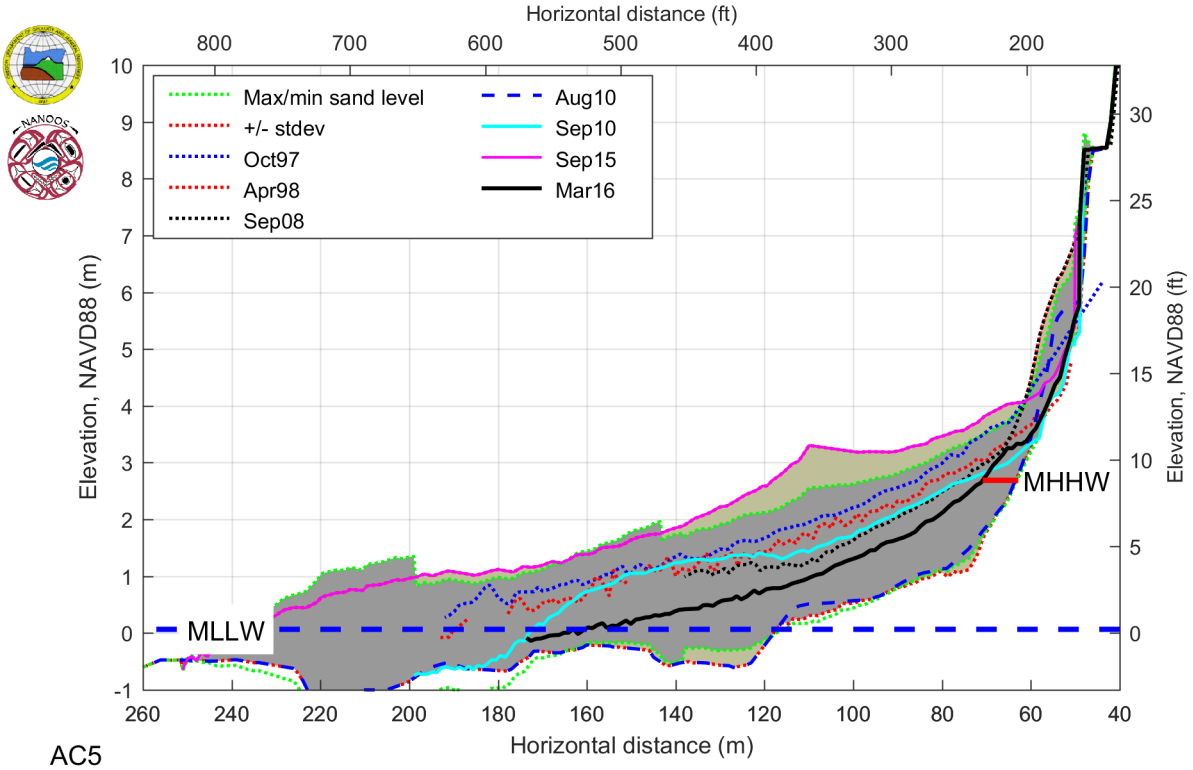
Horizontal distance (ft)
800
700
600
500
400
300
200
Max/min sand level
+/- stdev
Oct97
Apr98
Sep08
Aug10
Sep10
Sep15
Mar16
Elevation, NAVD88 (m)
Elevation, NAVD88 (ft)
MHHW
MLLW
260
240
220
200
180
160
140
120
100
80
60
40
Horizontal distance (m)

AC5

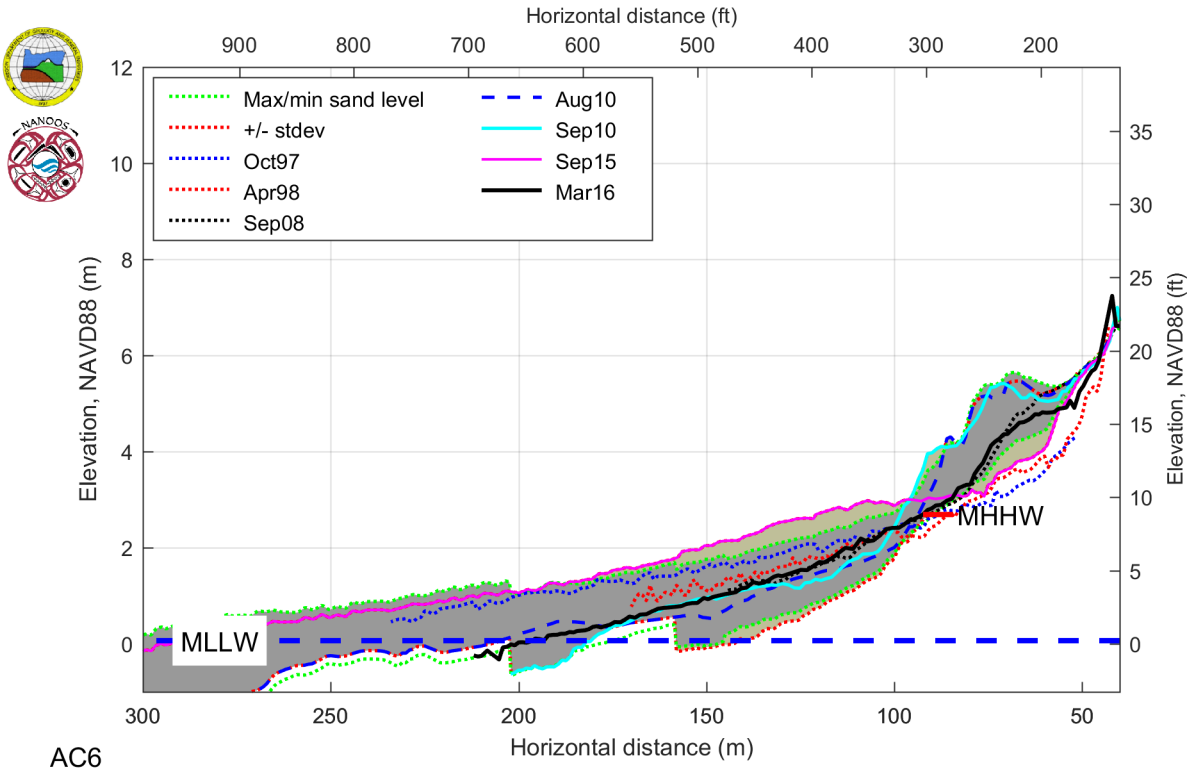
Horizontal distance (ft)
900
800
700
600
500
400
300
200
Max/min sand level
+/- stdev
Oct97
Apr98
Sep08
Aug10
Sep10
Sep15
Mar16
MHHW
MLLW
Elevation, NAVD88 (m)
Elevation, NAVD88 (ft)
Horizontal distance (m)
300
250
200
150
100
50

AC6

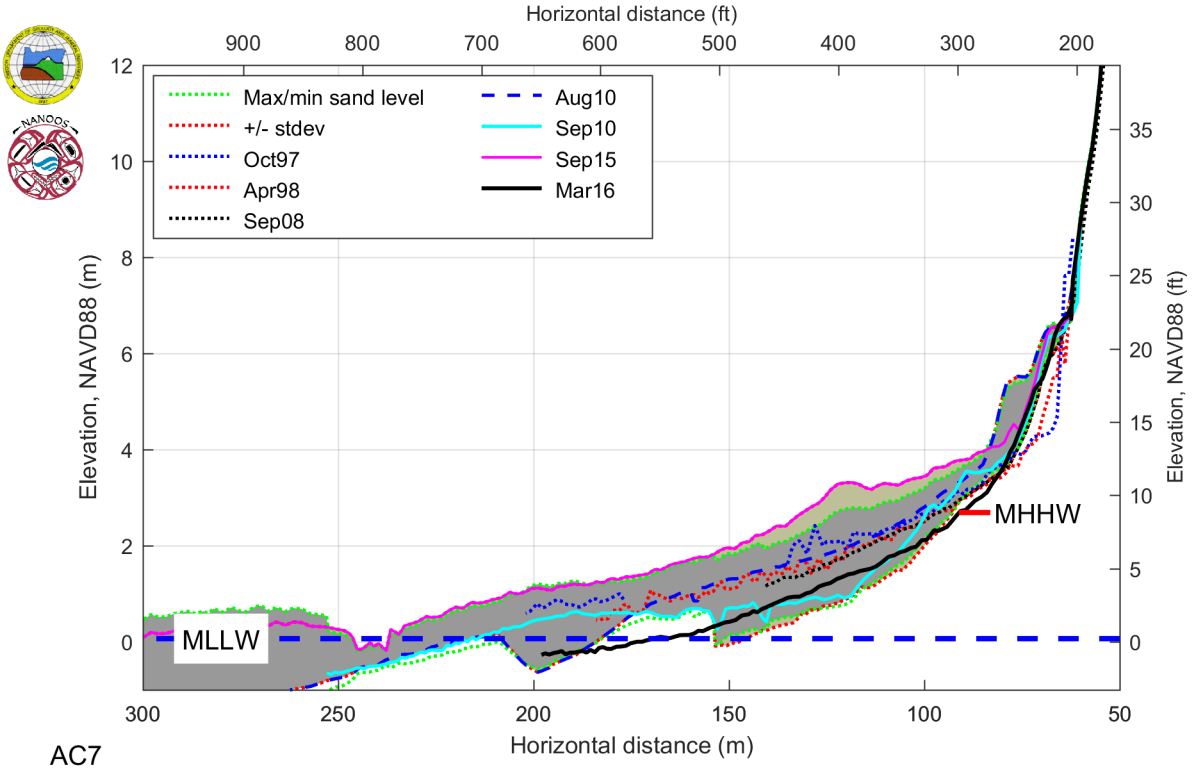
Horizontal distance (ft)
900
800
700
600
500
400
300
200
Max/min sand level
+/- stdev
Oct97
Apr98
Sep08
Aug10
Sep10
Sep15
Mar16
MHHW
MLLW
Elevation, NAVD88 (m)
Elevation, NAVD88 (ft)
Horizontal distance (m)
300
250
200
150
100
50

AC7

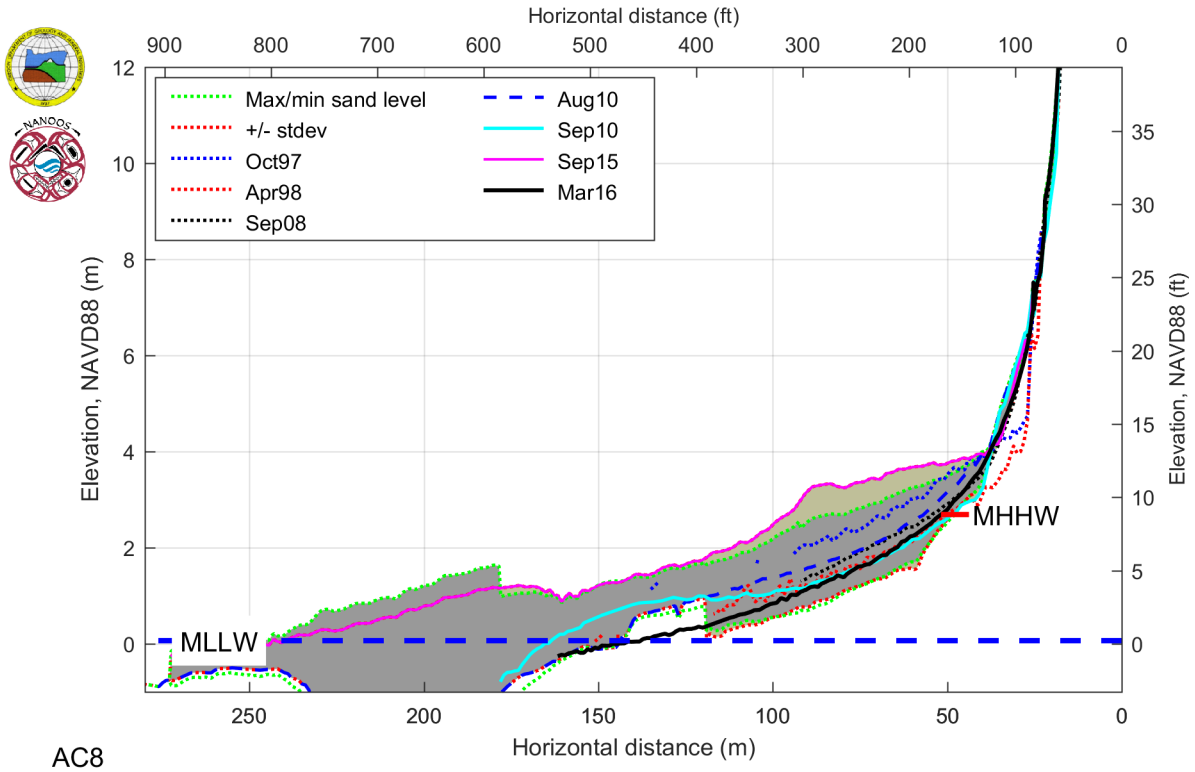
Horizontal distance (ft)
900
800
700
600
500
400
300
200
100
0
Max/min sand level
+/- stdev
Oct97
Apr98
Sep08
Aug10
Sep10
Sep15
Mar16
Elevation, NAVD88 (m)
Elevation, NAVD88 (ft)
MHHW
MLLW
250
200
150
100
50
0
Horizontal distance (m)

AC8

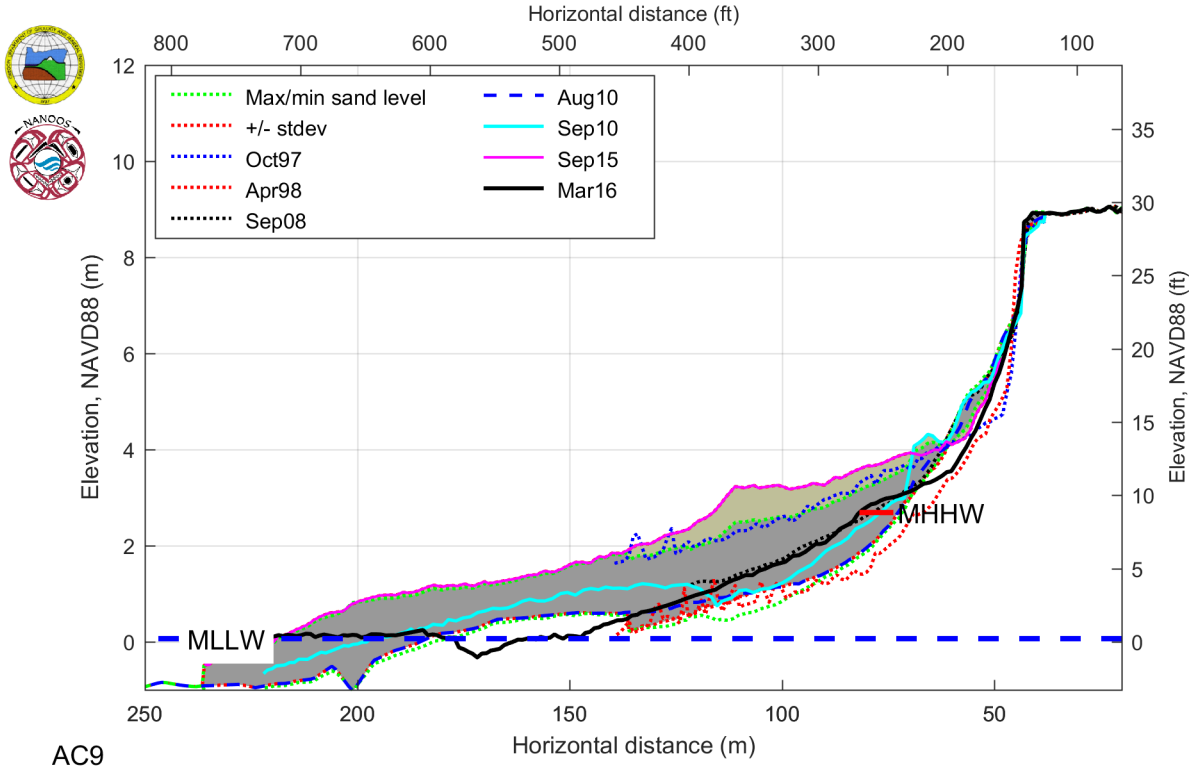
Horizontal distance (ft)
800
700
600
500
400
300
200
100
Max/min sand level
+/- stdev
Oct97
Apr98
Sep08
Aug10
Sep10
Sep15
Mar16
Elevation, NAVD88 (m)
Elevation, NAVD88 (ft)
MHHW
MLLW
250
200
150
100
50
Horizontal distance (m)

AC9

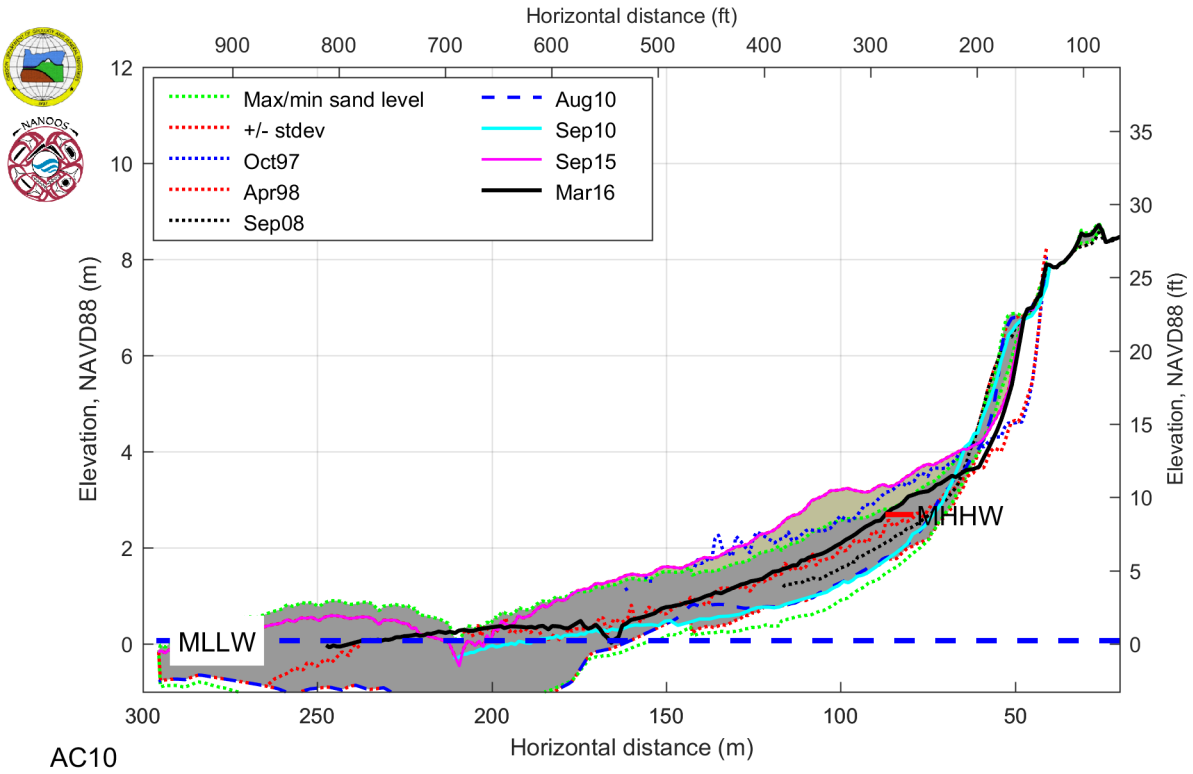
Horizontal distance (ft)
900 800 700 600 500 400 300 200 100
Max/min sand level
+/- stdev
Oct97
Apr98
Sep08
Aug10
Sep10
Sep15
Mar16
MHHW
MLLW
Elevation, NAVD88 (m)
Elevation, NAVD88 (ft)
300 250 200 150 100 50
Horizontal distance (m)

AC10

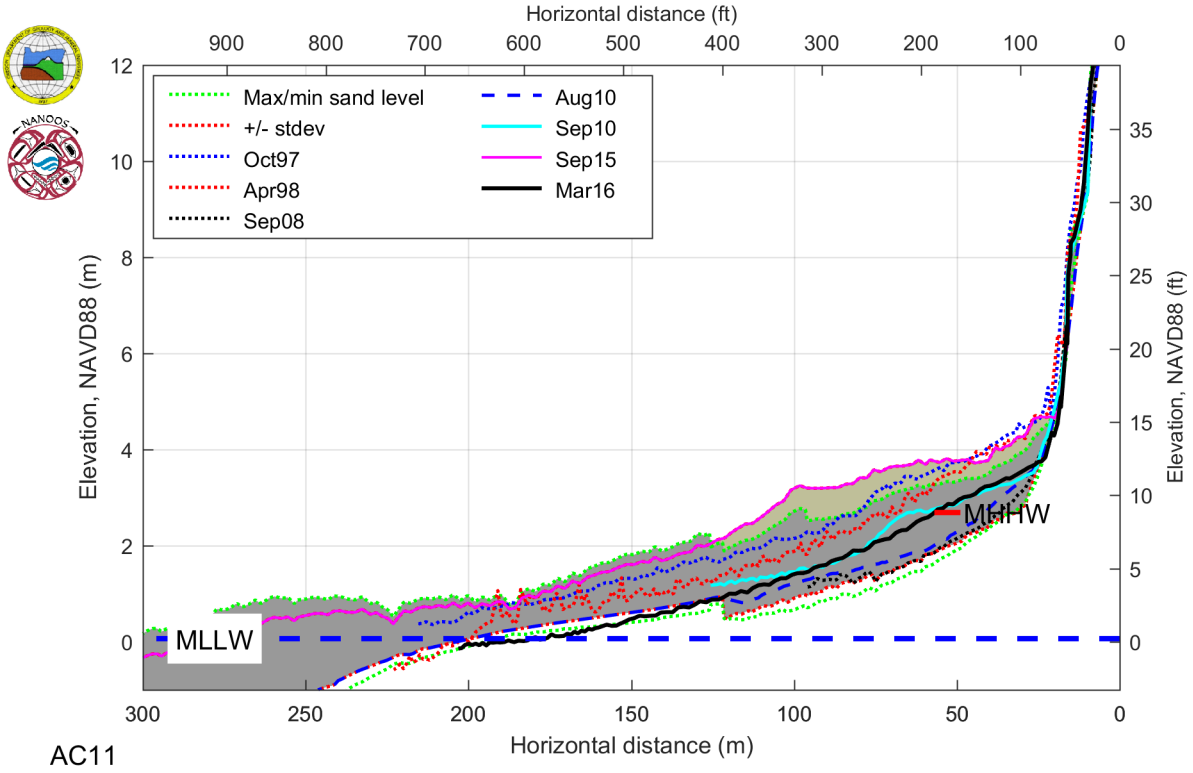
Horizontal distance (ft)
900 800 700 600 500 400 300 200 100 0
Max/min sand level
+/- stdev
Oct97
Apr98
Sep08
Aug10
Sep10
Sep15
Mar16
MHHW
MLLW
Elevation, NAVD88 (m)
Elevation, NAVD88 (ft)
300 250 200 150 100 50 0
Horizontal distance (m)

AC11

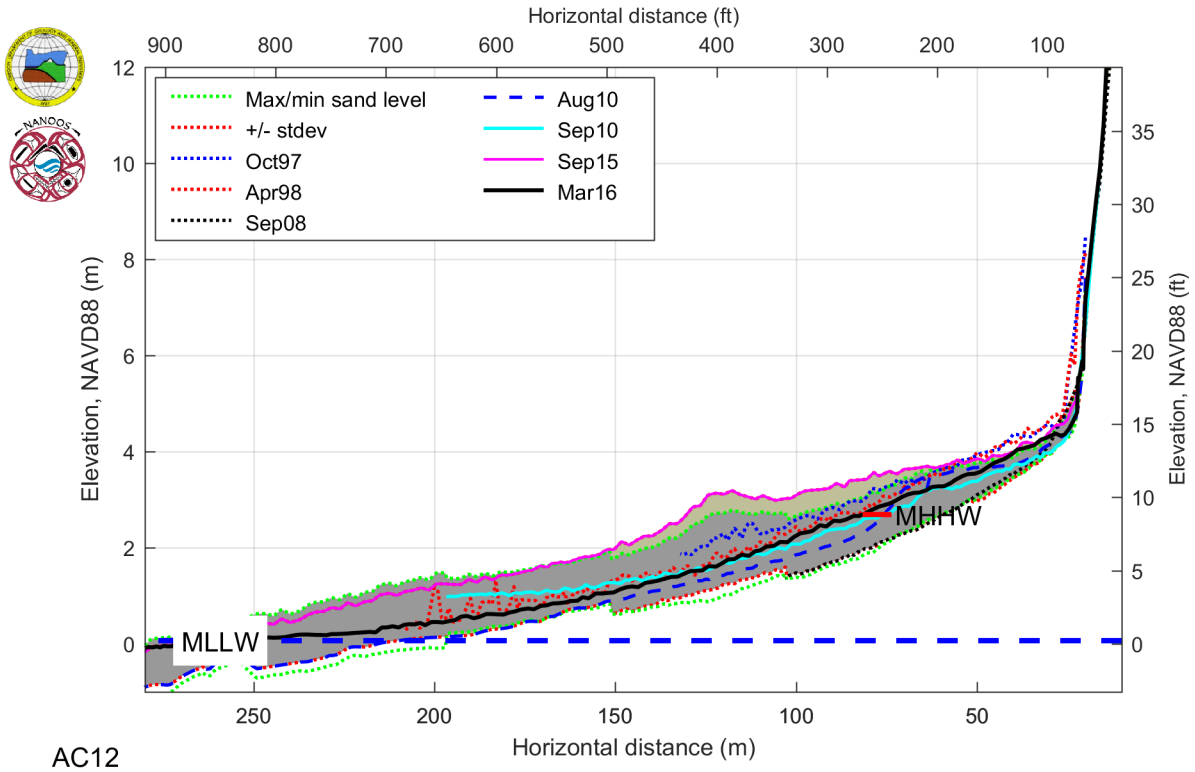
Horizontal distance (ft)
900
800
700
600
500
400
300
200
100
Max/min sand level
+/- stdev
Oct97
Apr98
Sep08
Aug10
Sep10
Sep15
Mar16
MHHW
MLLW
Elevation, NAVD88 (m)
Elevation, NAVD88 (ft)
250
200
150
100
50
Horizontal distance (m)

AC12

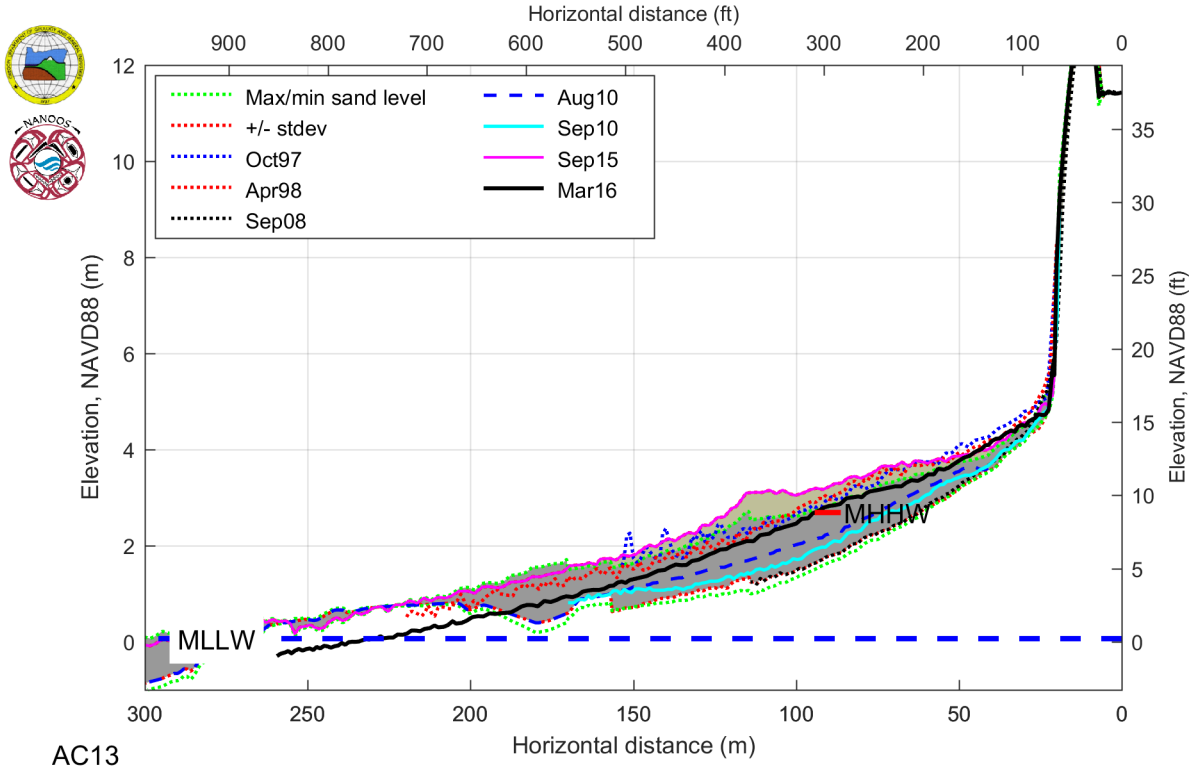
Horizontal distance (ft)
900
800
700
600
500
400
300
200
100
0
Max/min sand level
+/- stdev
Oct97
Apr98
Sep08
Aug10
Sep10
Sep15
Mar16
MHHW
MLLW
Elevation, NAVD88 (m)
Elevation, NAVD88 (ft)
300
250
200
150
100
50
0
Horizontal distance (m)

AC13

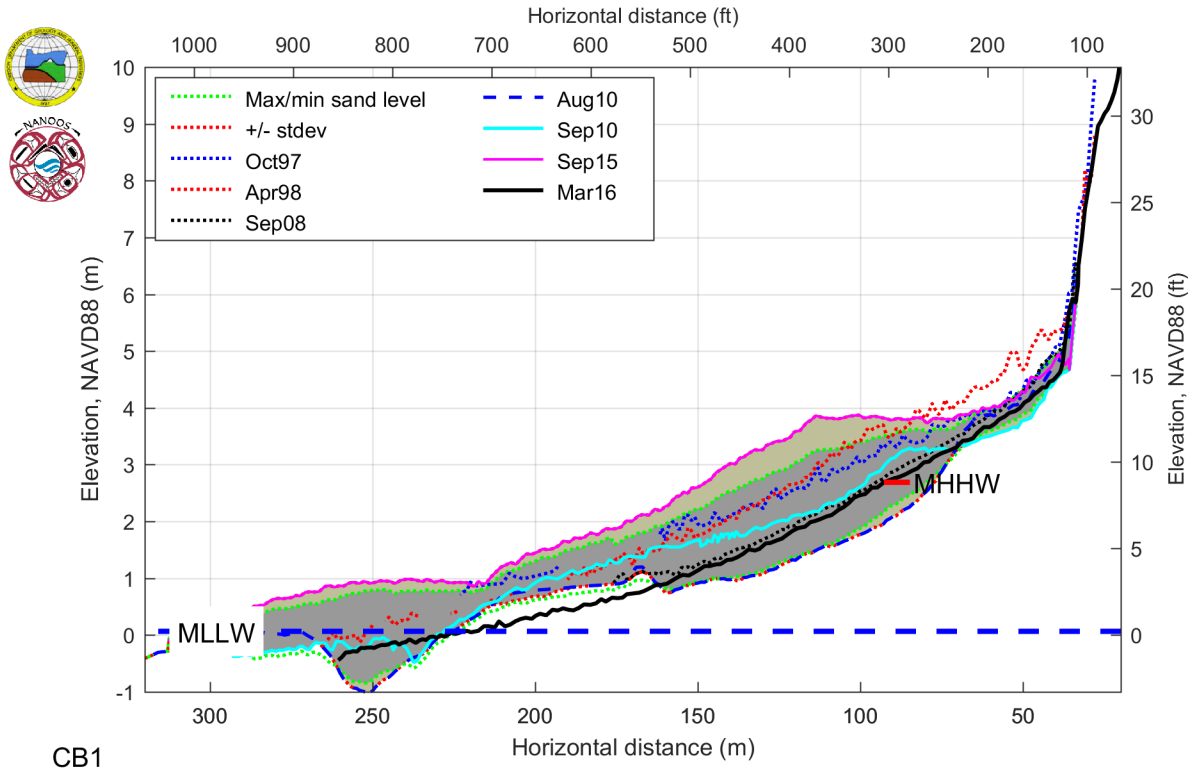
Horizontal distance (ft)
1000
900
800
700
600
500
400
300
200
100
Max/min sand level
+/- stdev
Oct97
Apr98
Sep08
Aug10
Sep10
Sep15
Mar16
MHHW
MLLW
Elevation, NAVD88 (m)
Elevation, NAVD88 (ft)
Horizontal distance (m)
300
250
200
150
100
50

CB1

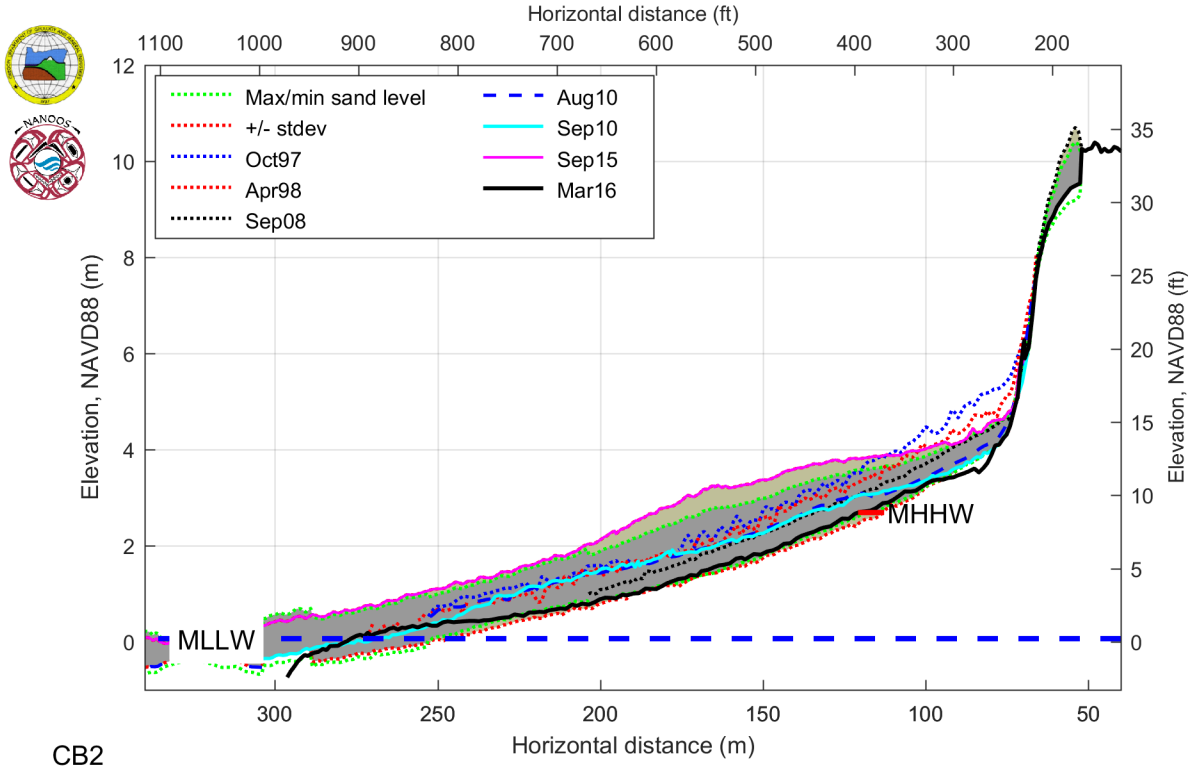
Horizontal distance (ft)
1100
1000
900
800
700
600
500
400
300
200
Max/min sand level
+/- stdev
Oct97
Apr98
Sep08
Aug10
Sep10
Sep15
Mar16
MHHW
MLLW
Elevation, NAVD88 (m)
Elevation, NAVD88 (ft)
Horizontal distance (m)
300
250
200
150
100
50

CB2

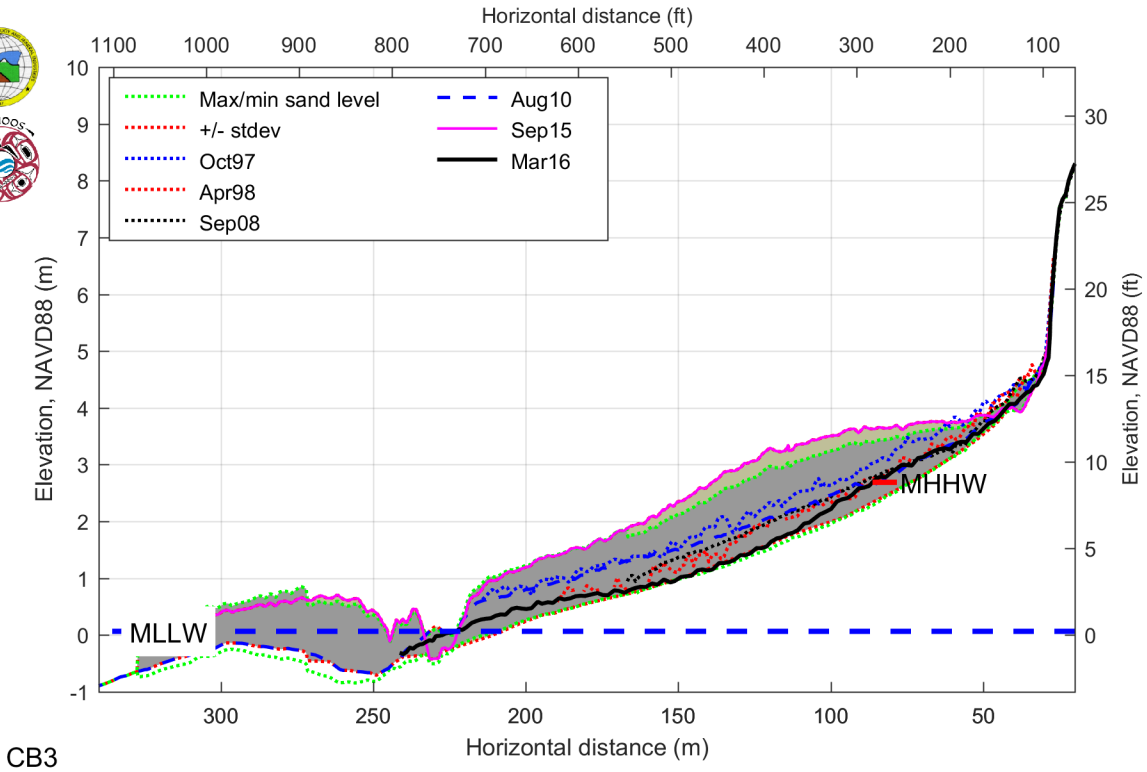
Horizontal distance (ft)
1100 1000 900 800 700 600 500 400 300 200 100
Max/min sand level
+/- stdev
Oct97
Apr98
Sep08
Aug10
Sep15
Mar16
MHHW
MLLW
Elevation, NAVD88 (m)
Elevation, NAVD88 (ft)
300 250 200 150 100 50
Horizontal distance (m)

CB3

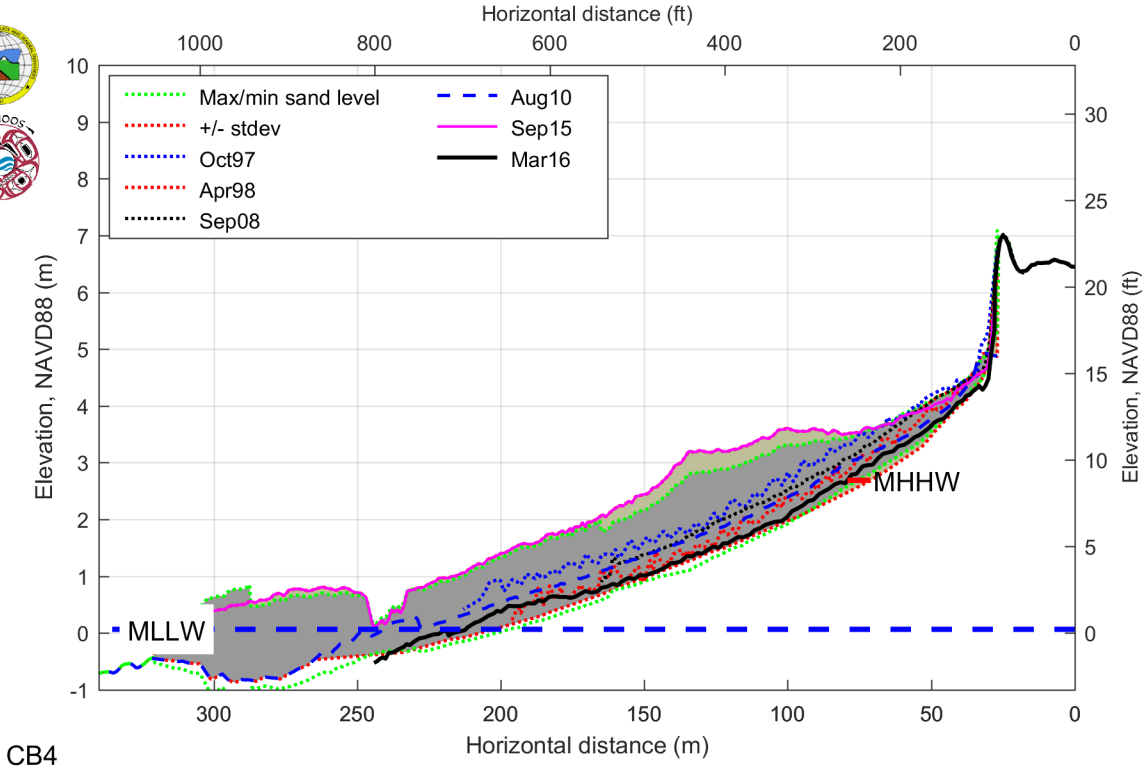
Horizontal distance (ft)
1000 800 600 400 200 0
Max/min sand level
+/- stdev
Oct97
Apr98
Sep08
Aug10
Sep15
Mar16
MHHW
MLLW
Elevation, NAVD88 (m)
Elevation, NAVD88 (ft)
300 250 200 150 100 50 0
Horizontal distance (m)

CB4

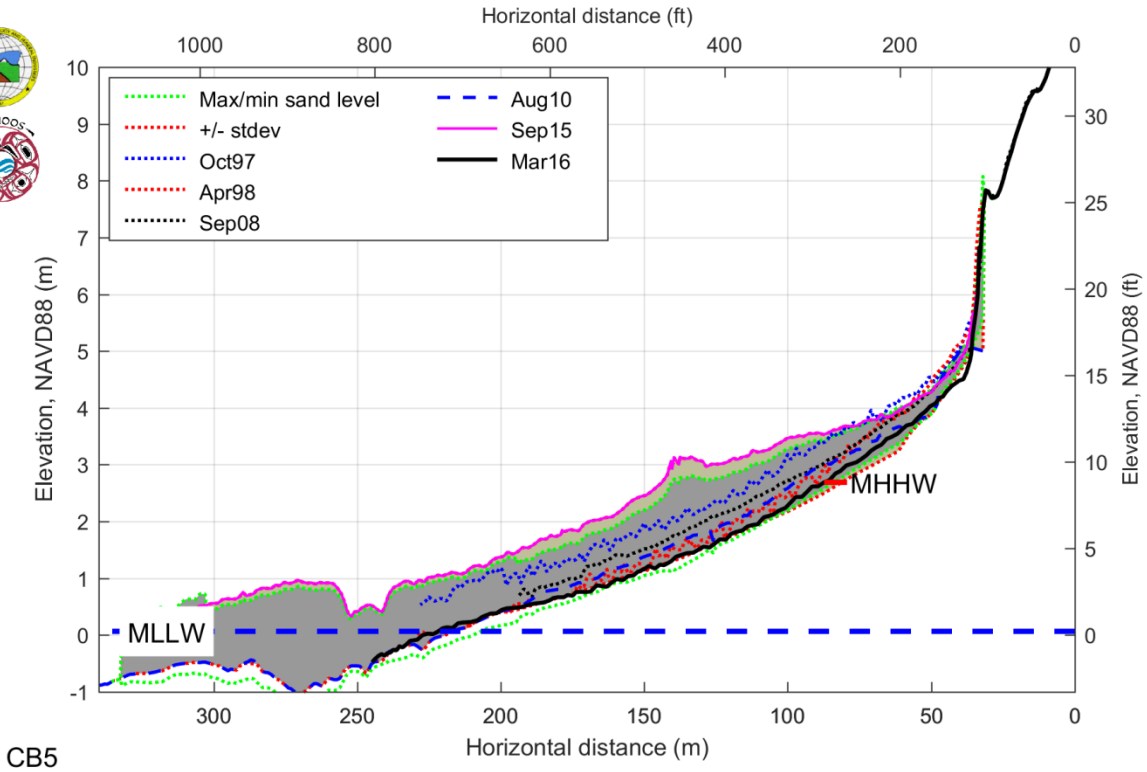
Horizontal distance (ft)
1000
800
600
400
200
0
Max/min sand level
+/- stdev
Oct97
Apr98
Sep08
Aug10
Sep15
Mar16
MHHW
MLLW
Elevation, NAVD88 (m)
Elevation, NAVD88 (ft)
Horizontal distance (m)
300
250
200
150
100
50
0

CB5

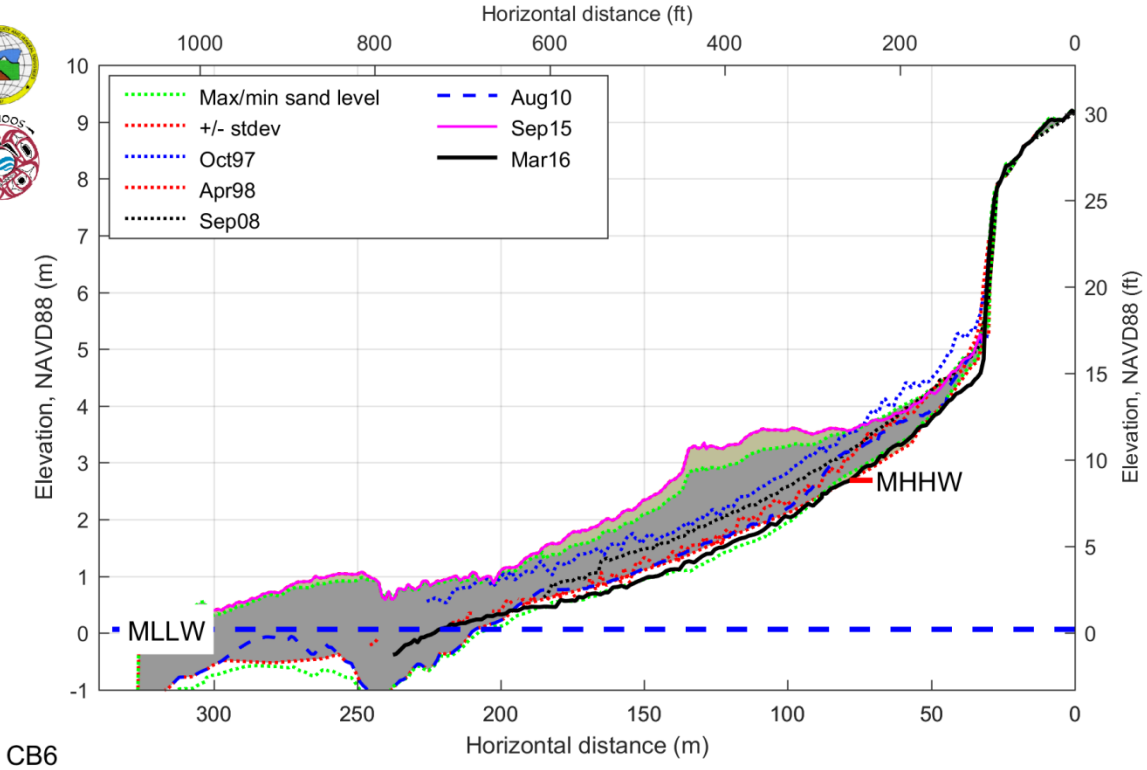
Horizontal distance (ft)
1000
800
600
400
200
0
Max/min sand level
+/- stdev
Oct97
Apr98
Sep08
Aug10
Sep15
Mar16
MHHW
MLLW
Elevation, NAVD88 (m)
Elevation, NAVD88 (ft)
Horizontal distance (m)
300
250
200
150
100
50
0

CB6

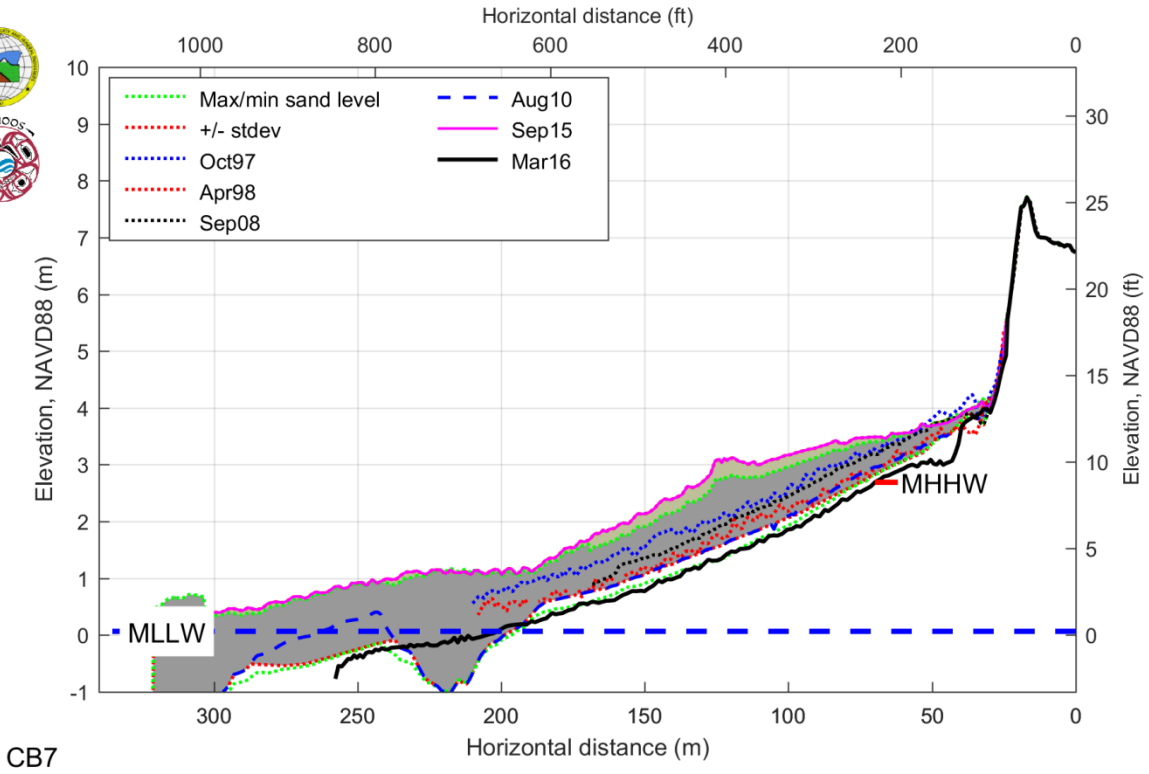
Horizontal distance (ft)
1000
800
600
400
200
0
Max/min sand level
+/- stdev
Oct97
Apr98
Sep08
Aug10
Sep15
Mar16
MHHW
MLLW
Elevation, NAVD88 (m)
Elevation, NAVD88 (ft)
Horizontal distance (m)
300
250
200
150
100
50
0

CB7

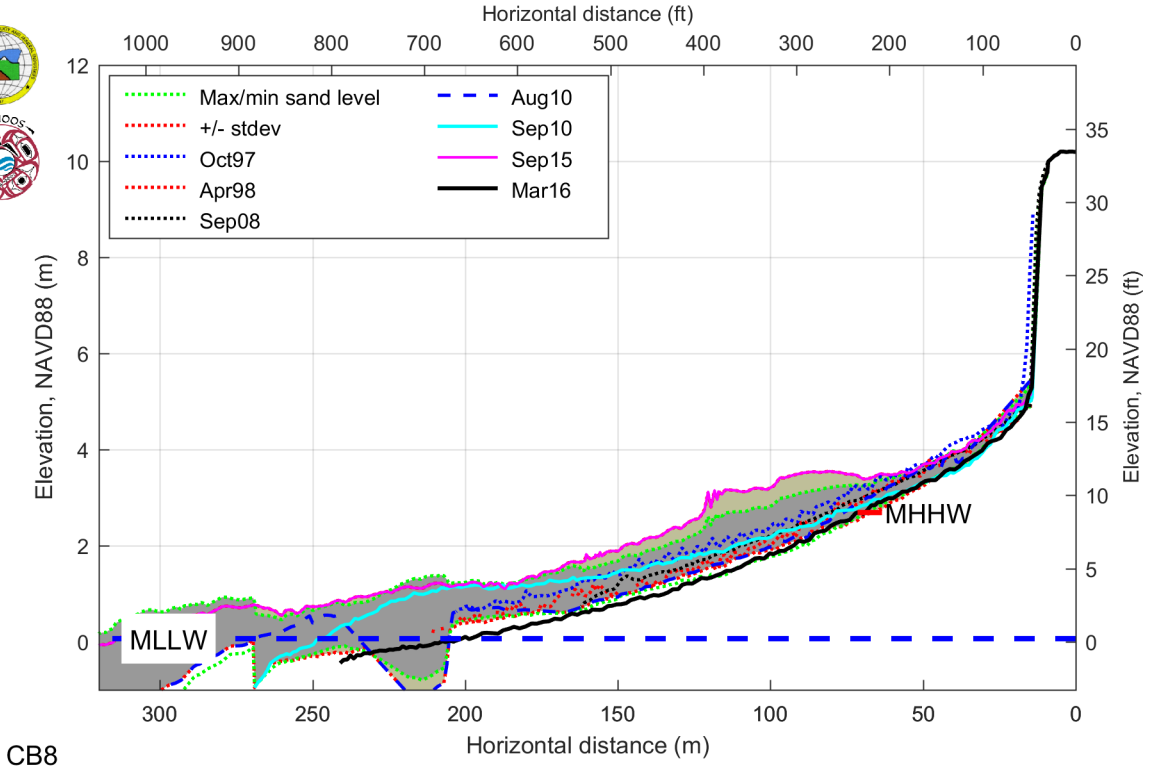
Horizontal distance (ft)
1000
900
800
700
600
500
400
300
200
100
0
Max/min sand level
+/- stdev
Oct97
Apr98
Sep08
Aug10
Sep10
Sep15
Mar16
MHHW
MLLW
Elevation, NAVD88 (m)
Elevation, NAVD88 (ft)
Horizontal distance (m)
300
250
200
150
100
50
0

CB8

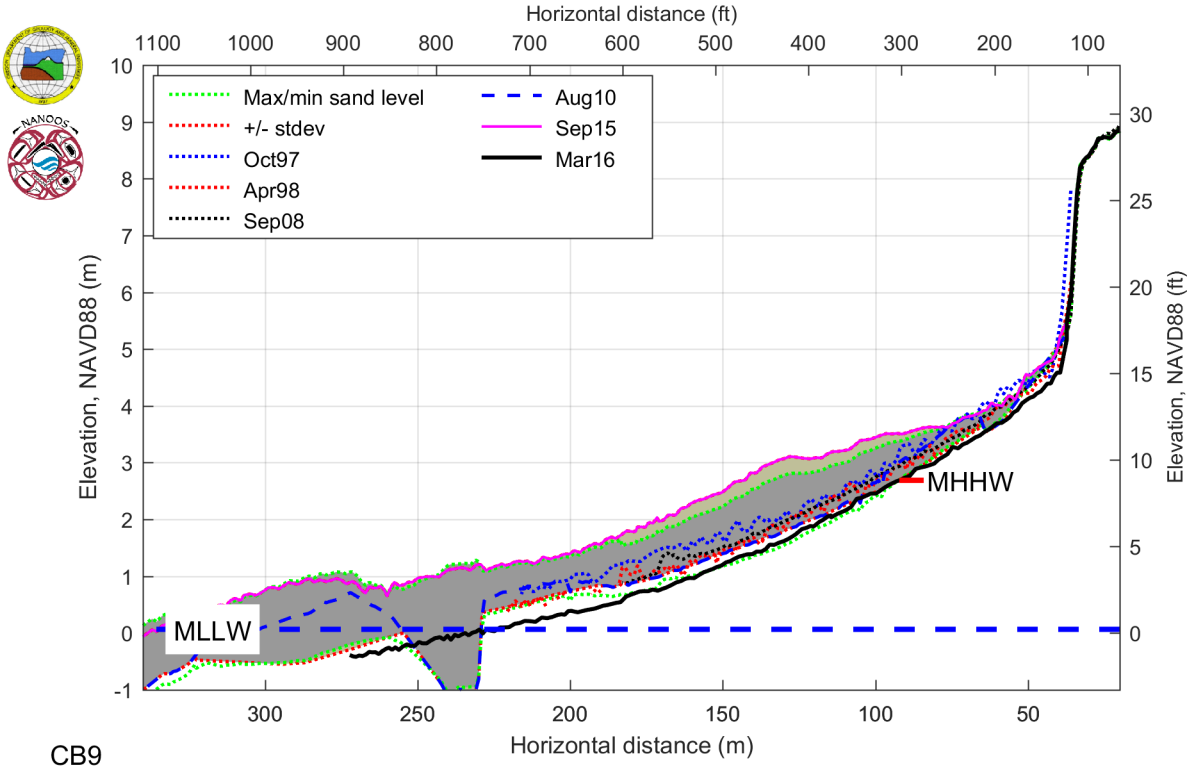
Horizontal distance (ft)
1100 1000 900 800 700 600 500 400 300 200 100
Max/min sand level
+/- stdev
Oct97
Apr98
Sep08
Aug10
Sep15
Mar16
MHHW
MLLW
Elevation, NAVD88 (m)
Elevation, NAVD88 (ft)
300 250 200 150 100 50
Horizontal distance (m)

CB9

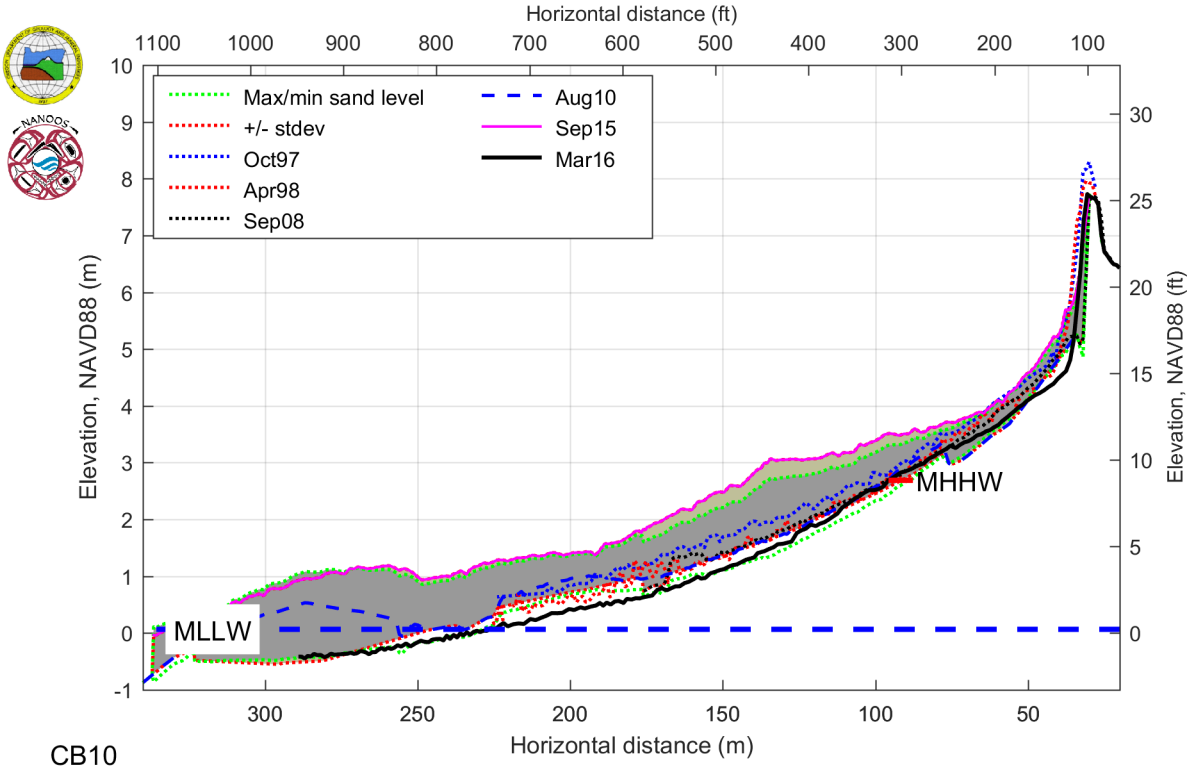
Horizontal distance (ft)
1100 1000 900 800 700 600 500 400 300 200 100
Max/min sand level
+/- stdev
Oct97
Apr98
Sep08
Aug10
Sep15
Mar16
MHHW
MLLW
Elevation, NAVD88 (m)
Elevation, NAVD88 (ft)
300 250 200 150 100 50
Horizontal distance (m)

CB10

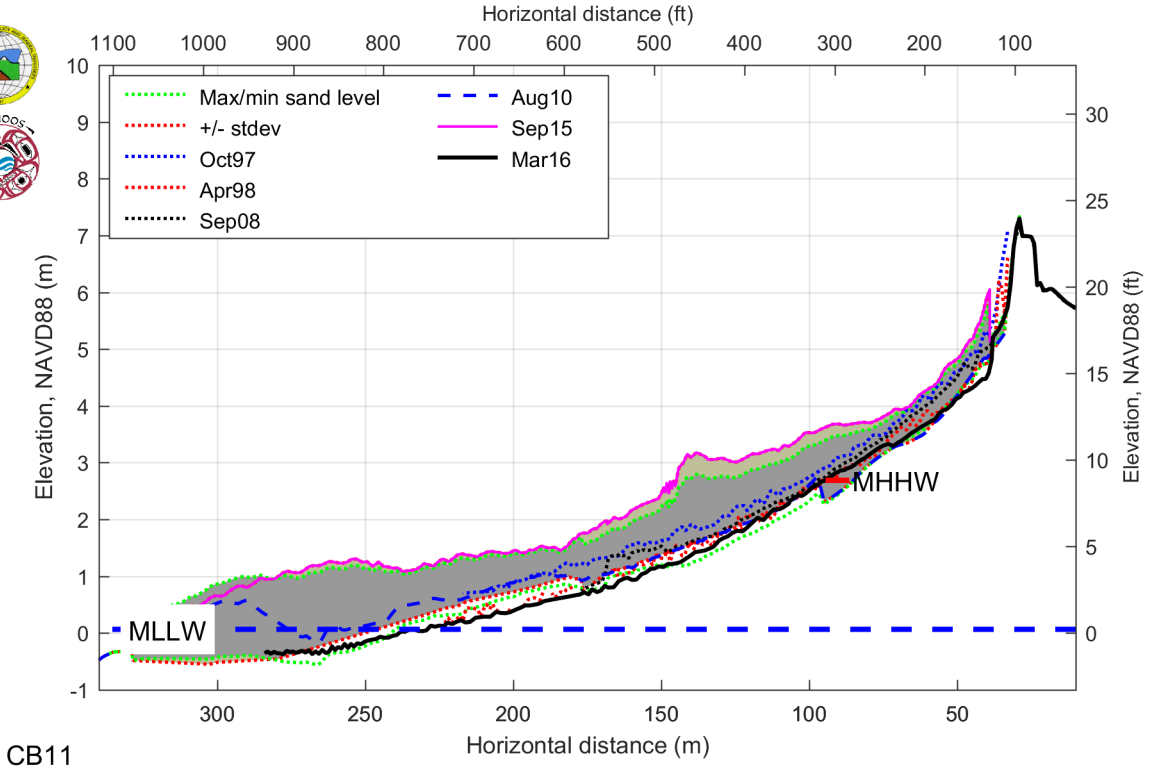
Horizontal distance (ft)
1100 1000 900 800 700 600 500 400 300 200 100
Max/min sand level
+/- stdev
Oct97
Apr98
Sep08
Aug10
Sep15
Mar16
MHHW
MLLW
Elevation, NAVD88 (m)
Elevation, NAVD88 (ft)
300 250 200 150 100 50
Horizontal distance (m)

CB11

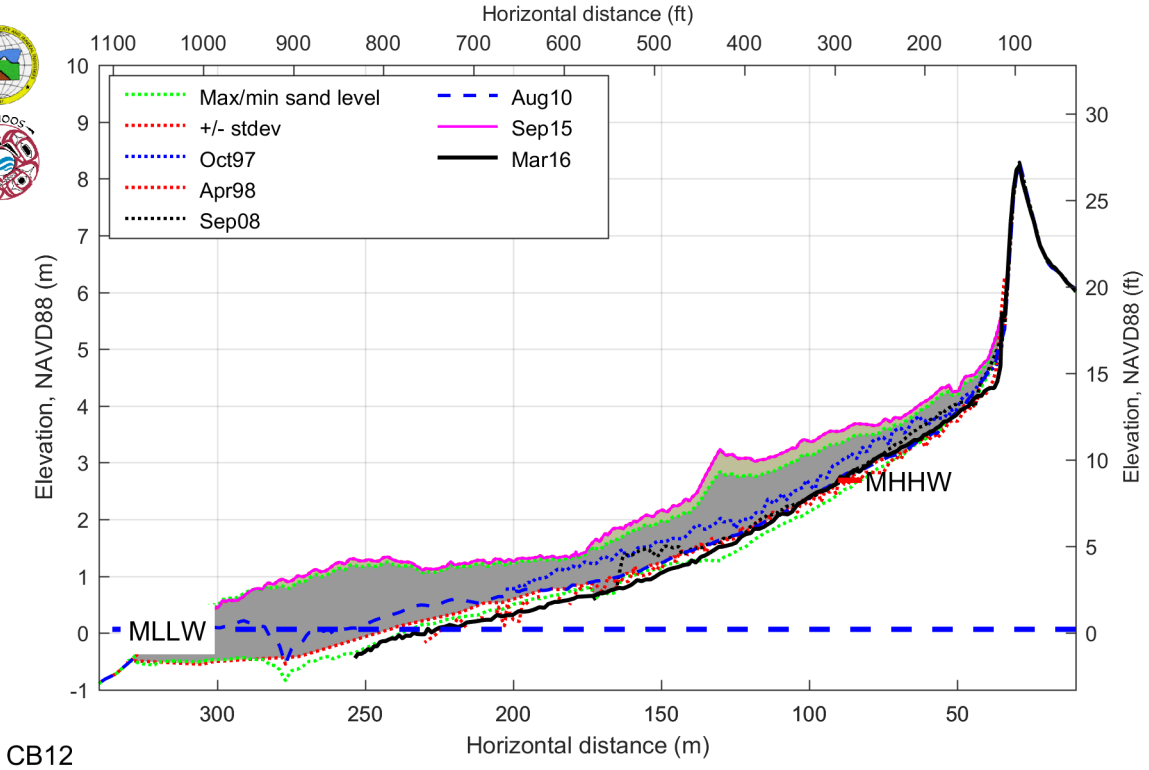
Horizontal distance (ft)
1100 1000 900 800 700 600 500 400 300 200 100
Max/min sand level
+/- stdev
Oct97
Apr98
Sep08
Aug10
Sep15
Mar16
MHHW
MLLW
Elevation, NAVD88 (m)
Elevation, NAVD88 (ft)
300 250 200 150 100 50
Horizontal distance (m)

CB12

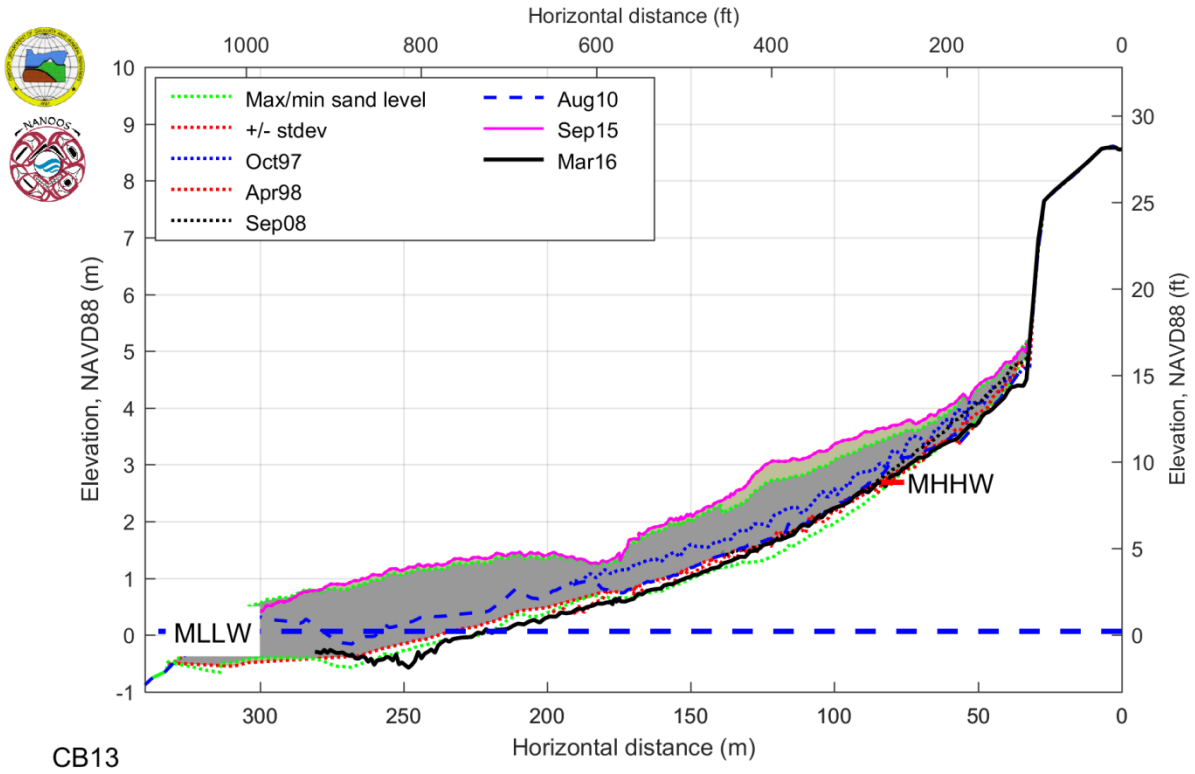
Horizontal distance (ft)
1000
800
600
400
200
0
Max/min sand level
+/- stdev
Oct97
Apr98
Sep08
Aug10
Sep15
Mar16
Elevation, NAVD88 (m)
Elevation, NAVD88 (ft)
MHHW
MLLW
300
250
200
150
100
50
0
Horizontal distance (m)

CB13

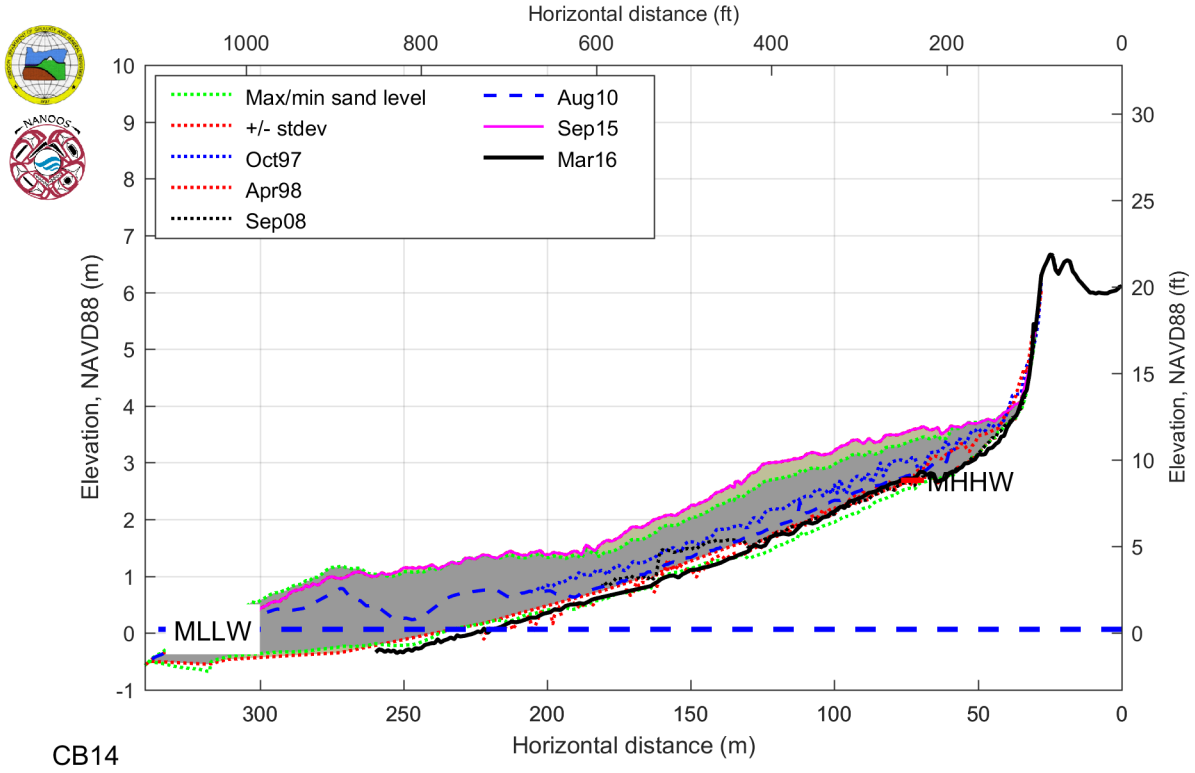
Horizontal distance (ft)
1000
800
600
400
200
0
Max/min sand level
+/- stdev
Oct97
Apr98
Sep08
Aug10
Sep15
Mar16
Elevation, NAVD88 (m)
Elevation, NAVD88 (ft)
MHHW
MLLW
300
250
200
150
100
50
0
Horizontal distance (m)

CB14

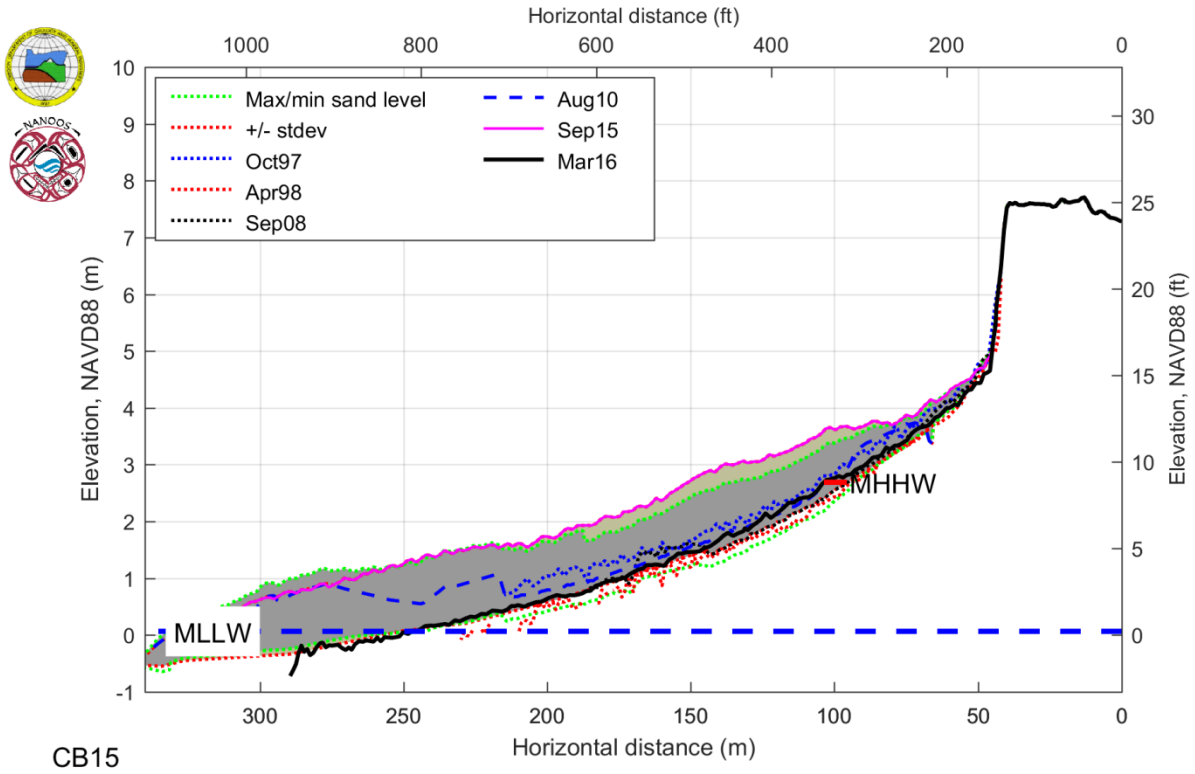
Horizontal distance (ft)
1000
800
600
400
200
0
Max/min sand level
+/- stdev
Oct97
Apr98
Sep08
Aug10
Sep15
Mar16
MHHW
MLLW
Elevation, NAVD88 (m)
Elevation, NAVD88 (ft)
Horizontal distance (m)
300
250
200
150
100
50
0

CB15

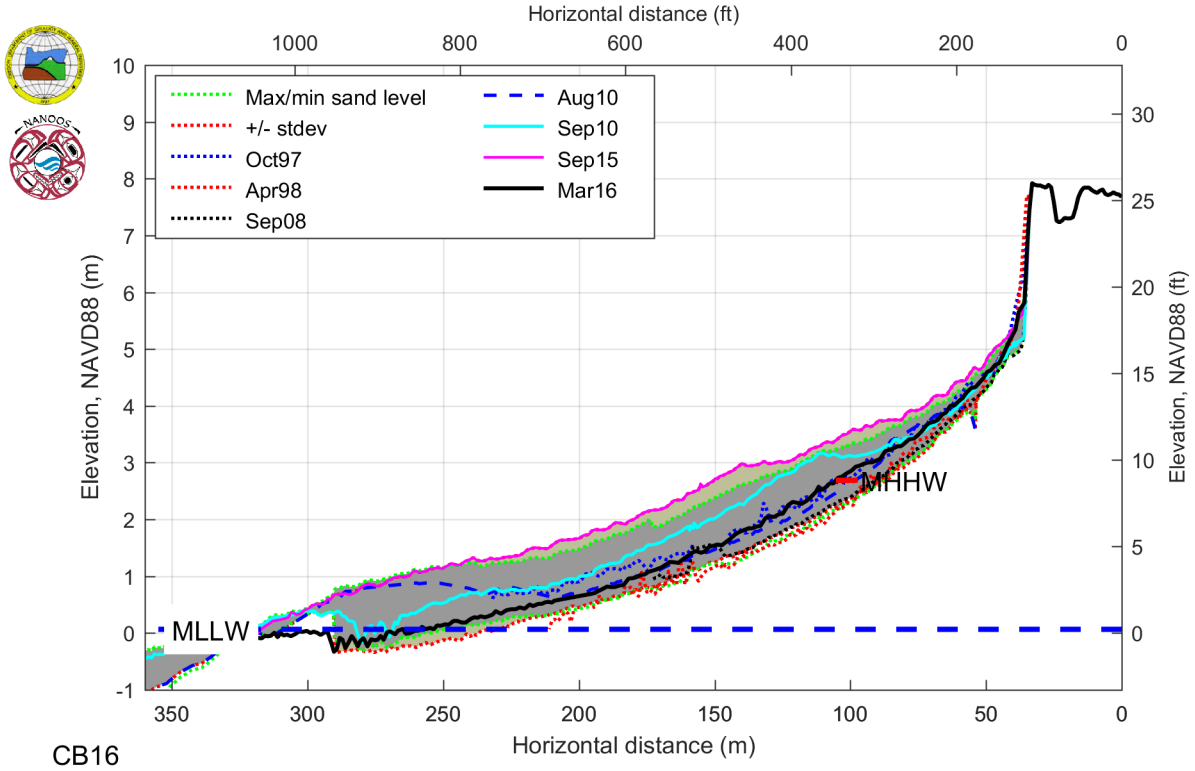
Horizontal distance (ft)
1000
800
600
400
200
0
Max/min sand level
+/- stdev
Oct97
Apr98
Sep08
Aug10
Sep10
Sep15
Mar16
MHHW
MLLW
Elevation, NAVD88 (m)
Elevation, NAVD88 (ft)
Horizontal distance (m)
350
300
250
200
150
100
50
0

CB16

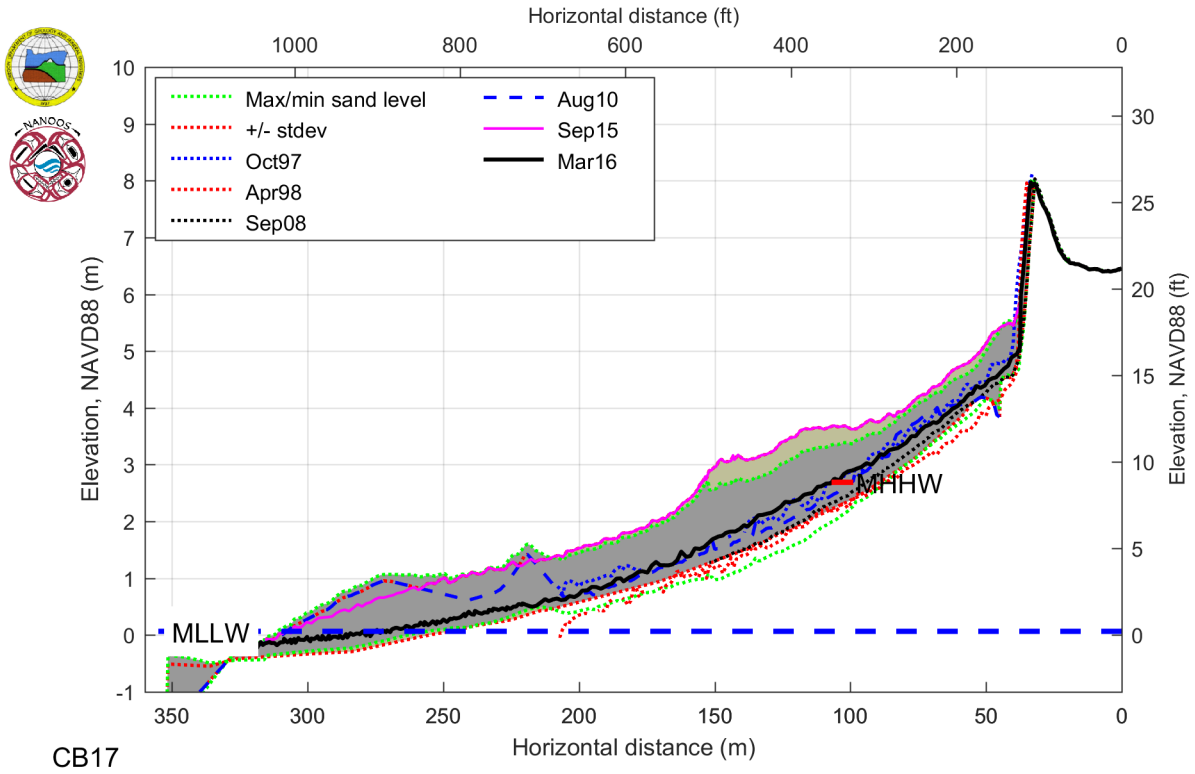
Horizontal distance (ft)
1000
800
600
400
200
0
Max/min sand level
+/- stdev
Oct97
Apr98
Sep08
Aug10
Sep15
Mar16
MHHW
MLLW
Elevation, NAVD88 (m)
Elevation, NAVD88 (ft)
Horizontal distance (m)
350
300
250
200
150
100
50
0

CB17

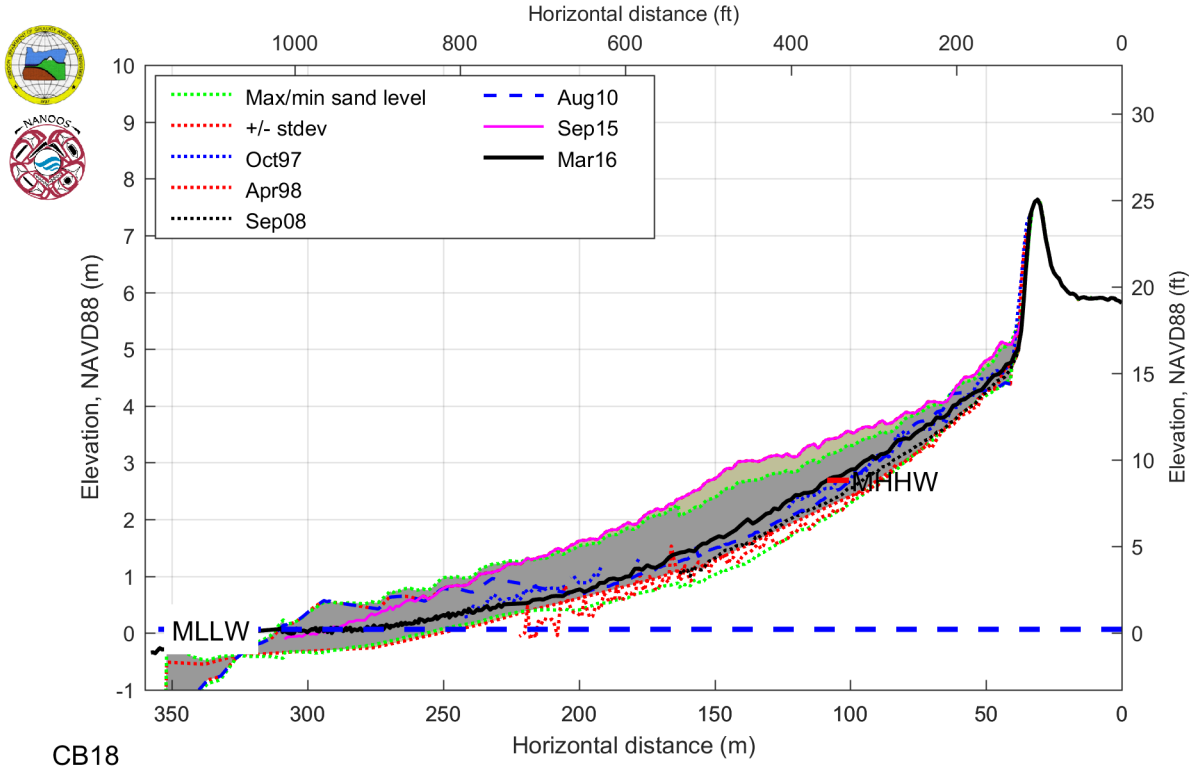
Horizontal distance (ft)
1000
800
600
400
200
0
Max/min sand level
+/- stdev
Oct97
Apr98
Sep08
Aug10
Sep15
Mar16
MHHW
MLLW
Elevation, NAVD88 (m)
Elevation, NAVD88 (ft)
Horizontal distance (m)
350
300
250
200
150
100
50
0

CB18

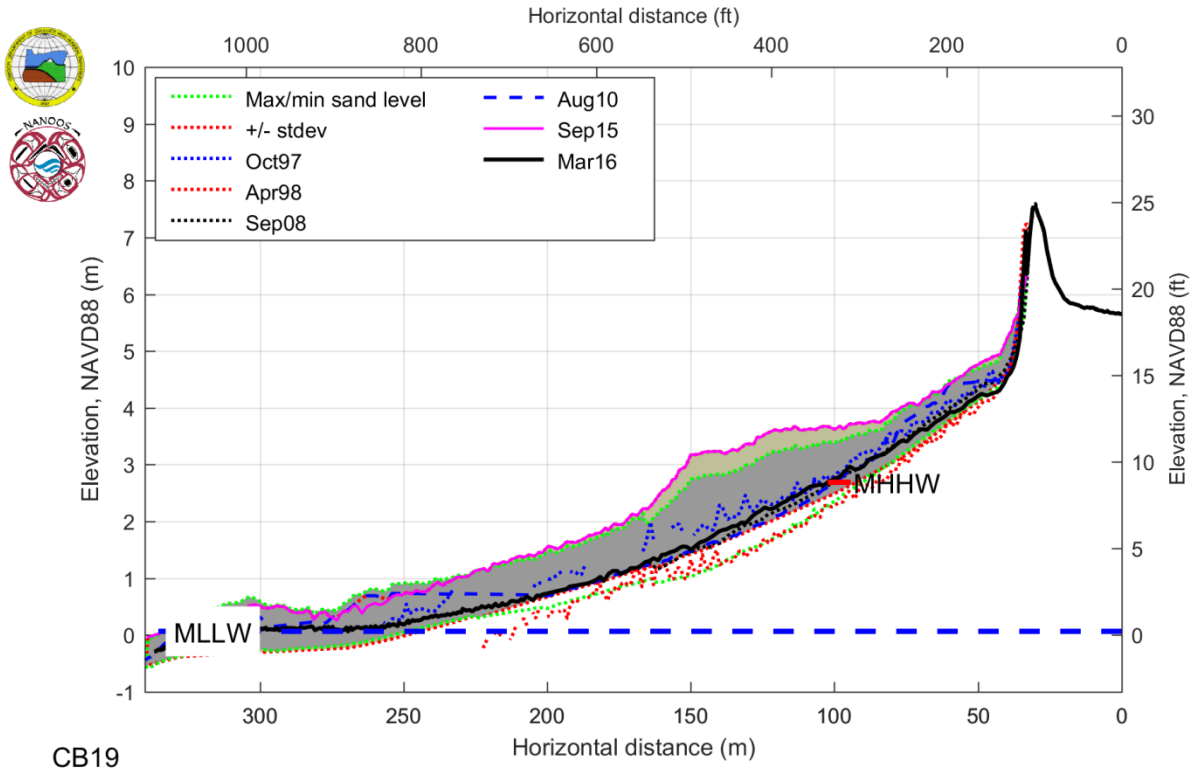
Horizontal distance (ft)
1000
800
600
400
200
0
Max/min sand level
+/- stdev
Oct97
Apr98
Sep08
Aug10
Sep15
Mar16
MHHW
MLLW
Elevation, NAVD88 (m)
Elevation, NAVD88 (ft)
Horizontal distance (m)
300
250
200
150
100
50
0

CB19

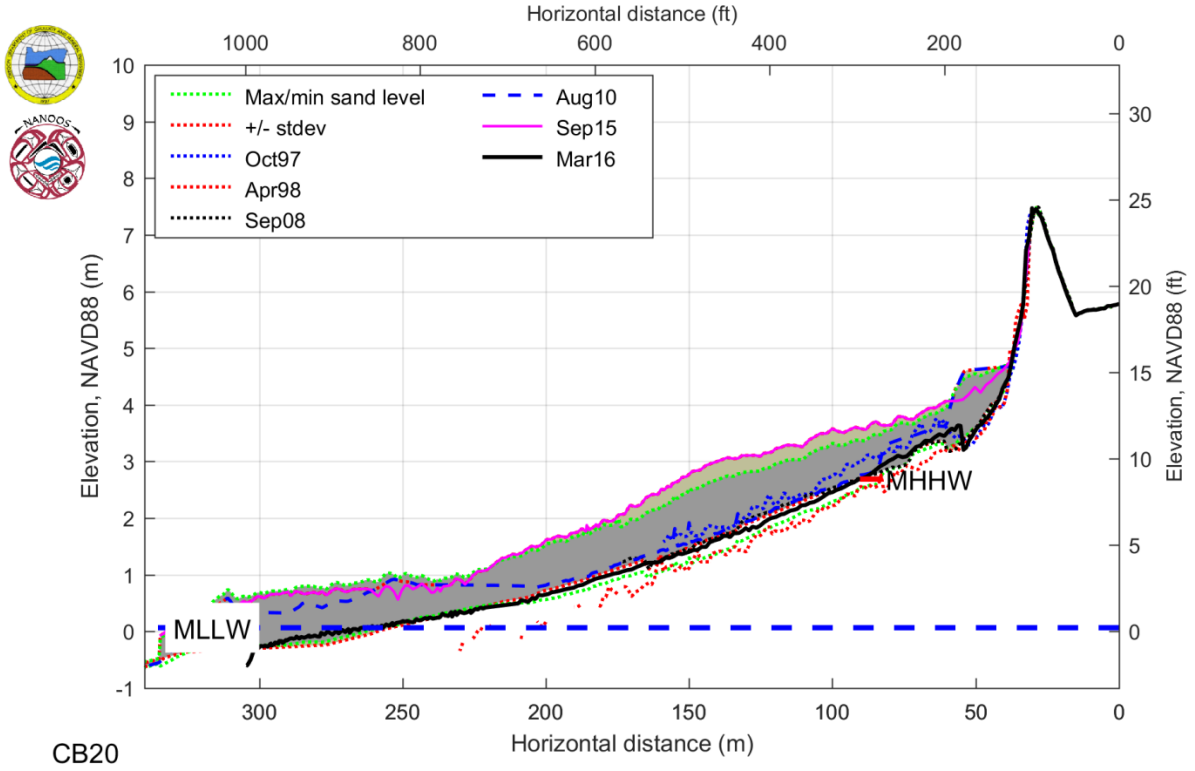
Horizontal distance (ft)
1000
800
600
400
200
0
Max/min sand level
+/- stdev
Oct97
Apr98
Sep08
Aug10
Sep15
Mar16
MHHW
MLLW
Elevation, NAVD88 (m)
Elevation, NAVD88 (ft)
Horizontal distance (m)
300
250
200
150
100
50
0

CB20

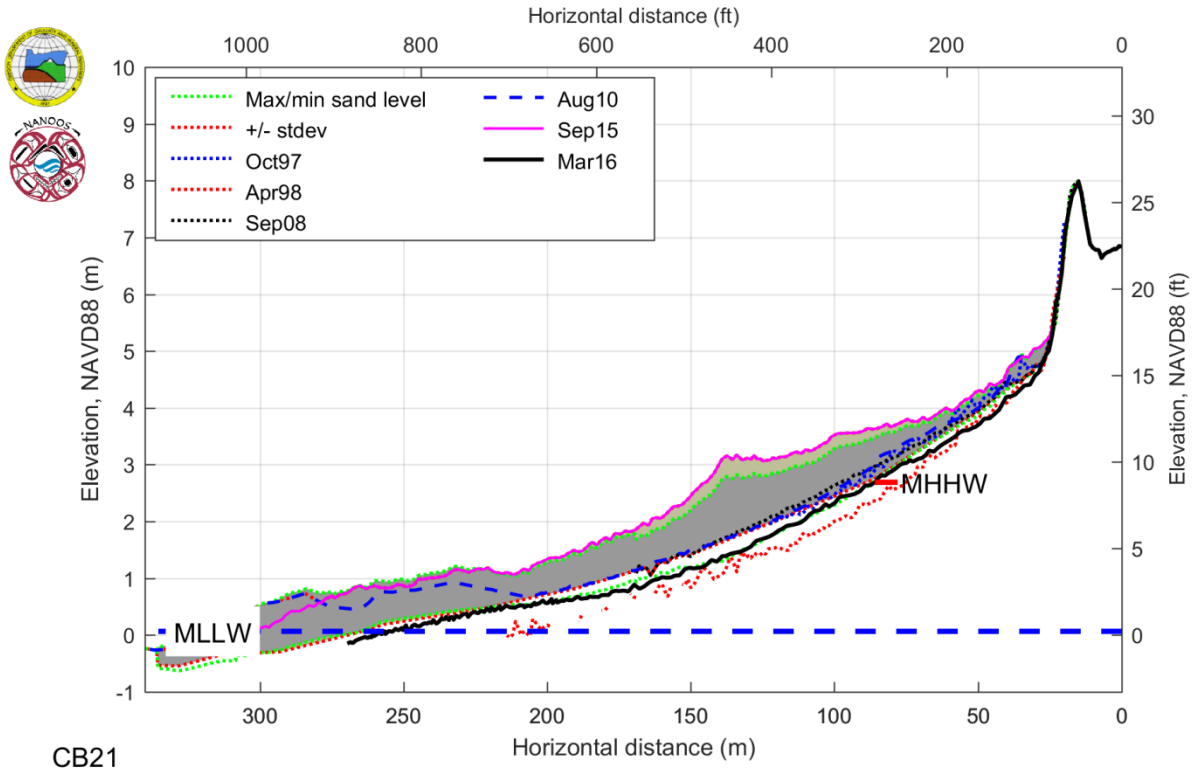
Horizontal distance (ft)
1000
800
600
400
200
0
Max/min sand level
+/- stdev
Oct97
Apr98
Sep08
Aug10
Sep15
Mar16
Elevation, NAVD88 (m)
Elevation, NAVD88 (ft)
MHHW
MLLW
300
250
200
150
100
50
0
Horizontal distance (m)

CB21

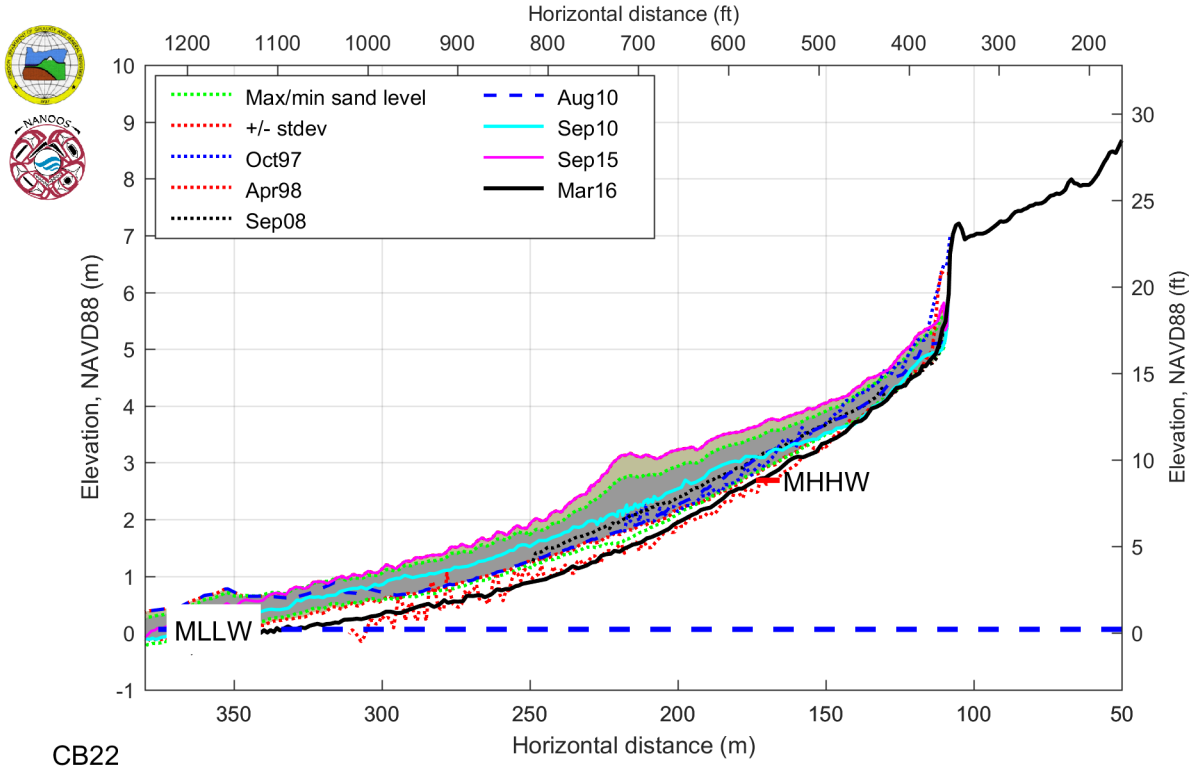
Horizontal distance (ft)
1200
1100
1000
900
800
700
600
500
400
300
200
Max/min sand level
+/- stdev
Oct97
Apr98
Sep08
Aug10
Sep10
Sep15
Mar16
Elevation, NAVD88 (m)
Elevation, NAVD88 (ft)
MHHW
MLLW
350
300
250
200
150
100
50
Horizontal distance (m)

CB22

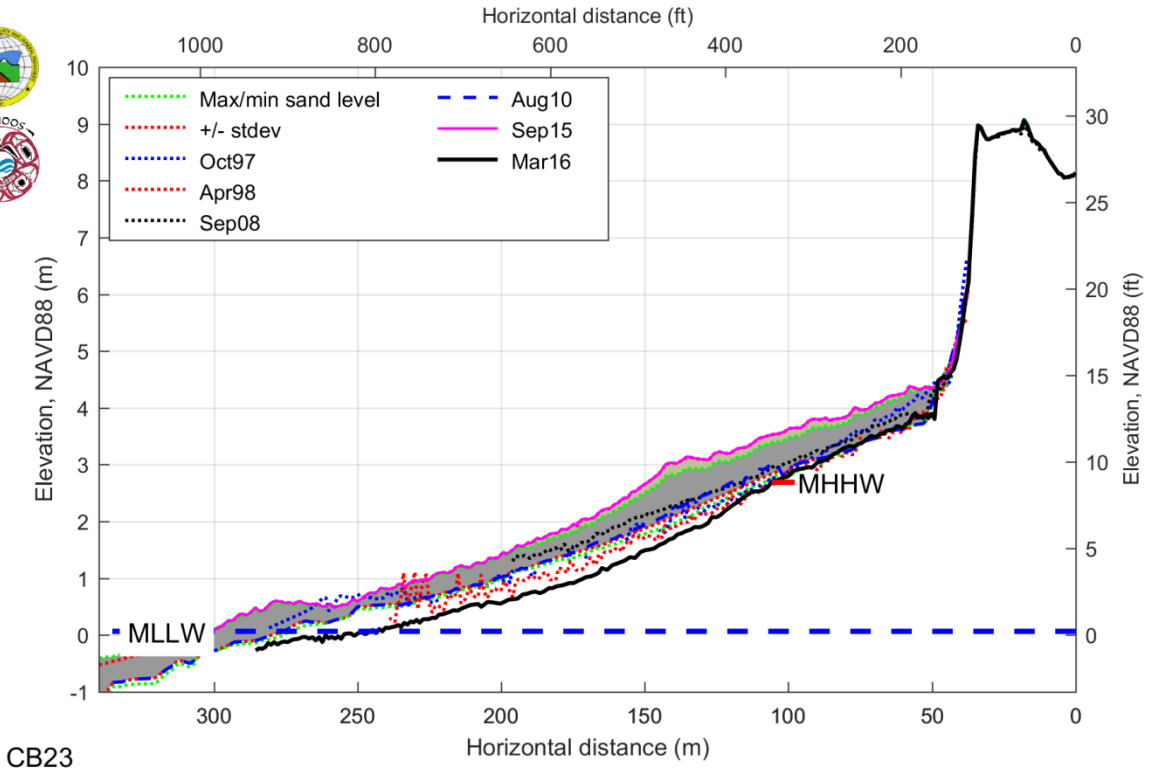
Horizontal distance (ft)
1000
800
600
400
200
0
Max/min sand level
+/- stdev
Oct97
Apr98
Sep08
Aug10
Sep15
Mar16
MHHW
MLLW
Elevation, NAVD88 (m)
Elevation, NAVD88 (ft)
Horizontal distance (m)
300
250
200
150
100
50
0

CB23

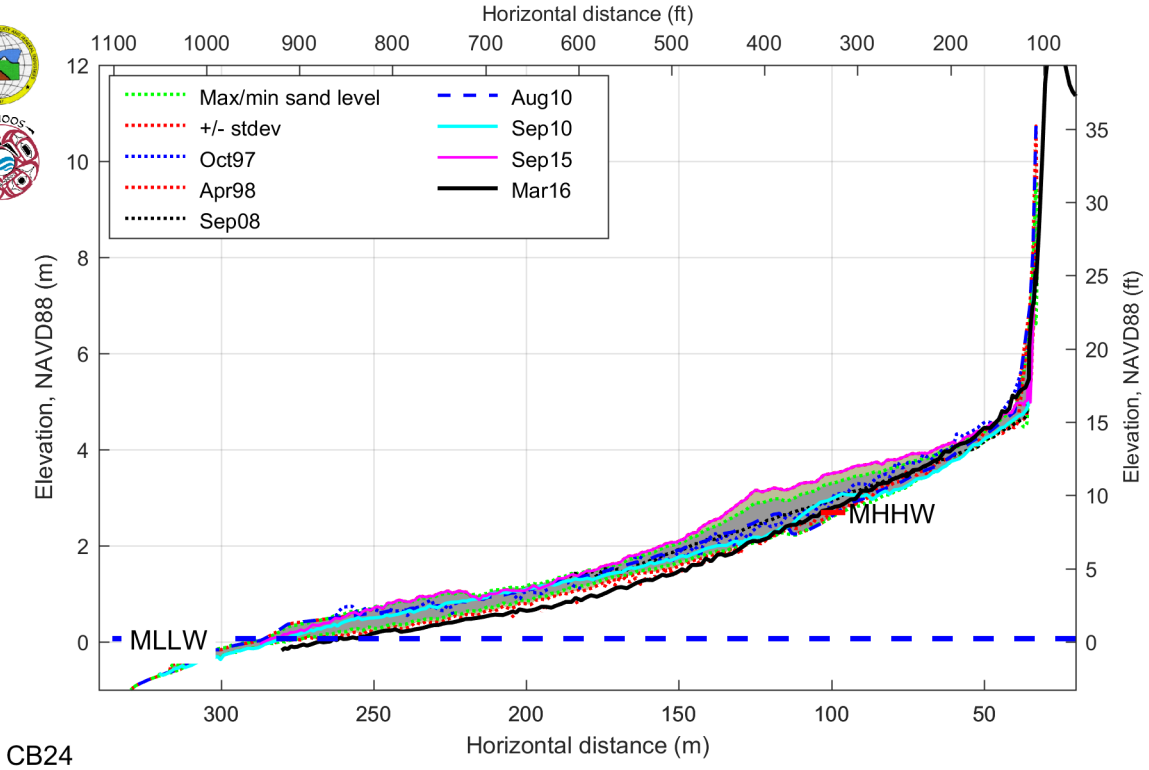
Horizontal distance (ft)
1100
1000
900
800
700
600
500
400
300
200
100
Max/min sand level
+/- stdev
Oct97
Apr98
Sep08
Aug10
Sep10
Sep15
Mar16
MHHW
MLLW
Elevation, NAVD88 (m)
Elevation, NAVD88 (ft)
Horizontal distance (m)
300
250
200
150
100
50
0

CB24

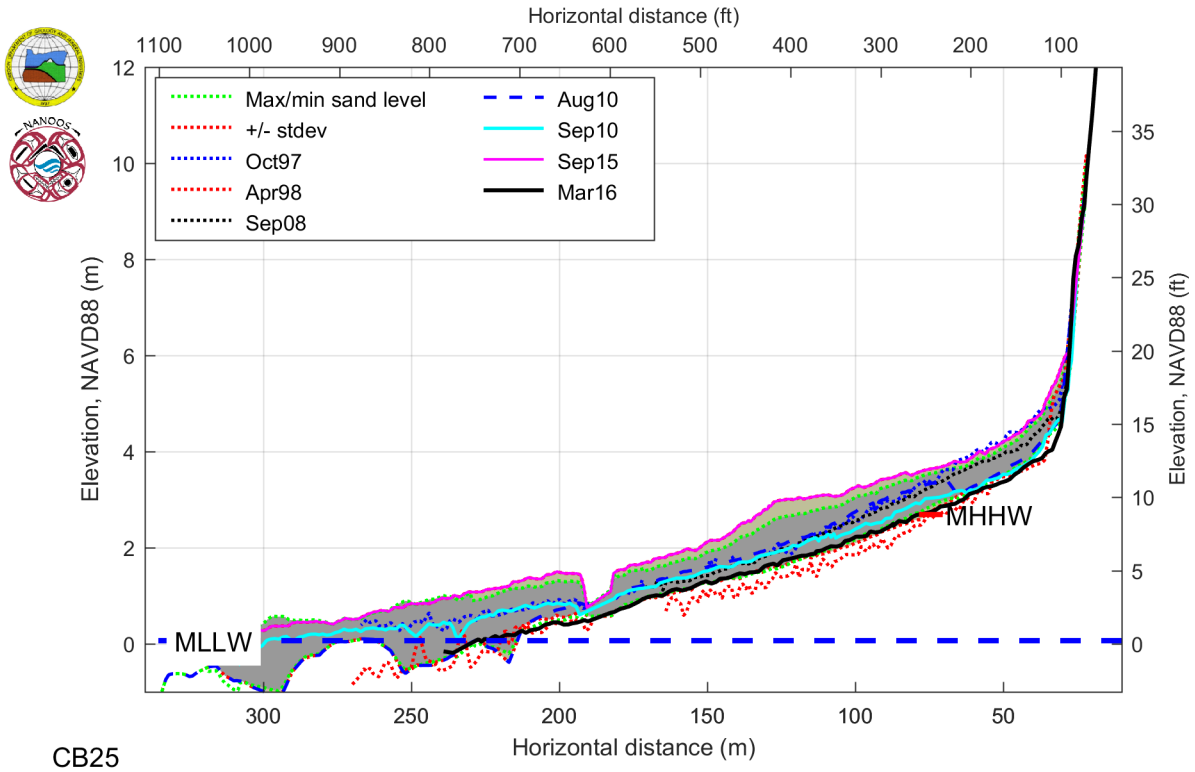
Horizontal distance (ft)
1100 1000 900 800 700 600 500 400 300 200 100
Max/min sand level
+/- stdev
Oct97
Apr98
Sep08
Aug10
Sep10
Sep15
Mar16
MHHW
MLLW
Elevation, NAVD88 (m)
Elevation, NAVD88 (ft)
300 250 200 150 100 50
Horizontal distance (m)

CB25

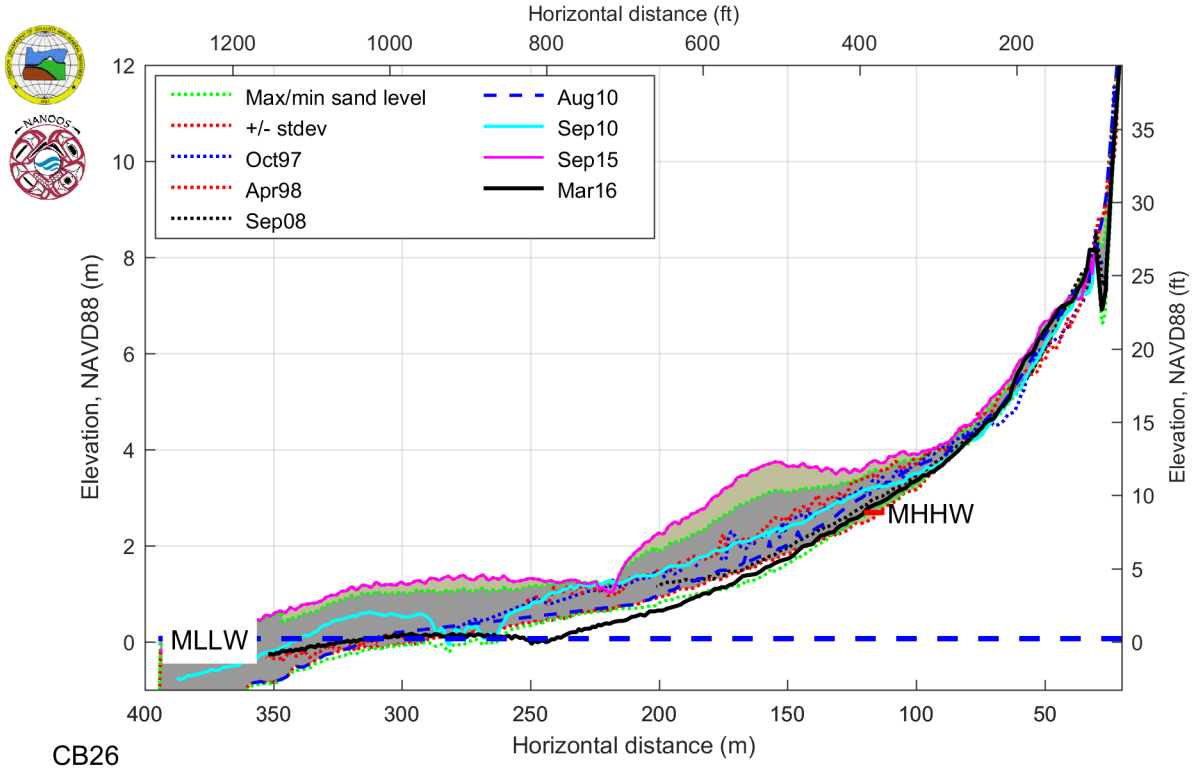
Horizontal distance (ft)
1200 1000 800 600 400 200
Max/min sand level
+/- stdev
Oct97
Apr98
Sep08
Aug10
Sep10
Sep15
Mar16
MHHW
MLLW
Elevation, NAVD88 (m)
Elevation, NAVD88 (ft)
400 350 300 250 200 150 100 50
Horizontal distance (m)

CB26

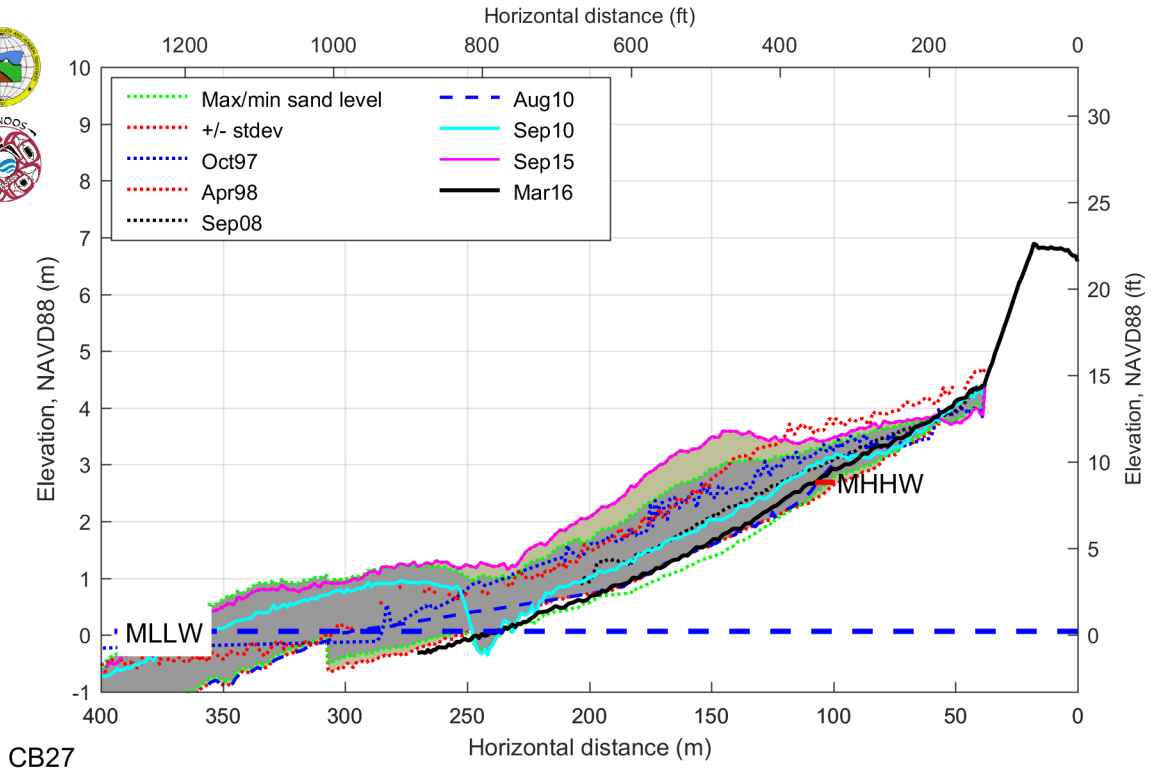
Horizontal distance (ft)
1200
1000
800
600
400
200
0
Max/min sand level
+/- stdev
Oct97
Apr98
Sep08
Aug10
Sep10
Sep15
Mar16
MHHW
MLLW
Elevation, NAVD88 (m)
Elevation, NAVD88 (ft)
Horizontal distance (m)
400
350
300
250
200
150
100
50
0

CB27

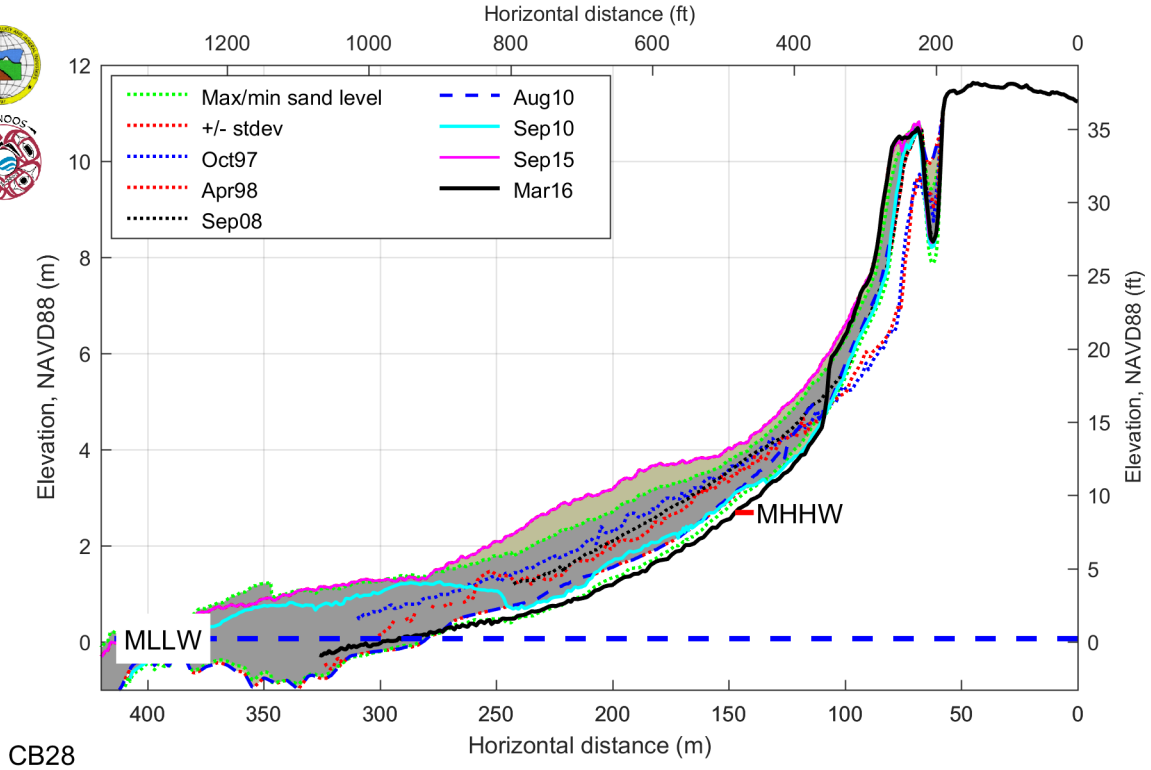
Horizontal distance (ft)
1200
1000
800
600
400
200
0
Max/min sand level
+/- stdev
Oct97
Apr98
Sep08
Aug10
Sep10
Sep15
Mar16
MHHW
MLLW
Elevation, NAVD88 (m)
Elevation, NAVD88 (ft)
Horizontal distance (m)
400
350
300
250
200
150
100
50
0

CB28

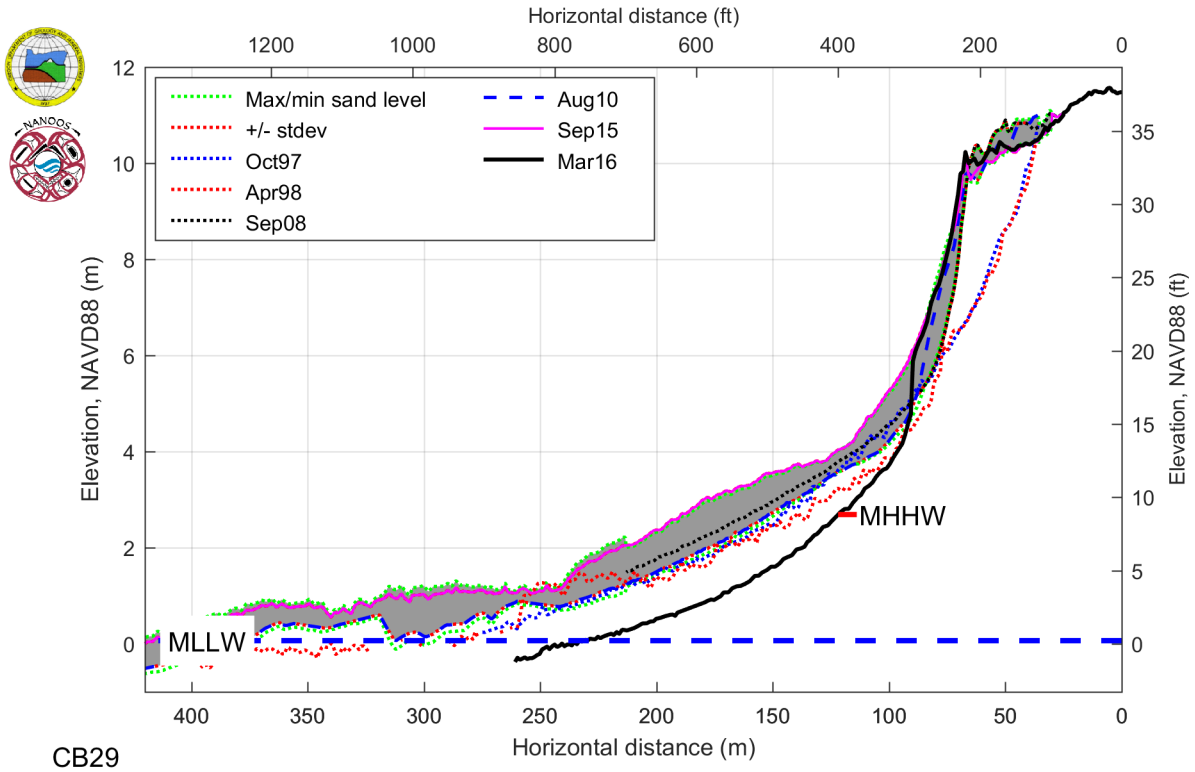
Horizontal distance (ft)
1200
1000
800
600
400
200
0
Max/min sand level
+/- stdev
Oct97
Apr98
Sep08
Aug10
Sep15
Mar16
MHHW
MLLW
Elevation, NAVD88 (m)
Elevation, NAVD88 (ft)
Horizontal distance (m)
400
350
300
250
200
150
100
50
0

CB29

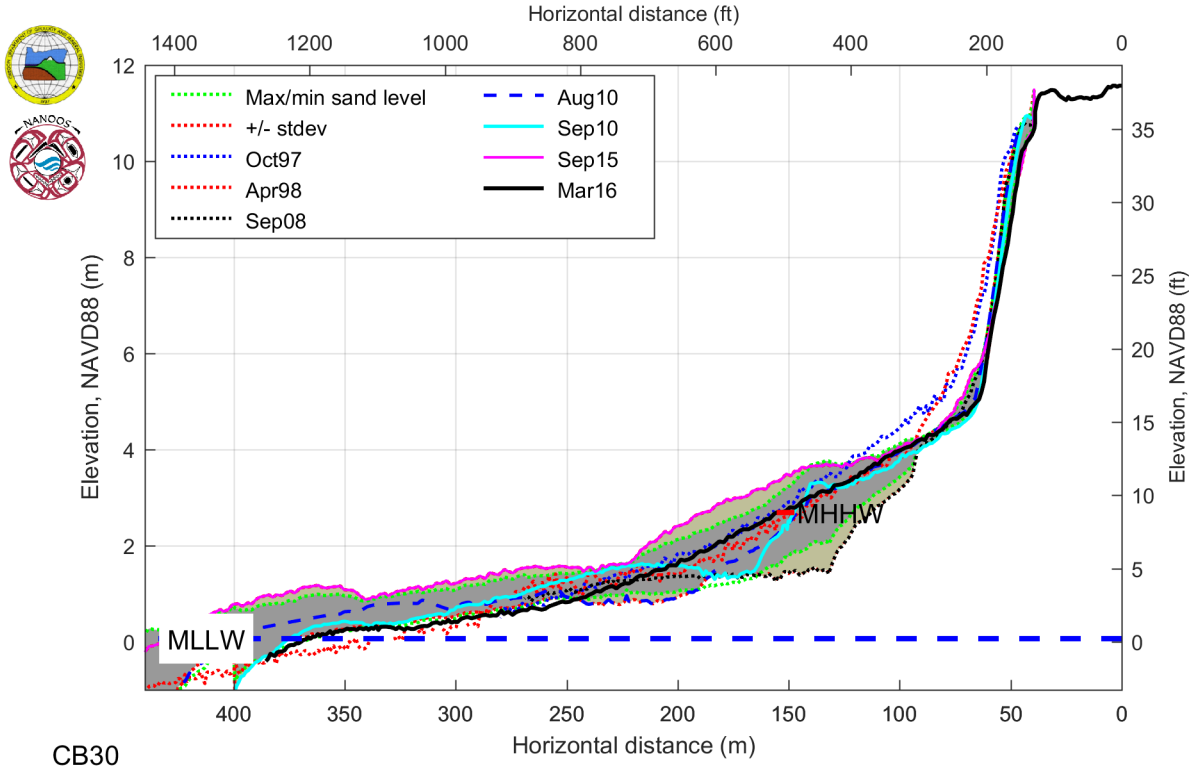
Horizontal distance (ft)
1400
1200
1000
800
600
400
200
0
Max/min sand level
+/- stdev
Oct97
Apr98
Sep08
Aug10
Sep10
Sep15
Mar16
MHHW
MLLW
Elevation, NAVD88 (m)
Elevation, NAVD88 (ft)
Horizontal distance (m)
400
350
300
250
200
150
100
50
0

CB30

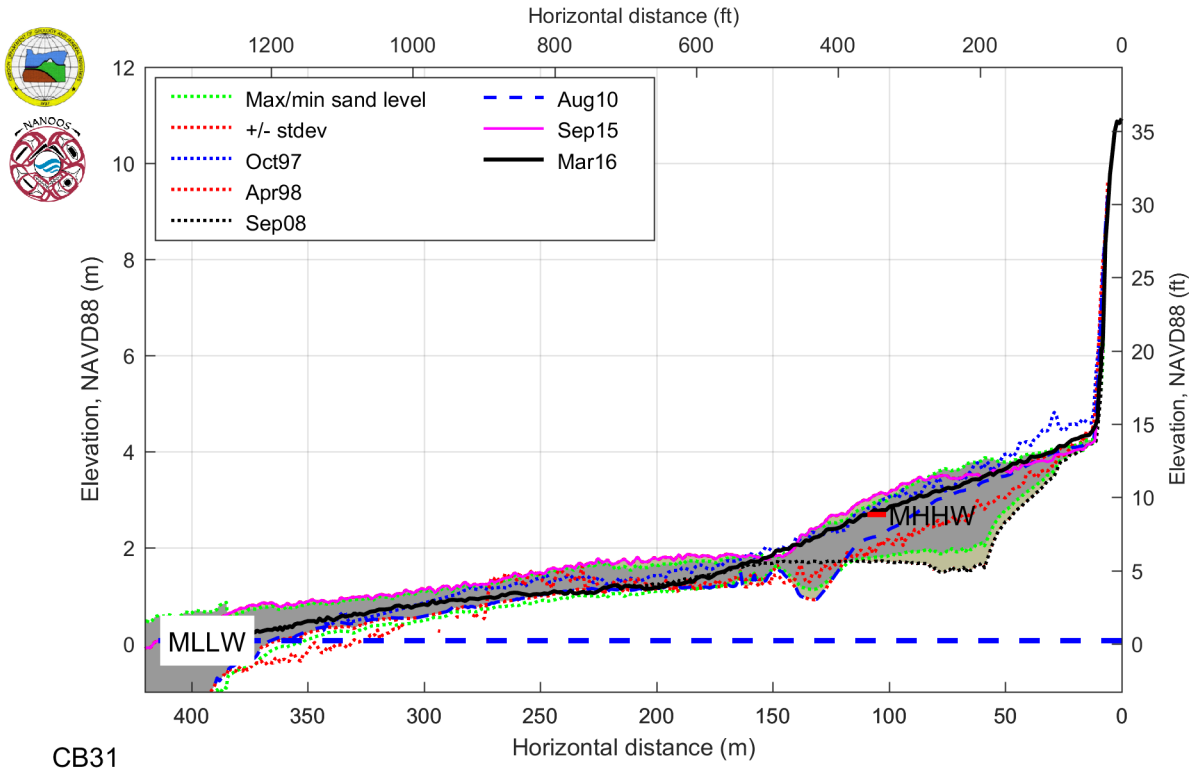
Horizontal distance (ft)
1200
1000
800
600
400
200
0
Max/min sand level
+/- stdev
Oct97
Apr98
Sep08
Aug10
Sep15
Mar16
MHHW
MLLW
Elevation, NAVD88 (m)
Elevation, NAVD88 (ft)
Horizontal distance (m)
400
350
300
250
200
150
100
50
0

CB31

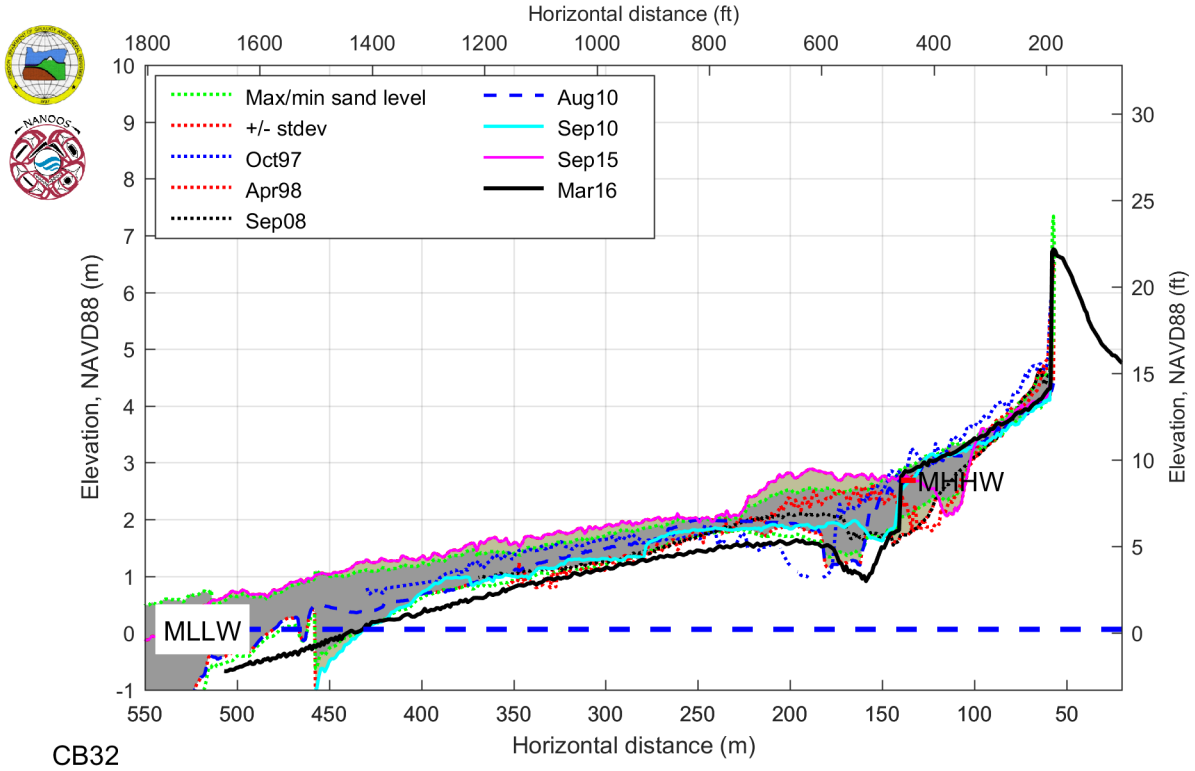
Horizontal distance (ft)
1800
1600
1400
1200
1000
800
600
400
200
Max/min sand level
+/- stdev
Oct97
Apr98
Sep08
Aug10
Sep10
Sep15
Mar16
MHHW
MLLW
Elevation, NAVD88 (m)
Elevation, NAVD88 (ft)
Horizontal distance (m)
550
500
450
400
350
300
250
200
150
100
50

CB32

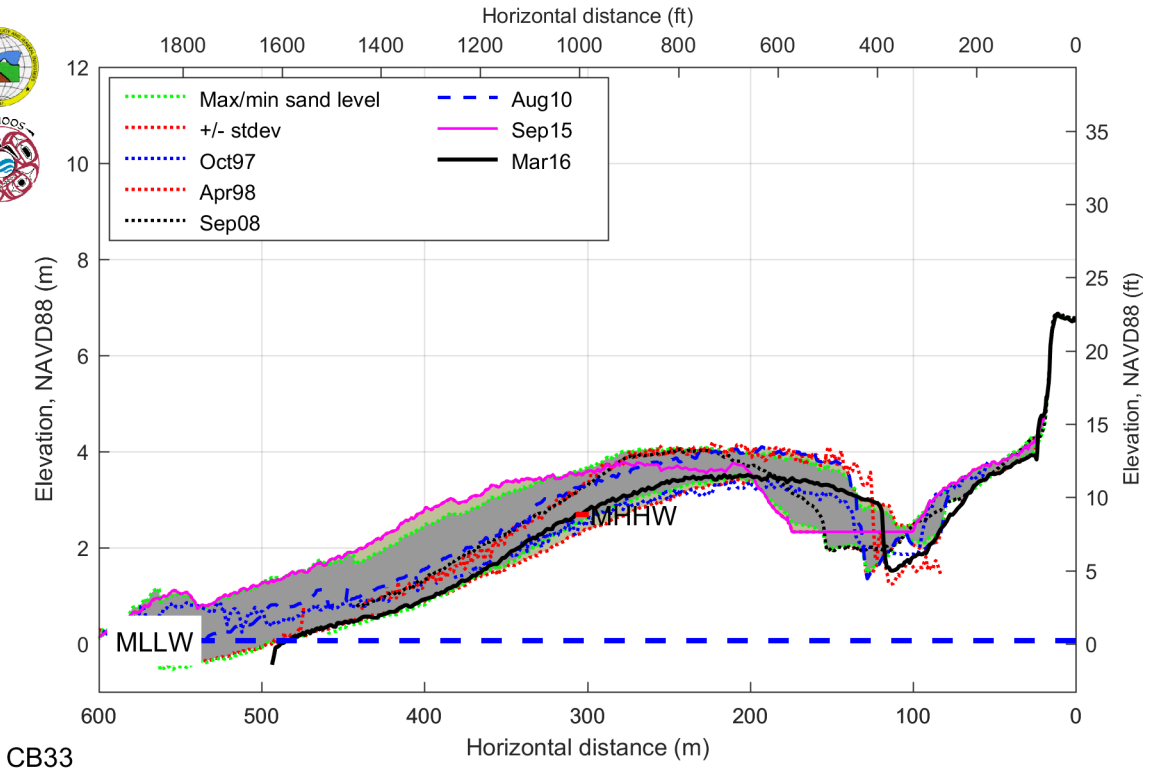
Horizontal distance (ft)
1800 1600 1400 1200 1000 800 600 400 200 0
Max/min sand level
+/- stdev
Oct97
Apr98
Sep08
Aug10
Sep15
Mar16
MHHW
MLLW
Elevation, NAVD88 (m)
Elevation, NAVD88 (ft)
600 500 400 300 200 100 0
Horizontal distance (m)

CB33

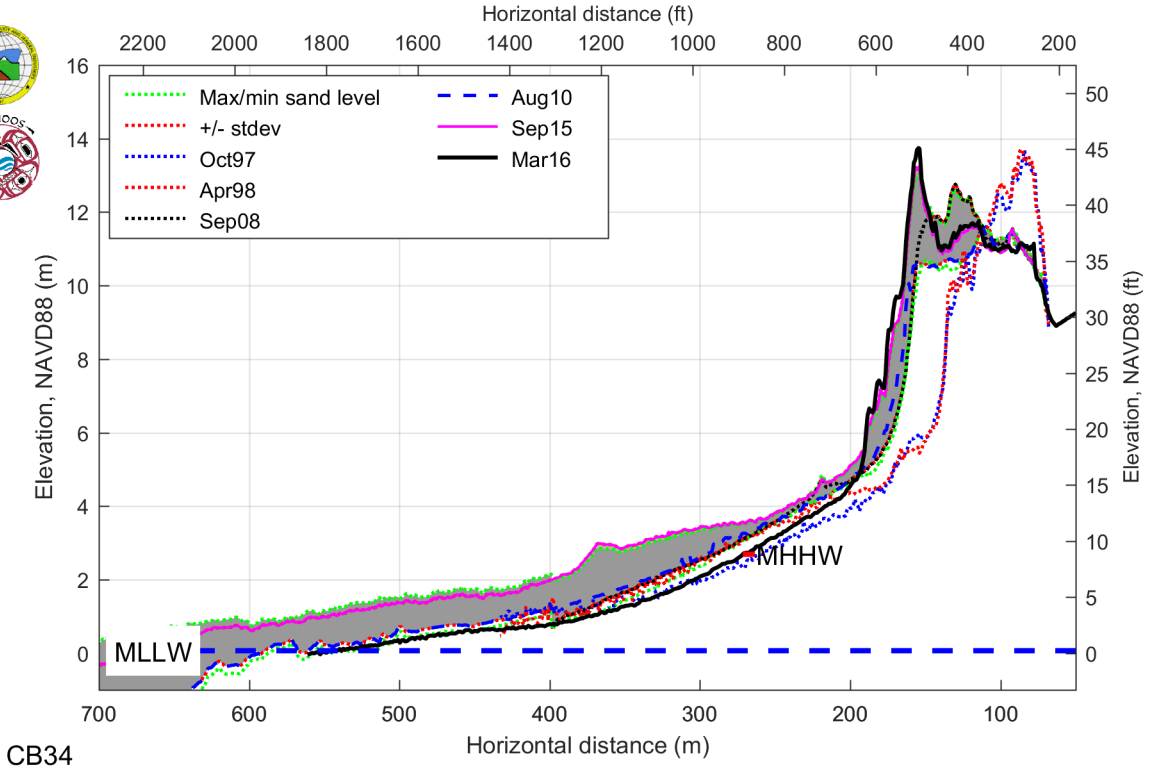
Horizontal distance (ft)
2200 2000 1800 1600 1400 1200 1000 800 600 400 200
Max/min sand level
+/- stdev
Oct97
Apr98
Sep08
Aug10
Sep15
Mar16
MHHW
MLLW
Elevation, NAVD88 (m)
Elevation, NAVD88 (ft)
700 600 500 400 300 200 100
Horizontal distance (m)

CB34

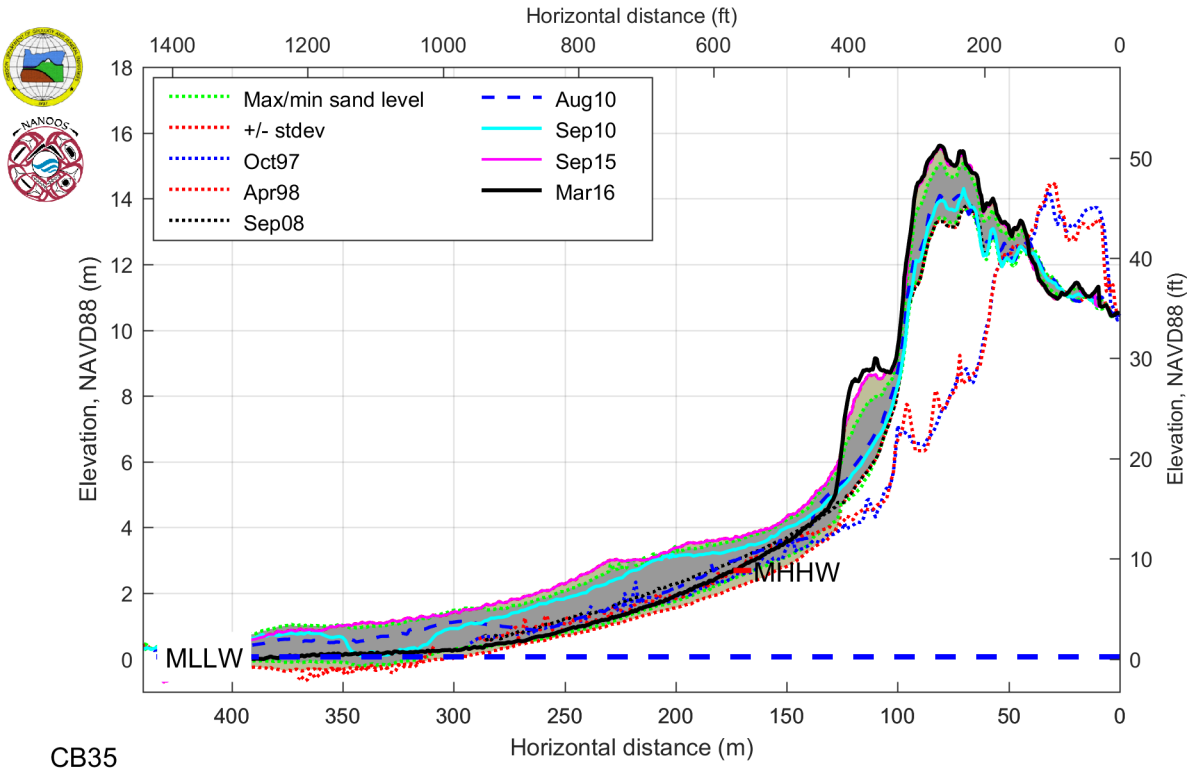
Horizontal distance (ft)
1400
1200
1000
800
600
400
200
0
Max/min sand level
+/- stdev
Oct97
Apr98
Sep08
Aug10
Sep10
Sep15
Mar16
MHHW
MLLW
Elevation, NAVD88 (m)
Elevation, NAVD88 (ft)
Horizontal distance (m)
400
350
300
250
200
150
100
50
0

CB35

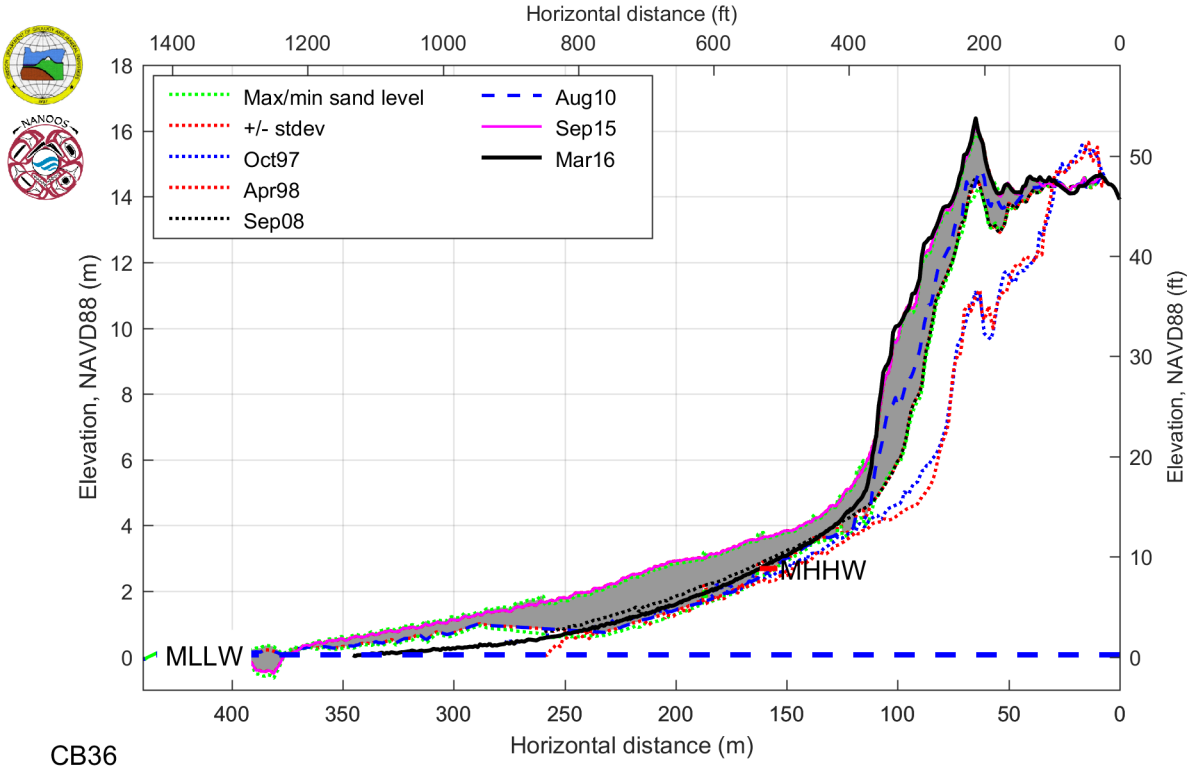
Horizontal distance (ft)
1400
1200
1000
800
600
400
200
0
Max/min sand level
+/- stdev
Oct97
Apr98
Sep08
Aug10
Sep15
Mar16
MHHW
MLLW
Elevation, NAVD88 (m)
Elevation, NAVD88 (ft)
Horizontal distance (m)
400
350
300
250
200
150
100
50
0

CB36

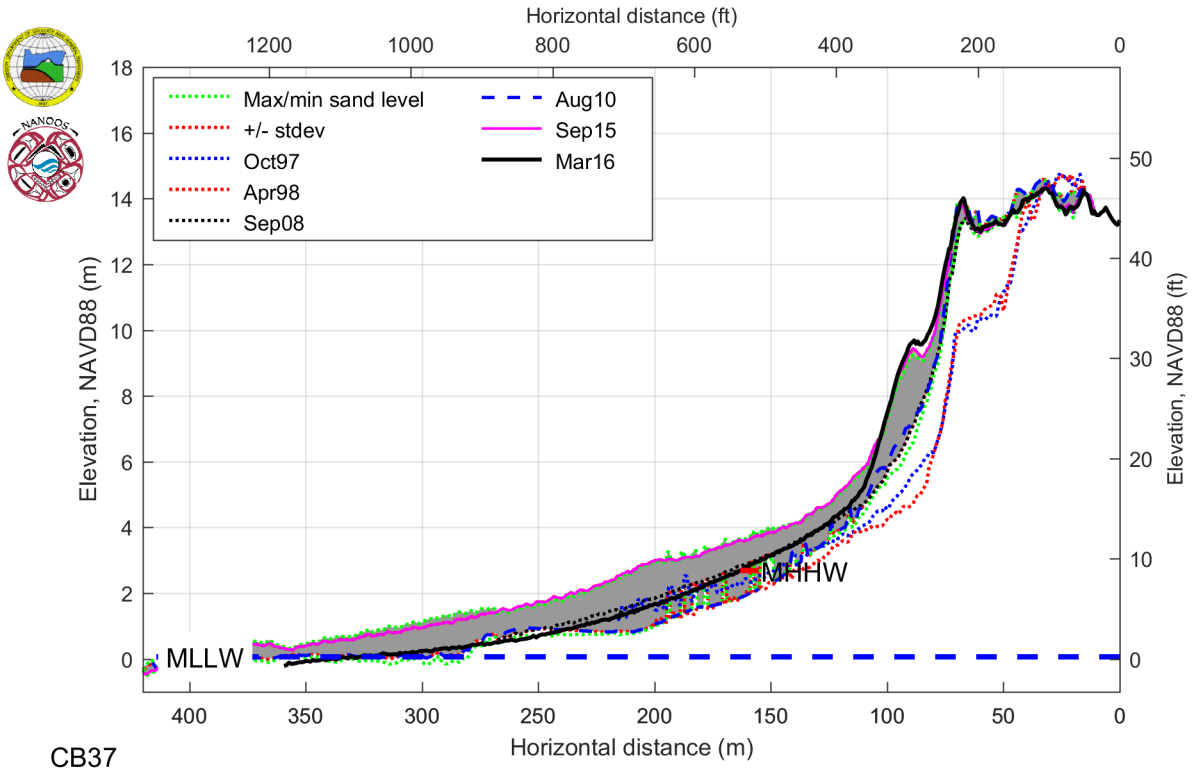
Horizontal distance (ft)
1200
1000
800
600
400
200
0
Max/min sand level
+/- stdev
Oct97
Apr98
Sep08
Aug10
Sep15
Mar16
MHHW
MLLW
Elevation, NAVD88 (m)
Elevation, NAVD88 (ft)
Horizontal distance (m)
400
350
300
250
200
150
100
50
0

CB37

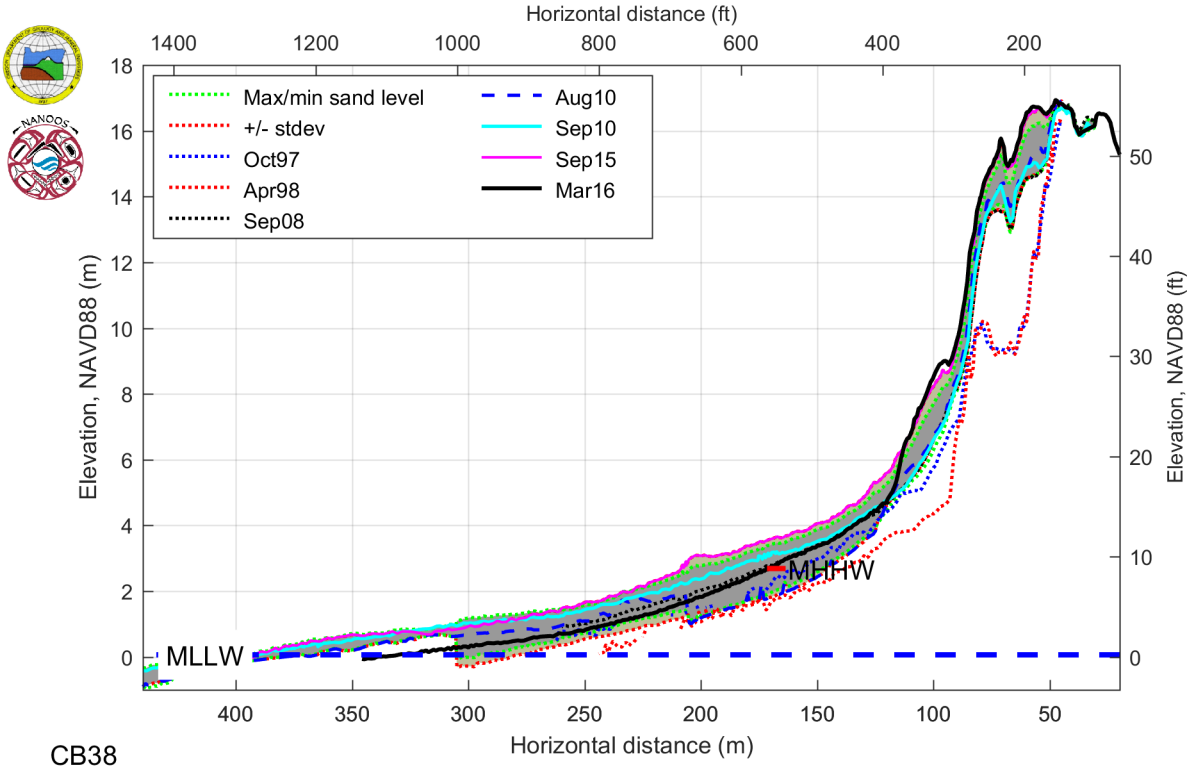
Horizontal distance (ft)
1400
1200
1000
800
600
400
200
0
Max/min sand level
+/- stdev
Oct97
Apr98
Sep08
Aug10
Sep10
Sep15
Mar16
MHHW
MLLW
Elevation, NAVD88 (m)
Elevation, NAVD88 (ft)
Horizontal distance (m)
400
350
300
250
200
150
100
50
0

CB38

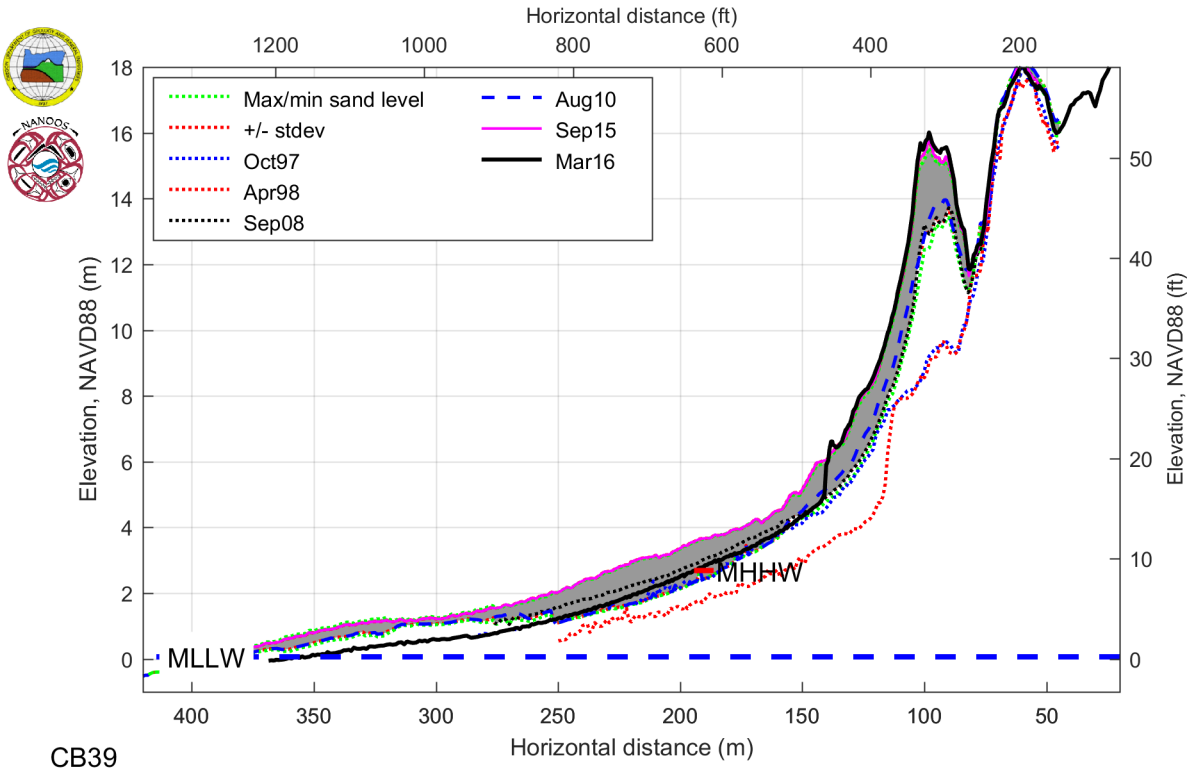
Horizontal distance (ft)
1200
1000
800
600
400
200
Max/min sand level
+/- stdev
Oct97
Apr98
Sep08
Aug10
Sep15
Mar16
MHHW
MLLW
Elevation, NAVD88 (m)
Elevation, NAVD88 (ft)
Horizontal distance (m)
400
350
300
250
200
150
100
50

CB39

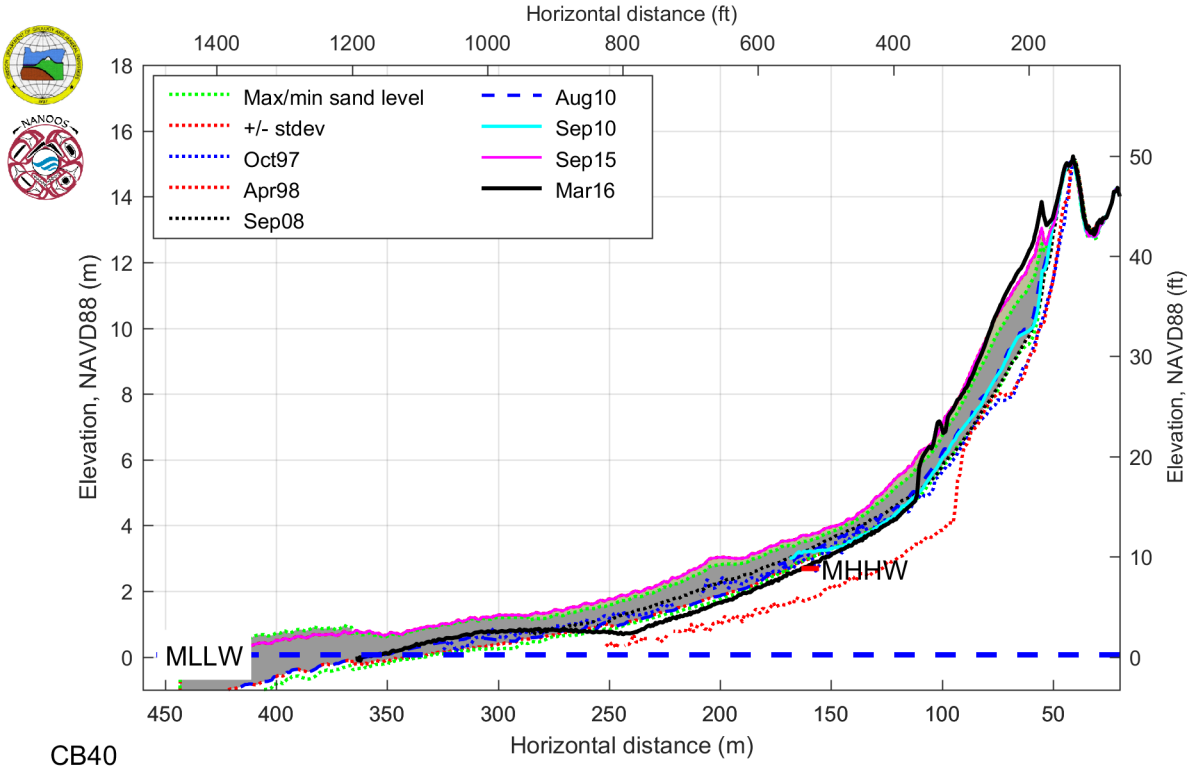
Horizontal distance (ft)
1400
1200
1000
800
600
400
200
Max/min sand level
+/- stdev
Oct97
Apr98
Sep08
Aug10
Sep10
Sep15
Mar16
MHHW
MLLW
Elevation, NAVD88 (m)
Elevation, NAVD88 (ft)
Horizontal distance (m)
450
400
350
300
250
200
150
100
50

CB40